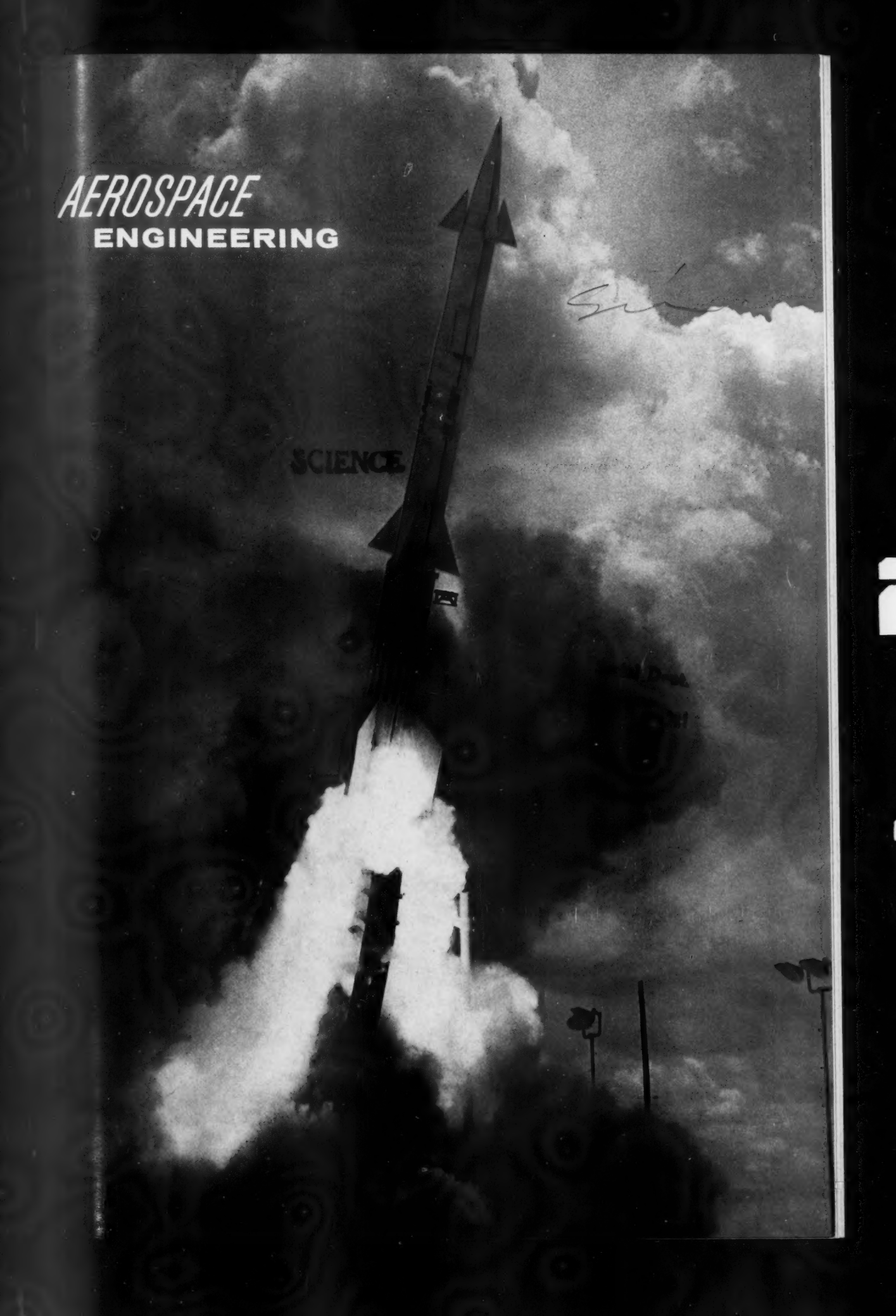
AEROSPACE
ENGINEERING
SCIENCE

To fly faster than time itself...

Here's how the Douglas trisonic jet would beat the clock on westbound flights

LV. NEW YORK 5:00 PM

AR. LOS ANGELES 3:30 PM
FLIGHT TIME – 1 HR. 30 MIN.

LV. SAN FRANCISCO 8:00 AM

AR. HONOLULU 7:35 AM
FLIGHT TIME – 1 HR. 35 MIN.

LV. TOKYO 9:00 AM

AR. BANGKOK 8:50 AM
FLIGHT TIME – 1 HR. 50 MIN.

LV. BEIRUT 12:30 PM

AR. LONDON 11:55 AM
FLIGHT TIME – 1 HR. 25 MIN.*

LV. PARIS MIDNIGHT

AR. NEW YORK 8:10 PM
FLIGHT TIME – 2 HRS. 10 MIN.*

**Includes take-off and landing time.*

Trisonic jets that would land you in Los Angeles 2 hours earlier than your take-off time in New York are feasible says a late Federal study. Douglas officials say they could be operational by the early 1970's.

A 2100 mph civilian jet transport that would fly 13 miles high, cross the continent in one hour and thirty minutes*, and use present jet runways is on the drawing boards at Douglas.

Such an airplane is needed – says a recent Federal Aviation Agency study made with White House approval – to maintain U.S. leadership in commercial aviation. This is important because the export value of aircraft and parts in 1960 was $1.4 billion or 5.2% of total U.S. exports!

The study also notes that substantial government assistance would be needed to underwrite the $500 to $550 million estimated development costs.

Douglas believes that the estimated market of 200 to 300 Mach 3 aircraft would more than repay these development costs.

They are backing this belief with continuing studies based on 15 years experience with missiles, supersonic and hypersonic aircraft...to bring the trisonic civilian jet transport to reality at the earliest possible date.

DOUGLAS

MISSILE AND SPACE SYSTEMS • MILITARY AIRCRAFT • DC-8 JETLINERS • RESEARCH AND DEVELOPMENT PROJECTS • GROUND SUPPORT EQUIPMENT • AIRCOMB® • ASW DEVICES

ARMA SYSTEMS

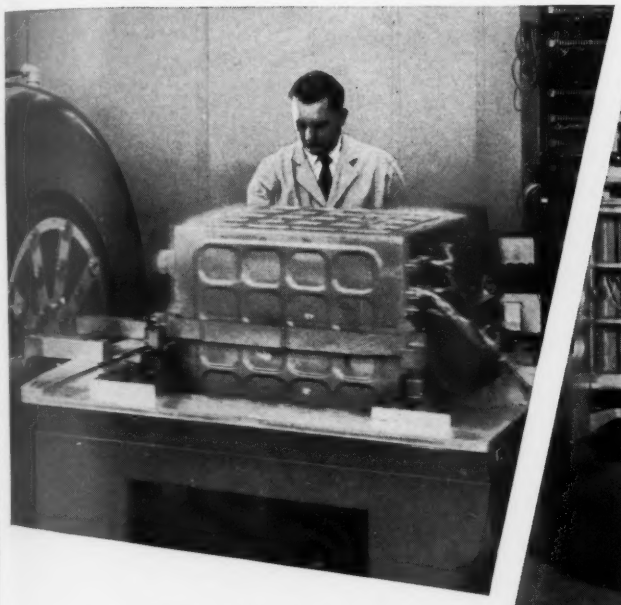

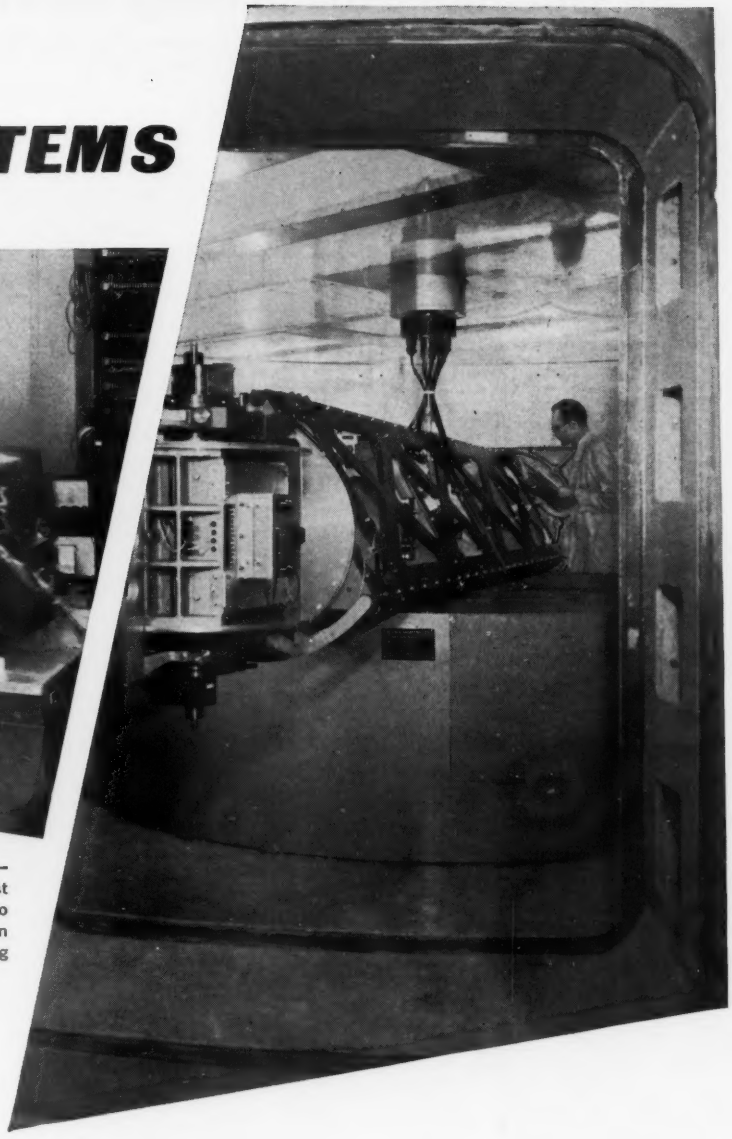

Vibration exciters, precision centrifuges—these are among Arma environmental test facilities used to subject weapons systems to performances far beyond actual operation—to assure reliability, accuracy and long service life.

predictable by test . . . proved by performance

In the receiving areas, in the materials test laboratory, on the production lines, in assembly and at the final test station . . . wherever you look in the Arma plant you'll see quality control and inspection equipment in use. Here rests the responsibility for maintaining the reliability of Arma systems.

And, Arma systems are famous for reliability: All-inertial guidance for the Atlas ICBM, a proved system of intercontinental range accuracy . . . the defense system for the B-52 . . . shipboard fire control and navigation systems . . . anti-submarine warfare systems.

Arma's chief contribution to our national defense effort is the ability to deliver reliable systems—on schedule and within the budget. All research and development, engineering and production are based on that philosophy. Arma, a division of American Bosch Arma Corporation, Garden City, New York.

2263

AMERICAN BOSCH ARMA CORPORATION

Do you share his driving determination to know?

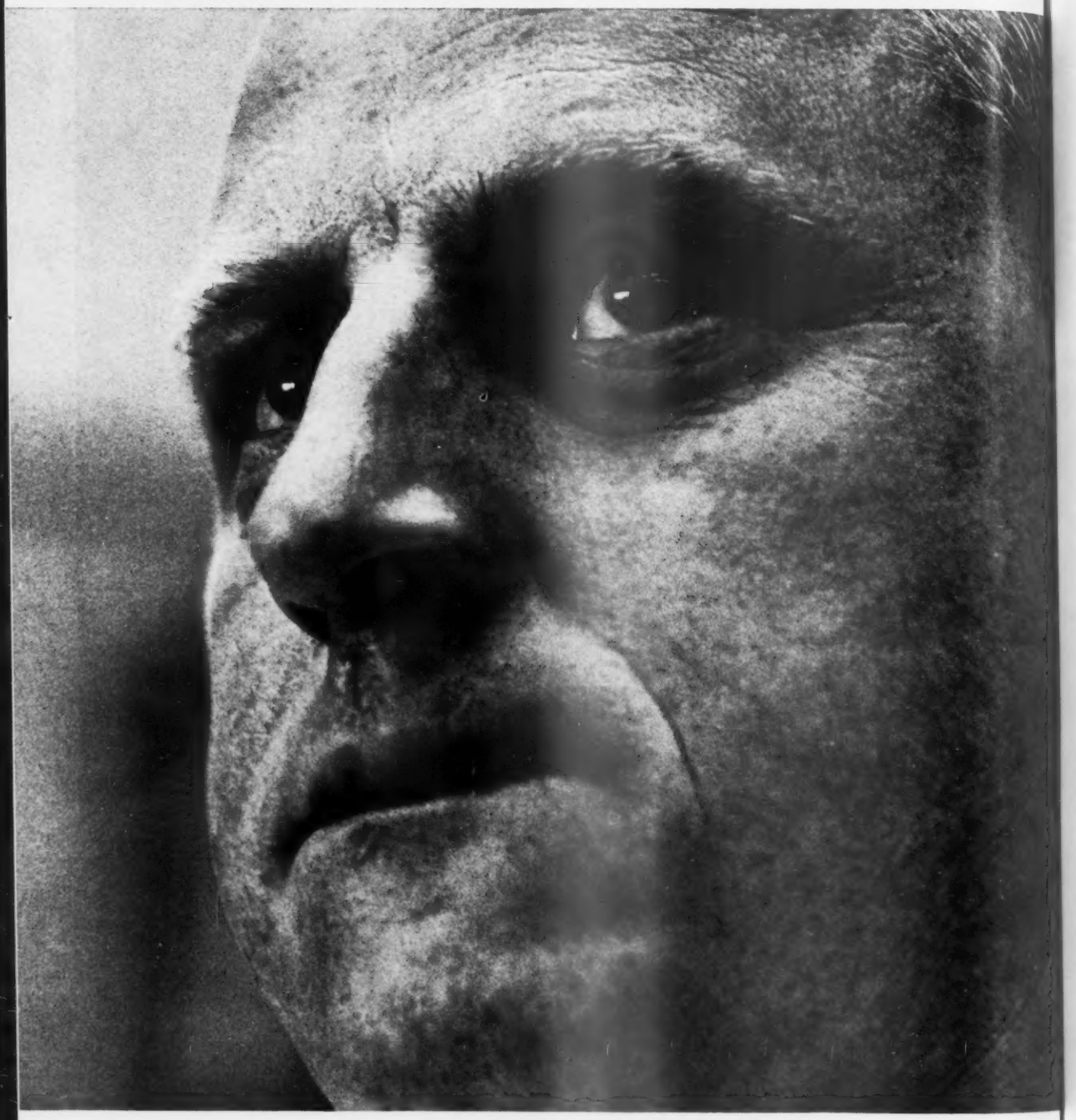

An unsolved problem is a nagging challenge to him. The word "impossible" is an impertinence.

Are you cut from the same cloth as this man? Then come to Northrop where you can work in the fringe of the future on such projects as space guidance and astronertial navigation systems, aerospace deceleration and landing systems, magnetogasdynamics, in-space rescue, repair and refueling techniques, laminar flow control, automatic test equipment and world-wide communications systems.

More than 70 such programs are now on the boards at Northrop, with many challenging problems still to be solved, and new areas of activity constantly opening up for creative research. Whatever your specialty, drop us a line now if you want to find out more about the Northrop challenge.

NORTHROP

NORTHROP CORPORATION, BEVERLY HILLS, CALIFORNIA

AN EQUAL-OPPORTUNITY EMPLOYER

"Written Exclusively
By Engineers—For Engineers

AEROSPACE ENGINEERING

– Established 1934 –

VOLUME 20 / NUMBER 10

OCTOBER 1961

Featured in this Issue

Editorial	9	The Next (X) Years—?
Rodney C. Wingrove and Robert E. Coate	10	Piloted Simulation Studies of Re-Entry Guidance and Control at Parabolic Velocities
Robert H. Smith and Joseph A. Menard	12	Supercircular Entry and Recovery With Maneuverable Manned Vehicles
J. H. Doolittle	14	Early Blind Flying
J. W. Smith and W. W. Vaughan	16	High-Altitude Wind Observations Above Cape Canaveral
Sitaram Rao Valluri	18	A Unified Engineering Theory of High Stress Level Fatigue
Joseph G. Wohl	20	Man-Machine Dynamics of Nose-Wheel Steering
Welko E. Gasich	22	Application of Laminar Flow Control to Transport Aircraft
Departments	24	Aerospace Technology as Seen by the Panels Vehicle Design—Some Notes on Aerospace Vehicle Design Trends . . . Adolph Burstein Flight Mechanics—Reliability—One of Today's Dominant Problems . . . C. B. Westbrook Management—Relating Industrial Research to Company Goals . . . Lewis A. Rodert
	27	Adventures in Engineering— Temperature Sensitivity in Germanium Transistors . . . James D. Mason
	55	Personnel Opportunities
	70	Sherman M. Fairchild Fund Papers
	70	IAS Special Publications
	96	Index to Advertisers

On our cover

A recent firing of Army's Nike Zeus. The antimissile missile test program has been under way at White Sands Missile Range for some time, and further testing will be conducted from Point Mugu, Calif., where White Sands limitations on range and altitude do not exist. Finally, at Kwajalein Atoll, Zeus missiles will be launched, controlled, and directed to intercept ICBM target missiles fired from Vandenberg AFB, Calif. Prime contractor for Nike Zeus is the Western Electric Company. Bell Telephone Laboratories is in charge of system research and design activities under direction of the Army Rocket and Guided Missile Agency.

AEROSPACE
ENGINEERING
ESTABLISHED 1934

EDITORIAL STAFF

Publisher: **Welman A. Shrader, AIAS**

Editor: **Allan Bernhardt, AIAS**

Editorial Production Manager: **Vehig S. Tavitian**

Editorial Assistant: **Helen S. Goldman**

Associate Editor: **Paul J. Burr, AFIAS**

Technical Consultant: **R. L. Bisplinghoff, FIAS**
Abraham Hyatt, FIAS

AEROSPACE TECHNOLOGY PANELS

* Indicates Chairman

Paul J. Burr, IAS Technical Services Director, Coordinator

Aerodynamics and Fluid Mechanics
Lester Lees*
Seymour M. Bogdonoff
Dean R. Chapman
Antonio Ferri
Paul Germain
Wayland C. Griffith
Hans W. Liepmann
C. C. Lin
Henry T. Nagamatsu
W. R. Sears
John R. Sellars
R. T. Whitcomb
Hideo Yoshihara

Aeroelasticity
R. L. Bisplinghoff*
Y. C. Fung
I. E. Garrick
Martin Goland
Kurt H. Hohenemser
J. C. Houbolt
W. P. Jones
W. J. Mykytow
Robert F. Speaker

Biomedical Sciences
Don Flickinger*
W. Ross Adey
Capt. William Augerson, USA
Stuart Bondurant
A. Scott Crossfield
Cdr. J. H. Ebersole, USN
W. R. Lovelace, II
Capt. Bruce Pinc, USAF
Stanley N. Roscoe
Foreign Correspondent,
Hilding Bjurstedt

Communication
P. C. Sandretto*
K. C. Black
James M. Bridges
Harvard L. Hull
Leonard Jaffe
David S. Little
Lt. Cdr. M. M. Macomber
Paul Rosenberg
William J. Sen
Arnold Shostack
Teck A. Wilson

Control & Guidance
Robert N. Brown*
B. Paul Blasingame
S. F. Eyestone
C. E. Gallagher
Percy Halpert
B. J. O'Connor
Robert L. Roderick
S. F. Schmidt
O. Hugo Schuck
H. Philip Whitaker

Energy Conversion
David Altman*
Robert Bromberg
M. U. Clauser
J. Preston Layton
Frank Marble
G. H. Markstein
A. M. Rothrock
Milton M. Slawsky
Martin Summerfield
T. Y. Toong

Flight Mechanics
H. J. Kelley*
Malcolm J. Abzug
H. Julian Allen
A. E. Bryson, Jr.
T. N. Edelbaum
William C. House
George Leitmann
Bernard Maggin
Angelo Miele
John D. Nicolaides
Charles B. Westbrook

Instrumentation
Paul F. Bechberger*
J. M. Hungerford
Max A. Lowy
Walter McKay
M. David Prince
Charles P. Sonett
George I. Toumanoff
Ralph H. Tripp
William A. Wildhack

Management
Edward A. Ledeen*
Garrett C. Covington, Jr.
Maj. Gen. Marvin C. Demler, USAF
Richard G. Folsom
Joel M. Jacobson
Boyd C. Myers
Sidney M. Robbins
Lewis A. Rodert
John H. Sidebottom
R. C. Siebold
T. Paul Torda

Meteorology
Thomas F. Malone*
Robert D. Fletcher
Henry T. Harrison
Joseph Kaplan
Donald T. Perkins
Herbert Riehl
Morris Tepper
Clayton Van Thullenar
Harry Wexler

Nuclear Applications
J. Donald Rauth*
Jack L. Armstrong
Robert W. Bussard
H. M. Dieckamp
R. L. Duncan
Harold B. Finger
Donald J. Keirn
Frank E. Rom
Raymer E. Schreiber
D. Roy Shoults
T. B. Taylor

Operations
Richard V. Rhode*
Maj. Gen. Otis Benson, USAF (MC)
Ernest A. Cutrell
R. Adm. E. E. Fawkes, USN
Melvin N. Gough
Benjamin S. Kelsey
Franklin W. Kolk
Col. J. L. Marinelli, USA
W. E. Rhodes
M. B. Spaulding, Jr.
D. N. Yates

Propulsion Systems
Bruce T. Lundin*
Robert H. Boden
George W. Brady
David Cochran
Elliot Mitchell
Perry W. Pratt
C. C. Ross
John G. Wilder, Jr.
Maurice J. Zucrow

Space Physics
John C. Evvard*
Herbert Friedmann
Leo Goldberg
C. F. Hansen
Arthur Kantrowitz
Bruno Rossi
S. F. Singer
Leo Steg
Fred L. Whipple

Structures and Materials
Nicholas J. Hoff*
Samuel B. Batdorf
Bruno A. Boley
Pol Duwez
R. R. Heldenfels
Samuel Levy
George N. Mangurian
S. S. Manson
Nathan E. Promisel
Ernest E. Sechler

Support
Ernest G. Stout*
Albert D. Brown
Edward I. Brown
Col. Paul T. Cooper, USAF
P. J. Daniel
Paul Hartline
Donald R. Hill
Capt. N. D. Hodson, USN
Lt. Col. George L. Lovett
R. R. Malik
John McKenna
Gilbert Rolan
Richard A. Schmidt
William R. Owens

Vehicle Design
C. E. Pappas*
Adolph Burstein
C. H. Christenson
A. J. Eggers, Jr.
Robert Lichten
E. V. Marshall
Rene H. Miller
John R. Ragazzini
George S. Schairer
George S. Trimble, Jr.

Aerospace Engineering (established 1934) is published monthly by the Institute of the Aerospace Sciences, Inc., at 20th and Northampton Streets, Easton, Pa. Headquarters and Editorial Offices: 2 East 64th Street, New York 21, N.Y. (TEmpleton 8-3800). Western Office: 7660 Beverly Blvd., Los Angeles 36, Calif. Subscription rates: United States and possessions, 1 year, $5.00; single copies, $0.50. Foreign countries including Canada (American currency rates), 1 year, $6.00; single copies, $0.50. Second-class mail privileges authorized at Easton, Pa. This publication is authorized to be mailed at the special rates of postage prescribed by Section 132.122. Notices of change of address should be sent to the Circulation Department, Institute of the Aerospace Sciences, Inc., 2 East 64th Street, New York 21, N.Y., at least 30 days prior to actual change of address.
© Copyright, 1961, by the Institute of the Aerospace Sciences, Inc. Statements and opinions expressed in *Aerospace Engineering* are to be understood as individual expressions and not those of the Institute.

BUSINESS STAFF

Business Manager and Advertising Production

John Phillips

Advertising Director

John R. Cockerell
116 So. Michigan Ave.
Chicago 3, Ill.
ANdover 3-6929

National Advertising Regional Offices

John Cockerell, Inc.

(Headquarters)
116 So. Michigan Ave.
Chicago 3, Ill.
ANdover 3-6929

3757 Wilshire Blvd.
Los Angeles 5, Calif.
DUnkirk 3-1135

380 Lexington Ave.
New York 17, N.Y.
OXford 7-9048

1501 Euclid Ave.
Cleveland 15, Ohio
TOwer 1-8338

915 Olive Street
St. Louis 1, Mo.
GArfield 1-0907

141 N.E. Third
Miami 32, Fla.
FRanklin 1-9941

Contributors Please Note

AEROSPACE ENGINEERING welcomes contributions of full-length technical articles, including manuscripts classified as technical notes, pertaining to all fields of interest in the Aerospace Sciences. (See headings of IAS Aerospace Technology Panels on opposite page.) Manuscripts in either category, which should be addressed to The Editor, *Aerospace Engineering*, 2 East 64th Street, New York 21, N.Y., are acknowledged on receipt. Editorial review—requiring from two to six weeks—is initiated with a promptness dependent upon conformance to standards discussed below. Authors are notified as soon as possible as to acceptance or rejection. To avoid delays and minimize correspondence, contributors are urged to supply the Editor with the original manuscript plus one or two legible (carbon or process) copies complete with clear copies of illustrations. Manuscripts should not exceed 17–20 pages (maximum of 5,000 words). Each should be typed (double-spaced) and every page must be typed with two-inch margins. For each illustration, deduct 350 words; for any tabular matter, deduct an equivalent number of words from text. Detailed instructions for preparation of manuscripts are published monthly on the inside back cover of the *Journal of the Aerospace Sciences*. *Aerospace Engineering* does not pay for contributions.

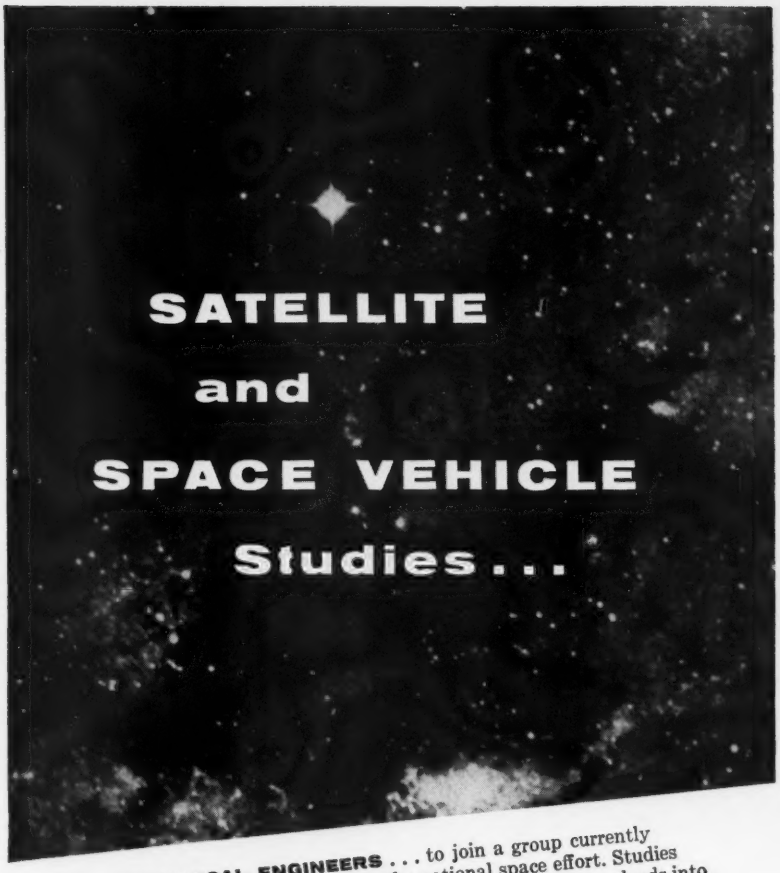

ASTRONAUTICAL ENGINEERS . . . to join a group currently making significant contributions to the national space effort. Studies include determination of economical methods for boosting payloads into orbit; maximizing payloads for inter-planetary missions; determination of satellite arrays for full-time weather observations of the earth's surface.

Requirements include an advanced degree in Aeronautical Engineering, Astronautics or Mechanics with a strong background in Applied Mathematics. A knowledge of celestial mechanics is desirable.

PRELIMINARY DESIGN ENGINEER . . . for a group responsible for analytical studies of advanced vehicle concepts and their propulsion systems. Work will include the selection of structure types and estimation of structure and component weights for space vehicles, missiles, conventional aircraft, and VTOL's.

The position requires a background of experience with broad studies in which structural weights have been developed on a generalized basis. Advanced degree in Aeronautical Engineering preferred, although consideration will be given to a B.S. with extensive applicable experience.

Respect for individuality Our overall organization is small. Office areas are designed to provide an environment for mental concentration. Widely circulated technical reports bear the signature of those responsible for the study; publication of papers is encouraged.

Advancement opportunities are excellent within our organization and in the operating divisions of UAC. Attractive, too, are the salary levels, fringe benefits, relocation allowances, and the fully-paid graduate study program. Work is primarily corporate-sponsored with inherent personal stability. Typical of the facilities available to our staff is a computational laboratory that ranks among the largest in our nation.

Please write to Mr. W. G. Walsh, Personnel Department:

RESEARCH LABORATORIES
UNITED AIRCRAFT CORPORATION
400 Main Street, East Hartford 8, Conn.

All qualified applicants will receive consideration for employment without regard to race, creed, color, or national origin.

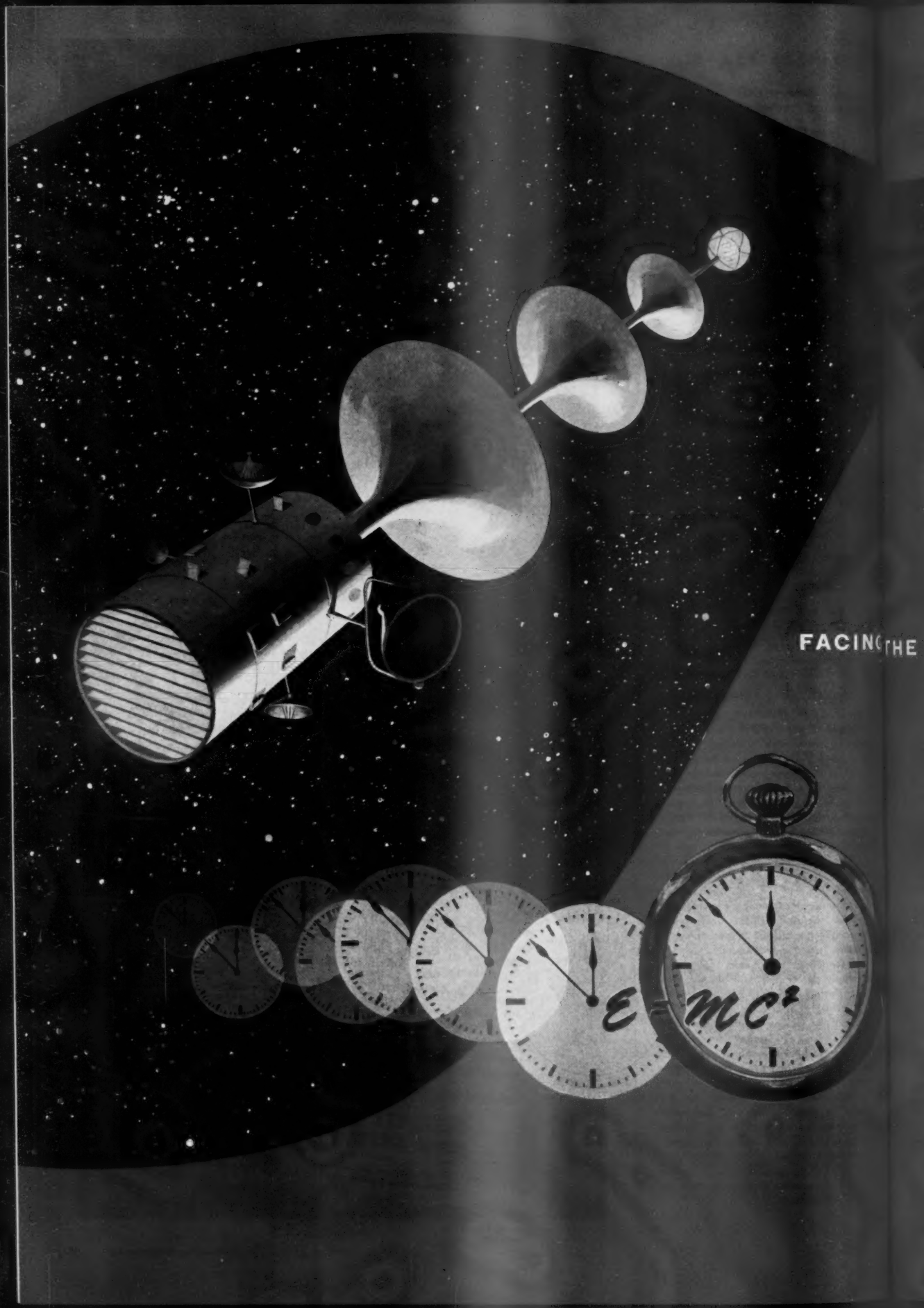
FACING THE
E = MC²

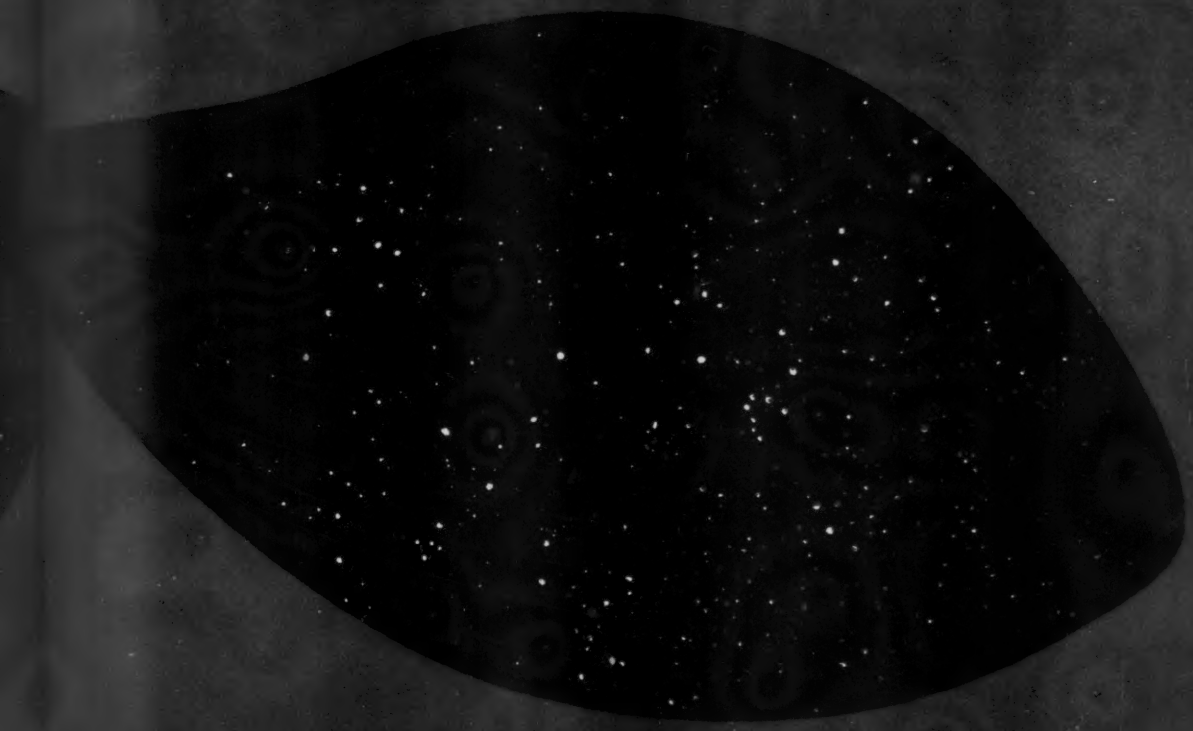

THE FOURTH DIMENSION IN PROPULSION DEVELOPMENT

Whether the universe has a "saddle shape," or any shape at all, is a matter of interesting conjecture. The matter of space travel, however, is the subject of intense experimentation. A nuclear/thermionic/ionic propulsion system, currently being studied at Lockheed Missiles & Space Company, might well become the power source for space vehicles.

Its design incorporates a nuclear reactor only one foot in diameter, generating heat at a temperature of 1850°K. This is transmitted to banks of thermionic generators, converting the heat directly into electrical energy for the ion beam motor which uses cesium vapor as a fuel. The entire system is designed without any moving parts, minimizing the possibility of failure.

Lockheed's investigation of propulsion covers a number of potential systems. They include: plasma, ionic, nuclear, unique concepts in chemical systems involving high-energy solid and liquid propellents, combined solid-liquid chemical systems. The fundamentals of magnetohydrodynamics, as they might eventually apply to propulsion systems, are also being examined. Just as thoroughly, Lockheed probes all missile and space disciplines in depth. The extensive facilities of the research and development laboratories—together with the opportunity of working with men who are acknowledged leaders in their fields—make association with Lockheed truly rewarding and satisfying.

Lockheed Missiles & Space Company in Sunnyvale and Palo Alto, on the beautiful San Francisco Peninsula, is an exciting and challenging place to work. For further information, write Research and Development Staff, Department M-24B, 962 West El Camino Real, Sunnyvale, California. U.S. citizenship or existing Department of Defense industrial security clearance required. An Equal Opportunity Employer.

LOCKHEED *MISSILES & SPACE COMPANY*

A GROUP DIVISION OF LOCKHEED AIRCRAFT CORPORATION

Systems Manager for the Navy POLARIS FBM and the Air Force AGENA Satellite in the DISCOVERER and MIDAS programs. Other current programs include SAINT, ADVENT and such NASA projects as OGO, OAO, ECHO, and NIMBUS.

SUNNYVALE, PALO ALTO, VAN NUYS, SANTA CRUZ, SANTA MARIA, CALIFORNIA • CAPE CANAVERAL, FLORIDA • HAWAII

GARRETT-U.S. AIR FORCE 'SPUR'

..one answer to America's future power needs in space

The joint U.S. Air Force-AEC Project SPUR is a research and development program being conducted by an industry team of Garrett, Aerojet-General Nucleonics (reactor) and Westinghouse, Lima (generator) to provide a power source to produce 300-1000KW electrical power in space for one year or more. Power is obtained by conversion of nuclear fission energy to mechanical (shaft) power with a potassium vapor turbine. Equipment includes: reactor, primary and secondary loop pumps, boiler, turbo-generator and condenser-radiator.

Long lead time is essential to the development of large nuclear space power systems. Present methods of power generation would require an impractical heat rejection surface nearly the size of a football field for a power output of one megawatt—power which will be needed for critical space missions already in the planning stage.

Garrett's AiResearch Divisions have now completed the initial SPUR design studies and proved the project's feasibility to supply continuous accessory power and low thrust electrical propulsion in space for long periods of time.

Cutting projected 1 MW power systems to 1/10th the size and 1/5th the weight of present power systems under development will be possible because of SPUR's capability to operate at higher temperatures, thereby sharply reducing the required radiator area.

Garrett has been working with the Air Force and the Atomic Energy Commission on SPUR as the prime contractor for more than one year and has more than five years of experience in space nuclear power development. Also an industry leader in high speed rotating machinery, heat transfer equipment, metallurgy and accessory power systems, the company is developing design solutions for SPUR in these critical component system areas.

THE GARRETT CORPORATION

AiResearch Manufacturing Divisions

Los Angeles 45, California • Phoenix, Arizona

Systems and Components for: AIRCRAFT, MISSILE, SPACECRAFT, ELECTRONIC, NUCLEAR AND INDUSTRIAL APPLICATIONS

EDITORIAL

The Next (X) Years—?

LATE IN AUGUST, as an integral part of the celebration of the first half century of Naval Aviation, the U.S. Navy and the IAS held a notable joint exercise in San Diego. This was not the first time that the Institute collaborated with our Senior Service, but the occasion was unique in many ways. It was marked by the successful flying demonstration by Test Pilot Don Germeraad of the IAS-built replica of the Navy's first airplane—the Curtiss A-1 (see *IAS News*, Sept. 1961). It included the dedication of an historic airfield to the memory of a great Naval hero—Admiral Halsey. But, more important from the Institute point of view, the 1,000-odd attendees at the three-day technical sessions heard scientists, engineers, economists, and policy planners discuss the blueprint for the future of the Navy's Air Arm.

The program was originally announced as a look at the "next 50 years of Naval Aviation." Almost to a man, however, participants backed away from such long-range prognostication on the grounds that the present state of affairs is so cloudy, and requirements and capabilities are changing so rapidly, that the effective range of the crystal gazer is far short of a half century. Most were willing to take a shot at the next decade—not beyond. It becomes too dangerous to base technical decisions upon extrapolations of extrapolations.

The IAS Council is now facing up to a similar problem. During the past several years a great deal of time and energy have been spent by your Officers and Council in providing the necessary flexibility in programs and in operations to meet the requirements of the IAS membership in this period of exploding technology. Although the results have been good, much of the work was, of necessity, done on an *ad hoc* basis. Events moved so rapidly that time to sit down to think connectedly about the long-range future was hard to come by. Long-Range Planning Committees were often concerned more with next year's budget than with questions as to where the Institute might be, or what it ought to look like a decade hence.

Now that some of the immediate problems have been dealt with, however, the attention of the Council has turned to the more distant future. At the last meeting (in Los Angeles, June 12) it was suggested that the next meeting be strictly a "think" session—that Officers and Council sit down together for a couple of days in some relatively quiet spot and plot the course for IAS for the foreseeable future. This struck a responsive chord, and plans are now well advanced for a week-end meeting of the Council and its Advisory Groups early in November, probably in the Palo Alto area.

It was early agreed (for the same reasons which influenced many prognostications at San Diego) that a "10-year look" was about the practical limit. Accordingly, the planning committee headed by IAS Vice-President Harold Luskin has come up with the Conference theme. *The IAS in 1970—A Plan for Growth and Development.* A four-part program has been laid down covering:

(1) Current services—their 1970 character.
(2) New and expanded services in 1970.
(3) Implementation—IAS organization in 1970.
(4) Implementation—IAS finances in 1970.

The end point of the exercise will be the formulation of a specific program to carry the work of the Institute forward through the next decade. We want to know where we are going, and what must be done to arrive at our selected goals.

During the past year we have made a number of extensive surveys of member opinion regarding IAS programs and policies. These have proved extremely valuable as groundwork for the up-coming exercise. If, however, any member wishes to give the Council the benefit of additional thinking as to future IAS operations—now is the time. Letters addressed to any Officer or Council Member on any subject of common interest will be brought to the Council's attention at the November meeting. Let us hear from you.—SPJ

✦ ✦ ✦

Piloted Simulation Studies of Re-Entry Guidance and Control at Parabolic Velocities

Rodney C. Wingrove • Robert E. Coate

Ames Research Center, NASA

THE GENERAL PROBLEM of concern here is that of designing pilot-operated systems to guide and control maneuverable vehicles through a planetary atmosphere to a desired touchdown point without exceeding specified deceleration limits. The guidance methods most discussed in the literature use either predetermined stored reference trajectories or an on-board prediction computer in which future decelerations and end points are repeatedly predicted as fast as possible from the present flight-path conditions.

While the former "fixed-trajectory" method can be quite accurate, it is inherently limited to the conditions or situations stored on board. A requirement for a more general approach able to cope with a wider range of emergency conditions, including aborts, led to the study that is reported in reference 1.

It is realized that an actual design choice between the two methods may depend on many factors outside the scope of a preliminary simulation study; these include compatibility with the mid-course guidance system, status of component development, and system weight and volume. However, it appeared desirable after completing the study[1] to perform a reasonably parallel study of a fixed-trajectory method for the identical vehicle and conditions. It was hoped thereby to permit at least a comparison of range and entry-corridor capabilities and of ability to avoid exceeding the pilot's time tolerance to deceleration.

Accordingly, both of these re-entry control techniques have been simulated, by use of an electronic analog computer. The vehicle is assumed to have a maximum L/D of 0.5 and to be entering the earth's atmosphere at an altitude of 290,000 ft at a velocity of 35,000 fps. Previous studies, references 2 through 4 for example, have considered end-point control from near-earth orbital conditions. Re-entries at the speed chosen here, which is slightly less than parabolic, require that the control system damp the phugoid oscillation so that the vehicle does not exceed a maximum g limit (arbitrarily set at 10g),

Mr. Wingrove graduated with a B.S. degree in aeronautical engineering from the University of Washington in 1955. Since that time he has been in Government service and at present is a research scientist with NASA, Ames Research Center. Mr. Wingrove is the author or coauthor of several NACA-NASA publications, as well as previous IAS and aerospace medicine technical papers. His early work was in the flight testing of experimental aircraft; stability and control analysis of handling qualities led to piloted-analog simulation; and his later work has been with fixed base, moving base, and centrifuge simulations for pilot control during re-entry.

Mr. Coate, research scientist at the NASA Ames Research Center, received his A.B. degree in mathematics "with distinction" from the San Jose State College in June 1950. Prior to his current employment he served as a pilot in the United States Air Force. Mr. Coate has specialized in manned-flight simulation techniques and has been associated with research in the fields of aircraft stability and control, and also in re-entry energy management systems.

▸ *Results of piloted simulation studies are presented and compared for two piloted re-entry guidance methods for controlling lifting vehicles through a planetary atmosphere to a desired touchdown point.*

▸ *It was found that the usable range with the fixed-trajectory method is about one third that with the prediction-control method, while the usable entry corridor is about the same for the two guidance systems.*

▸ *With either control system, this low L/D vehicle can be piloted in such a way that the pilot's time-tolerance-to-acceleration boundaries are not exceeded.*

Symbols

- A = acceleration factor, g units
- C_D = drag coefficient, $D/[(1/2)\rho V^2 S]$
- D = drag force, lbs
- g = gravitational acceleration unit, ft/sec²
- h = altitude, ft
- $\dot{h}$ = rate of climb, fps
- K = drag ratio, $\frac{C_D \text{ for desired trim condition}}{C_D \text{ for existing trim condition}}$
- L = lift force, lbs
- m = mass of vehicle, slugs
- r = distance from planet center, ft
- R_x = downrange value along great circle route in space, miles
- R_y = crossrange value normal to local great circle route in space, miles
- S = surface area, ft²
- u = circumferential velocity component normal to radius vector, ft/sec
- $\bar{u}$ = ratio of velocity to orbital velocity, $u/\sqrt{gr}$
- V = total velocity, ft/sec
- Y = side force, lbs
- Z = dimensionless function of $\bar{u}$ determined by Chapman equation and appropriate boundary conditions, $(\rho u/2)\ (C_D S/m)\sqrt{r/\beta}$
- β = atmospheric density decay parameter, ft^{-1}
- γ = flight-path angle relative to local horizontal direction; positive for climbing flight
- ρ = atmosphere density, slugs/cu ft
- φ = roll angle
- ψ = lateral deflection angle

Subscripts

- d = respect to destination
- f = respect to fixed trajectory
- i = initial condition
- max = trim for maximum L/D
- min = trim for zero L/D
- o = condition at roll angle 0°
- u = circumferential component normal to radius vector

and also does not skip out of the atmosphere (represented by a minimum limit of 0.075g). These L/D and g limits result in a permissible entry corridor of $-2.1°$ to $-6.2°$ flight-path angle (as determined by the methods of references 5, 6, and 7).

In addition to the general comparison mentioned previously, this paper will show how the deceleration limits influence the range attainable by the vehicle and how varying the entry angle affects the control problems. The maximum heating the vehicle and pilot can tolerate is, of course, another important limit. Although heating was not considered in these studies, it can easily be taken into account in either control method; it affects the attainable range and permissible entry corridor in a manner analogous to the demonstrated effects of deceleration.

(*Continued on page 28*)

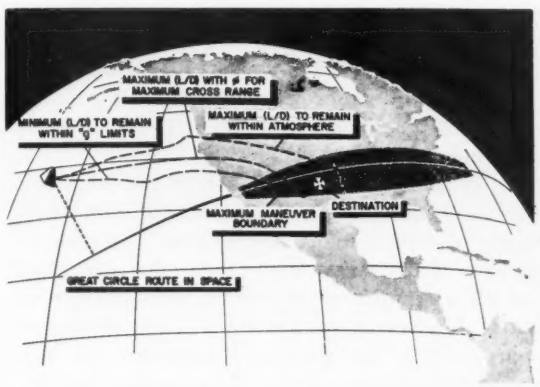
MAXIMUM (L/D) WITH φ FOR MAXIMUM CROSS RANGE
MINIMUM (L/D) TO REMAIN WITHIN "g" LIMITS
MAXIMUM (L/D) TO REMAIN WITHIN ATMOSPHERE
MAXIMUM MANEUVER BOUNDARY
DESTINATION
GREAT CIRCLE ROUTE IN SPACE

Fig. 1. Maneuver capability with prediction-control method.

Supercircular Entry and Recovery With Maneuverable Manned Vehicles

Robert H. Smith, MIAS • Joseph A. Menard, AIAS

The Boeing Company, Aero-Space Division

THE PRIMARY OBJECTIVE of any manned space mission is to perform some useful function in space at reasonable, if not minimum, cost. However, there is always an overriding responsibility to return the crew safely to their base. Resolution of these conflicting demands without compromise of either is a formidable problem. Several approaches to this problem are under consideration; each has its particular features and shortcomings. This paper, which is concerned with atmosphere entry and recovery of manned space vehicles, emphasizes the factors of crew comfort and safety, direct return to home base, and minimum interference with space mission planning.

Greater crew comfort and security can and should be provided by future entry vehicles. Current booster payload limitations, which place a premium on low vehicle weight, have almost forced 10*g* acceleration and ocean ditching into the status of standard operating procedures for entry vehicles. Such operations will surely be relegated to their former emergency-procedure status when payloads can include more sophisticated entry vehicles.

Entry and recovery with a high lift/drag ratio glider will offer, along with other advantages, a high degree of crew comfort and security. A glider is tolerant of deviations from ideal entry conditions and allows control of discomfort from acceleration loads. After entry, transportation to the home base is provided by the long-range capability and maneuverability of the glider. These features allow expanded freedom in space mission scheduling.

Mr. Smith is engaged in aerodynamics research on the staff of the Flight Technology Department, Boeing Aero-Space Division. He works in the hypersonic aerodynamics and space system performance fields and participated in the Dyna-Soar development during proposal stages. Before joining Boeing in 1953 he was on the research staff of the University of Washington Aerodynamics Laboratories. Mr. Smith is a graduate of the University of Washington, with a B.S. degree in aeronautical engineering (1946) and an M.S. in aeronautical engineering (1952).

Mr. Menard received a B.S. in aeronautical engineering (1954) and an M.S. in aeronautical engineering (1960) from the University of Washington. After serving 3 years in the Air Force Research and Development Command as a pilot and aerial weapons test officer, he joined the NASA Flight Research Center as an Aeronautical Research Engineer where he participated in the investigation of the landing performance of low *L/D* vehicles. For the past 18 months he has been affiliated with the Flight Technology Department, Boeing Aero-Space Division, working on superorbital entry vehicle performance.

Flight Plan

Direct single-pass entry will be used with controlled glide to the landing site. No power impulse is used and the glider stays in the atmosphere at all times after initial entry. The mission is considered in three essentially independent phases:

(1) Entry maneuvers involving a pull-out from the initial dive into the atmosphere and a pull-up to a suitable glide altitude just above satellite speed.

A concept is presented for atmosphere entry at parabolic speed with a hypersonic glider. The concept provides for glide, after entry, within the atmosphere to a preselected landing site. Three principal advantages of using a high lift/drag ratio glider for manned return-from-space missions are established:

(1) A very wide tolerance of entry angle is available if the crew endures acceleration loads approaching human limits.

(2) Entry angle tolerance is adequate even if acceleration loads are held to levels which are relatively comfortable for the crew.

(3) Controlled glide within the atmosphere to a preselected landing site is often possible regardless of the space-referenced location of the entry point.

(2) Global range control during trans-satellite glide.

(3) Subsatellite banked glide to the recovery site with lateral offset control and minor range control maneuvers.

A logical fourth phase, not considered here, is the landing maneuver. Fig. 1 is an altitude-velocity profile of typical trajectories to be considered.

Entry Maneuvers

Pull-Out

The entry pull-out begins at 400,000 ft altitude and 35,000 fps with the glider in maximum-lift attitude. For steep (undershoot) entries, this directs lift away from the earth and tends to minimize penetration of the atmosphere. The high drag associated with maximum-lift attitude is desirable at this time to reduce speed. Both effects, speed reduction and reduced penetration, are beneficial because they reduce the peak dynamic pressure and heating rate which will be reached near the bottom of the pull-out. When resultant acceleration load reaches a prescribed level, further increase is arrested by gradual reduction of angle of attack. During this attitude modulation, the resultant of lift and drag is held constant; hence, resultant acceleration load is constant in spite of rapidly increasing dynamic pressure. This mode of (*Continued on page 34*)

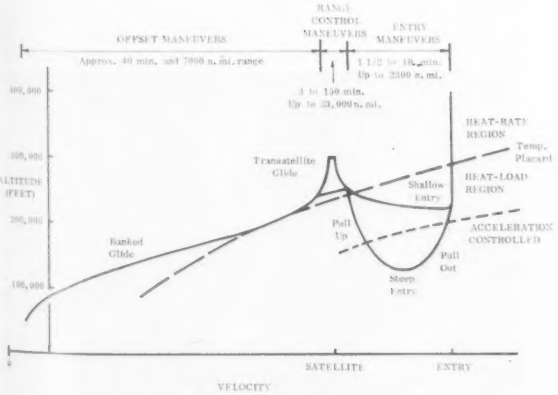

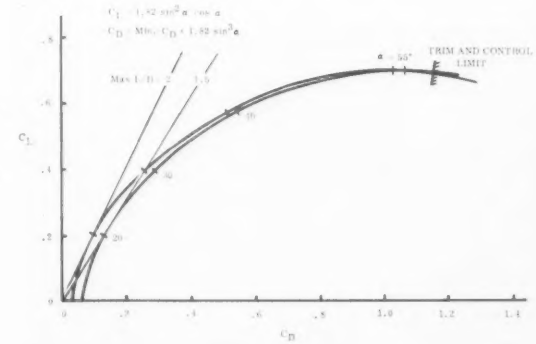

Fig. 1 (*left*). Entry and recovery maneuvers. Fig. 2 (*right*). Lift-drag polars.

YESTERDAY

Many honors, including his country's highest, have been bestowed upon this year's Gardner Lecturer. It was on May 19, 1942, that he received the Congressional Medal of Honor from President Roosevelt for having led the U.S. air raid on the Japanese mainland a month and a day earlier. Looking on *(above left)* are Mrs. Doolittle and Lt. Gen. H. H. Arnold. At right above is the 1961 Gardner Lecturer in his "open cockpit days." Gen. Doolittle recalls: "It was taken on Sept. 1, 1929, in Cleveland, just before taking off in a Curtiss P-1 to put on a stunting exhibition at the National Air Races. The airplane ...had a smaller radiator than the conventional P-1. As a result, it was somewhat cleaner and dived faster. While pushing under in a vertical dive the wings failed in reverse loading." Gen. Doolittle parachuted and about an hour later gave the scheduled exhibition in another airplane. In photo below, Gen. Doolittle receives the Daniel Guggenheim Medal the same year. *Left to right* are C. H. Colvin, G. W. Lewis, Brig. Gen. Doolittle, Glenn L. Martin, Joseph Hartson, Gen. Arnold, J. C. Hunsaker, and Lester D. Gardner.

This year's Gardner Lecture was presented on April 28 at the Massachusetts Institute of Technology, and repeated on September 28 at the Smithsonian Institution. The assistance of both these organizations in scheduling this enlightening document for publication in AEROSPACE ENGINEERING is gratefully acknowledged. The Lecture bears the name—in the words of the 1961 Lecturer—"of a great public servant and outstanding citizen," Lester D. Gardner, whose long career in aviation included founding of the IAS in 1932. His death occurred in 1956 and a bequest to M.I.T. provided funds to support a periodic address on the history of aeronautics. The initial lecture was given in 1959 by Grover Loening; the second in the following year by Igor Sikorsky. Photographs, rather than a written biography, recite some of the highlights in the career of the 1961 Lecturer. J. H. "Jimmy" Doolittle, who lived through, and in fact made, some of the history about which he writes, now is Chairman of the Board of Space Technology Laboratories.

On The Lecture, The Man Whose Name It Bears, And The 1961 Lecturer

Early

The Third

J. H. Doolittle, HFIAS

Space Technology Laboratories, Inc.

THE DEVELOPMENT OF flight has been a gradual, evolutionary process. There are, however, certain landmarks along the route. We may arbitrarily consider that there are roughly defined periods between these datum points.

In the very early days of flying, a slight breeze could cancel or delay a flight.

I recall seeing my first air show in the winter of 1909–10 at Dominguez Field near Los Angeles. In those old days it was customary for a pilot to wet his finger in his mouth and hold it up. If there was enough air movement to cause uneven evapora-

TODAY

Blind Flying

Lester Gardner Lecture

A Historical Review of Early Experiments in Instrument Flying

tion and make one side cooler than the other, then there was too much wind to fly.

Soon a modest wind was not a deterrent to flight and a good breeze was enjoyed because it shortened take-off and landing distance.

Next came the period when a pilot was happy only as long as he could see the visible horizon. He might fly in or through clouds, but he wanted clear air and a visible horizon when he came back through them.

This talk will deal with the next era, at the end of which a visible horizon was not required and during which it became possible to fly, and even land, without seeing outside an instrumented cockpit.

Today aircraft fly safely and reliably in all but the most inclement weather, and I look forward to the not-very-distant future when the airplane—or its successor—will fly absolutely regardless of weather and will then become not only the fastest but the most reliable form of transportation.

Whenever pilots got together for meditation and discussion in the immediate post World War I era, the subject of "flying instinct" or flying by the "seat of the pants" was apt to come up.

Views were divided. Some pilots believed that they could fly indefinitely without reference to the visible horizon—because they had. Others agreed that they had, but claimed it was not pilot skill but the inherent stability of their aircraft which made it possible.

In the early twenties the navigational instruments most commonly used were (*Continued on page 56*)

Many personalities mentioned in Gen. Doolittle's 1961 Gardner Lecture were present at both the initial presentation at M.I.T., and for its repeat at the Smithsonian Institution. These photos were taken at the M.I.T. event which took place on April 2. The first (*opposite page, bottom of Col. 2*) shows (from left to right) Jerome Lederer, Elmer Sperry, Jr., and C. Stark Draper. *Center:* Harry Guggenheim, James R. Killian, and Luis de Florez. *Right:* C. A. Frische, J. C. Hunsaker, and Vice Adm. Carl F. Espe.

High-Altitude Wind Observations

J. W. Smith • W. W. Vaughan

George C. Marshall Space Flight Center, NASA

DYNAMIC RESPONSE of a space vehicle during its flight depends not only on wind velocity, but also on the rate of change of velocity with respect to time. This rate of change of velocity is essentially determined by wind shear, which is the change of wind velocity with respect to altitude. Wind shear values have a significant influence on vehicle response even when associated with relatively small increases in wind velocity.[1] Optimum achievement of control response depends upon a broad knowledge of wind velocity, wind shear, and the gusts to be encountered. Current information concerning these factors is less adequate than is desired, especially for altitudes above 20 km where few observations have been made, and the accuracy of the data obtained doubtful.

High-altitude wind measurements over Cape Canaveral, Florida, are increasing in number, altitude, and accuracy; however, wind data continue to be relatively scarce and expensive to obtain in comparison to routine rawinsonde measurements. During the period from April 1959 through May 1960, 37 sounding rockets were launched successfully from Cape Canaveral. The objective of these firings was to gather information on high-altitude wind flow characteristics for use in missile and space vehicle design studies, and in the evaluation of test results obtained from ballistic missile test firings. The data* recorded are presented here, and, although the sample lacks sufficient size to have a definable statistical significance, it gives an indication of the general features of the atmospheric circulation at high altitudes over Cape Canaveral (Atlantic Missile Range).

An extension of rocketsonde observations to several geographical areas has been conducted under the direction of the Meteorological Rocket Network.[2] This effort, through the cooperation of the military services, the Weather Bureau, and the NASA, will provide valuable data in higher altitude regions.

* Data furnished through the cooperation of the U.S. Army Signal Research and Development Laboratories, the Air Force Cambridge Research Center, and the Air Force Missile Test Center.

Mr. Smith attended Oklahoma City University while working for the U.S. Weather Bureau, prior to World War II. During the war he served 4 years with the Army Air Force as an Instructor in Meteorology and as Personal Equipment Officer. He returned to the Weather Bureau after the war, and in 1957 transferred to the U.S. Army Ballistic Missile Agency, Huntsville, Ala. He has been a Meteorologist in the Aeroballistics Division of the Marshall Space Flight Center, NASA, since the creation of that agency in 1960. Mr. Smith is a member of the American Meteorological Society.

Mr. Vaughan received his B.S. degree in mathematics and physical sciences from the University of Florida in 1951, and did graduate work in meteorology at Florida State University while an officer with the USAF. In 1955, he joined the Air Force Armament Center, Eglin AFB, Fla., as an R&D Meteorologist. He then transferred to the ABMA, and since 1960 has been associated with the Aeroballistics Division, Marshall Space Flight Center, NASA. Active in the study and interpretation of atmospheric environmental data for development of missile and space vehicle design criteria and test performance evaluations, Mr. Vaughan is Chief, Aerophysics and Astrophysics Branch, Aeroballistics Div., MSFC. He is a member of the American Meteorological Society and the American Geophysical Union.

Above Cape Canaveral

A summary of 13 months' wind data from rocketsonde observations above 20-km altitude over Atlantic Missile Range at Cape Canaveral.
Wind speed, direction, shear, and components from April 12, 1959, to May 25, 1960, are analyzed on a seasonal, as well as annual, basis and the results are presented graphically.

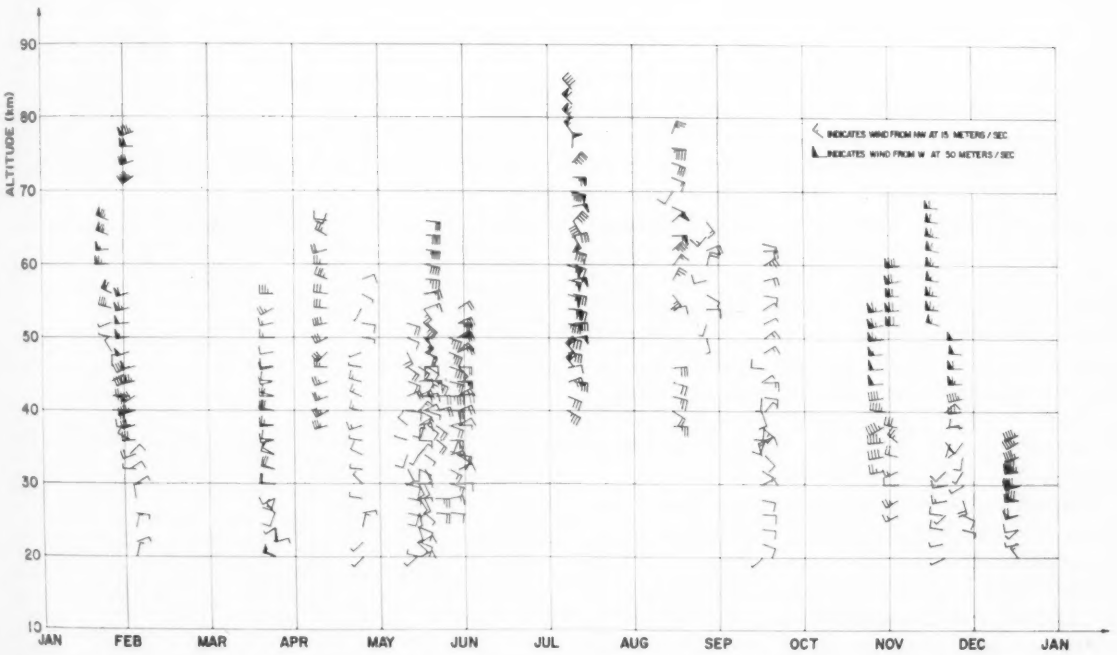

Fig. 1. High-altitude wind arrowgram by rocketsonde observation, April 12, 1959, to May 25, 1960, Cape Canaveral.

Origin of Data and Methods of Computation

The rockets used to obtain the data were of the unguided, solid-propellant type which eject a target near apogee a few minutes after firing.[3] The targets which consisted of either chaff, parachutes, or balloons were tracked by radar. The resulting tracking data were resolved by electronic computer to provide wind speed, direction, shear, components, and rate-of-fall of the target. The radar provided a record of the time, azimuth angle, elevation angle, and slant range at one-sec intervals. These data were converted to rectangular coordinates, and the resulting data were smoothed over 101 one-sec data points, using a second-degree polynomial. Allowance was made for the curvature of the earth. A three-point linear smoothing was then applied using 30-sec time-spaced data points, and wind variables were determined at 60-sec (*Continued on page 53*)

A Unified Engineering Theory of High Stress Level Fatigue

Sitaram Rao Valluri, AFIAS

California Institute of Technology

The author has been working in the Solid Mechanics group of C.I.T.'s Guggenheim Aeronautical Lab. since his graduation in 1954; at present he is Senior Research Fellow there. He received the B.Sc. in mechanical and electrical engineering from Banares University in India, the D.I.I.Sc. from the Indian Institute of Science in Bangalore, and the M.S. and Ph.D. in aeronautics from C.I.T. Interested in metal fatigue and, more recently, in the problems of fast propagating cracks and the phenomenon of spalling, Dr. Valluri's primary interest has been to see if the knowledge compiled by physical metallurgists in the dislocation theory of metals can be used by engineers for a better understanding of the engineering behavior of metals. He is an Associate Fellow of the IAS and a member of the American Society of Metals, Society of Experimental Stress Analysis, and Sigma Xi. He is also a consultant to Douglas Aircraft Company.

DURING THE LAST hundred years of research in fatigue, several theories concerning fatigue failure were suggested which held sway for some time and were subsequently discarded in the light of more recent information found to be inconsistent with the available theories.* Needless to say, any theories proposed now are necessarily subject to the same fate eventually. However, during the short period of its life, a theory will have served its purpose if it can explain consistently most of the available experimental information, can logically predict some results as yet unforeseen, and can be checked experimentally to establish its region of validity. It is with this end in view that the following theory of metal fatigue at high stress levels is proposed.

Limitations of a theory are almost always imposed by the explicit and implicit assumptions made in the development of the theory. In fatigue a test specimen or a structure may fail in the first loading or withstand several million cycles of loading before failing—or may not even fail at all. To be complete, a theory of fatigue, apart from explaining the dependence of fatigue upon the innumerable variables, must encompass the wide range of stresses over which failure may take place. Existing basic experimental observations show that failure under two fundamentally different deformational processes has been generally classified as fatigue. Under such circumstances, it becomes somewhat illusory to think in terms of a theory of fatigue that covers the whole range of stress and qualitatively, if not quantitatively, explains the dependence of fatigue on the several variables. If this idea is accepted, the next problem is one of defining a suitable mechanism, determining its range of validity, and discussing the dependence of the several variables. If one theory can be set apart from others, it will be because of the simplicity of the chosen model, the range of its validity, and the completeness with which it describes the dependence of the several variables.

In fatigue the number of items a theory has to explain are staggeringly large if we insist that the

This paper has been based upon research supported by the Aeronautical Research Laboratories, Air Force Research Division, ARDC, USAF, at the Wright-Patterson AFB, Ohio. The theory proposed here is discussed more extensively in a series of reports which will be published by the Laboratories and which are at present available as GALCIT Solid Mechanics Reports (references *a*, *b*, *c*, and *d*).

It is a pleasure to acknowledge the sponsorship and financial assistance of this agency, and the many helpful discussions with Profs. Y. C. Fung, E. E. Sechler, and M. L. Williams of GALCIT in the preparation of this paper. Thanks are also due to R. H. Christensen of Douglas Aircraft Company, Inc., for kindly supplying Figs. 2, 3, and 4.

* Symbols list appears on pages 68 and 69.

"An analytical theory of fatigue for high stress levels has been formulated based on a fairly simple model derived from a synthesis of the macroscopic elasto-plastic fracture theory and concepts derived from the dislocation theory of metals. The theory (1) predicts the shape of the stress vs. number of cycles curve in fatigue; (2) after determining two of the unknown constants from test results, makes quantitative predictions regarding the residual static strength, changes resulting from changes of stress ratio (and mean stress), cumulative damage due either to multiple step or to random loading; and (3) as a formal extension, gives a quantitative theory of acoustic fatigue."

explanation of all the ideas must come from the same basic model with at most a few (very few!) assumptions. Some of the various aspects which should be explained are shape of the stress vs. number of cycles curve in fatigue; existence or non-existence of an endurance limit; and effects of cold working, grain size, frequency, temperature, overstressing, understressing, and applying single overloads. One should also be able to discuss residual static strength; effect of changing test stress ratio or mean stress; cumulative damage (specifically, response to stress magnitude and response to the order of application of stress); response to random loading; and problems of acoustic fatigue. In addition, the theory should yield quantitative results with at most a few constants to be determined experimentally. If not immediately amenable, it should at least have the elements required to interpret the statistical distribution so characteristic of fatigue. Finally, it must be simple conceptually if not analytically.

It is nearly trite to comment that no theory has yet been devised which can do this over the whole stress spectrum in fatigue, especially for all the different materials. It therefore becomes necessary to restrict the scope of the theory. In order to do this, we shall have recourse to a brief survey of the available literature to ascertain basic facts that are sufficiently reliable, propose a hypothesis that is intuitively plausible, construct a quantitative theory, and find out to what extent the result so obtained can discuss the various aspects of fatigue in a systematic and consistent manner. (*Continued on page 68*)

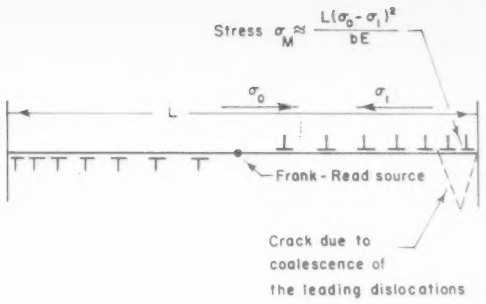

Fig. 1. Operation of a Frank-Read dislocation source leading crack formation.

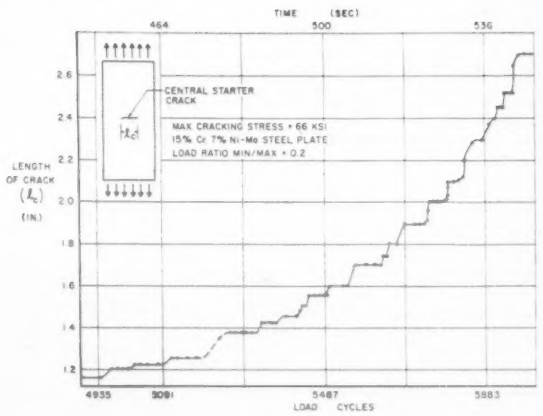

Fig. 2. Crack growth vs. number of load cycles in a damaging stress range.

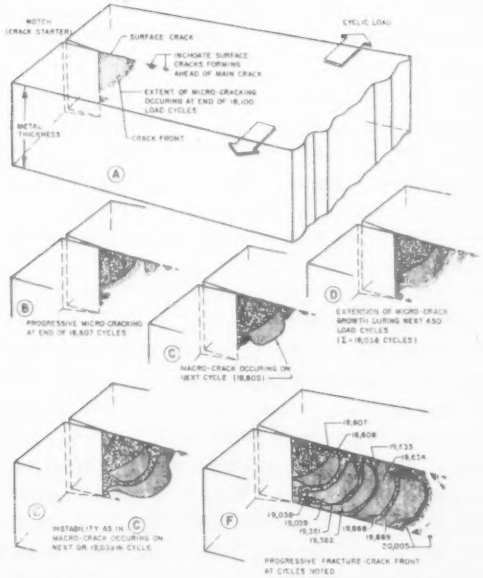

Fig. 3. Schematic representation of fatigue crack growth. Note repetitive and alternate periods of micro and macro cracking which result in "jumps" or "spurts" during progressive fracture. (Numbers of cycles of loading at various stages are from an actual test.)

Man-Machine

Joseph G. Wohl

Dunlap and Associates, Inc.

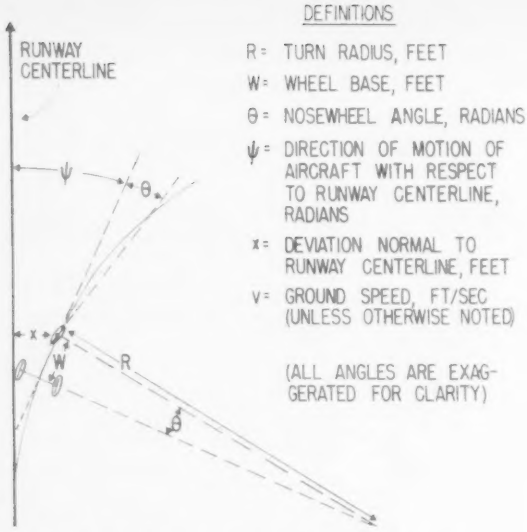

Fig. 1. Geometry of nose-wheel steering problem.

NEARLY ALL currently operational aircraft utilize landing gear systems with nose-wheel steering capabilities. Nose-wheel steering minimizes ground handling (towing) requirements and facilitates parking, taxiing, alignment on runway, and ground roll during landing and take-off. Control of nose-wheel steering is handled in most aircraft by the pilot through a separate steering wheel, and in a few through a direct linkage with the rudder bar. In either instance the pilot retains complete directional control of the aircraft throughout its so-called *ground phase*.

The essential thought of this paper is that a human operator (the pilot) must act as an element in a closed-loop servosystem. The functions of this human element are as follows:

(1) Selection of a reference (point, line, angle, curve, etc.) from which to determine the aircraft's misalignment or deviation—i.e., error.

(2) Detection of such errors.

(3) Establishment of an error criterion.

(4) Response to the detected error (via rudder bar or steering wheel) in such a manner as to maintain the aircraft within the established criterion limits throughout the ground phase.

These are complex functions for a servoelement of any type to perform. With this consideration in mind, it is a natural consequence to seek ways in which the ground steering task of the pilot could be made safer and simpler.

Analysis

In order to provide insight into the way in which the human functions as a servoelement in a nose-wheel steering system, the following simplified analysis of steering geometry is presented.

Fig. 1 illustrates the geometry of the nose-wheel steering problem during take-off. Certain simplifying assumptions are used for convenience:

$$\theta \leq 10^\circ$$
$$\sin\theta = \theta$$
$$\psi \leq 10^\circ$$
$$\sin\psi = \psi$$
$$v = \text{a constant}$$

(Effects of suspensions, cross wind, wheels, tires, skid or slip, inertia, etc., are neglected.)

Under these assumptions, the following simple and fundamental equations can be derived from the relationships illustrated in Fig. 1:

$$R = W/\theta \tag{1}$$
$$\dot{\psi} = v/R \tag{2}$$
$$\dot{x} = v\psi \tag{3}$$

where

R = turn radius, ft
W = wheel base, ft
θ = nose-wheel angle, rad
ψ = direction of motion of aircraft with respect to runway centerline, rad
v = ground speed, ft/sec
$\dot{x} = dx/dt$
$\dot{\psi} = d\psi/dt$

Substituting Eq. (1) in Eq. (2) results in

$$\dot{\psi} = v\theta/W \tag{4}$$

Taking the derivative of Eq. (3) with respect to

Dynamics of Nose-Wheel Steering

Aircraft ground steering dynamics are analyzed from a human factors standpoint, and a velocity-modulated steering system is proposed to reduce required variations in human steering sensitivity during the ground phase.

time (holding v constant) results in

$$\ddot{x} = v\dot{\psi} \tag{5}$$

Substituting Eqs. (3) and (4) in Eq. (5) results in

$$\ddot{x} = v^2\theta/W \tag{6}$$

Eq. (6) relates lateral acceleration with respect to the runway centerline to vehicle speed, wheel base, and nose-wheel angle, and represents a simplified model of the system dynamics at constant speed without the human operator.

Although several possible avenues of approach may be taken in analyzing human operation in the steering loop, a good starting place is the perceived information upon which the pilot might base his continuous judgment concerning steering.

The human perceptual problem is indicated more clearly in Fig. 2, which shows that there are at least six perceptual variables (the three shown plus their rates of change) with which the man might have to deal on an instantaneous and continuing basis.

From Fig. 2 we can infer that, for small angles ($\psi \leq 10°$),

$$x = D\psi \tag{7}$$

Differentiating this once, we obtain

$$\dot{x} = \dot{D}\psi + \dot{\psi}D \tag{8}$$

Solving this expression for $\dot{\psi}$ and substituting for $\dot{x}$ from Eq. (3), we get

$$\dot{\psi} = \psi[(v - \dot{D})/D] \tag{9}$$

Setting Eqs. (4) and (9) equal, we obtain

Mr. Wohl is Associate Program Director whose responsibilities include the human factors program of the Fleet Ballistic Missile System. He received a B.S. degree in physics and math from the University of Wisconsin in 1949 and has done graduate work at several universities. A Lecturer in man-machine systems engineering at Columbia University, he worked in the engineering psychology field at the Naval Research Laboratory and at ONR from 1948 to 1954, and for the ensuing 3 years was Senior Engineer and Group Leader at Sperry Gyroscope Company, performing duties involving systems engineering and preliminary design of drone and missile systems. He joined Dunlap and Associates in 1957, and holds memberships in several professional societies.

$$v\theta/W = \psi[(v - D)/D] \tag{10}$$

Solving Eq. (10) for θ, we obtain

$$\theta = \psi(W/v)\ [(v - \dot{D})/D] \tag{11}$$

If as in many aircraft and ground vehicles the steering system is *reversible*,* then the nose-wheel displacement θ is proportional to the force F applied by a human operator to the rudder bar or steering wheel—viz.,

$$\theta = kF \tag{12}$$

Eq. (11) can then be rewritten as

$$F = (\psi/k)\ (W/v)\ [(v - \dot{D})/D] \tag{13}$$

(*Continued on page 90*)

* In the *irreversible* case—e.g., certain aircraft flight control systems—the displacement θ may instead be proportional to the angle α through which the steering wheel or rudder bar is operated, with the disadvantage that there is no force feedback to the pilot. For a discussion of why the force-displacement concept is more desirable, see reference 3.

Application of Laminar Flow Control to Transport Aircraft

Welko E. Gasich, AFIAS, *Northrop Corporation*

MUCH HAS BEEN WRITTEN about the aerodynamic, propulsive, and structural aspects of laminar flow control. This paper discusses some of the areas which have received relatively less emphasis, and which are now commanding greater attention among aircraft designers and airline operators. In order to determine the applicability of laminar flow control to transport aircraft, one must compare the operating costs of normal aircraft having turbulent boundary layers with aircraft employing laminar flow control on wings and empennage. This consideration leads to the determination of manufacturing costs, maintenance costs, and operational considerations.

In order to demonstrate the practicality of laminar flow control, the United States Air Force has awarded Northrop Corporation a contract to construct and fly two demonstration aircraft. A brief description of this airplane configuration and the program objectives will be discussed.

LFC Definition

The definition of laminar flow is illustrated in Fig. 1. When the boundary layer air, or thin layer of air adjacent to the wing surface, moves in practically parallel air layers that do not intermix with each other, the air is said to be laminar and is of a low drag nature.

Turbulent flow is characterized by oscillating or fluctuating air movements. These disturbances or energy interchanges within the turbulent boundary layer are responsible for the relatively high turbulent friction drag.

Laminar flow control (LFC) prevents the formation of turbulent flow by pulling the slow-moving, turbulent-prone air adjacent to the wing surface through a large number of fine slots cut spanwise in the outer skin, and passing it through ducts inside the aircraft structure, then pumping it overboard.

A schematic diagram of a typical LFC system is shown in Fig. 2. The wake drag of the laminar surfaces and the equivalent suction energy required for the LFC process is balanced by a portion of the main engine thrust, the remainder of the main engine thrust being used to overcome induced drag and the drag of the fuselage and engine nacelles.

The equivalent suction energy C_s that is required is accounted for in the skin friction drag coefficients C_F quoted for LFC surfaces, giving a true picture of the net benefit resulting from LFC. The suction compressor can be driven by a free turbine, direct

The author would like to extend his appreciation to S. H. Brown and M. G. Huben of the Advanced Design Staff and to Dr. W. Pfenninger, Chief, Boundary Layer Research, for their contributions to this paper.

Mr. Gasich received his A.B. (mechanical engineering) and his M.S. (aeronautics) at Stanford University, and his professional degree of Aeronautical Engineering at California Institute of Technology. He joined Northrop in 1953 as Chief, Preliminary Design, and was promoted to his present position of Director, Advanced Systems Section, in 1957. Preparatory to his work at Northrop were associations with the Ames Aeronautical Lab. (NACA) as flight test and research engineer, Douglas Aircraft as structures engineer specializing in aeroelastics, and RAND Corp. where he was responsible for the aircraft design group performing design synthesis of various system studies. In his current position, Mr. Gasich directs the systems analysis and advanced design of new aerospace systems undertaken by the Norair Division. In addition to his affiliation with the IAS, he is a member of the Society of Automotive Engineers and Sigma Xi.

LFC is feasible from the following standpoints:

- ***Demonstrated drag reduction***
- ***Practicality of construction and maintenance***
- ***Possibility of lower operating costs in future subsonic transports***

shaft, bleed and burn turbine or by a separate turboshaft engine.[1]

Research Results

As described in the preceding section, laminar flow control appears elementary in concept and, although its advantages were understood in the late 1930's, it has commanded great attention only recently for the following reasons:

(1) It was easier for many years to make dramatic reductions in drag with developments such as cantilever wings, retractable landing gears, etc. These developments were a necessary part of the evolution to provide a smooth, streamlined airplane compatible with LFC.

(2) LFC required a comprehensive research program to bridge the gap between its theory and application.

Yet, LFC appeared to be the last significant step remaining in the history of friction drag reduction and thus posed a challenge. To solve the problem, a joint Air Force-Northrop effort was initiated in 1949 under the direction of Dr. Werner Pfenninger. The resulting 12-year program has covered extensive theoretical and experimental research, laboratory testing, wind-tunnel programs, and flight demonstrations to substantiate fully the friction drag figures quoted for LFC.

Some program results concerning drag coefficient vs. Reynolds number are shown in Fig. 3, with drag values of a typical production airfoil and a highly polished airfoil[2] shown for comparison. The F-94 airplane referenced in Fig. 3 was equipped with a 13 percent glove airfoil over a portion of the F-94 wing. Suction was applied to the upper glove surface through 69 slots. Full chord laminar flow was

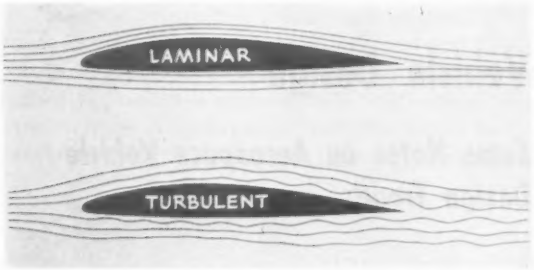

Fig. 1. LFC definition.

maintained up to 36 million Reynolds number—the test limit of the airplane. Over 200 flights were made with this airplane.[3]

The swept wing curve of Fig. 3 indicates the feasibility of LFC on a modern jet transport airplane. This curve is a result of tests that were conducted in the University of Michigan 5 by 7 ft tunnel and the Ames 12-ft tunnel on a wing of 30° sweep, with a modified 66-012 airfoil. As compared with a typical turbulent swept wing, the drag of the laminar wing is five to six times lower.[4]

A necessary part of achieving the low friction drags associated with LFC is a smooth airfoil surface. The smoothness required for the swept wing of a typical high subsonic airplane is shown as a function of altitude[5, 6] in Fig. 4.

To lend some physical feeling to the numbers quoted in Fig. 4, a few comparisons can be made. The roughness of 0.005 in. is approximately equivalent to fine sandpaper. This requirement is easily bettered by conventional sheet aluminum. Skin joints should be designed such that possible misalignments result in "up steps" instead of "down steps" to capitalize on maximum allowable step height. The "up step" allowable dimension of 0.017 in. at 40,000-ft altitude is approximately equivalent to the thickness of a playing card. This tolerance can be met in most areas with current manufacturing methods, although special attention is required where the leading and trail- (*Continued on page 44*)

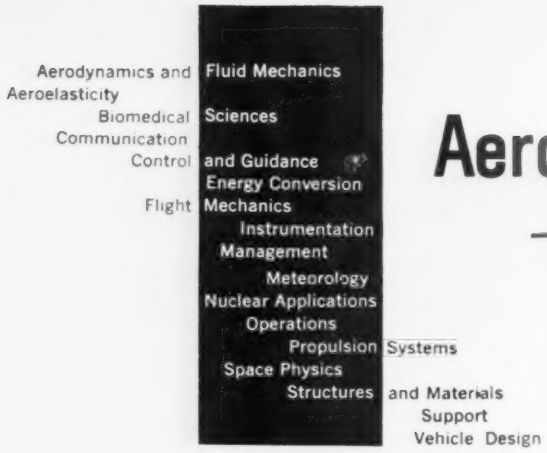

Aerospace Technology

—as seen by the panels

Vehicle Design

Some Notes on Aerospace Vehicle Design Trends

Adolph Burstein, AFIAS

The author is a member of the IAS Aerospace Technology Panel on Vehicle Design, and Assistant Chief Engineer, Research and Development, General Dynamics/Convair.

THE GENERAL ACCEPTANCE of jet transportation by the airlines and the public has been most gratifying and lends emphasis to several design trends.

Jet Transports—Present and Future

Subsonic Jet

There is a fast-growing use of jets on relatively short routes involving operations from limited fields. This leads to more extensive incorporation of high-lift and leading-edge devices and more sophisticated trailing-edge flaps.

The turbofan engines answer the need for both higher unit thrusts and greater fuel economy. Higher thrust engines coupled with lower take-off speeds made possible as a result of higher lift capabilities of the wing increase one-engine-out control difficulty. To solve this problem, several rearrangements of power plants from the current individual wing-mounted pod-pylon systems have been either used or proposed. The two most prominent approaches are tail-mounted or twin-pod, wing-mounted engines.

The greater thrust adds emphasis to the general desirability of increasing directional control and stability. Powered rudder systems were introduced because they offered greater control effectiveness than servotab actuated systems, while permitting low control forces. Another major advantage of the irreversible control system is that the rudder position is unaffected by aircraft yaw angle. The added complexity of powered controls had to be accepted to provide the desired effectiveness.

Supersonic Transport

Supersonic transport studies have indicated that a Mach 3 airliner carrying in the neighborhood of 130 passengers and designed for a range of some 3,500 miles could be operated economically in the 1970 time period. Since fewer aircraft will be required than in the subsonic jet fleet, the high development costs would make a privately financed venture highly unlikely.

Normal extensions of current technology would be required to produce a Mach 3 transport. A few illustrative problems and current conclusions are presented. Dry turbojets or turbofan engines appear to be most promising for operation in the vicinity of Mach 3. Sonic boom may be entering the power-plant selection considerations. Sonic boom is a major operational problem which may require that acceleration beyond $M = 1$ be restricted to altitudes above 40,000 ft. Turbofan cycle would be favored for such operation.

Obviously important in supersonic transport design is L/D. Two items of interest will be mentioned here. At supersonic speeds, the volume of the fuselage has much more influence on the total drag of the vehicle than in the subsonic case. To illustrate: reducing the fuselage volume standards from that used in subsonic jets to the Caravelle or DC-7 class will produce a direct operating cost reduction in the neighborhood of 15 percent. This certainly calls for a serious discussion of the luxury that needs to be provided for the supersonic transport passengers. Another drag item that we wish to

single out for comment is trim drag. Because of the center of pressure shift between subsonic and supersonic flight, methods must be found to minimize the penalty of trim drag during the supersonic cruise. Canard control surfaces offer interesting possibilities of providing efficient methods of achieving trim and desirable stability variation between subsonic and supersonic regimes.

Efficient structural design and selection of materials is important to minimize weight and cost penalties caused by the high speed. Both titanium and steel have to be considered. Cabin insulation, as well as wing tank insulation, are important problems. Much concern has been expressed about fuel temperature rise at the end of a Mach 3 mission.

Some operational problems should be mentioned. It is expected that supersonic transports will require field lengths similar to the current subsonic jets. Therefore, no special problem exists there. However, sonic boom will require major consideration and may affect airframe design as already mentioned. The major problem is the lack of supersonic operating experience. The only vehicle that has significant supersonic endurance, at the present time, is the B-58. This is compared to the thousands of hours that were accumulated on large, high-speed, subsonic, military jets prior to inauguration of passenger jet service. There is, and must be, serious planning to take full advantage of available means to gather maximum experience in preparation for supersonic passenger traffic. It is desirable that a program be instituted which will permit the development of safe operating procedures and the regulations to ensure such procedures.

Exoatmospheric Transports—The Aerospaceplane

This discussion is not complete without a brief look beyond the earth's atmosphere where it is possible to visualize a number of missions where men and material must be placed in earth orbits simply and economically. Such transports must be manned and therefore recoverable. They should approach the operational flexibility and safety of the transports discussed earlier. The various investigations show that this can be achieved in one stage by taking full advantage of the air-breathing engines to as high a speed as efficiency considerations permit, switching at that point to rockets. Right here we have a broad field for ingenuity and research in the area of air-breathing engine cycles. But propulsion is by no means the only problem area. In selecting the configuration for the aerospaceplane, the designer is faced with a set of formidable requirements, some of them conflicting. Aerodynamically, we must have an efficient, controllable configuration throughout the speed range from low subsonic to hypersonic re-entry velocities. We must take advantage of the pressure field underneath the wing or body for our air inlets; at the same time, we have to consider the increased local heating that will occur around the intersection of two surfaces formed by the intersection of a cowl and wing or body.

Structural heating and insulation problems are well known. Since liquid hydrogen is apt to be the fuel for this vehicle, we shall have a structure exposed to cryogenic temperatures on the inside and to over 2,000°F on the outside. (Higher temperatures would be experienced at the leading edges.)

Human factors, communication, and navigation, all present additional challenges.

A successful vehicle will indeed call for a most thorough and imaginative synthesis of the aerospace technologies to achieve the optimum combination.

Two-stage recoverable versions are interesting because of much greater payload potential and therefore place fewer demands on technology advances required to produce a useful vehicle. Of course, definite sacrifice in operational flexibility would be involved in going from single to two-stage design.

+ + +

Flight Mechanics

Reliability—One of Today's Dominant Problems

C. B. Westbrook, MIAS

Mr. Westbrook is a member of the IAS Aerospace Technology Panel on Flight Mechanics, and Chief of the Aero Space Mechanics Branch of the Flight Control Laboratory, USAF, at Wright-Patterson AFB, Ohio.

WITHOUT DOUBT, one of the dominant problems of the design of future aerospace vehicles is that of reliability. It is a subject, recently become fashionable, which, like the weather, many people are talking about. Also like the weather, a much smaller number are doing anything very constructive about it.

One of the problems in this respect is that not everyone is talking the same language or about the same missions and vehicles. For example, one person may be thinking of the reliability problem of operating the B-58 in service with a reasonable

utilization. Another may be thinking of the problem of reliable firing of an Atlas or Titan. A third may be concerned with reliable operation of an unmanned space vehicle for a year or more. There is a vast difference between the extent of the problem and the methods and procedures used to combat the problem for these various missions.

Some groups appear to believe that reliability can be "tested" into a system. While gradual and sometimes significant improvements can be made in this way by elimination of "bugs," it is certainly not the answer to the general problem.

Other groups appear to pin their faith on building the various components to the very highest quality and/or selecting high quality components from production. This approach is necessary and desirable in many cases where key elements must be in the system and the best is none too good.

It is disconcerting to note, at times, the emphasis placed on quality and reliability of certain classes of components when the overall gain in system reliability may not warrant it. For example, with regard to the flight control subsystem, relatively little effort has been placed on the electromechanical parts of the system as contrasted with the electronic portions, and yet a chain is only as strong as its weakest link.

The key factor in proper understanding and then design is the ability to analyze a proposed system early in the proposal stage. With this knowledge available, an engineer can identify the critical areas and plan what must be done. His first action no doubt would be to review his design to see if these critical points can be avoided by their outright elimination, redesign of the system to a simpler one, or substitution of other kinds of equipment. If a critical item is found to be indispensable, a proper course of action can be determined—development of a "super" component, use of redundancy, etc. Many times, unfortunately, flight control system designers accept requests for additions, frills, and niceties to the system as a challenge to their ability to perform the operation, with little regard to its effect on system reliability. Designers must learn to refuse such requests resolutely, based on concrete knowledge of what it will do to the system.

The mathematics of reliability analysis is relatively simple and straightforward. As with any analysis, however, the result is only as good as the data put into it. Efforts are being made to obtain these data particularly on electronic components. Industry has recognized the need enough to put aside its normal proprietary interest and share information under the IDEP program. In certain areas, however, our knowledge is weak or totally inadequate. For example, data and knowledge of how systems operate when turned on and off are practically non-

(*Continued on page 94*)

Management

Relating Industrial Research to Company Goals

Lewis A. Rodert, FIAS

Mr. Rodert is a member of the IAS Aerospace Technology Panel on Management, and Research Assistant to the Chief Scientist of Lockheed-California Co.

AMONG THE long-range planning problems the aerospace industry faces, none is more pressing than that involving research. Industry managers require better knowledge of how to return a profit on research investments. Research scientists and engineers want to know how to make recognized achievements in the industrial environment.

Ambitions, however, are not limited to the narrow point of view. Managers want their scientists to receive recognition for their achievements, and scientists want to see their ideas turned into profit. Yet, frustration beclouds many who hold to these objectives. The aerospace industry has problems to solve in harnessing the research function to company goals. Greater attention to long-range planning of industrial research arises directly from apprehensions that the research effort might fail to advance national scientific strength and promote industrial growth. The impact on the nation's strength and the dollar magnitude of industrial research[1] eliminate the possibility of ignoring the problem. Its complication[2,3] precludes solutions found quickly by casual processes conducted on a part-time basis.

Relating industrial research with company goals involves first identifying company goals encompassing (1) economic objectives, (2) product area plans, (3) resources to support the accomplishment of objectives, and (4) the environment in which the company is to compete.[4] A detailed enumeration of these items comprises one of the principal parts of relating research to company goals.

The other side of the balance sheet is concerned with how research may be described. Principal headings include programing, facilities, organization, and finance. An important decision in programing involves the selection of technical areas in which the company plans to be strong. Furthermore, the decision must be made that research will be conducted either to produce product line innovation or to preserve the continuity of the existing product lines and maintain technical ability. From these decisions many subordinate topics must be decided,

(*Continued on page 94*)

Adventures in Engineering

Temperature Sensitivity in Germanium Transistors

James D. Mason

The author is Supervisor, Piece Parts Reliability Standards Group, Product Reliability Department, Arma Division, American Bosch Arma Corporation. He received his B.E.E. degree from Syracuse University in 1949, joining Crouse-Hinds Co. as Development Engineer and Laboratory Supervisor. On becoming associated with Arma in 1957, he was assigned responsibilities in the Engineering Standards Section as a Semiconductor Specialist, shortly thereafter being assigned to his present position. Mr. Mason is a member of the IRE and the Standards Engineers Society.

TEMPERATURE SENSITIVITY of germanium transistors was discovered in the development of a guidance system for a major ballistic missile program. This guidance system uses approximately 1,000 germanium transistors. Cooling air is provided near 0°C prior to turn-on. Transistor malfunction occurred in approximately 0.1 percent of a given transistor population immediately after turn-on. The malfunction usually disappeared after a short warmup period, and was caused by a drastic excursion of I_{CBO} over a narrow temperature range. This problem was assigned to the writer and a task force of engineers was provided to help effect the solution.

The transistors had been purchased to a specification which included 100 percent leak testing and elevated temperature test.

When transistor temperature sensitivity appeared, an extensive program of failure analysis and test was indicated. As an interim step, all transistors of this type were subjected to a series of temperature cycles from −35 to +85°C with initial and post temperature cycling readouts of I_{CBO} and I_{EBO}. Any transistor exhibiting a change in excess of 2uA was rejected. This screening procedure was established deductively in an attempt to improve stocks and to require vendors to institute more stringent manufacturing controls.

Test results indicated that moisture contamination was the cause of difficulty. Vendors' manufacturing and assembly techniques indicated that moisture content was within limits when manufactured. Study indicated that transistor hermetic seals were adequate to exclude moisture from external sources for at least a period of time which exceeded the age of the transistors under study. Further investigation indicated that the internal structure of the transistor was outgassing under storage and use, increasing the moisture content of the atmosphere within the transistor housing.

Dew point testing was investigated as a possible screening mechanism. (The moisture level in the internal atmosphere of a transistor should be such as to exhibit a dew point below −65°C.)

Dew point testing was discarded as a screening or weeding mechanism for several reasons:

(a) Individual handling was required.

(b) A subjective decision was required.

(c) Characteristic anomalies, when present, were displayed very briefly.

(d) Test method caused operator fatigue.

(e) Precautions were required to avoid false indications from moisture condensation on the exterior of the transistor housing.

It became obvious that further work had to be done to evaluate, within a reasonable time, the efficiency of the temperature cycling screening mentioned earlier. Furthermore, immediate attention had to be given to recent developments in transistor construction.

The most noteworthy change in transistor construction at the time of investigation was the advent of the "gettered" transistor. A "getter" in a transistor consists of the addition of a molecular sieve material to the interior of the transistor. The molecular sieve mechanically traps moisture molecules and holds them within its structure over a wide temperature range. A test series was established using a temperature plateau test. This test consisted of exposing groups of transistors to temperatures in 10°C steps from −55 to +25°C with electrical measurements at each step or "plateau." Groups tested included:

(a) Transistors accepted via temperature cycling tests.

(*Continued on page 95*)

Piloted Simulation Studies (Continued from page 11)

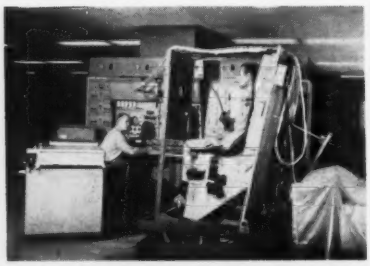

Fig. 2. Fixed cockpit and analog computer used in simulation of prediction-control method.

Methods of Control

Prediction Control

Basic concept: A brief description of the prediction method of end-point guidance and control is presented here for clarity. (Full details of this system are given in reference 1.) The aerodynamic range capability of the vehicle is predicted from existing conditions along the flight path by solving equations of motion for the constant trim conditions for maximum manuever. In this study the three constant trim conditions used were:

$(L/D)_{max} = 0.5$ and bank angle equal to zero ($\varphi = 0°$) for maximum range

$(L/D)_{min} = 0$ and $\varphi = 0°$ for minimum range

$(L/D)_{max} = 0.5$ and $\varphi = 45°$ for maximum crossrange

This area of aerodynamic range (shaded in Fig. 1) is solved repetitively, as "fast" as possible, for changing flight conditions by an airborne computer; the range and maximum manuever capability are thus known continuously as the vehicle parameters vary.

One of the major problems in a continuous prediction system is to choose the form of the equations of motion used in the airborne prediction computer so that a satisfactory compromise is achieved between the conflicting requirements for a reasonable amount of computing equipment, accuracy, speed, and easily obtainable input information. Chapman[8] has derived a mathematical model which defines the important variables for re-entry trajectories. A comparison is made below of the quantities needed to describe a trajectory for the standard equations of motion and those needed for the Chapman model.

Equation	Airborne Measurements	Vehicle Parameters
Standard	V, γ, h	$mC_DS, L/D$
Chapman	V, γ, A_u	L/D

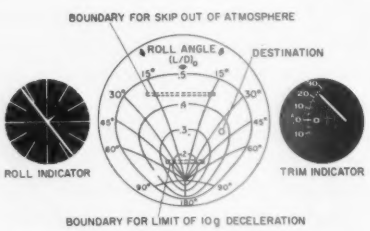

Fig. 4. Pilot's guidance and control display.

The Chapman model combines the vehicle's mass-to-drag ratio m/C_DS and altitude measurement into a deceleration measurement A_u which gives an effective "density altitude." This density altitude is then related to an exponential altitude density variation by the Chapman equation.

There are three factors which make the Chapman equation satisfactory for use in the airborne prediction computer. The first factor is that the computations are simplified by the use of acceleration (density-altitude) inputs. The second factor is that the relation between density and geometric altitude will usually be unknown during an actual re-entry; therefore, use of the effective density-altitude variation will provide a way of compensating for nonstandard atmosphere variation. The third factor is that the Chapman model does not use geometric altitude. White[9] shows large errors may be present in the measurement of geometric altitude during re-entry if an inertial platform is used for position information. Computations which use acceleration measurement instead of geometric altitude will be less affected by inherent inertial platform error. It is recognized that the continuous-prediction method must still use an inertial platform to measure longitudinal and lateral range. However, a cursory examination indicates this information would be available with the required accuracy.

Simulation details: The prediction method of end-point guidance and control was simulated by use of an electronic analog computer and a fixed cockpit (Fig. 2). The elements of the analog simulation important to the navigation study are shown in Fig. 3. The analog computer functioned to (a) accept control inputs about all three axes from the pilot and then solve the resulting six-degree-of-freedom motions of the vehicle, (b) compute the repetitive prediction equation, and (c) generate the pilot display information. Complete details of this simulation are given in reference 1, but for clarity a short discussion of the simulation will be given here.

The vehicle equations of motion describe six-degree-of-freedom dynamics along a great circle route (with small lateral displacements) over a nonrotating curved earth. The flight regime simulated was from 100,000 to 300,000 ft variation in altitude using the 1956 ARDC standard atmosphere, and from rest to 35,000 fps variation in velocity. The vehicle simulated had proportional reaction controls about all three axes, with constant gain damping augmentation included so that the short-period damping would be near-critical at the highest dynamic pressures. This damping along with very little cross coupling in the aerodynamic derivatives made the vehicle easy to fly in the short-period mode so that the pilot's function was mainly one of guidance control. The vehicle's aerodynamic characteristics, the re-entry altitude and velocity, and the allowable deceleration excursions imply[5-7] safe re-entry flight-path angles of $-2.1°$ to $-6.2°$.

The analog computer used in this simulation was not equipped with high-speed computer components. Because

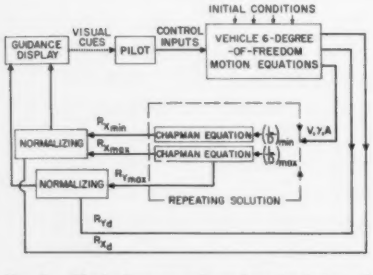

Fig. 3. Block diagram of analog simulation of prediction-control method.

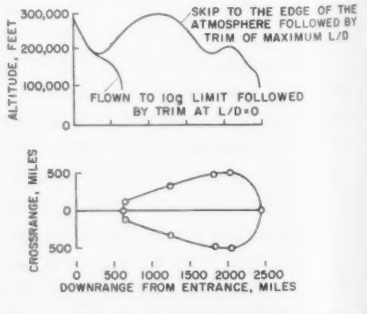

Fig. 5. Extremes of range possible using prediction-control method.

of this, the repetitive solution of the prediction equation could not be considered fast. The integration rate was $\frac{dw}{dt} = 0.2$/sec to which was added a 1-sec reset time. This means the solution from parabolic velocity was 8 sec, from satellite velocity 6 sec, and from one-half satellite velocity 3.5 sec. It can be seen that the repetition rate became more rapid as the vehicle neared its destination. One item of interest left unanswered by this simulation is to determine the effects of a truly fast solution time, particularly in the region in which pilot control was most sensitive. (This sensitive control region will be described later in this paper.)

The guidance display used in this simulation is shown in Fig. 4. The "footprint" or range envelope is a transparent overlay on the face of a 5-in. oscilloscope. The destination is a moving dot on the pilot's display oscilloscope presented in relation to the predicted range capabilities of the vehicle in the following manner:

$$y \text{ oscilloscope input} = \frac{Rz_d - Rz_{min}}{R_{zmax} - R_{xmin}}$$

$$x \text{ oscilloscope input} = \frac{R_{yd}}{R_{y_{max}}}$$

The correspondence then between the oscilloscope presentation for the pilot (Fig. 4) and the aerodynamic range capability of the vehicle (Fig. 1) can readily be seen. In fact, the oscilloscope display appears to the pilot as though he were looking through a window in the vehicle as it approaches its destination. The pilot's field of view through the window represents the maneuver capability of the vehicle. Then it is good procedure for the pilot to control so that his destination is in the center of his maneuver capability—that is, to fly the destination dot to the middle of the oscilloscope.

In this simulation it was decided to impose a maximum deceleration limit of 10g on the vehicle's trajectory as the arbitrary physiological acceleration limit on the pilot. It was also decided to impose a minimum deceleration limit of 0.075g to keep the vehicle from skipping out of the atmosphere. The effect of these g limits on the range capability of a vehicle entering at parabolic velocity is illustrated in Fig. 1. The repetitive prediction equations of range capability also predict the decelerations the vehicle will experience for fixed L/D. If the predicted value of deceleration for $L/D = 0$ exceeded the 10g limit, then an empirical relationship taken from references 5 and 8 was used to indicate on the oscilloscope (Fig. 4) the minimum L/D that could be held without exceeding the 10g limit. If the predicted value of deceleration for $L/D = 0.5$ was less than 0.075g (equivalent to a skip-out of the atmosphere), then the next repetitive maximum range solution included a value of $\Delta(L/D)$ proportional to the amount of overshoot, and this new L/D maximum value is displayed on the pilot's display (Fig. 4). Thus, the repetitive calculation is continually presenting to the pilot an L/D that if flown would cause the vehicle to reach the 10g deceleration limit, and another L/D that if flown would cause the vehicle to skip just to the edge of the atmosphere. The vehicle range capabilities could conceivably be extended beyond those of this simulation by allowing the vehicle to skip out of the atmosphere for added range.

Pilot technique and opinion: The method of pilot control for maximum or minimum range is illustrated in Fig. 5. For maximum range the pilot will trim to the L/D shown to be the boundary for skip-out of the atmosphere. The parabolic entry velocity will eventually diminish, and as it does the skip-out boundary will change until the pilot finds he is permitted to fly an L/D of 0.5. Conversely, to obtain minimum range, the pilot would trim to the L/D indicated by the boundary for the 10g deceleration limit and, as the vehicle velocity diminishes, the boundary will change until eventually the pilot can fly a trim of $L/D = 0$. Fig. 5 also shows the range area attainable by this vehicle when it is flown by this guidance method.

The pilot control technique used to fly to a desired end point is as follows: During the first part of the trajectory when the vehicle is at parabolic velocity and just entering the atmosphere, the pilot trims at those conditions which the guidance display indicates are necessary to reach the destination. If the destination mark on the guidance display should appear below the maximum deceleration boundary, the pilot just trims to that boundary. After the initial dive into the atmosphere and the point of maximum deceleration is passed, the pilot overcontrols slightly the destination to the center of the vehicle's range capability.

The pilots considered this system satisfactory. The pilot function needed here was to close the control loop between the bank and trim indicators and navigation display (Fig. 4), which involved keeping up with the changing trim conditions during the re-entry trajectory.

Pilots had no difficulty coping with emergency or abort re-entry conditions while using the continuous-prediction guidance and control system. Fig. 6 shows the piloted range capability for two typical abort trajectories. This ability of the guidance system to predict range and deceleration limits for any entry conditions makes it an almost universal control method.

NEW KODAK

METAL-ETCH RESIST

opens new chemical-milling applications

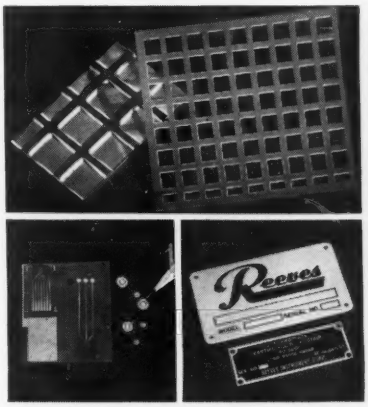

Speeds up, simplifies *deep etch* weight reduction and parts manufacture. Reproduces fine-line detail as in plating, dial and name-plate making. This new photographic process ends time-consuming handwork, results in high accuracy. Kodak Metal-Etch *Resist* withstands acids, alkalies, electrolytic fluids . . . adheres well to aluminum, titanium, magnesium, stainless and other alloy steels. High stability and strict uniformity simplify volume production. Send today for a detailed 16-page brochure that gives all the facts.

Text for this advertisement was set photographically.

No statement or suggestion is to be considered a recommendation or inducement of any use, manufacture or sale that may infringe on any patents now or hereafter in existence.

Graphic Reproduction Sales Division
EASTMAN KODAK COMPANY
Rochester 4, N. Y.
Please send me a copy of the booklet, "Etching, Chemical Milling and Plating with Kodak Metal-Etch Resist" (P-36).

Name _____
Company _____
Street _____
City _____
Zone ____ State _____

10-251

Kodak
TRADEMARK

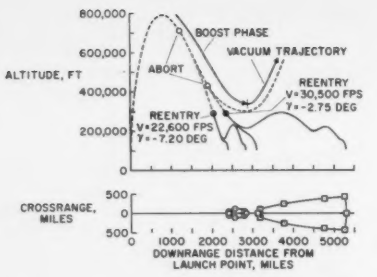

Fig. 6. Maneuver capabilities for typical abort re-entries.

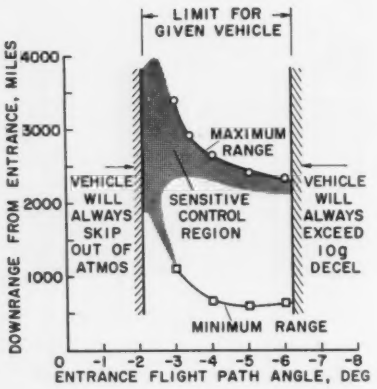

Fig. 7. Downrange and corridor limits for nearly parabolic re-entry.

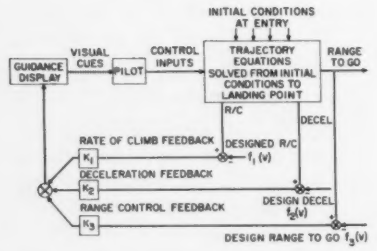

Fig. 8. Block diagram of a piloted fixed-trajectory control method.

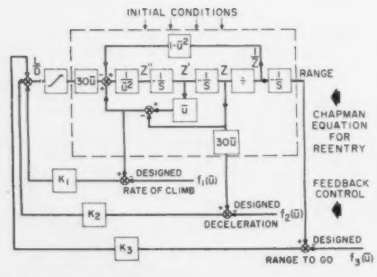

Fig. 9. Block diagram of analog simulation of fixed-trajectory control method.

Sensitive control regions: Flying those trajectories near the maximum deceleration boundary as indicated on the guidance display was not difficult. The procedure was to hold trim conditions just above the maximum deceleration boundary until the peak deceleration had passed and then to hold the trim conditions necessary to reach the destination. Flying to those destinations which required a skip to the upper limit of the atmosphere (300,000 ft for this simulation) to obtain the necessary range resulted in a sensitive control problem. For a maximum range trajectory (Fig. 5 is an example), little control effectiveness was available near the top of the skip (at maximum altitude), and the trajectory control exercised during the first dive into the atmosphere strongly influenced the rest of the trajectory. Fig. 7 is presented to show those values of range and entrance flight-path angle (h = 290,000 ft, V = 35,000 fps, and (L/D_{max} = 0.5 for all runs) for which pilot control was most sensitive—that is, the shaded area indicates entry conditions for which small changes in L/D control at the beginning of re-entry results in very large changes in range.

Fig. 7 is a good index of two major flying qualities problems of flight within the atmosphere at near parabolic velocities. The region of entry conditions acceptable to the pilot is squeezed between the sensitive control region and the limit of deceleration the pilot can tolerate with current restraint harness and control techniques. Research on both of these pilot-control problems is described in references 10 and 11. Further, Fig. 7 shows not only sensitive control regions, but also the range of readily controllable entry angles as related to maximum and minimum range obtainable by this guidance method.

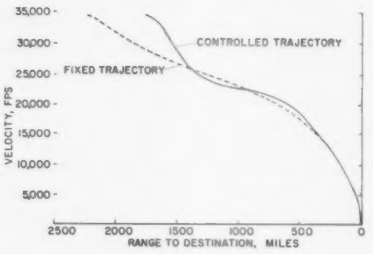

Fig. 10. Typical control to a fixed trajectory.

Fixed-Trajectory Control

Method of analysis: Fixed-trajectory control is conceived to be either a piloted technique (Fig. 8), which is analogous to the system for the continuous-prediction method, or possibly an automatic control method (Fig. 9) in which vehicle flight-path parameters are compared to the parameters of some precomputed design trajectory. In either case, the pilot or automatic controller simply initiates vehicle control inputs to null any error between the two. For purposes of direct comparison it would have been desirable to study the system as represented in Fig. 8; however, to expedite the study, the Chapman equations[5] were again used as the re-entry equations. The system as represented in Fig. 9 was then used in a closed-loop analysis; since the independent variable in these equations is velocity and not time, the human pilot could not be introduced. The particular comparisons in this paper are believed to be unaffected since the function of a human pilot in closing the control loop was closely approximated by the analytical method.

Fig. 9 shows the complete block diagram of the closed-loop method of analyzing this guidance system. The primary objective of a fixed-trajectory guidance system is to find a combination of predetermined trajectory and feedback control that will minimize the maximum range error at the end point from large variations in initial conditions. Typical control to a fixed trajectory is shown in Fig. 10. The outer loop or range control of Fig. 9 will cause the vehicle trajectory to converge to the design trajectory (Fig. 10). The inner-loop controls of Fig. 9, which are the deceleration and the rate-of-climb feedback, primarily affect the overshoots or oscillations about the fixed trajectory. The analysis of this system is made with the same limitations on the vehicle and its trajectories that were imposed on the prediction control method; $(L/D)_{max}$ = 0.5, deceleration limits of 10g maximum and 0.075g minimum, and entry conditions of h = 290,000 ft and V = 35,000 fps. These conditions imply a safe re-entry corridor −2.1° to −6.2° flight-path angle.

Simulation details: The use of the Chapman equation as the model for the vehicle trajectory equation of motion allows the important feedback quantities for range control to be recognized, and its relative ease of mechanization on an analog computer permits a straightforward method of investigation of fixed trajectory control. The control of range by the L/D input is essentially a third-order control system. The inner loop (rate of climb and deceleration feedback) which contribute damping by the control system can be seen in Fig. 9 to come from the Z' and Z terms. It is interesting to note the feedback loop from Z' and Z within the Chapman equation. The upper loop

He's solving a real estate problem

This AMF engineer's job is determining how best to move big missiles off shore for launching. Should they be floated out horizontally, flooded to an upright position, and then launched? Or, would it be more feasible to barge them out? Might they be moved to or assembled on "Texas Towers," or would a causeway or simply land-fill be the answer?

Behind the project is our shrinking real estate at launching sites, plus the hazards inherent in launching Saturn-sized missiles (and the coming, nuclear-powered missiles) near other installations. Off-shore launching may be the answer.

Feasibility studies of all types are an AMF specialty. What kind of remotely controlled machinery is required to service nuclear-powered aircraft? What kind of habitation could be built on (or under) the surface of the moon? What sort of machines (manned and unmanned) could survey the moon's surface without, for example, falling into a fissure? What is the best way to assemble a space station? All these are problems AMF engineers are presently investigating.

If your problem is the first of its kind, AMF will not, of course, have met it before. But AMF's long experience in accepting totally unique challenges gives it an advantage enjoyed by few other organizations concerned with ground support, launchability and space environment. To get further information write American Machine & Foundry Company, 261 Madison Avenue, New York 16, N. Y.

AMF

gineering and manufacturing AMF has ingenuity you can use...

AMERICAN MACHINE & FOUNDRY COMPANY

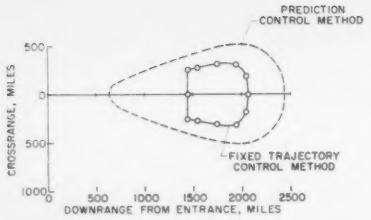

Fig. 11. Extremes of range possible using fixed-trajectory control method.

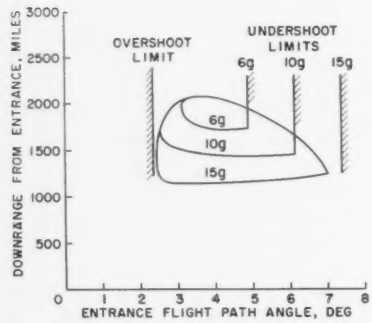

Fig. 12. Effect of maximum deceleration limit on range andentry corridor; fixed-trajectory method.

$(1-\frac{u}{u}^{-2})/Z$ is a stabilizing quantity for $\bar{u}$ less than one, but for $\bar{u}$ greater than one this loop is destabilizing. The lower loop $(\bar{u}Z'-Z)$ within the Chapman equation is a stabilizing loop that is essentially a rate-of-climb feedback loop that tends inherently to damp phugoid oscillation about a design trajectory.

The simulation of this control system has been done on an electronic analog computer in which $\bar{u}$ was the independent variable. It was assumed that the response times of control inputs would not greatly affect the overall trajectory motion. The constant-gain inner-loop quantities were taken as those measurements which may be available during a re-entry.

Crossrange control was simulated by a second-order system. The equation for crossrange was taken from Slye[12] and was expressed in terms of the heading angle ψ and the Chapman Z function. The present analysis considers only the control necessary to null the crossrange error to zero.

The equations that result from the analysis of longitudinal and lateral range control are of the following form:

$$L/D = K_1(h - h_f) + K_2(A - A_f)$$ inner-loop feedback

$$+ K_3(R_{x_d} - R_{x_{d_f}})$$ outer-loop range control

$$Y/D = K_4 R_{y_d}$$ crossrange control

These desired L/D and Y/D values are related to the vehicle control inputs, roll angle φ, and trim angle of attack $(L/D)_o$ in the following manner:

$$L/D = [(L/D)_o]_{min}^{max} \cos \varphi$$

$$Y/D = [(L/D)_o]_{min}^{max} \sin \varphi$$

This coupling was usually neglected in the past for high L/D vehicles where the desired L/D programs angle of attack and Y/D programs roll angle (φ is usually less than 45°). This study of a low L/D vehicle will consider the complete coupling.

Feedback control analysis: The flight-path conditions of a re-entry from the center of the safe entry corridor were chosen as the initial conditions for the design trajectory. The determination of such a trajectory for parabolic entry presents a problem. In studies of satellite re-entries, the design trajectory has usually been chosen as an equilibrium glide for a constant L/D in the middle of the vehicle's lifting capability. However, if constant L/D is used at parabolic velocities, the trajectory is unstable, and, therefore, an equilibrium glide condition cannot be used to define the design trajectory in this case. The trajectory chosen for parabolic re-entry was that which results from L/D control proportional to rate of climb. This simple rate-of-climb feedback loop is a very effective means of stabilizing the design trajectory. The gain of the rate-of-climb feedback

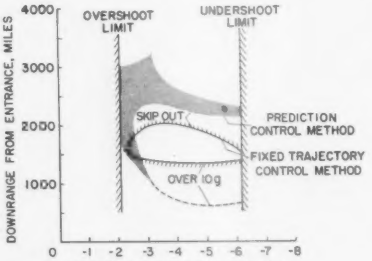

Fig. 13. Comparison of range and entry corridor limits.

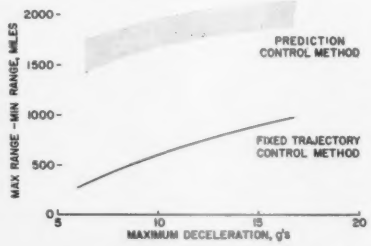

Fig. 14. Comparison of effects of maximum deceleration limit on range.

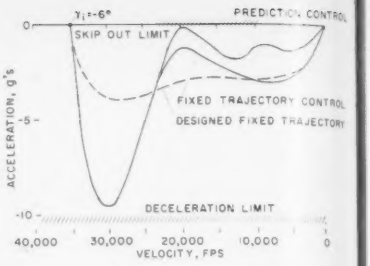

Fig. 15. Comparison of typical controlled trajectories with nearly maximum range.

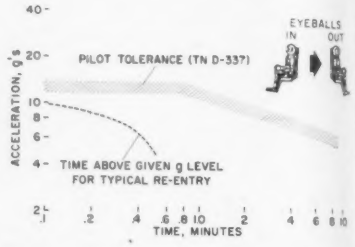

Fig. 16. Pilot's time tolerance to acceleration.

was chosen as that constant gain which commanded an L/D near the middle of the vehicle's lifting capability ($L/D \approx 0.3$) during the suborbital velocity portion of the trajectory.

The control of errors in range from the design trajectory was tried using only the rate-of-climb feedback for damping and range-to-go feedback for primary control. The results were unsatisfactory since the best control that could be expected gave end-point errors of ±25 miles for initial errors of ±100 miles.

Therefore, a third control loop, acceleration feedback, was added to the system to make the range control acceptable. The addition of this control loop allowed higher gains on the range control feedback for closer range control. The total system then gave end-point errors of ±5 miles for entry range errors from +100 to −500 miles. The acceptable control equation developed in this preliminary study is

$$L/D \pm^{+0.5}_{-0.5} = K_1\dot{h} + K_2(A - A_f) + K_3(R_{x_f} - R_{x_{d_f}})$$

where $K_1 = 0.001$/ft/sec, $K_2 = -0.33$/g and $K_3 = 0.006$/mile.

This system could be improved by programing optimum variations of K_1, K_2, and K_3 as functions of velocity instead of allowing these gains to be constant. For instance, if K_3 is programed to zero until just below satellite-velocity, then the available range capability would be about 2,000 miles compared with 600 miles for the constant gain system in this report.

Guidance capabilities: The ground area attainable using the fixed-trajectory method is shown in Fig. 11. This range capability is for control about a design trajectory having an initial entry angle of $-4.5°$ and should be compared with the prediction control range capability from Fig. 5.

The effect on maximum longitudinal range and permissible entry corridor of changing the maximum deceleration limit of the fixed-trajectory method of control is shown by Fig. 12. In general, doubling the maximum g limit doubles the longitudinal range and the entry corridor for the deceleration range considered in this study.

Comparison of Prediction Control and Fixed-Trajectory Control

The maximum and minimum range attainable by the prediction control and the fixed-trajectory control methods are compared in Fig. 13 for various entry angles. The figure shows that either control method can be used to keep from exceeding the peak deceleration limits of 0.075g and 10g for the same interval of entry angles, which was about $-2°$ to $-6°$. The main difference between the two methods is that the fixed-trajectory method of control provides only about one third of the range attainable by the prediction-control system.

The effect of changing the maximum deceleration limit on range capability has been shown for the fixed-trajectory control method in Fig. 12. A comparison of the effect of the maximum deceleration parameter on the range capability for the two control methods is shown in Fig. 14. The percentage change in range capability obtained by varying the peak deceleration limit for the prediction-control method is slight compared to the variation in range capability for the fixed-trajectory method.

Fig. 15 exemplifies the main reason for these differences in range capability. It shows the acceleration-velocity profiles for two maximum-range trajectories for which the initial conditions of the vehicle and flight path were identical. One was guided by prediction control and the other by the fixed-trajectory method. The main difference between the two methods of control is that the fixed-trajectory control technique inherently damps to the design trajectory, whereas the prediction-control method damps only to the end point. Therefore, the prediction-control technique spends more time at the lower deceleration levels (Fig. 15), thereby stretching the glide, than does the fixed-trajectory method.

Data presented in Fig. 15 correspond to a maximum range extension at a steep initial entry angle condition (close

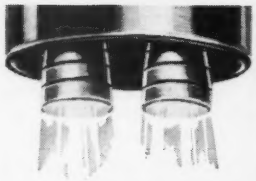

ALTITUDE

EGT (AUTOTEMP®)

TURBINE PRESSURE

FUEL FLOW & QUANTITY

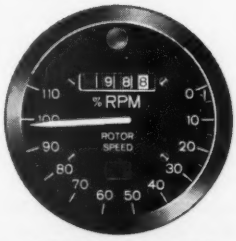

% R.P.M. (AUTOTAK®)

HOWELL
INSTRUMENTS

COMPREHENSIVE INSTRUMENTATION

HOWELL INSTRUMENTS are calibrated for use with all transducers for the measurement of the phenomena encountered in all phases of aircraft and missile development, test and operation. Each instrument is completely self-contained (miniaturized, silicon transistorized, servo-driven, hermetically sealed) with Zener reference, power supply, amplifier, servo motor, cold junction compensation as needed and the 144-inch slide-wire and punched tape to linearize e.m.f. for exact, counter-type digital readout. Needle pointers are provided for quick reference. Accuracies are within 0.1%. Available in 3"-dia. MS33639 and 2"-dia. MS33598.

Styled Series BH183 & 185—*The Instrument with the Tape-Slidewire*—these instruments are produced by the makers of the JETCAL® Analyzer, the only jet engine tester used throughout the world!

Full information is available for the asking.

Sales-Engineering Offices:
COMPTON, CAL., DAYTON, O., VALLEY STREAM, L.I., N.Y., WICHITA, KAN., TORONTO, ONT. *(George Kelk Ltd.)*, MITCHAM, SURREY, ENGLAND *(Bryans Aeroquipment Ltd.)*

HOWELL INSTRUMENTS, INC.
FORMERLY B & H INSTRUMENT CO., INC.
3479 WEST VICKERY BOULEVARD • FORT WORTH 7, TEXAS

to the limit shown in Fig. 13) for which it would be difficult to avoid the peak deceleration limit.

Fig. 16 is a graph, taken from reference 11, showing the pilot's time tolerance to acceleration as presently conceived for accelerations in the eyeballs-out or eyeballs-in direction. The dotted line on this graph indicates the length of time the pilot is at or above the corresponding g level for the two parabolic re-entries shown in Fig. 15—that is, Fig. 16 shows that for either guidance method the pilot will be above 5g for at most one-half minute and above 8g for at most one-third minute. For deceleration levels less than 5g, the time tolerance exceeds the total re-entry time of the vehicle, and thus is of no significance. Thus by either guidance method the pilot can maneuver so as not to exceed his time-tolerance-to-acceleration boundaries, and he is well within the region where he can perform a useful control function.

Concluding Remarks

The results of this study of two basic methods of terminal guidance and control during re-entry from a lunar mission show that either method can utilize nearly all the permissible re-entry corridor fixed g limits, but the range capability of the "continuous-prediction" guidance and control method is nearly three times the range attainable by the "fixed-trajectory" control method.

Finally, it has been found for entries from parabolic orbits that a vehicle can be maneuvered by either terminal guidance technique in such a manner that the present criteria for pilot's time tolerance to acceleration are not exceeded.

References

[1] Wingrove, Rodney C., and Coate, Robert E., *Piloted Simulator Tests of a Guidance System Which Can Continuously Predict Lading Point of a Low L/D Vehicle During Atmosphere Re-entry*, NASA TN D-787, 1961.

[2] Cheatham, Donald C., Young, John W., and Eggleston, John M., *The Variation and Control of Range Traveled in the Atmosphere by a High-Drag Variable-Lift Entry Vehicle*, NASA TN D-230, 1960.

[3] Lowry, James H., Jr., and Buehrle, Clayton D., *Guidance and Control of Point Return Vehicles*, Proc. National Specialists Meeting on Guidance of Aerospace Vehicles (sponsored by IAS), May 25–27, 1960.

[4] White, J. A., Foudriat, E. C., and Young, J. W., *Guidance of a Space Vehicle to a Desired Point on the Earth's Surface*, ARS Preprint 61-41, Jan. 1961.

[5] Chapman, Dean R., *An Analysis of the Corridor and Guidance Requirements for Supercircular Entry Into Planetary Atmospheres*, NASA TR R-55, 1960.

[6] Wong, Thomas J., and Slye, Robert E., *The Effect of Lift on Entry Corridor Depth and Guidance Requirements for the Return Lunar Flight*, NASA TR R-80, 1960.

[7] Teague, Roger, *Flight Mechanics of Re-Entry After Flight by Means of Various Lifting Techniques*, NASA, Marshall Space Flight Center, MNN-M-AERO-4-60, 1950.

[8] Chapman, Dean R., *An Approximate Analytical Method for Studying Entry Into Planetary Atmospheres*, NASA TR R-11, 1959.

[9] White, John S., *Investigation of the Errors of an Inertia Guidance System During Satellite Re-Entry*, NASA TN D-322, 1960.

[10] Sadoff, Melvin, McFadden, Norman M., and Heinle, Donovan R., *A Study of Longitudinal Control Problems at Low and Negative Damping and Stability With Emphasis on Effects of Motion Cues*, NASA TN D-348, 1961.

[11] Creer, Brent Y., Smedal, Harald A., Capt. USN (MC), and Wingrove, Rodney C., *Centrifuge Study of Pilot Tolerance to Acceleration and the Effect of Acceleration on Pilot Performance*, NASA TN D-337, 1960.

[12] Slye, Robert E., *An Analytical Method for Studying the Lateral Motion of Atmosphere Entry Vehicles*, NASA TN D-325, 1960.

✦ ✦ ✦

Supercircular Entry and Recovery With Maneuverable Manned Vehicles

(Continued from page 13)

entry pull-out for gliders was analyzed by Grant[1] and has been discussed by others.[2–4]

Peak dynamic pressure occurs just before the bottom of the pull-out, but modulation will generally continue. Beyond peak dynamic pressure, angle of attack is gradually increased to return the glider to maximum lift attitude. Throughout this process, lift and drag have been maintained at the highest level allowed by the prescribed acceleration limit, so penetration has been minimized and energy dissipation (speed reduction) has been maximized. This means, generally, that both heating rate and time of exposure have been held to a minimum so that the total heat load up to this point is as small as possible for the prescribed conditions.

The lowest acceleration limit which can be prescribed for a given entry angle is that which requires modulation to proceed from maximum-lift attitude at entry to nearly minimum-drag attitude at peak dynamic pressure. (Heat load in this case is rather large.) On the other hand, selection of a high acceleration limit requires less reduction of lift and drag so total heat load is reduced. Attitude modulation allows very steep entries with a high L/D glider without exceeding 10g. But the more significant advantage of attitude modulation is that resultant acceleration loads can be limited to more comfortable values at moderate entry angles. In either case, a heat load design penalty is incurred by extensive attitude modulation. A prospective glider design will involve a three-way compromise between design heat load, maximum resultant acceleration, and maximum entry angle or undershoot limit.

When operating at less than the maximum entry angle, it is important to recognize the different implications of heat-load limit and acceleration limit. Because of the concern for crew comfort, resultant acceleration load should always be reduced as far below the limit value as possible. But once a heat load limit is established and provision for it made in the design there is no incentive to hold heat loads to lower values. For entry angles less than the steepest provided for in the design, acceleration relief through attitude modulation should be used to the maximum extent allowed by the design heat load limit.

Pull-Up

At the bottom of the pull-out from a steep entry, the speed, dynamic pressure, and heating rate are still very high. A pull-up maneuver is desired which will avoid skip-out, continue control of acceleration, and avoid further accumulation of large heat load. Skip-out is prevented by banking, as required, to regulate the vertical component of lift. (In this paper *skip-out* is distinguished from *overshoot*; *skip-out* is defined as an exit from the atmosphere caused, in part, by inappropriate use of lift.) Resultant acceleration load is controlled by continuing the angle of attack modulation started during the

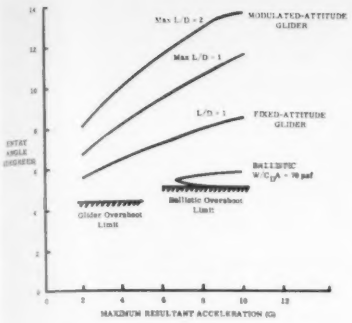

Fig. 3. Manned entry limits.

pull-out. Maximum drag consistent with the prescribed acceleration limit is maintained, as before, while the independent banking control regulates the flight path angle. The high drag tends to minimize heat load by keeping exposure time short. A considerable latitude in choice of trajectory is generally available.

The pull-up is controlled to allow termination of entry maneuvers above satellite speed at an altitude where glide with radiation cooling is possible. An inverted pull-over maneuver is required to establish level flight. For this study the terminal point is at 27,000 fps and 250,000 ft altitude. In the event that speed loss due to drag is too rapid to allow completion of the maneuver by bank angle control alone, the drag may be reduced by lowering angle of attack to allow more time. Greater heat load results from the additional exposure time.

It is recognized that the pull-up maneuver, which is generally completed within 3 min after entry, presents a difficult control system problem. This problem is being studied, but is beyond the scope of this paper. Analog computer studies have verified that the maneuver can be successfully controlled with the system proposed by Morth and Speyer.[5]

The small heading change from the use of banked flight during pull-up is an incidental assist to subsequent banked-glide maneuvers to reach the recovery site.

Overshoot Limit

Very shallow entries at supercircular speed can result in an overshoot which will make direct single-pass entry impossible. This is the result of insufficient penetration of the atmosphere; the glider will re-exit, and there follows a multipass series of entries over an extended period of time. At the overshoot limit, a pull-in maneuver is required in which maximum lift is used, but the glider is inverted so that the lift is directed toward the earth. This maneuver increases penetration to avoid overshoot. If there is any likelihood of overshoot, it is best to enter inverted. Directing the lift toward the earth steepens the flight path slightly, but roll to the upright attitude can be made, if necessary, after single-pass entry is assured and before atmosphere penetration is excessive.

Shallow entries bordering on the overshoot limit are completed by an inverted glide, within the heat-load region, to the terminal point at 27,000 fps and 250,000 ft altitude. It is recognized that constant attitude equilibrium glide above satellite speed is not stable. The rate of divergence from the speed-altitude schedule is low[6] which implies that control would present no problem. Entry at the overshoot limit involves low resultant acceleration, but considerable heat load accrues during the supercircular glide within the heat load region—i.e., below the temperature placard in Fig. 1.

Entry Corridor

Entry at an angle between the steep (undershoot) limit and the shallow (overshoot) limit is said to be within the entry corridor. The notion of a corridor[3] arises from a consideration of the virtual or no-atmosphere perigees of the undershoot and overshoot limit entries. The difference between perigee altitudes of these two hypothetical paths is a corridor width more easily visualized as an aiming slot for the returning space vehicle. Entry corridor expressed as an allowable range of entry angles may be converted to a corridor width by calculating the appropriate Keplerian perigees and observing the difference in perigee altitude.

An entry corridor is required to accommodate atmosphere irregularities and inaccuracies in approach guidance and control. A wide entry corridor may be desired to reduce the requirement for flight path deflection by impulse prior to entry. Corridor width is a major problem for vehicles with small maneuverability. However, when entry angle corridors of several degrees are available, there is freedom to make design trades between acceleration limits, heat load, and entry corridor.

Glide Maneuvers

Range and offset control are confined to the heating rate region where radiation cooling allows freedom for extended-time maneuvers. This restriction governs the maximum speed for beginning glide maneuvers. In this study, glide begins at 27,000 fps—about the highest speed allowed by the temperature placard for maximum L/D glide. The corresponding altitude is 250,000 ft. Equilibrium glide, which is essentially horizontal flight with no

NEW
STRAIGHT WALL
TANTALUM
CAPACITOR
CAN'T LEAK

Meets MIL C 3965-B, Style CL-64, CL-65.

A new space-saving approach to the design of wet tantalum capacitors ends mounting problems encountered with flanged types and yet will not leak.

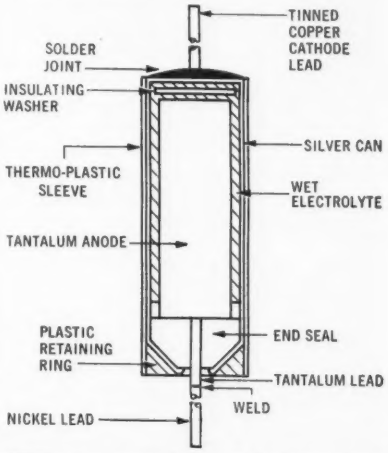

ITT's compact, sintered slug tantalum capacitor features a wedge-shaped seal held under compression by an epoxy retainer ring formulated for thermal characteristics inverse to those of silver. Ordinary, straight-wall capacitors leak along the lead when elastomer compression is reduced as the silver can expands. Not so with the new ITT design!

This new, compact capacitor conforms to specifications MIL C 3965-B, Style CL-64, CL-65 and provides both the compactness and rugged reliability required in missile, airborne and mobile equipment. For details, write today requesting Bulletin No. 610.

ITT
CAPACITOR DEPARTMENT
COMPONENTS DIVISION
INTERNATIONAL TELEPHONE AND TELEGRAPH CORPORATION, PALO ALTO, CALIFORNIA

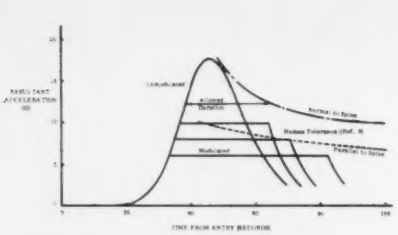

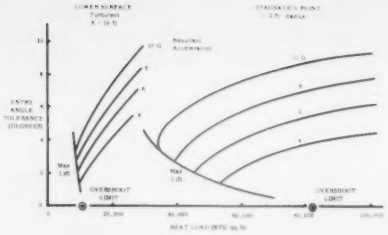

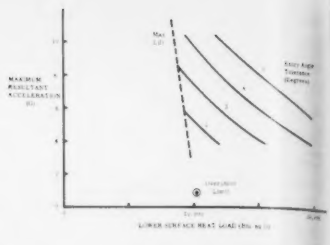

Fig. 4 (*left*). Acceleration magnitude and duration (glider with max L/D = 2; entry angle = 9 deg.). Fig. 5 (*center*). Entry heat load (glider with max L/D = 2). Fig. 6 (*right*). Entry design trades (glider with max L/D = 2).

vertical acceleration, is used from the end of entry maneuvers to arrival over the recovery site. During this phase, continuous response to range-to-go guidance is possible because aerodynamic control is maintained by always gliding within the atmosphere. The goal in the glide maneuver phase is to obtain range control which will allow landing anywhere in one circumnavigation while at the same time maintaining large lateral offset capability for all downrange distances within the range control capability. The result will be a belt of landing site coverage which is twice as wide as the offset available and which completely encircles the earth.

Trans-Satellite Glide

Control of range is the primary objective for glide from 27,000 to 25,000 fps. The very low dynamic pressures available in this region permit circumnavigating glide at maximum L/D with a transition through zero-lift attitude at satellite speed. Glide at a high-drag attitude along a temperature-placard trajectory for maximum allowable dynamic pressure allows very short-range flights. The small speed change, long-range requirement, and high flight speed in this phase make it impossible to deflect the flight path laterally more than a few degrees; consequently, this small added turn capability is neglected in favor of a simpler concept.

Subsatellite Glide

In the subsatellite glide phase beginning at 25,000 fps, substantial lateral offset can be achieved. Near-maximum lateral offset is obtained by a simple two-step maneuver consisting of glide at 45-deg bank angle until about an 80-deg heading change is obtained, then an unbanked glide is made to the maximum offset point. It is known that slight improvement can be obtained by following a more complex schedule of gradually diminishing bank angle.

The downrange distance at which maximum lateral offset is obtained is somewhat larger than half of the maximum no-turn range. Offset is the primary objective in subsatellite glide. Therefore, to avoid deviation from maximum offset capability, range control in this phase is limited to small corrections.

Glider Characteristics

Desired glider characteristics implied by the preceding discussion may be summarized as (1) high lift and high drag with the options of high L/D and low resultant aerodynamic force, (2) trim and control capability allowing the use of these options and all available conditions in-between, and (3) capability of withstanding the heating environments.

This general study is not based on a particular glider design but representative glider characteristics have been assumed. The assumptions are believed to be realistic in relation to currently recognized design possibilities.

Lift and Drag

Example glider lift-drag polars used for this study appear in Fig. 2. These are known as Newtonian polars because the lift and drag-due-to-lift are components of flat-plate normal force given by a modified Newtonian relation. (See equation in Appendix.) The modification, consisting of adjustment of the classic Newtonian coefficient from 2.0 to 1.82, gives more realistic values at high angles of attack. Minimum drag coefficient accounts for skin friction and other parasitic drag items, and it is selected to give the appropriate maximum L/D. Aside from being convenient for preliminary studies, lift-drag polars of this type furnish good approximations of hypersonic test results above the angle of attack for maximum L/D.

A maximum lift-coefficient of 0.7 with maximum L/D from 1.5 to 2.0 appears, on the basis of applicable test data and design experience, to be obtainable in the trans-satellite glide regime. Present indications are that higher L/D will not be easily obtained with gliders of reasonable size. Aerodynamic uncertainty is very great in the entry pull-out regime. But even if lower maximum L/D occurs in the entry phase, entry can still be performed satisfactorily. Maximum L/D of 2.0 or more is expected in the subsatellite glide phase.

Trim and Control

The lift-drag polars in Fig. 2 terminate just beyond maximum lift. Angles of attack beyond maximum-lift attitude are not considered in this study. Higher angles of attack give higher drag coefficients but lower lift coefficients. Some entry analyses[8] have indicated it is better to use angles of attack up to 90 deg for the principal purpose of obtaining low heat load. An opposing consideration is that trim and control difficulty increases at high angle of attack. At a 90-deg angle of attack an entirely different sort of control system and control surface arrangement would be required. Control dynamics and response characteristics deteriorate badly at extreme angles of attack. It is concluded that the heat load reduction obtained by flight above maximum-lift attitude does not justify the effort required to obtain satisfactory flying qualities. Furthermore, it is doubtful whether heat load reduction can be obtained without undesirable acceleration load or duration penalties.

Wing Loading

Glider weight will generally be lowest if the wing loading is the maximum allowed by material temperature limits. This study is based on assumed temperature limits of (1) 4,000°F at the 6-in. radius stagnation point and (2) 2,500°F on the lower surface in turbulent flow at an effective distance of 10 ft downstream of the leading edge. These limits define temperature placards which form the boundary between the heat load region and the heat rate region in Fig. 1. Aside from the entry maneuver, which necessarily plunges into the heat load region, the temperature placards are most closely approached during subsatellite banked glide. The critical points are at 22,000 fps for the stagnation point and 19,000 for the lower surface. At these design points, the wing loading is adjusted so that the glide altitude for maximum L/D attitude and 45-deg bank will not be below the placards. This

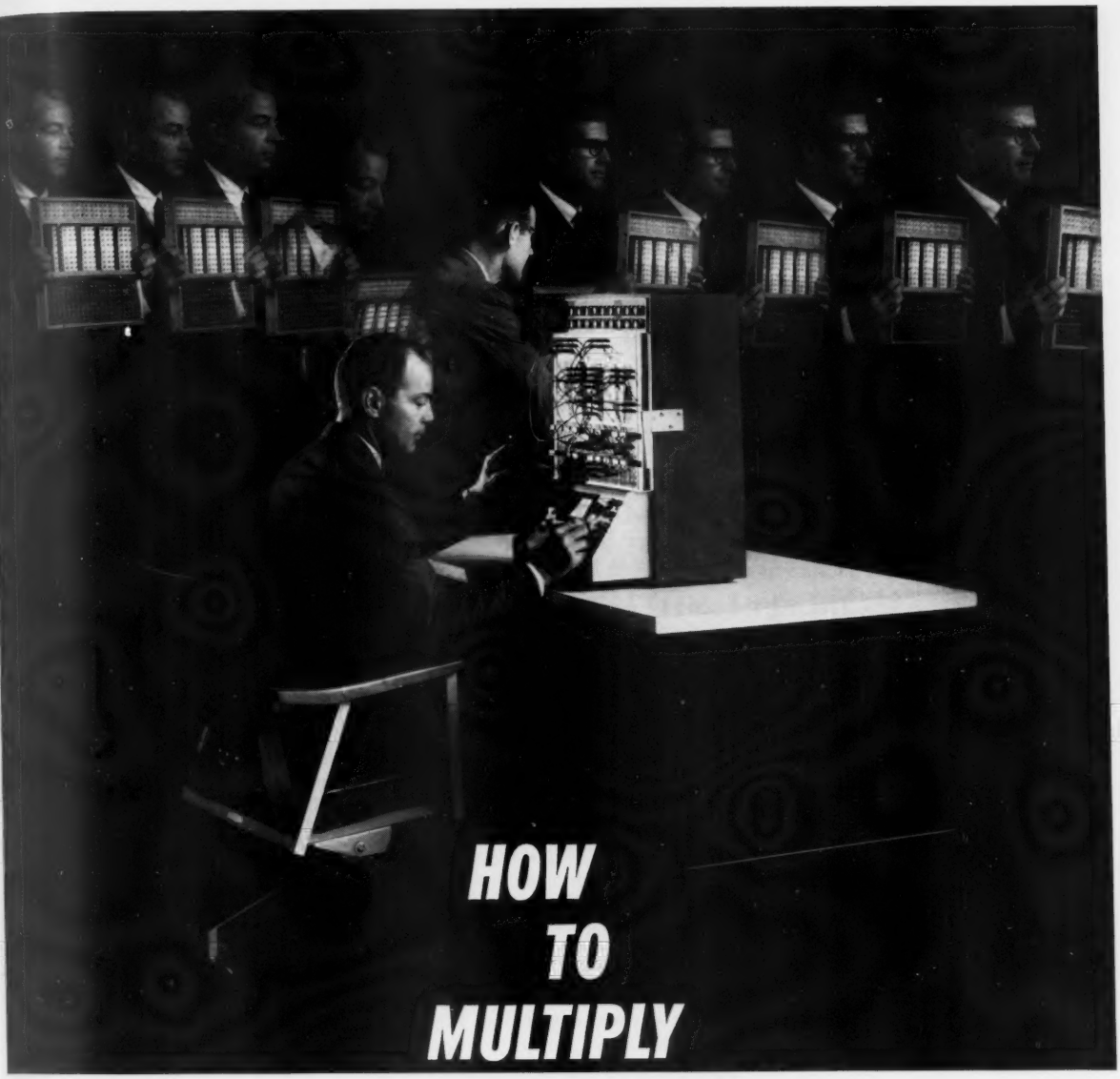

HOW TO MULTIPLY ENGINEERS

One engineer and an EAI PACE TR-10 transistorized desktop analog computer can be the equal of several men limited to conventional design tools. The TR-10 multiplies the design capabilities of the most able engineer. One TR-10, equipped with a removable patch panel, will serve the needs of a roomful of engineers. This new patch panel permits pre-patching of programs away from the computer. It plugs into the computer instantly — valuable computation time is conserved. ■ *Versatility of the TR-10 is unequalled. Unique simplicity makes it excellent for students or engineers unfamiliar with analog techniques. Accurate to a tenth of one percent, the TR-10 performs admirably for the experienced user in 95% of routine engineering problems. And with High-Speed Repetitive Operation added, or with several units slaved to operate as one, the TR-10 meets the demands of many advanced applications.* ■ *For technical data on this almost infinitely versatile computer, write for Bulletin No. AC 934.*

EAI ELECTRONIC ASSOCIATES, INC. *Long Branch, New Jersey*

Leader in Analogics Analog/Digital Computers Data Reduction Process Control Instruments Computation Service

condition restricts the wing loading to a maximum of 42 psf for glide at maximum L/D of 2.0 and 45-deg bank. If maximum L/D is lower, it will occur at a higher lift coefficient, and glide altitude will be higher unless wing loading is raised. For simplicity, wing loading is kept constant, and gliders with maximum L/D below 2 will operate with peak temperatures slightly below the limits.

Heat Protection

Survival during flight in the heat load region dictates the use of some type of protective system. No particular system will be specified in this paper, but, for illustrative purposes, an ablation system for entry maneuvers in conjunction with radiation cooling for glide maneuvers will be assumed.

Certain properties of the heat load have been observed which affect selection of a protection system. The heat load occurs as a pulse with duration as low as 90 sec. Driving enthalpies are large because of the high flight speeds. Hot gas radiation input has been ignored in this study; although this heat load component probably is not negligible in all cases considered, it is certainly not dominant. Some consideration of this factor will probably be required in the design of a heat-load protection system. Because the relatively thin ablation coatings over much of the glider will have limited insulation effectiveness, surface temperatures will probably have to be below the material limit temperatures—i.e., ablation temperature less than placard temperature. Convective heat loads presented in this study have been calculated for surface temperatures equal to the assumed material limit temperatures.

Entry Performance

Entry performance was calculated for the various entry maneuvers described in the Flight Plan section. Of primary interest is the heat load accumulation and acceleration loading prior to trans-satellite glide.

The performance of two hypersonic gliders, with maximum L/D of 1.0 and 2.0 and lift-drag characteristics described previously, was investigated. The wing loading of 42 psf was selected on the basis of critical temperatures on the lower surface as explained previously.

Basis for Calculations

Entry performance calculations for the initial entry pull-out and portions of the pull-up were programed for solution on the IBM 7090 high-speed digital computer. The complete equations of motion for a point mass with aerodynamic lift and drag were used.[10] A spherical nonrotating earth and a 1959 ARDC model atmosphere were assumed. The initial velocity and altitude were 35,000 fps and 400,000 ft, respectively.

The basic trajectory program has provisions for holding the resultant acceleration constant at a selected limit value by automatically reducing the angle of attack as the dynamic pressure increases above its corresponding limit value. This procedure maintains lift as high as possible, and the prescribed resultant acceleration is held constant.

The heating rate and heat load accumulation per unit area were calculated in a subroutine to the basic trajectory program. A modified Fay-Riddell heating rate equation was used for the nose stagnation point calculation. The reference temperature method for turbulent flow with adjustments for angle of attack variation was used for the lower surface reference point. These heating calculation procedures are given in reference 11. The radius of curvature at the nose stagnation point is selected as 1/2 ft, and the reference point for turbulent heating on the lower surface is 10 ft back from the leading edge. This choice of lower surface reference point gives, within 10 percent, the average heating rate for the entire undersurface of flat bottom delta wings with root chords from 35 to 90 ft. These heating data may be scaled to other reference lengths by applying the well-known rules that stagnation point heating varies inversely as the square root of the nose radius, and that lower surface turbulent heating varies inversely as the fifth root of the distance from the leading edge.

Undershoot-Overshoot Corridors

The results of the investigation of initial entry pull-out for 35,000 fps entry are shown in Fig. 3. The maximum permissible entry angle for a prescribed limit in resultant acceleration for the two gliders is shown by the upper two curves. At the maximum permissible entry angle, entry is made at maximum lift and attitude is modulated to nearly zero lift and minimum drag at peak dynamic pressure. These data confirm the conclusions of Grant.[1]

Results are also shown for the L/D 1.0 glider entering at fixed attitude. The attitude is that for maximum L/D (W/SC_L is 108 psf) which gives approximately minimum resultant acceleration for a fixed attitude entry. The minimum entry angle (overshoot limit) for these gliders is also shown. Both gliders have the same maximum lift coefficient and wing loading; therefore, both have the same overshoot limit.

Data for the ballistic vehicle, a peculiar feature of which requires explanation, is also shown in Fig. 3. When acceleration level is below about 8g, minimum entry angle is governed by acceleration rather than overshoot. Hildebrand[2] and Styer[12] have described a second peak acceleration which occurs below satellite speed for ballistic entries near the overshoot limit. It is this second peak acceleration which limits minimum entry angle in this case.

The entry corridors for the 10g limit converted to virtual perigee differences as suggested by Chapman are 9.5 nautical miles for the ballistic vehicle, 65 for the fixed attitude L/D 1.0 glider, and 185 for the attitude modulated L/D 2.0 glider. These corridors narrow slightly as entry velocity increases, and, as Chapman[3] has shown, all 10g ballistic corridors vanish at 46,300 fps.

The ability of an attitude modulated glider to limit the g level during steep entries depends upon the average lift throughout the pull-out. Average lift determines the depth of atmosphere penetration and, therefore, the peak dynamic pressure. If drag is low, lift can be larger for a given resultant acceleration; therefore low drag, high L/D gliders can control g level more effectively than aerodynamically inferior vehicles.

It is doubtful that the very large entry angle corridors shown will be required for manned entries; therefore, a trade for lower g's will be made.

Acceleration Magnitude and Duration

The attitude modulation mode of entry allows a limit to be placed on the magnitude of the g load, but this load must be sustained for a period of time. The added duration leads to concern that the g-time combinations might exceed human tolerances. Fig. 4 shows representative time histories of the resultant acceleration for entries at maximum lift unmodulated and modulated to lower g values. Also presented are human g-time tolerances for normal-to-spine and parallel-to-spine loadings as determined from human centrifuge tests and reported by Creer *et al.*[9] These data show that reduction of g level by attitude modulation improves the comfort level despite the extended duration of the reduced g level. The comfort level can be seen to increase rapidly as the resultant acceleration level is lowered. Comfort level is indicated by the amount the allowed duration exceeds the actual duration at a given acceleration level.

For the entries shown, the normal-to-spine tolerance is not exceeded even for the unmodulated entry. However, the parallel-to-spine tolerance is exceeded at greater than 8g resultant acceleration. When the pilot is seated upright in the glider, resultant acceleration is essentially parallel-to-spine between 15- and 55-deg angle of attack; thus the lower human tolerance curve in Fig. 4 will apply.

Heat Loads

The stagnation point and turbulent lower surface heat loads presented on Fig. 5 are the summation of heat loads accumulated during both the initial pull-out and the subsequent pull-up to the glide initiation point. The figure shows heat load per square foot plotted against entry angle tolerance. Entry angle tolerance is the difference between the undershoot and overshoot entry limits. The overshoot limit is fixed at 4.4 deg for this glider.

In Fig. 5 the stagnation point heat load per unit area appears to be dominant, but only a small area of the glider is involved. The lower surface heat load per unit area is more significant because it involves the entire wing lower surface.

The pull-up heat is up to 70 percent of the total heat for shallow entries and is as little as 10 percent for steep entries. When comparing these data with data from other general studies, it is important to note whether heat load beyond the pull-out has been included.

The maximum lift lines shown denote constant attitude entries at maximum lift and indicate the minimum heat load obtainable for a given entry angle. The heat load decreases as the entry is steepened because the higher average heating rate is more than offset by the shorter entry time caused by the higher average deceleration. When attitude modulation is employed to limit the g level, the heat load increases as the entry is steepened. Modulation involves deeper penetration into the atmosphere because the lift coefficient is reduced. The resulting increased average heating rate is the main reason for the higher heat load in this case. The lower surface heat load also reflects the secondary variation in heating rate resulting from changes in angle of attack during modulation.

Although the data presented are for a glider with maximum L/D of 2.0, this discussion applies also to lower L/D gliders. Analysis of heat loads for a glider with an L/D of 1.0 showed essentially the same results except that heat loads were somewhat lower. The difference is negligible for fixed attitude maximum lift entries, but up to 15 percent lower heat load occurs during modulated attitude entries. This reduction occurs because exposure time is shortened by the higher drag level of lower L/D gliders.

Entry Design Trades

The heat load, entry angle corridor, and resultant acceleration can be regarded as design variables. The lower surface heat load per unit area is indicative of heat protection system weight. An estimate of ablation system weight is obtained when heat load per unit area is divided by the wing loading

Increased technical responsibilities in the field of range measurements have required the creation of new positions at the Lincoln Laboratory. We invite inquiries from senior members of the scientific community interested in participating with us in solving problems of the greatest urgency in the defense of the nation.

RADIO PHYSICS and ASTRONOMY

RE-ENTRY PHYSICS

PENETRATION AIDS DEVELOPMENT

TARGET IDENTIFICATION RESEARCH

SYSTEMS:
Space Surveillance
Strategic Communications
Integrated Data Networks

NEW RADAR TECHNIQUES

SYSTEM ANALYSIS

COMMUNICATIONS:
Techniques • Psychology • Theory

INFORMATION PROCESSING

SOLID STATE
Physics, Chemistry, and Metallurgy

- *A more complete description of the Laboratory's work will be sent to you upon request.*

All qualified applicants will receive consideration for employment without regard to race, creed, color or national origin.

Research and Development
LINCOLN LABORATORY
Massachusetts Institute of Technology
BOX 23
LEXINGTON 73, MASSACHUSETTS

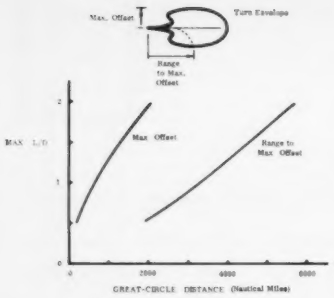

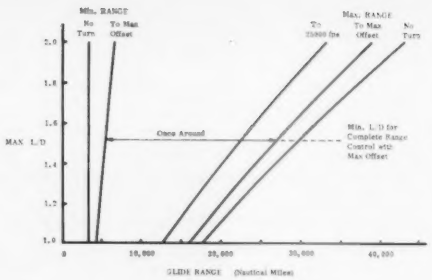

Fig. 7 (*left*). Subsatellite glide offset. Fig. 8 (*right*). Glide range (from 27,000 fps).

and effective heat of ablation. The result is the fraction of gross weight to be used for lower surface ablation material. The entry angle tolerance is selected on the basis of pre-entry guidance accuracy and approach path control considerations. Resultant acceleration is the crew comfort index. The designer's choice among these factors is shown in Fig. 6.

A representative glider design might have a design heat load limit for the lower surface of 15,000 Btu/sq ft. With 42 psf wing loading, an ablation weight of 6 percent of the total vehicle weight is required if an effective heat of ablation of 6,000 Btu/lb is assumed. This design heating limit provides for a maximum entry angle tolerance of 6 deg for maximum acceleration of 10*g*. With better control of entry angle so that the tolerance can be reduced to 3 deg (40 nm corridor), the resultant acceleration will not exceed 4*g*. For entries within the entry angle tolerance, lower heat loads could result, but it is preferable to lower the acceleration level.

Glide Performance

An evaluation of glide performance will reveal when and under what conditions it is possible to glide to a preselected landing site after entry has been achieved. Glide maneuvers beginning at 27,000 fps allow global range control and substantial lateral offset. These capabilities are expressed as a belt of landing site coverage which encircles the earth. The half-width of this belt is equal to the maximum lateral offset obtained during subsatellite glide. The freedom to land anywhere along this belt is obtained by control of range during trans-satellite glide. This evaluation, rather than determining specific flight paths to certain sites, will establish the limits of capability to reach preselected landing sites.

Trans-Satellite Glide

A wide variety of operating procedures is available for use in the trans-satellite speed regime (taken here to be from 27,000 to 25,000 fps.) Because range control, rather than range per se, is the objective in trans-satellite glide, procedures which allow the vehicle to leave the atmosphere are avoided. By gliding within the atmosphere, sufficient range control is obtained and continuous response to range-to-go guidance is possible. In general, control of range is obtained by regulating the rate at which energy is dissipated. In this case, range control involves an interdependent control of flight path and glider attitude. Low dynamic pressure flight paths and low-drag attitudes give long range. Conversely, high dynamic pressure and high-drag attitude give short range. The interdependence between flight path and glider attitude arises from the requirement for vertical force equilibrium. The flight path must be essentially horizontal to remain in the atmosphere; therefore, lift is required to maintain vertical forces in balance.

Long-Range Glide

Maximum trans-satellite glide range is obtained in a three-step maneuver following entry termination at 27,000 fps and 250,000 ft altitude. The altitude-velocity profile of the three steps is included in Fig. 1. The first step is flown inverted at maximum L/D attitude along the equilibrium-glide speed-altitude schedule for the corresponding lift coefficient and 42 psf wing loading. This step is terminated just above 300,000 ft altitude where the dynamic pressure has decreased to 1 psf and speed is about 100 fps above satellite speed. Through step 2 the dynamic pressure is held constant. The transition from constant lift coefficient glide to constant dynamic pressure glide requires a slight change in flight path angle. It is assumed that this transition maneuver will cause no range penalty. Vertical force equilibrium is maintained during step 2 by gradually reducing angle of attack until zero-lift attitude is reached at satellite speed. Then the glider is rolled upright and angle of attack is gradually increased a speed reduces. Maximum L/D at titude is regained about 100 fps below satellite speed, and the third step, a constant attitude glide to 25,000 fps, begins. The ranges in these three steps for a glider with maximum L/D of 2 are 11,600, 11,620, and 9,920 nm, respectively. (See equations in Appendix.) The total glide range is 33,140 nm for this trans-satellite maneuver. Range from the entry point adds an additional 450–2,300 nm. Maximum trans-satellite glide range for L/D from 1 to 2 is included in Fig. 8.

Short-Range Glide

Very short range results from operation at the highest allowable drag level. A dynamic pressure of 30 psf is available just above the temperature placard altitude, and a drag coefficient of about 1.0 occurs at maximum lift attitude. With wing loading of 42 psf, this combination yields a deceleration of about 0.7*g*. Speed will dissipate from 27,000 to 25,000 fps in about 90 sec; the distance flown will be under 400 nm. During this maneuver the vertical lift component is regulated to maintain the desired trajectory by varying bank angle from a nominal value of 90 deg. Because of the short duration this maneuver may require excessively rapid control response. To allow more time, the minimum trans-satellite glide range is assumed to be 900 rather than 400 nm.

Trans-Satellite Turn Performance

Lateral offset maneuvers are excluded from the trans-satellite glide phase as indicated in the Flight Plan discussion. Analysis of the trans-satellite turn performance with L/D of 2.0 confirmed that the operational complexity introduced is not yet justified by the available performance gain. To obtain an offset at a large downrange distance by continuous turning, it is necessary to alternate bank. The bank angle schedule required is different for each downrange distance. The theoretical maximum contribution to lateral offset using 90-deg bank turns between 27,000 and 25,000 fps is 465 nm. This is reduced to 306 nm when bank angles are limited to those allowed by equilibrium requirements and the temperature placard. Both of these values are accompanied by less than 4,000 nm range. The lateral offset contribution at a point one circumnavigation farther downrange is 114 nm. Because of the once-around range requirement, only the smaller contribution can be credited to widening the coverage belt. These contributions are not negligible, but they are small when compared with subsatellite lateral offset contributions.

Subsatellite Glide

Fig. 7 shows banked glide performance for maximum lateral offset with turns beginning at 25,000 fps. This maximum lateral offset will establish the width of the landing site coverage belt; the downrange distance at which maximum offset occurs is to be included in the glide range.

Maximum lateral offset for glide from 25,000 fps in a nonrotating atmosphere is approximately proportional to $(L/D)^{1.7}$ for L/D from 0.5 to 2.0. This variation has been suggested before[2] and has been verified by more exact analysis.[7] Downrange distance to maximum lateral offset varies from about 60 to 70 percent of maximum no-turn range as L/D varies from 2.0 to 1.0. The data in Fig. 7 are based on these approximate relations and a nominal maximum offset of 2,100 nm at an L/D of 2.0.

The maximum no-turn glide range from 25,000 fps is included in the maximum range shown in Fig. 8. (This range is given by the constant-attitude equilibrium-glide range equation presented in the Appendix.) The minimum no-turn range from 25,000 fps is assumed to be 2,400 nm for any L/D between 1.0 and 2.0. Even shorter range can be obtained by high angle of attack banked maneuvers similar to those suggested for minimum trans-satellite glide range. Note that Fig. 8 shows only glide range; range covered during the initial entry maneuver (450 to 2,300 nm) is not included.

Coverage Belts

Sufficient glide range data have been assembled to establish that a coverage belt extending around the earth is possible. The belt begins at the minimum range at which maximum offset can be obtained, and ends at the maximum range at which maximum offset can be obtained. When the difference between these limits equals or exceeds the circumference of the earth, the desired belt exists. As indicated in Fig. 8, this is true when maximum L/D is greater than 1.52.

The half-width of the belt is the maximum lateral offset given in Fig. 7. This varies from 1,325 to 2,100 nm for maximum L/D from 1.52 to 2.0. Landing site coverage belts for these two cases are shown over a Mercator map in Fig. 9. On a globe, the belt centerline or baseline is a great circle and the edges are parallel minor circles. The belts are shown at an arbitrarily chosen inclination of 45 deg to the equator. The map shows more than 360° longitude in order that the overlapping ends of the inner belt (L/D = 1.52) could be shown stretched out full length. The wider belt (L/D = 2.0) is longer and when stretched out extends outside the map borders.

The wider landing site coverage belt encloses the preselected landing site indicated in Fig. 9 for which Omaha has been chosen. Thus, landing there is possible by turning left with a glider having maximum L/D of 2.0. The belts are fixed in space, and earth rotation will shift Omaha to the right as time elapses. About one hour later, landing at Omaha will be possible for a glider with maximum L/D of 1.52. About 13 hours later, Omaha will be outside both belts on the right. This example illustrates the effect of time on accessibility of a preselected landing site. The baseline inclination and landing site were arbitrarily selected. Choice of another inclination and/or landing site latitude would alter the situation.

Because the belts circle the earth, the entry point could be located anywhere along the space-fixed baseline without changing coverages. A new entry point location would require a different glide program to reach a given site within the belt, but the definition of the belt ensures that the site can be reached.

Space Mission Planning and Conditions at Entry

Round-trip space missions must be scheduled to terminate with entry conditions which are suitable for the vehicle used.

The approach trajectory leading to the atmosphere entry point can be specified by the following entry point conditions: (1) entry speed, (2) entry altitude, (3) entry angle, (4) space-referenced (or inertial) entry longitude, (5) approach plane inclination to the equator, and (6) time at entry.

Desired entry conditions may be specified in advance and the entire space mission scheduled to suit the resulting restrictions. Because inevitable space trajectory dispersions and perturbations will cause variations from intended entry conditions, provisions will be made for enroute path corrections. Some space mission objectives may be impossible without major impulsive maneuvers to obtain specified entry conditions. Thus, space mission scheduling is either hampered or penalized in weight by advance specification of entry conditions, but these difficulties cannot be avoided where entry vehicles with small maneuverability are used. The relaxation of entry condition restrictions by the use of more sophisticated entry vehicles will allow greater freedom in space mission scheduling.

Consider, for example, moon-earth trajectories when entry angle is the only entry condition specified. Entry speed is essentially constant for practical trajectories. Time of arrival at the entry point will depend almost directly

work in the fields of the future at NAA

DYNAMICS ENGINEERS

Immediate openings for Structural Dynamics, Vibration, and Flutter Engineers to work on advanced present and future manned aerodynamic vehicles.

Graduate Engineers in Aeronautical, Mechanical or Applied Mechanics needed for:

Vibration Prediction
Structural Vibration Analysis
Dynamic Response Calculation
Oscillatory Aerodynamics

Specialists or Senior Engineers have excellent opportunities in the fields of vibration, dynamic analysis, structural response, and flutter. Openings available at all levels of experience and responsibility.

Experience in at least one of these fields, plus an advanced degree in AE, ME, or Applied Mechanics required.

Write: Mr. H.K. Bowman, Engineering Personnel, North American Aviation, Inc., Los Angeles 45, California.

All qualified applicants will receive consideration for employment without regard to race, creed, color, or national origin.

LOS ANGELES DIVISION

NORTH AMERICAN AVIATION

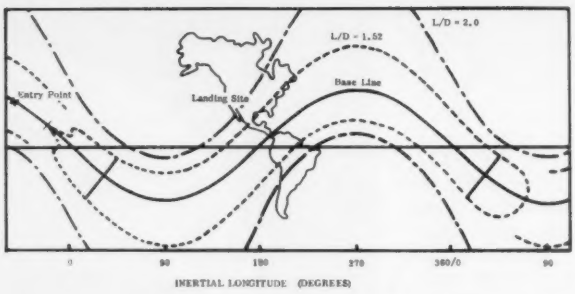

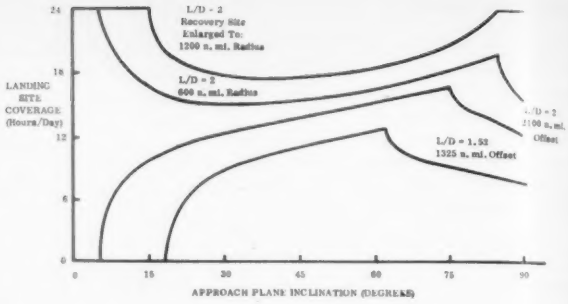

Fig. 9 (*left*). Landing site coverage belts. Fig. 10 (*right*). Landing site coverage (recovery site at 40° latitude).

on time of departure from the moon for a given type of trajectory—i.e., energy level, direct or retrograde, etc. Entry point inertial longitude will vary with calendar time of departure at about 13° per day. It will also vary with entry angle and type of trajectory. Approach plane inclination is the most uncertain item because it varies greatly with minor variations in trajectory near the moon. It appears that relaxation of restrictions on approach plane inclination will be most beneficial because this would reduce requirements for path corrections. Relaxation of time and longitude restrictions will increase freedom to launch the mission any time during the day and on any day of the month.

The time of day determines the geographic longitude of the entry point for a given inertial longitude, and time of the month determines inertial longitude of the entry point. This relationship and its consequences were implied in the discussion of coverage belts on the Mercator map.

Landing Site Coverage

In the discussion of space-fixed coverage belts on the Mercator map (Fig. 9), it was shown that landing site coverage is independent of entry point location along the baseline. This means that inertial longitude of the entry point does not affect ability to glide to a preselected site. It was also observed that landing at the selected site was possible during a period of several hours. Thus, entry could take place any time during a period of the same duration. It was noted that results would change for a different landing site latitude and/or baseline inclination. (Baseline and approach plane inclinations are nominally the same.) Fig. 10 shows how the combined effects of these factors determine the prospects for landing at a 40° latitude site. Landing site coverage is expressed as the number of hours per day that the landing site can be reached from the entry point.

The two cases shown on the map (Fig. 9) are included in Fig. 10 as points on the two lower curves at 45-deg approach plane inclination with 11- and 14-hour coverage. The curves show the variation of coverage for other approach plane inclinations. A substitute for lateral offset is enlargement of the site to a circular region and acceptance of a landing anywhere in the circle. The increase in coverage for circular recovery areas centered at 40° latitude is shown by the upper pair of curves in Fig. 10. A 3,300-nm radius would be required to always obtain 24-hour coverage for the glider with L/D of 2.0. Such a large recovery area is impractical; but, perhaps since daylight landings are preferred, only 12-hour coverage is needed.

Fig. 10 shows that equatorial entry (zero approach plane inclination) with point landing sites is excluded for both gliders. If the site were moved south 300 nm (to 35° latitude), 12-hour coverage would be available to the higher L/D glider. However, there will be a slight sacrifice in coverage at high inclinations. Similar results for the glider with L/D of 1.52 would require a landing site at 22° latitude.

Another possibility exists for allowing equatorial return. The approach plane inclination can be adjusted, in effect, by heading changes achieved before the glide phase. For steeper entry angles and modulation to low acceleration limits, there is opportunity for significant heading change during the pull-up. Banked flight is used to control the flight path angle, and heading changes up to 7 or 8 deg occur incidentally. Shallow entries yield smaller heading changes which approach zero for overshoot entries. Note that these heading changes are more useful than those which might be obtained during trans-satellite glide because they occur before, rather than during, long-range glide. For an adjustment of approach plane inclination due to heading change during pull-up, the horizontal scale of Fig. 10 is displaced to the right or left an amount equal to the heading change. A 7-deg heading change adjustment, when available, will give about 6-hour coverage for the glider with L/D of 2.0 on an equatorial approach plane. Another feature of Fig. 10 should be noted. For high inclinations, to the right of the break in the three lower curves, the coverage occurs in two equal periods. In this case, the coverage belts go over the poles and are intercepted twice a day by the landing site as it rotates with the earth.

Many possibilities are suggested by these limited data but the point is that a high L/D glider can land at some specified United States base after entry at any space-referenced longitude or approach plane inclination with a tolerance on entry time approaching half a day. This capability gives a high degree of operational convenience and allows great freedom in scheduling the space mission.

Other Possibilities

The utilitarian advantages of highly maneuverable gliders for entry and recovery are believed to be unique. It may, however, be possible to obtain comparable entry and recovery performance with aerodynamically less sophisticated vehicles by including impulsive maneuvers of various kinds. One especially interesting possibility is injection into a near-earth waiting orbit after a direct entry has reduced speed to near-satellite speed. Then de-orbit could be arranged to allow widespread choice of landing sites. In this type of recovery operation with a less maneuverable vehicle, entry angle would necessarily be more closely controlled not only to get comparable comfort levels for the crew, but also to ensure capability of achieving the desired waiting orbit.

Many other schemes will be advanced for refining the comfort and utility of entry vehicles by the time their application is required. In choosing among the various possibilities, low system weight will always be a major factor of merit. Because of the current booster situation, low system weight is the dominant factor now amounting to a GO–NO-GO feasibility criterion. But in the future the opportunity will be available to trade weight for

utility. Then there will be a demand for entry vehicles with greater maneuver capability. This capability will allow entry with low acceleration loads on the crew and recovery with greater flexibility in mission planning.

Conclusions

The use of a hypersonic glider for direct entry into the atmosphere at escape speed and subsequent controlled flight to a preselected landing site has been considered and found promising.

Entry corridors on the order of 60 miles wide can be maintained with acceleration levels controlled to 6g or less by attitude modulation. Thus, crew comfort levels consistent with really reliable crew performance are assured. This entry performance can be achieved with feasible heat protection system weights. After entry, controlled glide to a previously selected landing site is possible regardless of the approach path location or orientation, while return from space can occur any time within a period of several hours.

These are the predominant performance advantages of a glider used for entry and recovery; they are the product of the basic maneuverability of a glider. The remaining question is whether these advantages justify the weight penalty that may reasonably be expected when a glider is compared with less aerodynamically sophisticated vehicles. This concept of refined entry and recovery maneuvers using a high L/D glider is submitted with the expectation that our rapidly expanding space technology will soon require such refinements and a reasonable weight penalty will be justified.

Appendix

Newtonian Lift-Drag Polars

The lift and drag coefficients for a Newtonian polar are

$$C_L = N \sin^2 \alpha \cos \alpha$$

$$C_D = N \sin^2 \alpha + \min C_D$$

where N = Newtonian coefficient, and α = angle of attack (positive values only).

The classic Newtonian coefficient is 2.0, but it is modified to 1.82 for this study as explained under Glider Characteristics. These additional relations follow from the foregoing basic Newtonian polar equation.

$$\sin \alpha_0 = \{K[1 - K^2 + (1 - 2K^2)^{1/2}]\}^{1/3} + \{K[1 - K^2 - (1 - 2K^2)^{1/2}]\}^{1/3} - K$$

$$\max L/D = \frac{\sin^2 \alpha_0 \cos \alpha_0}{K + \sin^2 \alpha_0}$$

$$\max C_L = 0.385N$$

where N = modified Newtonian coefficient, K = min C_D/N, and α_0 = angle of attack at maximum L/D.

Maximum C_L occurs at a 54$^3/_4$ deg angle of attack in all cases.

Range Equations

All glide operations are performed with essentially horizontal flight—i.e., the flight path angle is very small (less than 1/10 deg for L/D of 2) and changes very slowly with time. This allows simplification of the equations of motion leading to this familiar expression for calculating glide range in steps 1 and 3 of trans-satellite glide

$$\Delta R = (r/2)\ (L/D) \cos \phi \ln \left(\frac{1 - \bar{V}_2^2}{1 - \bar{V}_1^2} \right)$$

where ΔR = range increment, r = radius of earth, ϕ = bank angle, and $\bar{V}$ = ratio of velocity to circular satellite velocity. Subscripts 1 and 2 refer to initial and final conditions.

This equation works above and below satellite speed; but, because constant L/D and bank angle have been assumed, it is discontinuous at satellite speed.

Glide across satellite speed requires variation of attitude—either bank angle or angle of attack or both—to satisfy the equilibrium rules implied by the assumption of horizontal flight.

The following general equation works through satellite speed because bank angle has been varied to satisfy equilibrium requirements. Because angle of attack and dynamic pressure are held constant, it is a constant-drag glide. This equation is not directly applicable to the step 2 trans-satellite glide but will be modified for use as explained here:

$$\Delta R = (r/2)\ (W/C_D\ Sq)\ (\bar{V}_1^2 - \bar{V}_2^2)$$

where W/S = wing loading, C_D = drag coefficient, and q = dynamic pressure.

In step 2 of the trans-satellite glide, the initial and terminal points are on constant-attitude equilibrium glide speed-altitude schedules. For this special case, it can be shown that the last factor in the foregoing equation is given approximately by the following:

$$(\bar{V}_1^2 - \bar{V}_2^2) = \frac{2qC_L^* |\cos \phi^*|}{W/S}$$

where C_L^* = life coefficient of glide preceding 1 and following 2, and ϕ^* = bank angle of glide preceding 1 and following 2.

Step 2 of the trans-satellite glide involves variation of angle of attack at zero (or 180 deg) bank angle in order to maintain equilibrium. Angle of attack varies between zero lift and maximum L/D attitudes. The drag coefficient varies between the minimum and the value at maximum L/D. Within this variation there is an effective constant value which yields equivalent results.

NOW AVAILABLE

High Speed Aerodynamics and Jet Propulsion: Volume VIII

HIGH SPEED PROBLEMS OF AIRCRAFT AND EXPERIMENTAL METHODS

Edited by A. F. Donovan, H. R. Lawrence, F. E. Goddard, and R. R. Gilruth. **Topics include methods of performance calculation at high speed, stability and control, aeroelasticity and flutter, principles of model testing, design considerations, wind tunnel measurements, objectives of free flight research, instrumented models in free flight, free flight range methods. 994 pages. $22.50**

Princeton University Press
Princeton, N. J.

PRINCETON AERONAUTICAL PAPERBACKS

Coleman duP. Donaldson, General Editor

Presents the most-demanded portions of the important 12-volume series, *High Speed Aerodynamics and Jet Propulsion*

The newest titles:

FUNDAMENTAL PHYSICS OF GASES
Karl F. Herzfeld, Virginia Griffing, Joseph O. Hirschfelder, C. F. Curtiss, R. B. Bird, Ellen Spotz. **131 pages. #7 $1.95**

FLOW OF RAREFIED GASES
Samuel A. Schaaf, Paul L. Chambre. **55 pages #8 $1.45**

TURBULENT FLOW
Galen B. Schubauer, C. M. Tchen. **123 pages. #9 $1.45**

STATISTICAL THEORIES OF TURBULENCE
C. C. Lin. **60 pages #10 $1.45**

Please write for complete descriptive circular on the ten Princeton Aeronautical Paperbacks

Princeton University Press
Princeton, N. J.

The effective value of drag coefficient was found to be approximately

$$\text{effective } C_D = \min C_D + 1/3\ [(C_D \text{ at max } L/D) - (\min C_D)]$$

For modified Newtonian polars these drag coefficients can be expressed in terms of α_0 when higher order terms are omitted.

$$C_D \text{ at max } L/D = 3\ (\min C_D) \cos^2 \alpha_0$$

$$\text{effective } C_D = (\min C_D) \times (2/3 + \cos^2 \alpha_0)$$

Substituting the alternate form for the velocity factor and effective C_D for C_D in the range equation above and recognizing that $C_L{}^*$ is now C_L for maximum L/D and ϕ^* is either zero or 180 deg, the equation for range in step 2 is obtained:

$$\Delta R = r(\max L/D) \frac{3 \cos^2 \alpha_0}{2/3 + \cos^2 \alpha_0}$$

where α_0 = angle of attack for max L/D on the Newtonian Polar, and r = radius of earth.

Note that this range increment depends only on lift-drag characteristics and is unaffected by the altitude (or dynamic pressure) at which step 2 crosses satellite speed. This is reasonable because a lower altitude (higher dynamic pressure) crossover for which drag would be larger would also have a larger speed difference and, therefore, more energy to dissipate. However, crossover at lower altitude would reduce range in steps 1 and 3.

References

[1] Grant, Frederick C., *Modulated Entry*, NASA TN D-452, Aug. 1960.

[2] Hildebrand, Robert B., *Manned Reentry at Supersatellite Speeds*, IAS Paper 60-83, June 1960.

[3] Chapman, Dean R., *An Analysis of the Corridor and Guidance Requirements for Supercircular Entry into Planetary Atmospheres*, NASA TR R-55, Aug. 1959.

[4] Lees, L., Hartwig, F. W., and Cohen, C. B., *The Use of Aerodynamic Lift During Entry into the Earth's Atmosphere*, Jet Propulsion, Sept. 1959.

[5] Morth, Raymond, and Speyer, Jason L., *Control System for Supercircular Entry Maneuvers*, Boeing Airplane Co., Aero-Space Div., Document D2-9812, April 1961.

[6] Morth, Raymond, and Speyer, Jason L., *Divergence from Equilibrium Glide Path at Super-Satellite Velocities*, ARS Journal, March 1961.

[7] Slye, Robert E., *An Analytical Method for Studying the Lateral Motion of Atmosphere Entry Vehicles*, NASA TN D-325, Sept. 1960.

[8] Bryson, A. E., Denham, W. F., Carroll, F. J., and Mikami, K., *Determination of the Lift or Drag Program that Minimizes Re-Entry Heating with Acceleration or Range Constraints Using a Steepest Descent Computation Procedure*, IAS Paper 61-6, Jan. 1961.

[9] Creer, Brent Y., Smedal, H. A., and Wingrove, R. C., *Centrifuge Study of Pilot Tolerance to Acceleration and the Effects of Acceleration on Pilot Performance*, NASA TN D-337, Nov. 1960.

[10] Hildebrand, R. B., *Manned Return from Space*, paper presented to International Aeronautical Federation, Zurich, Sept. 1960.

[11] Flight Technology—Structures Technology Staff, *Handbook for Aerodynamic Heat Transfer Computation*, Boeing Airplane Co., Aero-Space Div., Document D2-5107, Jan. 1960.

[12] Styer, Eugene F., *A Parametric Examination of Re-Entry Vehicle Size and Shape for Return at Escape Velocity*, American Astronautical Society Preprint No. 60-87, Aug. 1960.

✦ ✦ ✦

Application of Laminar Flow Control (Continued from page 23)

ing edge sections are attached to the main structural box. There is obviously no difficulty in providing spanwise or chordwise gaps less than 0.10 in. wide.

A typical wing structure that satisfies LFC smoothness criteria is shown in Fig. 5. The slot spacing on a jet transport size wing would average approximately 2 in., being closer together near the leading and trailing edges and farther apart near the maximum thickness point of the airfoil. It should be noted that the leading and trailing edge sections serve as full depth LFC ducts. In the area of the main structural box where suction requirements are lower, ducts are part of the skin panel, and integral fuel volume is provided similar to a conventional turbulent-type wing. Wing assembly procedures are discussed in the Manufacturing Techniques section of this paper. Another paper[2] presents some structural aspects of a typical LFC wing. The type of wing structure shown in Fig. 5 is utilized on the demonstration aircraft program.

Demonstration Aircraft Program

In August 1960, the Norair Division of Northrop Corporation was awarded an Air Force contract to modify two B-66 aircraft to a laminar flow control demonstration airplane configuration. The B-66 was chosen because of its ability to simulate in size and speed the operating Reynolds number range of transport aircraft, while at the same time meeting cost and schedule considerations. The basic objectives of the program are:

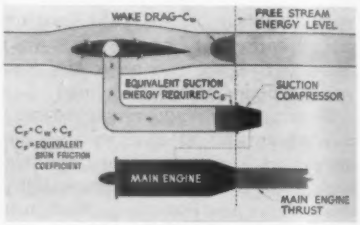

Fig. 2. LFC schematic.

(1) To demonstrate the practicality of LFC

(*a*) *Design*—To show the feasibility of integrating LFC requirements with the smoothness criteria, fuel capacity, access provisions, and fatigue integrity expected in a typical, sound wing structure.

(*b*) *Manufacturing*—To prove that LFC structure can, in fact, be fabricated successfully at reasonable cost, utilizing present state-of-the-art manufacturing techniques.

(*c*) *Operation and maintenance*—To demonstrate the compatibility of LFC with various weather conditions

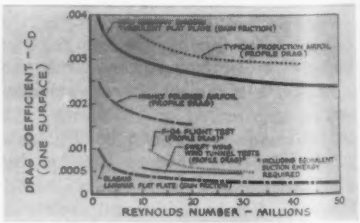

Fig. 3. Research results.

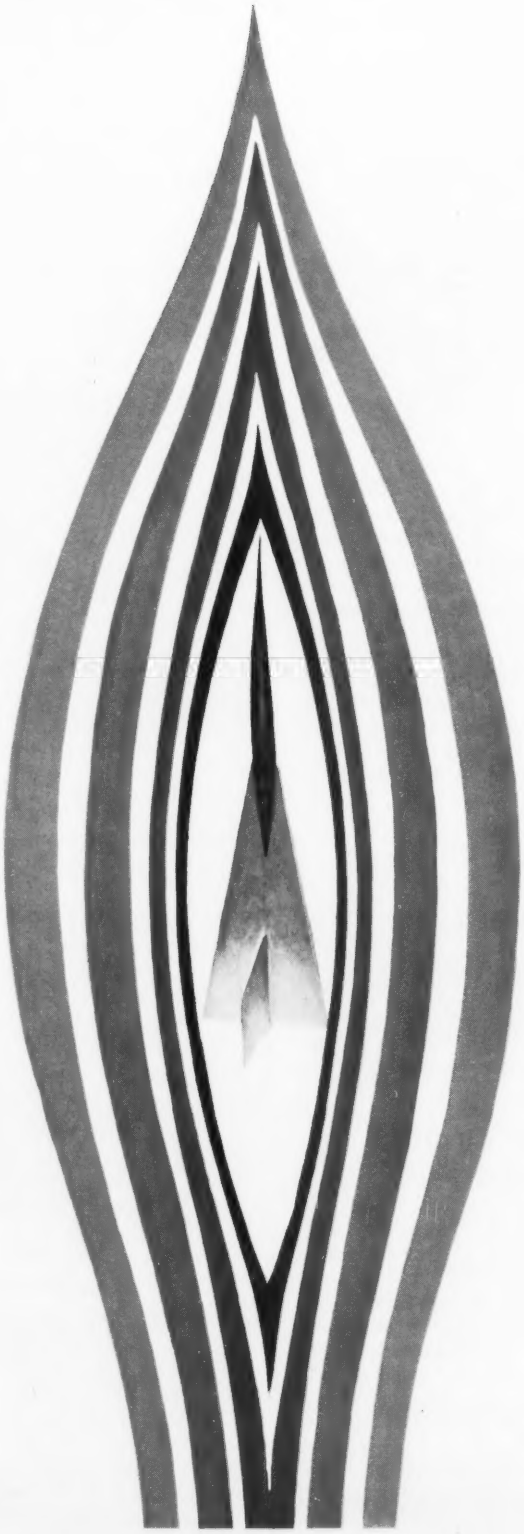

AIMED AT THE FUTURE

V/STOL vehicles for land and carrier based operations... Close Support Aircraft... expanding studies in Variable Sweep Wing Technology... antenna design and electrical-electronics systems development... these are just a few of the projects in which Boeing / Wichita engineers are engaged.

If you are a SENIOR ENGINEER qualified by experience and education to do Research, Design and Test Studies on advanced projects, you'll be interested in the career positions now open at BOEING / WICHITA.

We are seeking qualified engineers with a minimum of five years experience, either working toward or already possessing an advanced degree, preferably with experience in any of the following areas: STRUCTURAL DESIGN OR DYNAMICS, STRESS ANALYSIS, AERODYNAMICS, AUTOMATIC CONTROLS, ELECTRICAL OR ELECTRONICS, ACOUSTICS, SYSTEMS DESIGN OR APPLIED PHYSICS.

If you qualify and would like information regarding specific assignments and living conditions in Wichita, write in strict confidence to Mr. Melvin Vobach, Dept. OAO, The Boeing Company, Wichita Division, Wichita 1, Kan.

BOEING / WICHITA

An Equal Opportunity Employer

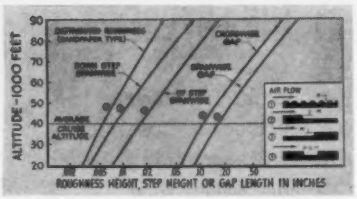

Fig. 4. Smoothness requirements.

and other operational environments normally encountered by a service-type airplane, and to establish the LFC maintenance requirements.

(2) To provide data for direct application to future aircraft systems.

The LFC airplane, illustrated in Fig. 6, offers such significant changes from the original airplane as increased wing area, aft-mounted engines, and pumping nacelles underneath the wing.

The wing area was increased from 780 to 1,250 sq ft to establish characteristics similar to typical operational LFC

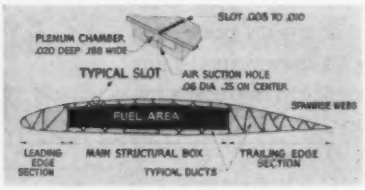

Fig. 5. Typical LFC wing section.

airplanes, such as the optimum cruise aerodynamic condition, the laminar area percentage of total airplane wetted area, take-off and landing characteristics, representative amount of fuel in the wing, and wing structural similarities. The new wing will have, for test purposes, electrical cyclic deicing equipment on a 10-ft section of the leading edge.

The aft-fuselage engine location was selected to broaden the range of LFC experimentation on the wing itself. A wide spectrum of test conditions including many off-design points has been planned to establish firmly the limits of

Fig. 6. LFC airplane.

LFC operational effectiveness, and this is most efficiently accomplished with fuselage-mounted engines. Wing-mounted turbofan engines are compatible with LFC using established acoustic criteria and sound suppression techniques.[8]

Pumping nacelles are located on the wing, as they would be on a typical jet transport. A cutaway of the LFC demonstration aircraft pumping nacelle

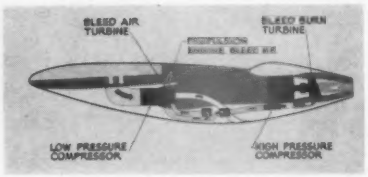

Fig. 7. LFC pumping system.

is shown in Fig. 7. The suction compressors in this case are driven by bleed and bleed-burn turbines operating on air from the main propulsion engines. In a jet transport with wing-mounted engines, the pumping system would be located within the engine pylon.

Status of the LFC demonstration aircraft program is highlighted at present by the "finalized" design of LFC slots, hole sizes, and complete duct system. Wing tooling fabrication is in progress, and ground tests of the complete airplane will start in October 1962, followed by the first flight in January 1963.

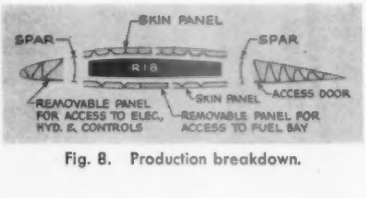

Fig. 8. Production breakdown.

Manufacturing Techniques

A typical LFC wing production breakdown is shown in Fig. 8. A notable manufacturing feature of this wing is the extensive use of proved bonding techniques to satisfy the LFC contour and smoothness requirements while assuring production costs per pound equal to conventional structures.

The upper and lower skin panels and the leading edge and trailing edge sec-

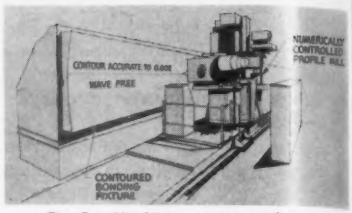

Fig. 9. Machining contoured fixture.

tions are bonded assemblies. These, in turn, are attached to each other and to the ribs and spars with mechanical fasteners.

One of the first steps in manufacturing the wing is the construction of a number of bonding fixtures approximately 4 by 20 ft in size to serve as pressure bases in the bonding operation. These fixtures match the wing surface to an accuracy of 0.002 and are wave-free. The fixture material is aluminum tooling plate, machined with a numerically controlled profile mill as illustrated in Fig. 9.

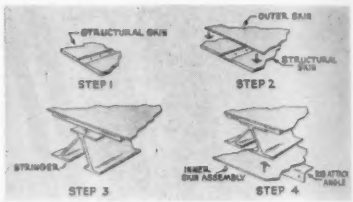

Fig. 10. Skin bonding.

Skin panels are then formed, machined as required, and put through several consecutive bonding operations as shown in Fig. 10. All bonding is accomplished by use of the previously mentioned bonding fixture as a pressure base.

In step 1 (Fig. 10), the plenum chamber grooves and suction holes are machined and drilled in the structural skin utilizing an accurately indexed tooling fixture. In step 2, the structural skin and outer cover, still unslotted, are

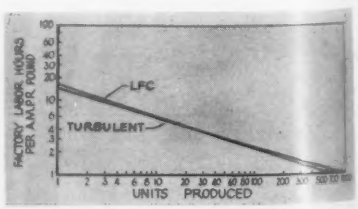

Fig. 11. Manufacturing cost comparison.

bonded together. Next, the stringers are bonded to the outer skin assembly; finally, the inner skin assembly, complete with bonded rib-attach angles, is bonded to the stringers.

The complete skin panel, approximately 4 by 20 ft in size, is then slotted using a radial-type saw attachment, accurately indexed to the same tooling fixture used in machining the plenum chamber slots and in drilling the suction holes. Slotting is accomplished on the upstroke movement of the saw blade, thus avoiding burrs on the slot edges inside the plenum chamber.

A manufacturing cost comparison between conventional turbulent structure and LFC-type structure is shown in Fig. 11. The turbulent structure referred to here is the conventional skin-

	FLIGHT LINE		PERIODIC	
	OPERATION	MAN HRS / FLT HR	OPERATION	MAN HRS / FLT HR
SURFACES	WIPEDOWN VISUAL INSPECTION	1.45	CLEANING, INSPECTION, WAVINESS CHECK, GAP CLEARANCE CHECK, SLOT CLEANOUT, REPAIR	.64
INSTRUMENTATION	RUN-UP CHECK	.19	REPAIR, CALIBRATION	.08
SUCTION EQUIPMENT	RUN-UP CHECK	.09	INSPECTION, REMOVE & REPLACE OR REPAIR COMPONENTS	1.31
	SUB-TOTALS ——	1.73		1.80

TOTAL = 3.53 MAN-HOURS OF MAINTENANCE PER FLIGHT HOUR FOR LFC, PLUS THE AVERAGE OF 15 MAN-HOURS PER FLIGHT HOUR FOR CURRENT JET TRANSPORTS

Fig. 12. LFC maintenance.

stringer-spar type of construction which actually becomes more expensive per pound than the LFC structure when large numbers are produced. This is primarily the result of fewer parts in the LFC wing, with its large bonded assemblies and lower tooling requirements.

The information shown in Fig. 11 is the result of (1) extensive manufacturing research on LFC-type structures, including tool development and operational experience, and (2) firsthand experience in the fabrication of conventional jet transport wing structures.

Conceivably, the conventional wing could be redesigned for bonded construction, but the significant feature of Fig. 11 is the fact that the high accuracy requirements of the LFC wing have been more than compensated for, from the point of view of cost, relative to conventional construction.

Maintenance Estimates

The maintenance of an LFC airplane is generally similar to that of a current jet transport. Emphasis is placed on maintaining clean, smooth LFC surfaces, primarily a wipedown operation performed at the flight line. Periodic maintenance on such items as waviness checks, trouble shooting, repairing or replacing suction equipment, etc., re-

WORLD'S MOST ACCURATE OPTICAL DIVIDING HEAD

VINCO GUARANTEES the Optical Master Inspection Dividing Head to be accurate within ± 1 second of arc; the ball bearing spindle runout to be 25 MILLIONTHS of an inch, total indicator reading; the master disc graduations to be spaced to an accuracy within ± ½ second of arc.

Shown above is a heavy duty dividing head and a dual recorder console with a ball slide electronic indicator stand. This ultra precision equipment will check and record tooth to tooth errors and accumulated errors to within 50 millionths of an inch on a 15" D.P. gear. Single recorder consoles are available.

DIVIDING HEAD APPLICATIONS

- **Inspection of missile guidance system components.**
- **Measurement of gear and spline spacing and bore relationships.**
- **Calibration of index plates, involute and master involute profiles.**
- **Calibration of lead bars or helical precision components.**
- **Inspection of two and three dimensional cams as well as ellipses, cycloids, etc.**
- **Measurement of angular transmission of motion by gears and gear trains.**
- **Measurement of angular displacement of turntables.**

SEND FOR THIS FREE EIGHT PAGE BROCHURE. THE DIVIDING HEAD IS FULLY ILLUSTRATED AND EXPLAINED.

A 720 TOOTH, 32 D.P. 14½° P.A. PRECISION GEAR

Tolerances on this 22.500" P.D. gear are .0002" involute profile; .0003" T.T.E.; .0006" T.C.E. The same craftsmen who build the world's most accurate dividing head produce gears of even closer tolerances daily for use in missile guidance systems, jet aircraft, instrumentation or wherever needed. **Call Vinco on your sub-contract requirements.**

VINCO DIV., VINCO CORP.

9111 SCHAEFER HIGHWAY • DETROIT 28, MICHIGAN

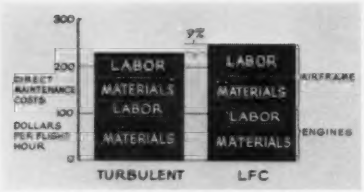

Fig. 13. Maintenance cost per flight hour.

quires no unusual skills or equipment. LFC malfunction is not a safety-of-flight item.

Northrop has accumulated 12 years' experience in the maintenance aspects of LFC through laboratory testing, exposure of test panels to various climates over extended periods of time, wind-tunnel experiments, and actual operational experience on the F-94 test airplane. This background is being further expanded through the demonstration aircraft program now in progress.

Utilizing this experience, maintenance requirements have been established to assure satisfactory LFC operation. These requirements have been applied to current jet transport aircraft maintenance procedures as shown in Fig. 12.

The 3.53 man-hours of maintenance per flight hour is in addition to the average figure of 15 man-hours for current jet transports. This is an increase of 23 percent resulting from LFC. Converting these maintenance man-hours and material costs to maintenance costs per flight hour (using the 1960 ATA formula), the results indicate only a 9 percent cost increase attributable to LFC (Fig. 13).

This 9 percent is accounted for in the direct operating costs of the LFC airplanes shown in the Design Studies section which follows.

Design Studies

Results of the research, analytical, and design efforts to date form the basis for this section of the paper, which compares performance and direct operating costs of subsonic turbulent and LFC jet transports.

Historically, as shown in Fig. 14, the rate of reduction in the skin friction drag coefficient has come to a standstill; current jet transports have reached the lowest drag levels feasible for turbulent airplanes. The coefficients shown are for the complete airplane.

The limiting condition, as indicated by the dotted line of Fig. 14, is the drag level of a smooth turbulent flat plate at approximately 40 million Reynolds number. The fact that a turbulent jet transport, with its curvatures and intersections, manages to approach this flat plate limiting condition so closely is attributable to clean aerodynamic design and to local areas of laminar flow on the airplane.

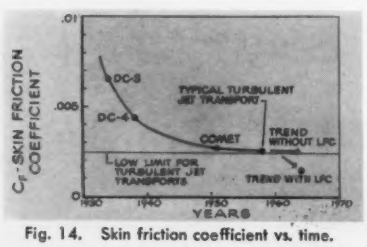

Fig. 14. Skin friction coefficient vs. time.

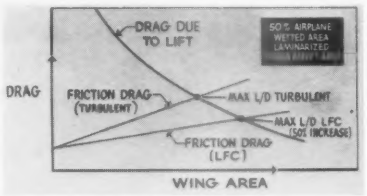

Fig. 15. Optimum wing area.

The only method of substantially changing the trend of friction drag coefficients is through LFC. The jet transport with laminar wings and empennage, potentially available in 1965, shows a friction drag of 60 percent of its turbulent counterpart.

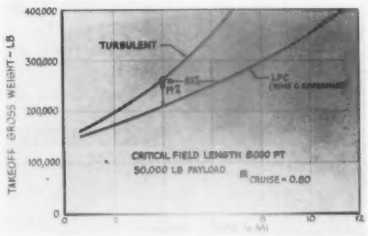

Fig. 16. Parametric comparison.

One basic result of LFC is a greater optimum wing area for the same take-off weight. The interrelation of wing area, friction drag, and drag due to lift is illustrated in Fig. 15.

The drag due to lift, primarily a function of span loading, decreases with increasing wing area, for fixed aspect ratio and fixed take-off weight (Fig. 15). But friction drag (a direct function of area) increases as the wing area increases; however, this increase is at a much slower rate for LFC airplanes because of the lower skin friction coefficients associated with laminar surfaces. The intersections of the drag due to lift curve and the friction drag curves represent the points of maximum lift-to-drag ratio for the respective airplanes, with the LFC airplane achieving its maximum lift-to-drag ratio at a lower drag level and larger wing area than the turbulent airplane. This effect raises the typical lift-to-drag ratio approximately 50 percent.

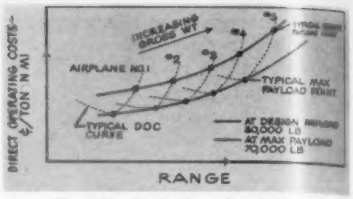

Fig. 17. Derivation of cost data.

Parametric Aircraft Analysis; Variable Gross Weight

In examining the various benefits of LFC as applied to jet transports, a parametric study was made to determine the direct operating cost variation as a function of design range for both turbulent and LFC transport aircraft. The study utilized a design payload of 50,000 lbs. at the design range. A maximum payload capability of 70,000 lbs was allowed for at the original gross weight of the design payload-range point by off-loading fuel.

As is typical of most parametric analyses, the assumption of scaled engines was included. Turbofan engines with a thrust-to-weight ratio of 4.25 and a cruise sfc of 0.78 were used. These engine characteristics are typical of current values. The wing areas are primarily a function of cruise requirements rather than take-off requirements, although no configuration used in the study exceeded an 8,000-ft critical field length. The airplanes were similar in appearance to current jet transports, and all airplanes had the same size passenger-type fuselage. The LFC air-

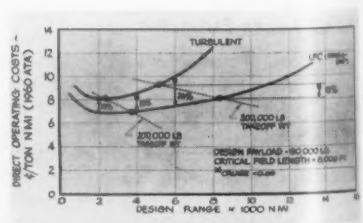

Fig. 18. Direct operating costs, parametric analysis.

WILEY BOOKS

BALLISTIC MISSILE AND SPACE VEHICLE SYSTEMS

Edited by H. S. SEIFERT, *Stanford Univ., and* KENNETH BROWN, *John Wiley & Sons, Inc.* Covers engineering design principles of missiles and space vehicles which resemble each other in everything but the trajectories followed. Attention is focused on engineering rather than on biological or space physics problems. It provides a thorough survey of the ballistic problem, including vehicle stabilization and re-entry dynamics and support system planning. The vital relationships among the many complex parts of a missile or space system are given great stress.

The whole is based on a course taught by a team, each member of which is now working at high levels in important space and missile programs.

1961. 526 pages. $12.00

STATISTICAL ANALYSIS AND OPTIMIZATION OF SYSTEMS

By E. L. PETERSON, *General Electric Co.* Analysis, synthesis, and optimization of systems where statistical uncertainty is involved in the process dynamics. Gives analytical foundations, describes computation procedures, and numerical results of specific examples.

1961. 190 pages. $9.75

ANALYSIS OF NONLINEAR CONTROL SYSTEMS

By DUNSTAN GRAHAM, *Princeton University and* DUANE MCRUER, *Systems Technology, Inc.* Key word is *analysis.* Offers basic mathematical tools for problems of stability, accuracy, and response of nonlinear systems. Illustrated with practical problems, design data.

1961. 482 pages. $9.75

TEMPERATURE MEASUREMENT IN ENGINEERING, Volume II

By H. D. BAKER, *Columbia Univ.*, E. A. RYDER, *United Aircraft, and* N. H. BAKER, *Columbia Univ.* Methods for measurements in situations arising in shop, laboratory, and field. *1961. 510 pages. $13.00*

Vol. I, 1953. 179 pages. $4.95

PROCEEDINGS OF THE FIRST SYMPOSIUM ON ENGINEERING APPLICATIONS OF RANDOM FUNCTION THEORY AND PROBABILITY

Edited by J. L. BOGDANOFF *and* F. KOZIN, *Purdue Univ.* Record of the first symposium devoted to general engineering applications of stochastic processes.

1961. In press.

DESIGN DATA IN AERONAUTICS AND ASTRONAUTICS

Edited by RICHARD B. MORRISON, *assisted by* MELVA J. INGLE, *both of University of Michigan.* Brings together information previously unpublished or scattered widely throughout the literature. All data are presented in forms convenient for analysis and computation relating to industrial, research, teaching, and military needs. Correlated data and nondimensional parameters are given wherever possible, and graphs rather than tables are used when it is desirable to show trends.

Special feature—a *Mollier Diagram for Equilibrium Air.* Includes: Atmospheric properties; thermodynamic properties of gases; fluid flow properties; aerodynamics; aerothermodynamics; performance; materials; aerothermochemical data; human tolerances.

1961. Approx. 608 pages. Prob. $12.50

THE MECHANICS OF INERTIAL POSITION AND HEADING INDICATION

By W. MARKEY *and* J. HOVORKA, *M.I.T.* A concise, rigorous treatment of the synthesis of inertial navigation systems, which can be immediately applied to practical work in the field. *1961. 92 pages. $3.95*

A GUIDE TO FORTRAN PROGRAMMING

By D. D. MCCRACKEN, *McCracken Associates, Inc.* First practical book on FORTRAN, the computer language designed primarily for scientific and engineering programming. A self-study book for those who want to program problems but don't care about computer mechanics *per se.* Includes exercises.

1961. 88 pages. $2.95

OPTIMUM DESIGN OF MECHANICAL ELEMENTS

By R. C. JOHNSON, *Yale Univ.* Introduces a method of design which is explicit in nature, can be applied to innumerable problems, minimizes cut-and-try, and takes into account inherently unavoidable limitations confronting the design engineer.

1961. 535 pages. $11.50

INTRODUCTION TO SPACE DYNAMICS

By W. T. THOMSON, *UCLA.* Stresses analytical techniques in the areas of coordinates for space motion; orbits in central force field; gyroscopic theory applied to instruments, missiles, satellites; generalized theory of dynamics from a variational approach; optimization techniques applied to rockets and trajectories.

1961. Approx. 352 pages. Prob. $11.50

Send now for your on-approval copies

JOHN WILEY & SONS, INC. 440 Park Avenue South, New York 16, N.Y.

planes had LFC on the wing and empennage.

The results are shown in Fig. 16, where each curve represents a series of airplanes, with each airplane optimized for maximum range for the weight shown. A 63 percent range improvement for the LFC airplane is shown at 260,000 lbs, a take-off weight typical of current jet transports. In comparing both airplanes at the same range of 4,000 nautical miles, the LFC airplane shows a take-off gross weight 19 percent lower than that of the turbulent airplane.

Direct operating costs as a function of range were calculated by 1960 ATA methods for each of five different gross weights for both the turbulent and LFC airplanes. These direct operating costs were plotted separately for the turbulent and LFC airplanes as represented by the numbered curves of Fig. 17.

Assuming that the curves of Fig. 17 typify turbulent aircraft, the cost curves for the LFC airplanes have the same general characteristics but are of a lower cost magnitude. In both cases, turbulent and LFC, envelope curves were drawn through the design payload points as shown by the solid line, and through the maximum payload points as indicated by the dashed line. It is evident that minimum direct operating costs are achieved at less than design range and

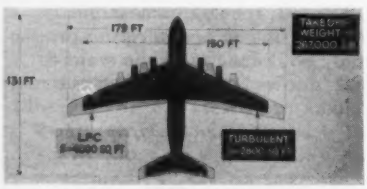

Fig. 19. Planform comparison.

at the maximum payload; but in the cost comparisons that follow, the design payload values are used to maintain a consistent relationship with the design ranges quoted. Cost reduction for LFC is relatively constant for both design and maximum payloads.

The envelope cost comparison, derived by the method of Fig. 17, for the

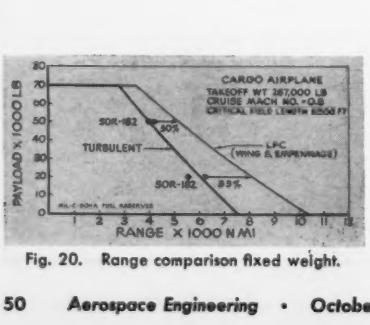

Fig. 20. Range comparison fixed weight.

turbulent and LFC aircraft at the design payload condition is shown in Fig. 18. The LFC aircraft direct operating costs vary from 14 to 26 percent lower than the turbulent aircraft over ranges of 2,000 to 6,000 nautical miles.

It is also apparent (Fig. 18) that the cost reduction through an LFC airplane is substantial when compared to a turbulent airplane of the same weight—for example, a 13 percent reduction at a gross weight of 300,000 lbs.

As impressive as these cost reductions are through LFC, it must be appreciated that these curves show optimized airplanes for each specific range, on a parametric basis, and therefore do not necessarily represent the practical operational case due to the unavailability of fractionally sized propulsion units.

In summary, it has been shown that when comparing an optimized LFC airplane to an optimized turbulent airplane

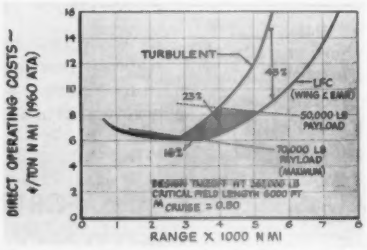

Fig. 21. Direct operating costs fixed weight.

for the same design payload-range condition, the LFC airplane provides a significant reduction in direct operating costs.

Specific Aircraft Analysis; Fixed Gross Weight

Cargo Transport

The parametric analysis showed that the optimum LFC airplane would be somewhat smaller in weight and would exhibit superior operating cost characteristics as compared to the optimum turbulent design. Consider now an existing airplane modified by incorporating LFC on a new wing and empennage. A contemporary turbulent design that meets the USAF SOR-182 requirements is considered here because of its familiarity to the industry. This design uses programed turbofan engines and meets the 6,000-ft critical field length requirement. The payload-range requirements are 50,000 lbs for 4,000 nm and 20,000 lbs for 5,500 nm.

The existing and modified airplanes are shown in the planform comparison

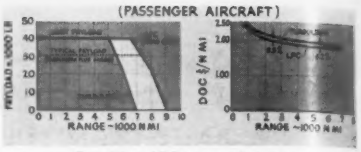

Fig. 22. LFC cost reduction.

of Fig. 19. The fuselages, wing geometry, and tail volumes are identical for each airplane. Also, they each have the same cruise speed of 0.80 Mach number.

The wing area on both airplanes is a compromise between take-off and maxi-

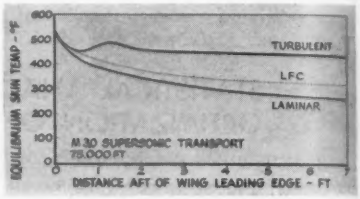

Fig. 23. Skin temperature.

mum range requirements. The take-off characteristics require that the wings are oversized, such that a 1 to 2 percent range reduction occurs. The lower drag of the LFC airplane allows the use of engines of 30 percent lower thrust than the turbulent airplane, but the take-off requirements can be maintained on the LFC airplane because of its larger wing area. The same take-off lift coefficients are used in all cases. The payload-range characteristics of the two airplanes are shown in Fig. 20.

The LFC airplane carries a 50,000-lb payload approximately 30 percent farther and the 20,000-lb payload 33 percent farther than the turbulent airplane at the same gross weight.

Fig. 21 compares the 1960 ATA direct operating costs as a function of range for the two aircraft. The LFC airplane is slightly more economical below the 2,500-nm range point. At the design payload-range point of 4,000-nm the LFC airplane shows a 23 percent reduction in direct operating costs compared to the same weight turbulent airplane. The operational advantages of the LFC airplane, carrying the same payload as the turbulent airplane, are shown by the shaded area of Fig. 21. For trans-Atlantic or Hawaii-to-Japan routes (approximately 3,500 nm), the cost reduction is approximately 18 percent for the LFC. At ranges greater than design range, such as a flight from Los Angeles to Paris (approximately

5,500 nm), the cost reduction with the LFC is dramatic—a 43 percent reduction as compared to the direct operating cost of the turbulent airplane. It is also evident from Fig. 21 that the LFC airplane carries the design payload 30 percent farther than the turbulent airplane and at a lower cost.

In summary, incorporation of LFC on an existing airplane can provide low operating costs over a broad spectrum of ranges. Small savings are available below the maximum payload point, and increasingly greater savings are available above this point. This ability to operate over greater ranges at low cost with LFC increases operational flexibility and precludes the necessity of purchasing several sizes of aircraft to obtain low operating costs at the various ranges between 2,000 and 6,000 nm.

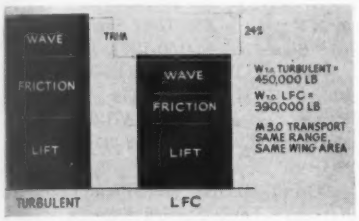

Fig. 24. Drag breakdown.

Passenger Transport

Consider now the economic advisability of LFC application to a contemporary turbofan passenger transport. Assume, in this case, that LFC is installed on the wing alone. From the payload range curve (Fig. 22), it is seen that with a nominal payload of 30,000 lbs the range is extended about 33 percent. This enables the airplane to operate on several routes that were previously impossible even with zero payload.

Fig. 22 also compares the direct operating costs in dollars per nautical mile as a function of range for the turbulent airplane and its LFC counterpart with LFC on the wing alone. For a payload of 30,000 lbs and 10 hours per day utilization, a cost reduction of approximately 6.5 percent over a wide spectrum of operating ranges results for the LFC installation. This 6.5 percent reduction in operating costs represents a saving of $2.1 million over a 10-year period. If it is assumed that the modification cost for a new wing and LFC suction system is about $1.0 million, the earning power of the passenger transport is increased by $1.1 million.

In summary, it can be seen that through the application of LFC to the wing alone on a passenger-type transport, the operational flexibility is increased, the direct operating cost is reduced, and over a wide spectrum of operating ranges the earning power of the airplane is significantly increased during its operational lifetime.

Future Trends

LFC will influence the future trends of subsonic and supersonic jet transport designs to a much greater degree than generally envisioned today. Just as the introduction of cantilever monoplanes made it worthwhile to cowl engines and retract landing gears, LFC will cause evolutionary changes in the design of airplanes to augment the basic advantages of laminar flow. These changes could substantially improve range and operating costs.

Subsonic

Initially, subsonic LFC jet transports are expected to resemble current designs for traditional reasons but will gradually change in appearance while becoming more efficient because (1) induced drag will form a larger part of the airplane drag and thus pose a challenge to develop wings of greater span while retaining present structural-weight efficiencies; (2) further aerodynamic cleanup will be worthwhile (smoother windshields, fewer bumps and fairings, lower interference drag, and more highly streamlined bodies); and (3) further reductions in friction drag will be possible through application of LFC to the fuselage and other turbulent areas.

The investigation of laminar flow on bodies, including bodies of revolution, is currently the subject of a research program at Northrop under Air Force contract. This program includes wind-tunnel testing at high Reynolds numbers and will help determine the practicality of LFC on bodies.

If LFC is applied to the major portion of the fuselage and engine nacelles of the jet transport shown in Fig. 16 (which had a design payload turbulent range of 4,000 nm and range of 6,500 nm with LFC on the wings and empennage), the range would be approximately 7,400 miles, or 85 percent greater than the original turbulent airplane.

Supersonic

The feasibility of supersonic LFC was demonstrated in 1958 with wind-tunnel tests at Mach numbers 2.23 and 2.77 on a 5 percent biconvex airfoil at a relatively low chord Reynolds number of 12.5 million.[9] Additional research is now in progress at Northrop under Air Force contract to investigate LFC on bodies and wings at high Reynolds number in wind-tunnel experiments from Mach 2.5 to 3.5.

Maintaining laminar flow on a supersonic transport has two potential advantages, lower skin temperatures and reduced friction drag. The cooler skin is due to a large reduction in the convective heat-transfer coefficient resulting from LFC (essentially a function of the lower velocity gradient in the laminar boundary layer), coupled with the effect of surface radiation. The temperature reduction is shown in Fig. 23.

All temperatures in Fig. 23 are equilibrium values and are reached in approximately 10 min. The example chosen for analysis was Mach 3.0 at an altitude of 75,000 ft. The calculations are based on simple flat plate heat-transfer coefficients for turbulent and laminar flow. LFC skin temperatures are somewhat higher than natural laminar flow, as shown. The suction air will have a total temperature only slightly higher than the external laminar surface temperature, so the duct wall temperatures will approximate those of the external surface. Results of Fig. 23 may be summarized as follows:

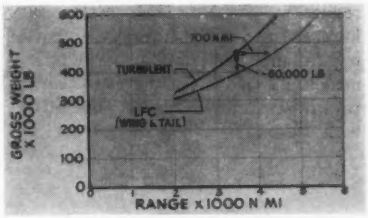

Fig. 25. M = 3.0 transport comparison.

(1) Application of LFC to the wing could reduce the equilibrium surface temperature by as much as 100°F from the turbulent boundary layer value.

(2) Equilibrium surface temperature over a large portion of the wing might be maintained below 350°F with LFC for $M = 3.0$ flight. This fact introduces the feasibility of construction materials other than steel.

(3) Application of LFC to the fuselage appears advantageous. In addition to further reducing the total vehicle drag, reducing the structure equilibrium temperature, and lowering the boundary layer noise, the cabin conditioning heat load is substantially reduced. This reduction would be about 35 percent of the turbulent flow heat load.

Friction drag continues to be a substantial percentage of the total airplane drag at Mach 3.0 and probably will increase in percentage with time as new methods develop to reduce wave drag. A typical drag breakdown for a Mach 3.0 transport, representative of airplane

types presented at the recent IATA supersonic transport conference, is shown in Fig. 24. For a fixed range of 3,500 nm, the LFC wing area remains approximately equal to that of the turbulent wing. This similar wing area provides the optimum lower wing loading for the LFC airplane as a function of less fuel and less propulsion system weight. Wave drag remains constant with the fixed percentage thickness ratio of the airfoil and the fixed wing area. Since drag due to lift is reduced only slightly, in proportion to the wing loading, the LFC reduction in friction drag contributes most significantly to the 24 percent reduction in the total airplane drag. The friction drag reduction shown assumes LFC on the wing and tail only. The resulting performance improvement shown in Fig. 25 includes a weight penalty for the LFC system.

At a design range of 3,500 nm the weight of the Mach 3.0 transport could be reduced by approximately 60,000 lbs, or the range could be increased by 700 nm. The most advantageous choice is considered to be the weight reduction from several standpoints—lower cost, present runway compatibility, take-off and landing speeds commensurate with current subsonic jet transports, and less sonic boom (lower wing loading).

Studies indicate the desirability of continuing the present research to advance supersonic LFC technology to the same high confidence level now existing at subsonic speeds.

Conclusions

Application of LFC technology is desirable for the following reasons:

(1) LFC is feasible from the standpoint of demonstrated drag reduction and practicality of construction and maintenance.

(2) LFC provides for the possibility of appreciably lower operating costs in the future development of subsonic transports.

(3) Preliminary examinations show that lower skin temperatures and lower take-off weights are made possible through the application of LFC to the supersonic transport.

References

[1] Connors, J. W., Pfenninger, W., and Smith, C. B., *Propulsion Systems for Laminar Flow Aircraft*, AEROSPACE ENGINEERING, Vol. 20, No. 8, pp. 16, 17, 70–79, Aug. 1961.

[2] Gray, W. E., and Fullam, P., *Comparison of Flight and Tunnel Measurements of Transition on a Highly Finished Wing (King Cobra)*, RAE TN Aero 2383, June 1950.

[3] Groth, E. E., Carmichael, B. H., Whites, R. C., and Pfenninger, W., *Low Drag Boundary Layer Suction Experiments in Flight on the Wing Glove of an F-94A Airplane. Phase II—Section Through 69 Slots*, Northrop Corp., Norair Div., Report NAI-57-318 (BLC-94), Feb. 1957.

[4] Pfenninger, W., and Bacon, J. W., Jr., *About the Development of Swept Laminar Suction Wings With Full Chord Laminar Flow*, Northrop Corp., Norair Div., NOR-60-299 (BLC-130), Sept. 1960.

[5] Carmichael, B. H., *Critical Reynolds Numbers for Multiple Three-Dimensional Roughness Elements*, Northrop Corp., Norair Div., Report NAI-58-589, July 1958.

[6] Carmichael, B. H., *Surface Imperfection Experiments on a Swept Laminar Suction Wing*, Northrop Corp., Norair Div., Report NOR-59-454, Aug. 1959.

[7] Wieder, J., and Pfenninger, W., *Structural Aspects of Low Drag Suction Airfoils*, IAS Paper No. 61-150-1844, June 1961.

[8] Rooney, T. R., Carmichael, R. F., and Eldred, K. M., *Investigation of Noise With Respect to the LFC, NB-66 Aircraft*, Northrop Corp., Norair Div., Report NOR-61-10, April 1961.

[9] Groth, E. E., and Pfenninger, W., *Boundary Layer Suction Experiments on a 5% Thick Biconvex Airfoil Section at M = 2.23 and 2.77*, Northrop Corp., Norair Div., NAI-58-195 (BLC-105), March 1958.

IAS/Army Aviation Meeting Proceedings

This 68-page book contains *unclassified* papers and figures presented at the IAS/Army Aviation Meeting, April 13–14, 1961, Washington, D.C.

IAS Member Price—$2.50 Nonmember Price—$5.00

Frontiers of Science and Engineering Proceedings

Contains papers and figures presented at the Frontiers of Science and Engineering Symposium, cosponsored by the Los Angeles Section of the Institute of the Aerospace Sciences and the University of California, Sept. 16–17, 1959.

IAS Member Price—$5.00 Nonmember Price —$10.00

Special Publications Dept., IAS, 2 E. 64th St., New York 21, N.Y.

High Altitude Wind Observations (Continued from page 17)

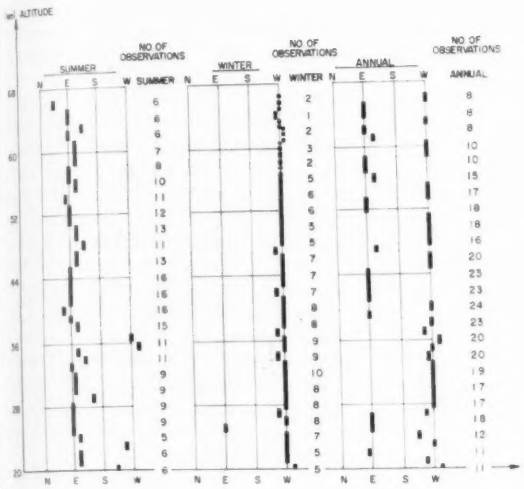

Fig. 2. High-altitude prevailing wind by rocketsonde observation, April 12, 1959, to May 25, 1960, Cape Canaveral.

intervals. The data were interpolated at 500-meter intervals of altitude. Shear was then computed for each 1,000-meter altitude layer and attributed to the midpoint of the layer.

Care should be exercised in interpreting the reduced wind data because smoothing methods used in the computer operations tended to reduce certain wind speed and shear values. Also, in some cases the use of chaff targets gave abnormally high wind speeds and shears. The chaff targets dispersed over an area of several square kilometers, and the radar focused on the point of strongest signal return which often shifted from one point to another. Such abrupt shifts caused abnormal speeds, shears, and directions to appear in the reduced data, thereby requiring careful editing.

Simultaneous tracking of the rocketsonde targets by two or more radars has made a comparative check of the computed wind values possible. Similar comparisons of the overlapping portions of the rawinsonde wind measurements show that there exists an uncertainty in the rocketsonde wind speed of approximately 8 meters/sec or 10 percent of the computed wind speed, whichever is greater. With careful investigation and correction of the more radical data points measured, averages should be reasonably accurate even though individual data points are questionable. This agrees favorably with other comparable error analyses.[4,5]

Presentation

While data from 37 soundings were used, not more than 24 observations were available for any single altitude level. When fewer than five observations were available for a given altitude level, the data are shown on the graphs by dashed lines. Data were summarized for the winter months of October through March, for the summer months of April through September, and for the entire year. Because of dissipation of the chaff targets, few observations extended below 20-km altitude. No observations were made at altitudes above 84.5 km; consequently, most of the graphical data are confined to the 20- to 66-km altitude range.

Analysis of Data

Inspection of the arrowgram (Fig. 1) shows that winds from any direction can occur at almost any altitude or during any season, at least occasionally. However, when the measured winds are summarized (Fig. 2), it becomes apparent that easterly winds prevail during summer months and westerly winds prevail during winter months. On the rare occasions when easterly winds do occur in winter months or westerly winds in summer months, they seem to be characterized by low velocity at altitudes up to approximately 70 km. Annual prevailing winds—i.e., those directions which occur most frequently—fluctuate between easterly and westerly according to the data presented here, probably because more observations were made during summer months when easterly winds prevail than in winter when westerly winds prevail. If an equal number of observations had been made during winter and summer months, it is likely that the annual prevailing winds would be predominantly westerly at almost all altitudes.

A minimum wind speed was observed at an altitude of 23 km[6] (Fig. 3). Above this point, mean wind speed increases with altitude up to at least 64 km, and possibly higher, to another region of

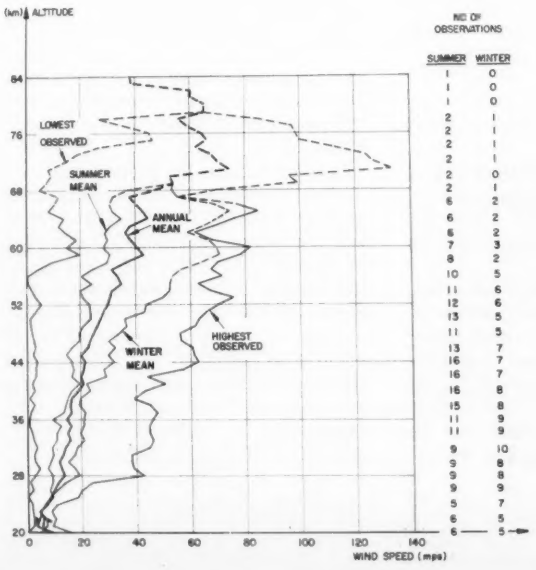

Fig. 3. High-altitude wind speed by rocketsonde observation, April 12, 1959, to May 25, 1960, Cape Canaveral.

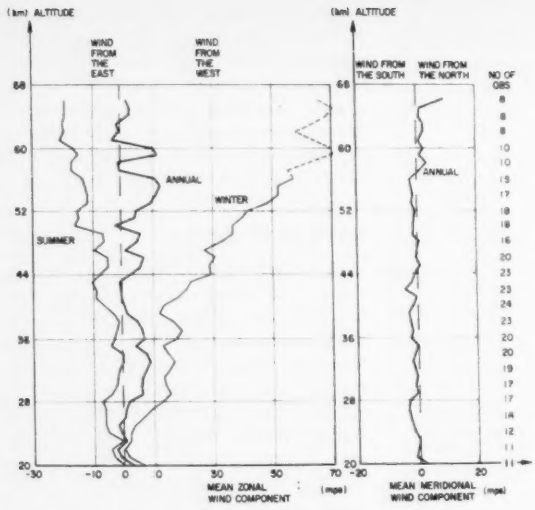

Fig. 4. High-altitude wind components by rocketsonde observation, April 12, 1959, to May 25, 1960, Cape Canaveral.

maximum wind speeds apparently centered near 70 km.[5,7] The maximum wind speed observed in this rocketsonde series was 133 meters/sec from the southwest at an altitude of 71 km; it occurred in winter. The summer maximum was 99 meters/sec from the east-southeast at 69-km altitude. Winter winds were considerably stronger than summer winds, except at the wind speed minimum which occurs at an altitude of approximately 23 km. The stronger winter winds were especially noticeable at higher altitudes. These observations agree favorably with the findings of other studies.[8]

Easterly winds first appear at altitudes above 50 km in late April, and westerly winds first occur in late October. Unfortunately, no observations were made in early October, and very few were made during the month of April. More observations will be required to confirm the date at which the reversal of prevailing wind occurs; however, it appears likely that this reversal occurs within a very few days.

Meridional wind components are generally small, and the annual meridional wind resultant is nearly zero, although southerly winds seem to occur slightly more often at altitudes below 57 km (Fig. 4). Seasonal meridional wind components reverse so frequently that they are omitted.

The summer zonal wind components are easterly, and the winter zonal wind components are westerly and much stronger than the summer easterlies (Fig. 4). While approximately 60 percent of the observations were made during the summer months and 40 percent were made during the winter,

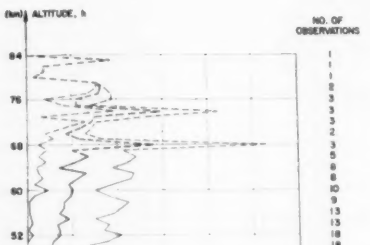

Fig. 5. High-altitude wind shear by rocketsonde observation, April 12, 1959, to May 25, 1960, Cape Canaveral. (Shear Δh = 1,000 meters.)

the combined resultant for the annual summation is mainly westerly because the wind speed is greater for the westerly winds.

The wind shear, the partial derivative of the wind vector with respect to altitude, averages less than 0.01 inverse sec/1,000-meter altitude layer up to 60 km (Fig. 5). The highest shear in this study, 0.0523 inverse sec/1,000-meter altitude layer, was measured at an altitude of 68 km. Because of errors inherent in the method of observation,[5] the values of shear data obtained might not be exact, but there is evidence to substantiate an increase in the magnitude of wind shear at higher altitudes.

Conclusion

The mean rocketsonde wind speed observed in the high altitudes above Cape Canaveral ranges from 5 meters/sec at an altitude of 20 km to 40 meters/sec at an altitude of 58 km. Individual observations range from nearly zero to 133 meters/sec. Winds from any direction can occur at almost any altitude or during any season, but summer winds are predominantly easterly and winter winds are predominantly westerly and stronger. Meridional wind components are small, and zonal wind components are westerly and strongest in winter. Wind shear ranges from nearly zero to more than 0.05 inverse sec/1,000 meters and increases in magnitude with increases in altitude. At altitudes up to 59 km, the mean wind shear is less than 0.01 inverse sec/1,000-meter layer.

The data on high-altitude wind characteristics presented here are intended for the use of design and operations personnel concerned with missile and space vehicle test flights from Cape Canaveral (AMR), Florida.

References

[1] Geissler, E. D., *Problems in Altitude Stabilization of Large Guided Missiles*, Aerospace Engineering, Vol. 19, No. 10, pp. 24–25, 68–72, Oct. 1960.

[2] aufm Kampe, H. J., *The Meteorological Rocket Network*, Weatherwise, Vol. 13, No. 4, pp. 192–195.

[3] Webb, W. L., and Jenkins, K. R., *Application of Meteorological Rocket System*, Journal of Geophysical Research, Vol. 64, No. 11, pp. 1855–1861, Nov. 1959.

[4] Smith, Lawrence B., *The Measurement of Winds Between 100,000 and 300,000 Feet by Use of Chaff Rockets*, Journal of Meteorology, Vol. 17, No. 3, pp. 296–310, March 1960.

[5] Rapp, R. R., *The Accuracy of Winds Derived by the Radar Tracking of Chaff at High Altitudes*, Journal of Meteorology, Vol. 17, No. 5, pp. 507–514, May 1960.

[6] Armstrong, C. L., and Garrett, R. D., *High Altitude Wind Data from Meteorological Rockets*, Monthly Weather Review, Vol. 88, No. 5, pp. 189–190, May 1960.

[7] Batten, E. S., *Wind Systems in the Mesosphere and Lower Ionosphere*, Journal of Meteorology, Vol. 18, No. 3, pp. 283–291, June 1961.

[8] Murgatroyd, R. J., *Winds and Temperatures Between 20 km and 100 km—A Review*, Quarterly Journal of The Royal Meteorological Society, Vol. 83, No. 358, pp. 417–449, 1957

Personnel Opportunities

This section is for the use of individual members of the Institute seeking new connections and eligible organizations offering employment to specialists in the aero/space industry. Any member or eligible organization may have requirements listed without charge by writing to the Secretary of the Institute.

Wanted

Engineers and Scientists—Electronics Research Directorate of the Air Force Cambridge Research Laboratories announces professional staff vacancies for **Engineer** (Electronics); **Physicist** (Electronics, Electromagnetics, Plasmas, Solid State); **Mathematician**; **Chemist** (Physical, Analytical, Nuclear). These vacancies are within the Federal Civil Service and offer liberal leave benefits, payment of expenses incurred by employees and their families in moving to Bedford, an extensive program of sponsored education, and an opportunity to pursue a stable program of non-time-oriented research. Graduate level scientific personnel interested in positions described are invited to write or call Francis McWilliams or John Cooney, at CRestview 4-6100, Ext. 3633 or 3758 at Hanscom Field, Mass.

Professors—The Air Force Institute of Technology, Wright-Patterson AFB, Ohio, has a vacancy in the Department of Mathematics. Most of the work is at advanced undergraduate and graduate levels. One quarter out of four free of teaching duties for research or other academic pursuits, plus vacation. Working conditions comparable to those in leading universities. Employment will be effected in accordance with Civil Service regulations. Rank and salary will depend upon qualifications of applicant and may be anywhere between assistant professor, GS-11, $7,560, and full professor, GS-14, $12,210. Applications should be made on Standard Form 57, available at any Post Office or by letter to Head of the Department of Mathematics.

Aerodynamicists—Cornell Aeronautical Laboratory has attractive openings for qualified scientists to perform research in the following areas: (1) magnetoaerodynamic effects on the flow over blunt bodies; (2) flow field analyses at hypersonic velocities and low densities; (3) aerodynamic characteristics of simple geometry hypersonic configurations; (4) aerodynamic aspects of air-data sensing at hypersonic flight conditions; (5) base heating of clustered rocket nozzle configurations; (6) structure of air heat transfer due to turbulent boundary layers at hypersonic Mach numbers. The Laboratory provides a desirable combination of the best features of industry as to financial and facilities resources coupled with a university associated atmosphere conducive to R&D activity at the highest level. Salary commensurate with qualifications and experience. Send complete résumé to A. A. Rentschler, Cornell Aeronautical Laboratory, Inc., 4455 Genesee St., Buffalo 21, N.Y.

Notices of all change of address should be sent to the Circulation Department, Institute of the Aerospace Sciences, Inc., 2 East 64th Street, New York 21, N.Y., at least 30 days prior to change of address.

The number preceding the notice represents the Box Number of the Institute of the Aerospace Sciences to which inquiries should be addressed.

138. Professor of Aerospace Engineering—Positions now available in department of aerospace engineering of state university. Openings are in areas of aerospace structures, aerodynamics, and magnetoaerodynamics. Rank and salary will depend upon qualifications of applicant. Liberal research and consulting policies. Furnish résumé with reply.

Available

137. British Aircraft Designer (AFIAS)—Interested in consultation and formation of design team in United Kingdom. Would be prepared to consider any design consignment. Work would be completed rapidly and at nominal cost. Résumé on application.

136. Aeronautical Engineer—Thirty years' experience—civil approval of power plants, power-plant supervisor with aircraft manufacturer, chief of AEDC engine test facility; also manager, engineering sales and advanced proposals. Desires engineering applications and Government contacts for advanced propulsion and space systems. B.S. in M.E. and LL.B. Ohio resident.

134. Project or Engineering Manager—Broad background in aeronautical and ballistic missile design and management. Experience in establishing structural design, criteria, performance of operational analysis, and weapon system analysis and development. Considerable experience as project manager handling all phases of design, budgeting, program planning, and support activities for an operational military system. Age 44. AFIAS. Reg. Prof. Eng. Desires position in program planning, project management, engineering management or at staff level.

133. Aeronautical Engineer—Thirteen years' experience in high-speed wind-tunnel testing, data reduction, and data analysis. Ten years in a supervisory capacity. Experience includes research activities, technical report preparation, and aerodynamic data analysis. Work also accomplished in the field of plasma generation in connection with arc-heated wind-tunnel development and employment as a testing facility. West Coast location desired; other locations considered. Résumé furnished on request.

132. Director—Research, Engineering, or Planning—Age 39, M.S. in A.E., Registered P.E., AFIAS. Eighteen years' extensive experience in scientific and management fields as consultant, director of research, and general manager with well-known company in aerospace and related fields. Has proved capabilities in planning, organizing, and administering successful programs—completed on schedule and at a profit. Familiar with USAF, USN, Army, and many commercial companies' plans. Desires responsible position with dynamic growth company.

131. Engineer—M.E., M.S. Fifteen years' experience in research and development on electromechanical devices and systems. Includes 9 years in design and evaluation of inertial guidance components and systems. Now Manager of Analysis for large manufacturer.

130. Engineer - Designer - Draftsman—Age 50. Thirty years' experience in drafting, design, and engineering of airframes. turbine engines, automotive parts, fans, blowers, superchargers, airmotors, valves, and fittings. Two years in aircraft engine stress analysis. Registered Professional Engineer (M.E., Indiana). Salary open. Résumé on request.

129. Aero/Mechanical Project Engineer—Seeking position with a growing, stable company. Over 10 years' diversified background as a project, development, and application engineer in aircraft structural and mechanical design; electromechanical, hydraulic, and pneumatic controls; rotating machinery including small turbines. Familiar with control dynamics, filament wound fiberglass structures, and cryogenics. B.S. Aero Engineering, Post Graduate Industrial Management. Former USAF and civilian pilot. Prefer a medium-sized equipment company in Northeastern coastal location. All replies considered. Résumé on request.

An Authorized Binding for *Aerospace Engineering*

Arrangements have been made by the Institute of the Aerospace Sciences for members and subscribers to have their magazines bound carefully and economically. Simply write for details to:

Publishers' Authorized Bindery Service Ltd.
430 West Erie St.
Chicago 10, Ill.

Early Blind Flying (Continued from page 15)

"On September 4–5, 1922, I flew a DH-4...It was the first time the North American continent had been crossed in less than 24 hours." *(IAS Photo, gift of Albert R. Crocker, from the Sherman Fairchild Collection of Aeronautical Photographs)*

the magnetic compass, the altimeter, and the airspeed indicator.

It was customary on cross-country flights to follow railroads, or less frequently, highways, and the maps generally used were the standard Rand McNally maps of the individual states. These state maps were each about the same size so, unfortunately, were usually not to the same scale.

Please excuse me if in the following I seem to talk too much about myself. The personal experiences are related to illustrate conditions which affected all fliers of the era.

On September 4–5, 1922, I flew a DH-4 airplane in which additional gasoline and oil tanks had been installed from Pablo Beach, Fla.—near Jacksonville—to Rockwell Field at San Diego, Calif., with one intermediate stop for fuel at Kelly Field, San Antonio, Tex. The elapsed time was 22 hours and 35 minutes. It was the first time the North American Continent had been crossed in less than 24 hours.

It was also the first airplane in which I had used a bank and turn indicator. To obtain the instrument, it was necessary to go the the Army Air Service Engineering Base at old McCook Field in Dayton, Ohio, and "promote" an experimental model through the help of cooperative technical friends. This instrument, invented in 1917 by Elmer Sperry, Sr., built by Elmer Sperry, Jr., and first flight tested by Lawrence Sperry with Elmer, Jr., as passenger, was not yet in common usage or generally available.

Took off just after dark and arrived at Kelly Field soon after daylight. Was quickly refueled and immediately proceeded to Rockwell, arriving there in the late afternoon. Had chosen a moonlight night to facilitate night flying, but about 4 hours out ran into solid overcast and then severe thunderstorms.

For a while the lightning flashes were almost constant and, in the otherwise black night, so intense as to light up the ground clearly for a considerable area. Some flashes were so close that their familiar ozone odor could be detected, but, although it seemed that one could reach out and touch them, none struck the plane.

The air was extremely turbulent and the airplane was violently thrown about its axes as well as up and down and, despite its excellent stability characteristics, was held on a relatively even keel only with great concentration and effort. After the lightning died away, the turbulence appeared to intensify and there was about an hour in the jet black darkness when no ground reference point could be seen; it would have been quite impossible to maintain proper attitude and course without the blessed bank and turn indicator.

Although I had been flying for almost five years "by the seat of my pants" and considered that I'd achieved some skill at it, this particular flight made me a firm believer in proper instrumentation for bad weather flying.

In 1925 I did a thesis here at M.I.T. for a Doctor of Science degree in aeronautics.

At first I had hoped to study, through carefully controlled flight tests, the possibility—or impossibility—of a specially trained pilot orienting himself without flight instruments and determining certain phenomena, such as wind direction, without reference to a visible horizon or point on the ground.

The original subject matter was not sufficiently abstract for the doctorate, so it was changed to an analysis of "The Effect of the Wind Velocity Gradient" employing flight tests, wind-tunnel data, and mathematical analyses.

The thesis starts:

There has long been an uncertainty in the minds of avia-

Forging a metal spectrum for any flight environment

Whether design criteria be Mach 2 or escape velocity — the part a wing spar or rocket motor nozzle — most of the significant advances in forging conventional, exotic and refractory materials come from Wyman-Gordon. Here, technical breakthroughs in size, complexity and strength-to-weight ratios of forged airframe hardware and propulsion components have materially raised performance ceilings for every type of vehicle — global bomber to deep space probe capsule. Always impatient with state-of-the-art concepts, Wyman-Gordon engineers and metallurgists constantly explore ways to bring hitherto "unforgeable" metals and alloys into operational use — broadening the spectrum of ultimate-performance materials available for advanced vehicle designs. Consultation on your project requirements can help achieve better correlation of materials to service environment.

CURRENTLY FORGING THESE AERO-SPACE MATERIALS

Aluminum	Beryllium
Titanium	Molybdenum
Magnesium	Tantalum
Columbium	Zirconium
Hafnium	Tungsten
Inco 718	René 41
Astroloy	Waspaloy
Stainless steels	Vacuum-melt alloys
Nickel-base alloys	Iron-base, high-temperature alloys
High-strength die steels	20-27 Nickel steels

EST. 1883

WYMAN-GORDON

FORGINGS

of Aluminum Magnesium Steel Titanium . . . and Beryllium Molybdenum Columbium and other uncommon materials

HARVEY ILLINOIS — WORCESTER MASSACHUSETTS — DETROIT MICHIGAN

GRAFTON MASSACHUSETTS — LOS ANGELES CALIFORNIA — PALO ALTO CALIFORNIA — FORT WORTH TEXAS

tors regarding the effect of the wind on the flying qualities of an airplane.

Some pilots claim that it is much easier to turn into the wind than with it, and that at any altitude they can tell the wind direction by the feel of the ship in a turn and this even though in a dense cloud which would preclude the possibility of obtaining their relative motion from any stationary object.

Other pilots maintain that, regardless of the wind velocity or the proximity of the ground, there is no difference in the feel of the plane when turning into the wind and when turning with it. They claim that any apparent difference is due wholly to the psychological effect on the pilot, resulting from the difference in ground speed in the two cases, and if there is any difference in the ships' performance, from a time altitude standpoint, it is because the pilot handled the controls differently. In other words, if the pilot were blindfolded, he could not tell the wind direction when turning, and a turn made into the wind would be identical with a turn made with the wind. This is, of course, considering the turn in relation to the medium in which it is being executed and not in relation to the curves traced out on the ground.

There is a similar difference of opinion regarding the effect of a strong wind on the rate of climb. Experienced pilots are about evenly divided, half feeling that a plane climbs better into the wind, and the other half feeling that the wind makes absolutely no difference.

Seven of the leading pilots of the day were questioned regarding the effect of the wind on flying performance. The answers given were far from consistent, as might be expected from such a group of individualists. There was therefore still considerable confusion—and controversy—among the experts.

The conclusions from the thesis, somewhat oversimplified, were that, in airplane flight,

(1) There is no measurable effect in level flight, at altitude, due to wind direction so long as the wind is steady.

(2) There is no effect on climb due to wind except very near the ground, and there the wind velocity gradient increases the rate of climb slightly when flying into the wind and decreases it slightly when flying with the wind.

(3) A steady wind has no effect on turning except very near the ground when the wind velocity gradient causes a slight tendency to settle when turning away from a head wind and a slight tendency to climb when turning into it. This is most noticeable in strong winds and when flying at a large angle of attack or at minimum power.

SUMMING UP: A steady wind exercises no measurable effect on airplane performance at altitude—except, of course, on ground speed and direction of flight. Very near the ground, however, the effect of wind velocity gradient can be serious, particularly in the case of a heavily loaded airplane. The danger is increased by a strong tendency on the part of the pilot to pull the nose up or in beyond the most efficient angle of attack. This increases any tendency to settle and may even cause the airplane to stall and spin in.

In the early and middle 1920's the Jones-Barany revolving chair test was given to all military pilots as a part of their periodic physical examination for flying. Normally, this test was given with the pilot's eyes open, and the flight surgeon looked for variations in times and amount of the rhythmic side-to-side movement of the eyes called nystagmus.

In early 1926, Capt. (later Col.) David A. Myers,

"The first important expenditures made by the Full Flight Laboratory were for two modern airplanes." One, relates Gardner Lecturer Doolittle, was a Consolidated NY-2 military training plane which mounted a special landing gear with long oleo action instead of pontoons. This is the NY-1. *(IAS Photo, from the Sherman Fairchild Collection of Aeronautical Photographs)*

an outstanding Air Corps flight surgeon, decided to augment the routine test by giving an additional test consisting of several rotations of the chair with the pilot's eyes closed. After the rate of rotation became steady, a normal pilot, with eyes closed, could not tell which way he was turning. If the rate of rotation was slowed down and stabilized at a somewhat lower speed, the pilot thought the rotation had been stopped and, when the rotation actually was stopped, he thought he was turning in the opposite direction.

The explanation is that man normally maintains his equilibrium by sight, touch, hearing, muscle, and vestibular sense. Touch and hearing are not important in flight orientation. By using the three remaining senses he can usually ascertain and maintain his position, accurately sense the rate and direction of his motion, and generally orient himself with relation to the earth. Sight is by far the most reliable of these three senses, and when sight is lost, we must get our sense of balance and motion from the muscles and from the fluid movement sensors in the vestibular canals. If an individual is merely displaced, the fluid motions return to zero very rapidly, but if one is rotated it may take from 5 to 25 seconds for the fluid motions to stop. During this period an individual can experience a false sense of motion called vertigo. This, of course, explains why early-day pilots flying in dense fog or clouds frequently became completely confused and occasionally spun in and crashed.

Captain (later Col.) William C. Ocker, an early and extremely competent Army Air Corps pilot and flight researcher, had long been interested in instrument flying and in 1918 had tested the then new bank and turn indicator.

In mid-1926 he took Captain Myers' new "blindfold test." His first reaction was that Captain Myers had played a trick on him or, if not, that his senses had failed him. After further consideration he decided that there was proof positive that no normal pilot could consistently fly "blind" without instruments.

Ocker, who had had considerable experience flying with the bank and turn indicator—he frequently carried one, a quickly attachable unit complete with venturi, in his flight baggage—believed this instrument could correct the pilot's faulty senses. He designed a lightproof "black box" which contained a bank and turn indicator and a magnetic compass. This box was mounted on the front of the Jones-Barany chair. The pilot sealed his face against the opening in the box and observed the bank and turn indicator and compass. With this piece of equipment he could correctly identify the direction and rate of his rotation. After the rotation stopped and the compass settled down, he could then determine heading.

Myers and Ocker continued their experiments, and the arrangement of black box and revolving chair were patented and subsequently used in the training of pilots. Later some pilots were to learn to fly by instruments alone before they learned to fly under normal visual conditions.

In the late twenties and early thirties, Capt. Ocker and 1st Lt. (later Col.) Carl J. Crane collaborated on the study of instrument flying techniques and developed, among other things, a unitary arrangement of instruments which would give the pilot a maximum of useful flight information with a minimum of effort and fatigue. They referred to this as a "flight integrator."

In 1932, Maj. Ocker and Lt. Crane wrote *Blind Flight in Theory and Practice* (published by the Naylor Printing Company). This book gave an excellent analysis of the problems inherent in instrument flying and their solution. It was for many years the standard reference on instrument flying.

Daniel Guggenheim was one of the great industrialists, philanthropists, and citizens of the 20th Century. He was interested in everything that could lead to a fuller life and a better world. One of his many great contributions was the Daniel Guggenheim Fund for the Promotion of Aeronautics. It

Latest in . . . CAMBRIDGE AERONAUTICAL SERIES

THE THEORY OF SUBSONIC PLANE FLOW

by L. C. Woods

Fellow of Balliol College, Oxford University

A concise and systematic treatment of two-dimensional subsonic, inviscid fluid motion and its aeronautical applications.

Part I — Survey of the relevant fluid dynamics. (Assumes knowledge of fluid dynamics at introductory level)

Part II — Development of the methods of conformal mapping and Cauchy integrals — useful for the treatment of elasticity and diffusion problems, as well as aeronautical ones. (Assumes elementary understanding of complex variable theory)

Part III — Applications of the methods to several important problems in fluid and aerodynamics. This is the first book to give an extensive account of mixed boundary-value problems and to treat such examples as occur in ventilated wind-tunnel theory, jet-flap theory, and unsteady Helmholtz motions.

The book is fully indexed and contains a valuable table of references. *$22.50*

CAMBRIDGE UNIVERSITY PRESS
32 East 57th Street, New York 22, N. Y.

was established for the purpose of promoting the advancement of the art, science, and business of aviation. It proved to be a very effective medium in the accomplishment of that purpose.

The Fund was established in January 1926 with a grant of $2.5 million. (The previous year $500,000 had been given to New York University for the purpose of starting aeronautical education.) The Fund, in cooperation with the Government, was to be administered by a board of trustees composed of men of "eminence and competence." Harry Guggenheim, gifted son of Daniel and a World War I naval aviator, was chosen president of the Fund. In the initial stages of its organization, Rear Adm. H. I. Cone, an outstanding naval officer, was vice-president. Then, until the Fund's work was completed, Capt. (later Vice Adm.) Emory S. Land of the Construction Corps of the U.S. Navy held this position. The strength of character, sound judgment, organizational ability, understanding, and capacity for cooperation of Harry Guggenheim and Capt. "Jerry" Land were, in large part, the cement which held the Fund together, enabled it to function efficiently, and permitted its considerable contributions.

The general purposes of the Fund were defined as follows:

(1) To promote aeronautical education both in institutions of learning and among the general public.

(2) To assist in the extension of fundamental aeronautical science.

(3) To assist in the development of commercial aircraft and aircraft equipment.

(4) To further the application of aircraft to business, industry, and other economic and social activities of the nation.

The basic concept of the Fund was "to maintain a simple, inexpensive directing organization depending on established outside agencies, whenever possible, to carry out the aims of the Fund." It was to be a primer—a spark plug—to stimulate interest and promote action.

From the first it was understood that flight safety and reliability were important considerations and that one phase of the Fund's work might certainly be to study means of assuring safe and reliable flight despite weather conditions. With this in mind, a special committee of experts was organized to define the problem, and a directive was prepared which authorized study regarding

(1) Dissipation of fog.

(2) Development of means whereby flying fields may be located from the air regardless of fog.

(3) Development of instruments to show accurately the height of airplanes above the ground so as to replace barometric instruments now in general use showing height above sea level.

(4) Improvement and perfection of instruments allowing airplanes to fly properly in fog.

(5) Penetration of fog by light rays.

To assist in carrying out pertinent parts of this directive, the directors of the Fund decided in 1928 to establish a Full Flight Laboratory at Mitchel Field, Long Island, N.Y., with all necessary facilities and equipment. In August 1928, I was borrowed from the Army Air Corps to head this laboratory. Professor William G. Brown of the Aeronautics Department of M.I.T. joined us as technical assistant in February 1929. Bill Brown worked with the Fund's Full Flight Laboratory from then until it was dissolved at the end of 1929. His technical knowledge and unbounded enthusiasm provided a constant help and inspiration.

This was a most interesting period in my life. The Good Book says, "No man can serve two masters for . . . he will hold to one and despise the other." I had three—an Army boss, Lt. Col. (later Maj. Gen.) Conger Pratt, Commanding Officer of Mitchel Field where I was stationed; Capt. Land of the Navy; and Mr. Guggenheim, a civilian. They were all such fine, understanding, and cooperative people that my existence, instead of being complex, was uncomplicated and extremely pleasant.

Our first activity in the Full Flight Laboratory

The second Full Flight Laboratory aircraft was a Navy-type Vought Corsair O2U-1 "to be used for cross-country practice flying." *(IAS Photo, from the Sherman Fairchild Collection of Aeronautical Photographs)*

IAS/ARS JOINT MEETING

LOS ANGELES, JUNE 13–16, 1961*

IAS/ARS MEMBER PRICE—$0.50 each **NONMEMBER PRICE—$1.00 each**

61-88 -1782 Trends in Air Cargo—H. Carter & J. Jackovich

61-89 -1783 Factors Underlying the Future Domestic Market for Air Cargo Service—G. Busch & K. Mayer

61-91 -1785 Air Trailer Transportation—W. Ligon

61-92 -1786 Economics of Air Eligibility—L. Regan & G. Harris

61-95 -1789 Maximizing Reliability for One-Shot Space Missions—S. Morrison

61-96 -1790 One-Shot Mission Success for Minimum Cost—W. Cox & W. Harter

61-104-1798 Short Haul Air Transportation—W. Kennedy

61-105-1799 Aerodynamic Characteristics of Subsonic V/STOL Transport Airplanes—M. Kelly & C. Holzhauser

61-106-1800 Application of Laminar Flow Control to Transport Aircraft—W. Gasich

61-115-1809 Prediction of Optimum Approach & Landing Techniques-Manned Reentry Gliders—L. Gaines & T. Surber

61-116-1810 Second Order Theory of Entry Mechanics into a Planetary Atmosphere—W. Loh

61-118-1812 Instrument Flight Simulator Study of VTOL Controllability-Control Power Relationship—J. Patierno & J. Isca

61-119-1813 Design Characteristics of a Lifting Fan V/STOL Logistic Transport—E. Kazan & W. Bergen

61-120-1814 Influence of Two-Dimensional Stream Shear on Airfoil Maximum Lift—R. Vidal

61-123-1817 Age Concept of Management for Ground Environment Area—S. Tremaine

61-124-1818 Universal Program-Comparator Checkout Equipment & Logistical Considerations—E. Metsker & M. Beeson

61-125-1819 Role of Operational Analyses in Planning Effective Missile Ground System—S. Firstman

61-126-1820 Compiling of Automatic Test Equipment Programs—E. Quinn and C. Chipps

61-129-1823 Study of Solid-Fuel Ramjet Applications—P. Munter

61-134-1828 Description of Weapons Assignment Research Model (WARM)—R. Totschek

61-135-1829 General Purpose Simulator for Airborne Computers—E. Carter

61-143-1837 Design Alternatives for In-Flight Maintenance—R. Demaree

61-144-1838 Human Engineering Principles of Design for In-Space Maintenance—L. Pigg

61-146-1840 Predicting Human Reliability-Implications for Operations & Maintenance in Space—R. Kaufman, T. Oehrlein and M. Kaufmann

61-147-1841 Some Experiments of Human Maintenance Behavior—M. Grodsky

61-149-1843 Unified Engineering Theory of High Stress Level Fatigue—S. Valluri

61-150-1844 Structural Aspects of Low Drag Suction Airfoils—J. Wieder and W. Pfenninger

61-151-1845 Leading Edge Design with Brittle Materials—F. Anthony and A. Mistretta

61-158-1852 Mercury Animal Program—J. Henry and J. Mosely

61-162-1856 The Mini-Recorder System—J. Renfro

61-183-1877 Directive Non-Oriented Reflectors as Passive Satellites in Long Distance Communications—Y. Stahler and A. Johnson

61-190-1884 The Magnetic Particle Clutch–A Versatile Control Element for Rocket Systems—B. Grau & B. Chubb

61-194-1888 X-15 Flight Simulation Program—N. Cooper

61-195-1889 Piloted Simulation Studies of Re-entry Guidance & Control at Parabolic Velocities—R. Wingrove & R. Coate

61-196-1890 The Simulator as a Human Factors Research Tool for Manned Space Flight—G. Simon

61-210-1904 Flow Past Slender Blunt Bodies–Review & Extension—R. Capiaux and L. Karchmer

*See page 70 for other IAS publications available.

Order by number from: Special Publications Dept., IAS, 2 E. 64th St., New York 21, N.Y.

✦ ✦ ✦

The IAS Library

Publications treated in *International Aerospace Abstracts* are maintained by the Library for use by the IAS Membership. They are *not* for sale but are made available through the facilities of the Library.

LENDING SERVICES: Institute members, both Individual and Corporate, may borrow periodicals, reports, and books for a period of 2 weeks, excluding time in transit. Excepted are certain reference books and those IAS publications that may be purchased.

PHOTOCOPY SERVICES: The Library is equipped to provide, as a service, positive photocopies of certain materials in its collections. Rates on request.

For detailed information about these and other services, write to:

John J. Glennon, Manager
Technical Information Service
Institute of the Aerospace Sciences, Inc.
2 East 64th Street
New York 21, New York

was to study and endeavor to analyze the work previously done on blind landing in fog.

In England tethered balloons had been lined up with the landing field and used with some success in still air and when the fog was not thick. This concept we abandoned at once as unsatisfactory, for experience had indicated that the fog layer might be very thick and still air could not be depended upon at all times when visibility was restricted—for example, in a blizzard.

In both England and France the lead-in cable idea was tried. In this system an electrified cable circled the field and led into a landing. It required very sensitive sensing equipment in the airplane, and it was necessary to make a precision turn into the field at low altitude. This turn presented considerable difficulty.

Lieutenant LeRoy Wolf of the Army Air Corps also experimented with the electrified cable concept at Wright Field.

The U.S. Navy had some success, with an electromagnetic cable guide at the Lakehurst Naval Air Station.

The low-frequency radio range had been developed by the Bureau of Standards and the Army and was in limited use for aerial navigation. An adaptation of this radio range in the form of a radio homing beacon seemed to offer the greatest promise for our use. It could also be readily tied in with the radio receiver and other conventional airborne equipment.

Actual blind landings had been attempted with dragging weights and long tail skids. These either gave an indication upon touching the ground or were rigged to actuate the aircraft control.

There was additional background information but the material outlined here was fairly representative.

The first important expenditures made by the Full Flight Laboratory were for two modern airplanes. One, a Consolidated NY-2 military training plane mounting a J-5 engine, was to be used in the instrument landing experiments and to test instruments, equipment, or devices that might be helpful in overcoming fog flying problems. It had the large wings used by the Navy for pontoon seaplane training, but mounted, in place of the pontoons, a specially reinforced landing gear with long oleo action. As a training plane it had a very high factor of safety, was extremely rugged, and was inherently stable about all three axes. (Special flying and landing wires permitted the rigging in of additional dihedral.)

The acceptance test flight on this airplane was made November 3, 1928, at the factory near Buffalo, and the airplane was flown to Mitchel Field the next day. It was flown considerably in November and December and then delivered to the Radio Frequency Laboratories in Boonton, N.J., to have voice radio installed. It was at Boonton for 4 weeks this first time and frequently thereafter.

The second airplane was a Navy-type Vought Corsair 02U-1. It mounted a Pratt & Whitney Wasp engine. It was to be used for cross-country practice flying and was an excellent airplane for the purpose. It was a fast, good-flying airplane, but not so rugged and stable as the NY-2. The 02U-1 was delivered to the Fund on November 21, and the first cross-country flight—to Boston, with Harry Guggenheim as passenger—was made on the same day.

The Army Air Corps made a hangar available at Mitchel Field for the use of the Full Flight Laboratory. It was initially provided for the safe airplane competition, another important contribution of the Fund. The Army also provided the full-time services of an excellent mechanic to maintain the Laboratory's aircraft. This was Cpl. (later Sgt.) Jack Dalton. The continued excellent mechanical condition of the two aircraft thereafter was largely the result of his competence and devotion.

Lieutenant (later Brig. Gen.) B. S. Kelsey was made available by the Army Air Corps as flight assistant and safety pilot. When flights were made under the hood it was necessary, in the interest of safety, to have another pilot in the airplane to look out for other aircraft and also to make sure that the pilot under the hood did not get into difficulty because of instrument or equipment failure. Ben, from the start, was a full-fledged member of the team and did much of the experimental work. His piloting help, criticism of tests carried out, sound technical counsel, and ever-pleasant personality contributed greatly to the results achieved.

As the preliminary practice flights progressed, it soon became apparent that, even with the very stable and sturdy NY-2, the available instruments were not adequate. For determining heading when maneuvering and when landing, the compass, because of the northerly turning error, was entirely unsatisfactory and the bank and turn indicator, though excellent for its purpose, was more a qualitative than a quantitative measuring instrument. Also, at the moment of touch-down in a blind landing, it was desirable that the wings be level with the ground. This was not easy to assure, particularly when the wind was gusty.

An accurate, reliable, and easy-to-read instrument showing exact direction of heading and precise attitude of the aircraft was required, particularly for the initial and final stages of blind landings.

Two German artificial horizon instruments, the Anschutz and the Gyrorector, were studied but were not deemed entirely satisfactory.

I sketched a rough picture of the dial for an instrument which I thought would do the job and showed it to Elmer Sperry, Sr., a great engineer and inventor who had established and headed the Sperry Gyroscope Company and who was very interested in aviation. It was, in substance, the face of a directional gyro superimposed on an artificial horizon. He advised that a single gyroscopic instrument could be designed to meet the requirements

but recommended, for simplicity of construction, two separate instruments. I agreed and he then assigned his ingenious son, Elmer, Jr., to work with us and to be responsible for the design and fabrication of the two instruments. We could not have had a better colleague. Elmer also soon became a member of the team and spent as much time at the hangar and at the evening "discussion" sessions in our quarters on Mitchel Field as the rest of us. Out of this, as you know, came the Sperry artificial horizon and the Sperry directional gyroscope which still, with their descendants, are on the instrument panel of every airliner and military airplane today.

As time progressed, literally hundreds of blind and simulated blind landings were made. To make a landing, the airplane was put in a glide at 60 mph, with some power on, and flown directly into the ground. Although this was about 15 mph above stalling speed, the landing gear absorbed the shock of landing and, if the angle of glide was just right, the airplane didn't even bounce. Actually, after a while, it was possible to make consistently perfect landings by this method. To assure just the right amount of power in the glide, a mark was placed at the proper place on the throttle quadrant.

Excellent cooperation was obtained from every organization and individual with whom we worked. Among them were the Pioneer Instrument Company, the Taylor Instrument Company, the Radio Corporation of America, and the Bell Telephone Laboratories, who installed the modern radio transmitter and provided miniature earphones with molded plugs. Along with the other BTL personnel, Capt. Russell Luff Meredith and Capt. Ray Brooks, recently retired from the Army Air Corps, were very helpful, as was the Aircraft Radio Corporation of Radio Frequency Laboratories which installed the excellent radio receiver. Dr. L. M. Hull, the President, Dr. A. W. Parkes, Dr. F. H. Drake, and all members of the staff were most cooperative. Plus the Kollsman Instrument Company, the Sperry Gyroscope Company, and many other industrial concerns, scientists, engineers, inventors who helped and just well-wishers. All helped.

Valuable support was received from the Bureau of Standards which designed and installed most of the ground and airborne radio navigation equipment. Dr. Harry Diamond and his associates of the Bureau spent much time with us and could not have been more cooperative.

While aural signals were satisfactory for rough aerial navigation, it soon became apparent that a visual indicator would be much better for the precise directional control required in blind landings.

To meet this requirement, the Bureau of Standards, working with the Airways and Radio Division of the Department of Commerce, designed a 2-kw, semiportable, two-leg range, which was used as a homing beacon, and a fan-type marker beacon. The homing range was installed on the west side of Mitchel Field. The marker beacon sat on the leg of the homing range and was located on the east side of the field.

The indicator for the former, carried in the airplane, was a pair of juxtaposed vibrating reeds. If to the right of the course, the right reed vibrated through the greater amplitude. If to the left of the course, the left reed vibrated more vigorously. If on course, both reeds vibrated through the same arc. As the station was approached, the amplitude of vibration increased. If the amplitude of vibration became too great, it could be reduced through use of a rheostat.

A single reed started to vibrate as the fan-type marker beacon was approached. It reached maximum amplitude, then quickly dropped to zero when the airplane was directly overhead, rapidly built up to maximum again, and then tapered down. The homing range indicator also had a distinct null when the airplane was directly over the range station.

As the tests progressed, the instrumentation and equipment were constantly improved until toward the end of 1929, during the final stages of the flight tests, the following instruments and equipment were carried:

(1) Normal engine instruments
(2) Magnetic compass
(3) Earth inductor compass
(4) Bank and turn indicator
(5) Directional gyro
(6) Artificial horizon
(7) Air-speed indicator
(8) Altimeter
(9) Rate of climb indicator
(10) Outside air thermometer
(11) Vibrating reed homing range indicator
(12) Vibrating reed marker beacon indicator

Considerable thought was given to the location or arrangement of each instrument in order to facilitate reading and reduce pilot fatigue. Fatigue led to errors, and piloting errors could not be tolerated in instrument landings.

Small instruments were preferred to the more conventional, larger ones because, even though somewhat harder to read individually, the small instruments permitted more compact and logical arrangement and were easier to read and interpret en masse. It was soon determined that small instruments could be made easier to read by the use of broader hands with white or radium paint applied to the outer half of their length.

It was found that the instruments could be read more quickly, and over a longer time period with less fatigue, if the arrangement of instruments and the position and direction of motion of the indicating hands was "natural." Also, any abnormality or improper indication should be detectable automatically by a quick glance at the instrument panel. This did not "solve" instrument flight but did simplify it.

The airplane, in addition to its flight instruments, carried a RFL radio receiver, a BTL radio trans-

mitter, two 6-inch Pyle national landing lights, and a parachute flare.

A larger-than-customary Leece-Neville generator was installed on the engine to assure an adequate and continuous electrical supply.

The mast-type receiving antenna, which was employed to minimize directional effect, required considerable development before a tendency to vibrate under certain flight conditions could be corrected.

A trailing wire antenna was used for transmission in normal flight. This was reeled in, and a fixed wire antenna was used for transmitting when landing.

The specialized ground equipment consisted of a radio receiver and transmitter which provided voice communication with the aircraft and a Kollsman sensitive altimeter with which the altimeter in the airplane was synchronized by radio.

In addition, there were the visual homing range and the visual fan-type marker beacon previously mentioned, and, of course, the standard Mitchel Field Army-type aural beacon to lead an aircraft to the vicinity of the airfield.

Two problems that were available very much on the minds of the Fund directors were collision of aircraft in the air and formation of ice on the wings, structure, propeller, and in the carburetor of aircraft, when atmospheric conditions were conducive to icing.

Dr. W. C. Greer and Dr. Merrit Scott at Cornell University carried out work, under Fund sponsorship, on the underlying causes of ice formation on aircraft.

The Fund also sponsored the work done by John P. Kilgore of New Haven, Conn., on an electrically heated wing blanket for deicing.

The Full Flight Laboratory did no development work on deicing equipment, but many test flights were made under icing conditions to determine effects and limitations.

The NY-2 was frequently out of commission while new instruments or equipment were being installed. These were convenient periods for cross-country flying practice under unfavorable weather conditions in the O2U-1. This airplane had all necessary flight instruments but no blind landing equipment.

An extreme example of a cross-country bad weather flight took place on March 15, 1929. I took off from Buffalo in the O2U-1 headed for Mitchel Field. It was night and the weather was fair and improving at Buffalo but marginal to the south and east. This was to be a difficult flight but possible and just the sort of thing required to establish flight "limitations." In a pinch I could return to Buffalo any time up to the point where nearly half of the gasoline supply was used up.

I well realized that the pilot who flew within his limitations would probably live to a ripe old age, whereas the pilot who flew beyond them would not. I also knew that different pilots had different limitations.

This was pointed up in the mid-twenties when I was a test pilot at old McCook Field. At that time there were few facilities and little ground equipment to do environmental testing on new airborne devices. It was therefore necessary to test them out in flight, and the test pilots spent many hours flying around the airfield to see how a new device held up under the accelerations, vibrations, and changes in temperature and pressure experienced in flight.

Lieutenant Alex Pearson always spent these hours practicing precision flying—for instance, holding constant speed and altitude. As a result he became extremely proficient and could fly a better speed course or do a smoother saw-tooth climb than any of the rest of us.

I spent the hours flying low in the vicinity of McCook Field and on the main air routes in and out memorizing the terrain. I knew every high building, tree, silo, windmill, radio tower, and high-tension line in the area. I could therefore fly in—or under—adverse weather safely when other equally experienced pilots didn't fly. This was not because I was a better or more daring pilot than my colleagues. Constant practice had just extended my limitations.

The trick was to learn your limitations, gradually expand them, but never go beyond them.

I thought I was being pretty sharp but the Commanding Officer, learning that I frequently flew in that area when other pilots did not, thought differently. Unaware of my training plan, he removed me from the job of chief pilot in the flying section, advised me that I didn't have judgment enough to be a pilot, and assigned me to the airplane section as an aeronautical engineer.

All of these things went through my mind as the weather deteriorated. I planned to fly contact all the way so, in order to avoid the mountains, took the route Buffalo, Rochester, Syracuse, Utica, Schenectady, Albany, and then down the Hudson River.

There was no particular problem getting to Albany, but from there on the ceiling and visibility became marginal.

Soon I had passed "the point of no return" and no longer had gasoline enough to go back to Buffalo.

At one place I found it expedient to slow down and hover with the left wing of the airplane over a brightly lit southbound passenger train traveling along the east side of the Hudson River. Presently it went through a cut and wiped me off. This was too hazardous, so I left the train behind and followed the river bank. Considered crossing the river and landing in the parade ground at West Point, but abandoned this idea as the weather remained flyable—barely.

Upon reaching the lights and heat of the City of New York, the ceiling and visibility improved

slightly. Flew south to the Battery hoping to be able to get to Mitchel Field from there, but the East River and the area to the south were "socked in" so I could not go on. Tried to get to Governor's Island and land on the drill ground, but it was fog-shrouded.

Turned north back up the Hudson intending to land on the Yonkers Golf Course which I knew well, but the fog was below the river bank so had to abandon that idea.

Returned to the Battery with the intention of crash-landing in Battery Park. A chap ran out into the middle of the Park and waved me off. He apparently thought I mistook it for a flying field.

It is interesting to note that the George Washington Bridge across the Hudson at 179th Street was under construction at this time. There were as yet no suspension cables or other horizontal structure. Only the great vertical piers on each side of the River had been completed. I had passed the east pier three times without seeing it.

About this time it appeared that a crash-landing in the River might be necessary, so I removed my parachute in order to be able to swim ashore.

The water, on closer inspection, looked uninviting so decided on a final try—this time for Newark Airport—and headed across the Hudson. As soon as the River was crossed and the lights south of Jersey City appeared, it became obvious that this last chance was impractical. Thereupon pulled up into the fog and climbed through it. It was only about a thousand feet thick and crystal clear above. Intended to fly west until past the highly populated part of the metropolitan area and then jump. The gasoline gage had been fluttering on zero for some time. Noted about this time that my parachute harness was off and promptly put it on.

About over Kenilworth, beyond Elizabeth, saw a revolving beacon through a hole in the fog and a flat-looking area adjacent to it with no lights. Hoping it might be an emergency field or at least an open area (although realizing that it might be a wood or lake), turned the landing lights on and dived through the hole and scouted the area. The bottom of the fog was still very low, and I tore the left lower wing badly on a tree top. The airplane still flew, although almost completely out of gasoline, so I returned to the most likely spot and crash-landed. Took the impact by wrapping the left wing around a tree trunk near the ground. The O2U-1 was completely washed out—quite beyond repair—but I was not even scratched or bruised.

The moral of the story is that with the NY-2 mounting blind landing equipment and the Full Flight Laboratory radio station alerted at Mitchel, this would have been a routine cross-country flight with "no sweat."

The flight pointed up the importance of constant radio communication between the aircraft and the ground and the need for frequent and accurate weather reports obtainable by radio during flight in order to assure safe continuation or indicate suitable alternate destinations. It also indicated the desirability of a special light to mark emergency fields for night landings. Later green lights were used.

In general, the weather a pilot could fly in safely was a function of airplane characteristics, ground facilities and procedures, ground and airborne equipment and instrumentation, general pilot skill, and his specialized knowledge of the local aids to air navigation, the terrain, and the weather conditions to be expected in the area.

An important requirement in instrument landing was to have a precise measure of altitude when approaching the ground for a landing.

The conventional barometric altimeters of the day measured, at best, to the nearest 50 or 100 feet. It would be handy if an altimeter were available that, near the ground, would measure to 10 or even 5 feet.

The Kollsman Instrument Company developed such an instrument and on August 30, 1929, I was very pleased to take Paul Kollsman and his new instrument up on its first test flight (in the second O2U—a more modern O2U-2 purchased after the crash of the O2U-1). Mr. Kollsman held the sensitive altimeter in his lap during the flight and it performed perfectly. Here was another important addition to flight instrumentation. We promptly obtained one and installed it in the NY-2.

This instrument had two hands and a multiplication factor of twenty between them. Actually the fast-moving hand made one complete revolution for each 1,000-foot change in altitude, which meant a movement of about $^{5}/_{32}$ inch for 20 feet altitude. This was over an order of magnitude more accurate than earlier altimeters.

Although the Kollsman altimeter provided a considerable advance in instrumentation, it still measured the barometric altitude or height above sea level. An instrument which would measure the height above the ground regardless of changes in barometric pressure would be of great value.

With this idea in mind, several companies were encouraged to work on a sonic altimeter. One built by Sperry was tested out in the NY-2. A note on a frequency of about 950 cycles was directed at the ground from a megaphone on the bottom of the airplane and picked up by a detector on the airplane after having been reflected back from the ground. The elapsed time interval was measured, as in a marine "fathometer," and the altitude above the ground thus determined. The concept was theoretically sound, but in its initial form the equipment caused considerable drag and was unduly large, heavy, difficult to install, and complicated. It also appeared that a radio altimeter measuring the phase

difference of radio waves reflected back from the ground offered more promise.

Several radio altimeters were under development—with Fund encouragement—so the sonic altimeter experiments were abandoned.

Although major emphasis was given in the Full Flight Laboratory to flight tests designed to permit flying safely and reliably despite fog, the Fund, and the Laboratory, were also interested in experiments on the penetration of fog by light rays and on the dispersal of fog.

Studies on fog penetration were made by Dr. Anderson of the University of Washington and Dr. Barnes of Bryn Mawr College under Fund sponsorship, and by Dr. Julius A. Stratton of M.I.T. for Col. E. H. L. Green. The visual, infrared, and ultraviolet parts of the spectrum were carefully explored.

It was concluded that, though there was some difference in penetration due to wave length, there was little likelihood of finding any visual light which would penetrate thick, dense fog. Dr. Stratton's further investigations gave some promise that at very short wavelengths—below one centimeter—there was a possibility that fog might be penetrated by dispersal.

In addition to the scientific studies carried out, various inventors presented ideas for fog penetration, all of which received careful consideration.

Four basic methods of fog dispersal were originally considered:

Mechanical

Here the concept was to have a large propeller or series of propellers "churn up" the fog.

Chemical

Experiments carried out by Henry G. Houghton, Jr., of M.I.T., using hygroscopic materials, showed some promise both in the Laboratory and in full-scale tests which were conducted on the estate of Colonel Green in South Dartmouth, Mass.

Electrical

From the early 1920's Dr. Warren of Hartford, in collaboration with the Army Air Service, had been experimenting with cloud and fog dispersal by means of electrified sand particles dropped from an aircraft. He was occasionally successful in dispersing small clouds.

Mr. Flowers experimented with fog dispersal through the use of electrified water particles and achieved some interesting results.

Heat

Experimentation on, and the actual accomplishment of, fog dispersal by heat has been carried on until fairly recent times.

FIDO—Fog, Intense Dispersal of. FIDO was effectively used in World War II on three of the long emergency and ten of the main landing fields in England. It consisted of powerful heat sources at intervals along the runways which heated the air to a temperature above the dew point, and the nearby fog was thereby dispersed.

Approximately 2,500 bombers and fighters—mostly RAF but including some USAF—returning from missions and finding their home base, and much of England, covered in pea soup fog were directed to the cleared "tunnels in the fog" over these FIDO fields and safely landed.

Perhaps I should mention here that the Eighth Air Force Bomber units in England were being trained and equipped to operate "blind"—without FIDO—and at the end of the war two groups could take off and land regardless of fog. In short time, the entire force would have been so trained.

In the late forties successful FIDO experiments were carried out at the Naval Air Base at Arcata on the coast of northern California. Arcata was chosen because it was in one of the foggiest areas on the entire Pacific Coast. Southwest Airways successfully used the Navy fog dispersal system from November 1947 until November 1949.

In 1953, a FIDO installation was made at the Los Angeles International Airport. The cost for installation, modification, and test was $1,325,000. While the installation appeared to handle moderate fogs fairly well, it did not satisfactorily disperse dense fogs where the visibility was one eighth of a mile or less. The dispersal difficulties seemed to arise from the great amount of heat required, the airport configuration, and the movement and intrusion of the fog. Further operational problems resulted from infrequent use of equipment and the high cost of installation, maintenance, and operation. It was also anticipated that there would be difficulty experienced in moving passengers to and from the airport and in moving aircraft to and from the cleared runway when the fog was really dense. The following year the FIDO program was abandoned at Los Angeles.

It appears that FIDO would be a successful way of coping with intense fog only when the air is comparatively still. When there is any considerable movement of the air—and fog—particularly if the movement has a component across the runway, the cleared air mass moves on and new fog comes in faster than it can be dispersed. Difficulties are also experienced in an absolutely dead calm because of conduction, particularly at runway intersections and elsewhere where there are no burners.

The Full Flight Laboratory's first experience with FIDO—of sorts—occurred in 1929.

Mr. Reader of Cleveland operated a gravel pit and utilized a large blowtorch type of heater to dry the gravel and sand. He observed that if there was an intense fog when he turned the heater on, the fog in the immediate area dispersed.

Learning of the Guggenheim fog flying experiments, he wrote giving information of his experience and advising that he was interested in helping solve the fog problem.

He was invited to bring one of his heaters to Mitchel Field where it was installed just east of the last hangar.

For several months thereafter we waited in vain for a dense fog. Finally, on September 24, 1929, it came. Someone, I think it was Jack Dalton, awakened just before daylight and noted that there was a zero-zero fog covering the area. Our gang was quickly called together.

We immediately notified Mr. Reader who arrived shortly thereafter. Mr. Guggenheim was also notified but he had to come from Port Washington and didn't arrive until later.

The equipment was fired up, but the fog did not disperse except in the immediate vicinity of the blow torch. The experiment was a disappointing failure. At the time we considered the concept impractical and the equipment was removed.

In retrospect, it appears that the trouble was probably fog movement or possibly the absence of a mineral mass to store and reflect the heat. Also, for satisfactory fog dispersal over a considerable area, about two orders of magnitude more heat energy would seem to be required.

Though we were all disappointed we were there, and the fog was there, so I decided to make a real fog flight.

The NY-2 was pushed out of the hangar and warmed up. The ground radios were manned and the radio beacons were turned on. I taxied out to the middle of the field and took off. Came through the fog at about 500 feet and made a wide swing coming around into landing position. By the time I had landed 10 minutes after take-off, the fog had just started to lift.

At about this time Mr. Guggenheim, along with several other people, arrived so we decided to do an "official," under the hood, flight. I'd just made a real flight in the fog so wanted to go alone, but Mr. Guggenheim insisted that Ben Kelsey be taken along as safety pilot. The fog had lifted considerably by this time and he was afraid there might be other aircraft in the vicinity.

We both got into the airplane and the hood over my cockpit was closed.

The engine was again warmed up and I taxied the airplane out and turned into the take-off direction on the radio beam. Took off and flew west in a gradual climb. At about 1,000 feet the airplane was leveled off and a 180° turn was made to the left. This course was flown several miles and another 180° to the left was made. The airplane was lined up on the leg of the radio range located on the west side of Mitchel Field and a gradual descent started. Leveled off at 200 feet above the ground and flew at this altitude until the fan beacon on the east side of the airfield was passed. From this point the airplane was flown into the ground, using the instrument landing procedure previously developed. Actually, despite previous practice, the final approach and landing were sloppy. This entire flight was made under the hood in a completely covered cockpit which had been carefully sealed to keep out all light. The flight, from take-off to landing, lasted 15 minutes. It was the first time an airplane had been taken off, flown over a set course, and landed by instruments alone. This was just 10 months and 3 weeks from the first test flight of the NY-2.

The tests carried out thus far indicated, among other things, that before all-weather flying would be practical there was a need for

(1) Better coordination between the long-range aural beam and the short-range visual landing beam.

(2) Accurate measurement of distance along the landing beam.

(3) A slant glide beam at right angle to the vertical landing beam which might be curved to become tangent to the earth rather than intersect it in a straight line.

(4) The possibility of automatic volume control on the receiving radio.

(5) A good gyro pilot to assist the pilot in flying the aircraft. This could be, and later was, tied in with the instrument landing systems.

(6) Much more work on ignition shielding not only to reduce noise but to permit flight in heavy rain.

At the end of 1929, the Fund was disbanded. It was felt that it had made the necessary initial contribution and that further development could better be carried out by other organizations. The Full Flight Laboratory went out of existence with the Fund, and the NY-2 was turned over to the U.S. Army Air Corps and moved to Wright Field where instrument landing experimentation and development were continued under the direction of 1st Lt. (later Maj. Gen.) Albert Hegenberger.

The Bureau of Standards and the Bureau of Air Commerce of the Department of Commerce also continued their work and on March 20, 1933, James L. Kinney, with William La Violette as mechanic and Harry Diamond as passenger, flew a Bellanca airplane by instruments alone, from College Park, Md., to Newark Airport, a distance of about 200 miles. He landed blind using the recently developed bent landing beam. The weather was actually below minimum.

The Collier Trophy is awarded each year to an individual or group "for the greatest achievement in aviation in America, with respect to improving the performance, efficiency, or safety of aircraft, the value of which has been thoroughly demonstrated by actual use during the preceding year."

In 1934 the Collier Trophy was awarded to Capt. Albert Hegenberger, U.S. Army Air Corps, for the development and demonstration of a successful blind landing system.

On May 9, 1932, Capt. Hegenberger made the

first solo blind flight, alone in the plane, depending solely upon instruments from take-off to landing.

Over a period of years he and his colleagues had greatly improved the equipment previously used and developed additional equipment. He devised a blind landing procedure which became standard military practice. This system was put into actual use in 1934.

Flying by instruments had outgrown the early experimental phase. It was a practical reality, and aviation had entered a new era.

✦ ✦ ✦

High Stress Level Fatigue

(*Continued from page 19*)

Experimental Basis of the Theory

Generally speaking, the fatigue damage from which the crack is formed is localized near the surface of the specimen.[1] The cracks start in broad slip bands, traces of which persist during electropolishing treatments, and the fatigue cracks are found to start quite early in the life of the specimen.[1] Grooves and ridges are formed on the surface of the specimen along the slip bands, and the ridges sometimes develop into thin tongues of metal.[2] The mechanism of the formation of these tongues of metal and the holes, more familiarly called extrusions and intrusions, seems to be independent of temperature in the sense that the phenomenon was observed at liquid air temperatures. So it appears that, while a thermally activated mechanism may play a part in fatigue failure, it is not an essential feature of fatigue. However, the thermally activated mechanisms can definitely compliment, enhance, and accelerate the deterioration characteristics in fatigue. The crack formation generally observed seems to occur in the intrusions on the surface. Indications are that this is a purely geometric process[3] in the sense that it may be understood as a consequence of the motion of dislocations in the several intersecting crystallographic planes.

It is appropriate at this stage to introduce the findings of Wood.[4] He shows, on the basis of fairly conclusive evidence, that two essentially distinct types of failure have been hitherto classified as fatigue. One predominates at large amplitudes of stress and the other at small stress amplitudes where the curve of stress vs. number of cycles in fatigue tends to turn parallel to the cycle axis. These two ranges are termed by Wood the *H* and *F* ranges, respectively. The mode of deformation in the *H* or hardening mechanism range is substantially the same as in static deformation. The process of deformation is essentially one of coarse

Symbols

A	= area of plastic enclave ahead of crack
A_o	= area of cross section of test specimen
C	= $(C_1 \times L_m)/b$, an experimental constant to evaluate Eq. (19)
C, C_1, C_2, C_p	= constants
E	= Young's modulus
E_S	= secant modulus
E_∞	= E
K	= a constant representing width of hysteresis loop of enclave material after it strain-hardens; an experimental constant to evaluate Eq. (19)
K_1, K_2, K_3, K_4	= constants
K_T	= theoretical stress concentration factor in vicinity of a notch
K_σ	= a plane stress factor associated with A in elastoplastic solution for area of plastic enclave
L	= grain size
L_m	= mean grain size
N_a	= actual number of stress pulses after which failure may be expected in completely random loading consisting of N_T stress pulses
N_f	= total number of cycles to failure in fatigue at a single stress σ_o, Eq. (21)
N_q	= total number of cycles to failure at stress level σ_q
N_{S-1}	= total number of stress pulses in random sequential loading which can be applied before failure occurs; subscript (S − 1) indicates block number
N_T	= total number of cycles assumed to be applied during anticipated design life of a test specimen in random loading
$(N_e)_r$	= equivalent number of cycles at reference stress corresponding to application of N_T cycles in completely random loading
$(N_r)_L$	= total number of cycles to failure at reference stress level corresponding to maximum stress in either program type, random, or acoustic loading
N_{TP}	= total number of cycles to failure in program type loading = $n_s \times \Delta n_{TP}$
N_0	= cycles associated with failure at ultimate tensile strength, $N_0 = 1/4$
N_1, N_2	= fatigue life at stress levels σ_1 and σ_2, respectively, in discussion of two-step cumulative damage
N_2'	= N_2
N_1'	= number of cycles at stress level σ_1, beyond which idea of cumulative damage has no meaning in two-step cumulative damage
N_{12}	= total number of cycles to failure in cumulative damage when stress σ_1 is applied first and then σ_2 is applied, $\sigma_1 < \sigma_2$
N_{21}	= total number of cycles when order of application of stress σ_1 and σ_2 is reversed, $\sigma_1 < \sigma_2$
ΔN	= sum of cycles of applied stress for dormant period and active incremental growth of crack $\Delta N = \Delta N_1 + \Delta N_2$

ΔN_1 = dormant period in incremental crack growth

ΔN_2 = active period in incremental crack growth

N_{mean} = mean number of cycles at which failure may be expected in random loading consisting of possible application of N_T cycles

N_{max} = maximum number of cycles after which failure may be expected

$(N_r)_{mean}$ = equivalent number of cycles at reference stress corresponding to N_{mean}

P_{rs} = residual static strength of test specimen after subjecting it to fatigue for n cycles, Eq. (23)

R = ratio of minimum stress amplitude σ_o' to maximum stress amplitude σ_o in tension

S = surface energy density in Griffith theory of cracks

S_{12} = sum of fractional lives in two-step cumulative damage when order of stress application is σ_1, σ_2 ($\sigma_1 < \sigma_2$)

S_{21} = same as S_{12} when order of application of stress is σ_2, σ_1 ($\sigma_1 < \sigma_2$)

W = initial area of hysteresis loop of plastic enclave ahead of crack before it hardens

W_N = final area of hysteresis loop after enclave hardens

W_P = width of plastic enclave; $W_P \approx A^{1/2}$

b = Burger's vector, a characteristic lattice spacing

l = crack length at any stage

l_S = length of a Frank-Read source

l_{cr} = length of a crack which is just critical for given applied tensile load

l_m = mean length of crack when variations of grain size are taken into account

l_0 = crack length at the end of N_0 cycles of applied stress, assumed here to be equal to Griffith crack length for failure at σ_{ult}

l_1, l_2 = crack lengths in discussion of cumulative damage after application of n cycles of stress σ_1 and σ_2, respectively

Δl_1 = incremental length of crack when original crack length is $(l + \Delta l)$

n = arbitrary number of cycles at any stress level

n_D = number of dormant periods in fatigue, $n_D = N/\Delta N_1$

n_S = number of blocks to failure in program type of loading

n_q = number of cycles of stress applied at stress σ_q in cumulative damage

$n(L)$ = distribution function of grain size

$n(l_S)$ = distribution function of Frank-Read source lengths

n_1, n_2 = equivalent number of cycles at stress levels σ_1 or σ_2 in two-step cumulative damage when n cycles are applied first at σ_2 or σ_1, respectively

n_1', n_2' = number of cycles at stress σ_1 and σ_2 applied in cumulative damage in familiar cumulative damage notation

Δn_{TP} = total number of cycles in a block in program type of loading $\Delta n_{TP} = \sum_{q=1}^{q} \Delta n_q$

Δn_q = number of cycles at σ_q in program loading

$(\Delta n_e)_r = \sum_{q=1}^{q} (\Delta n_r)_q$

$(\Delta n_r)_q$ = equivalent number of cycles at reference stress level σ_r corresponding to Δn_q cycles at a stress level σ_q

Δn_{erq} = total equivalent number of cycles at reference stress level corresponding to stress cycles at different frequencies in acoustic fatigue

t_A = actual time to failure of panel in acoustic fatigue

t_r = time to failure at reference stress level and reference frequency

$t_{er} = \sum_{q=1}^{q} t_{erq}$

t_{erq} = equivalent time at reference stress level and frequency corresponding to Δn_{erq} cycles

α_1, α_2, β_1, β_2 = functional constants in discussion of cumulative damage in two-step loading

η = number of dislocations piled up in a grain due to operation of a Frank-Read source

μ = shear modulus

ρ_1, ρ_2 = normalization factors of distribution functions used in discussion of fatigue under random loading

σ_M = maximum tensile stress at leading-edge dislocation of a pile-up of dislocations

σ_i = internal tensile stress in direction of applied stress for which τ_i is appropriate shear stress; also interpreted as endurance limit or natural elastic limit

σ_q'' = Rayleigh peak amplitude stress for rms stress $\overline{\sigma_q}$ at ω_q

σ_q, $\sigma_q - \sigma_q'$ = an arbitrary stress and its range in discussion of multiple-step and random loading

$\overline{\sigma_q}$ = rms stress peak in acoustic fatigue at frequency ω_q

σ_t = tensile stress appropriate for τ_{oct} in a tension test

σ_o = maximum applied tensile stress in a fatigue cycle for which τ_o is appropriate resolved shear stress

σ_o' = minimum stress amplitude in a fatigue cycle

σ_1, σ_2 = stresses in discussion of two-step cumulative damage

σ_∞ = stress far away from local discontinuities

σ_{rs} = residual static strength in psi; $\sigma_{rs} = P_{rs}/A_c$

σ_{ult} = ultimate tensile strength

σ_{iR} = endurance limit in fatigue when test stress ratio is R

σ_{mq} = mean stress in acoustic fatigue at frequency ω_q

σ_{mqi} = endurance limit in fatigue when mean stress is σ_{mq}

τ_i = internal shear stress that opposes dislocation motion

τ_o = resolved shear stress in slip plane in slip direction when a tensile stress σ_o is applied

τ_{oct} = limiting octahedral stress in elastoplastic theory of cracks

ω_q = frequency of a mode of vibration in acoustic fatigue

ω_r = reference frequency in acoustic fatigue analysis

slip and appears to occur primarily through the operation of Frank-Read sources.[5] Accordingly, Wood calls the fatigue failure in the high stress range a "delayed static fracture." It is delayed because the hardening process, which appears to precede the nucleation and propagation of cracks,

SHERMAN M. FAIRCHILD PUBLICATION FUND PAPERS

No.		Member	Nonmem.
FF-29	Design Principles for a General Control Computer—R. Alonso and J. H. Laning, Jr.	$3.00	$6.00
FF-28	Elementary Mechanics of Turbulent Fluid Motion—Max M. Munk	2.00	4.00
FF-27	A Magnetic Support for Floated Inertial Instruments—P. J. Gilinson, Jr., W. G. Denhard, and R. H. Frazier	2.00	4.00
FF-26	2nd Supersonic Transport Proceedings—L. J. Line, D. J. Maglieri, H. H. Hubbard, J. B. Pearson, Jr., R. J. Pfeiffer, B. C. Monesmith, R. A. Bailey, and R. H. Miller.	1.50	3.00
FF-23	A Matrix Approach to Flutter Analysis—William P. Rodden.	0.75	1.50
FF-22	Methods of Boundary-Layer Control for Postponing and Alleviating Buffeting and Other Effects of Shock-Induced Separation—H. H. Pearcey and C. M. Stuart.	1.50	3.00
FF-18	On the Mein Spray Generated by Planing Surfaces—Daniel Savitsky and John P. Breslin.	0.75	1.25
FF-17	Atomic Reactors (a Symposium).	1.25	1.75
FF-14	Engineering Management Philosophies (a Symposium).	0.50	1.00
FF-12	Transonic Testing Techniques (a Symposium).	1.85	2.50
FF-10	Improved Solutions of the Faulkner and Skan Boundary-Layer Equation—A. M. O. Smith.	0.75	1.25
FF-9	A Hydrodynamic Study of the Chines-Dry Planing Body—Experimental Towing Tank, Stevens Inst. of Tech.	1.20	1.60
FF-7	Natural Flight and Related Aeronautics—James L. G. Fitz Patrick.	2.65	3.50
FF-4	Finite Deflections of Curved Sandwich Plates and Sandwich Cylinders—F. K. Teichmann and Chi-Teh Wang.	$0.50	$0.85
FF-3	The Penetration of a Fluid Surface by a Wedge—Experimental Towing Tank, Stevens Inst. of Tech.	1.20	1.60
286	Linearized Treatment of Supersonic Flow Through Axi-Symmetric Ducts with Prescribed Wall Contours—Charles E. Mack, Jr., and Ignace I. Kolodner.	0.75	1.25
229	Wave Profile of a Vee-Planing Surface, Including Test Data on a 30° Dead-Rise Surface—Experimental Towing Tank, Stevens Inst. of Tech.	1.20	1.60
170	Wave Contours in the Wake of a 10° Deadrise Planing Surface—Exp. Towing Tank, Stevens Inst. of Tech.	1.20	1.60
168	Wave Contours in the Wake of a 20° Deadrise Planing Surface—Exp. Towing Tank, Stevens Inst. Tech.	1.20	1.60
167	On the Pressure Distribution for a Wedge Penetrating a Fluid Surface—Experimental Towing Tank, Stevens Inst. of Tech.	0.75	1.00
106	Measurement of Ambient Air Temperature in Flight—W. Lavern Howland.	0.35	0.50
104	Tensor Analysis of Aircraft Structural Vibration—Charles E. Mack, Jr.	1.85	2.50
102	Electrical Resistance Strain Gages Applied to Wind-Tunnel Balances—Elmer C. Lundquist.	0.60	0.80
101	Introduction to Shock Wave Theory—J. G. Coffin.	2.65	3.50
100	Blade Pitching Moments of a Two-Bladed Rotor—R. W. Allen.	0.75	1.00

Order by number from: **Special Publications Dept., IAS, 2 E. 64th St., New York 21, N.Y.**

IAS SPECIAL PUBLICATIONS

	Member	Nonmember
Aerospace Engineering Index - 1958	$10.00	$15.00*
Aeronautical Engineering Index - 1956 and 1957 (each)	10.00	15.00*
Aeronautical Engineering Index - 1947 through 1955 (each)	3.00	5.00*
IAS/Army Aviation Meeting Proceedings - 1961 (68 pp.)	2.50	5.00*
National Midwestern Meeting on Air Logistics Proceedings - 1960 (116 pp.)	5.00	10.00*
Weapons Systems Management - National Midwestern Meeting Proceedings - 1957 (60 pp.)	1.50	2.50*
National Symposium on Hypervelocity Techniques Proceedings - 1960 (176 pp.)	5.00	10.00*
Recovery of Space Vehicles Symposium Proceedings - 1960 (104 pp.)	4.00	8.00*
National Specialists Meeting on Dynamics & Aeroelasticity Proceedings - 1958 (136 pp.)	3.50	6.00*
1961 National Telemetering Conference Report	3.50	5.50*
1960 National Telemetering Conference Report	4.50	6.50*
1959 National Telemetering Conference Report	3.00	4.00*
Frontiers of Science & Engineering Symposium Proceedings - 1959 (132 pp.)	5.00	10.00*
Fourth Turbine-Powered Air Transportation Meeting Proceedings - 1959	2.00	4.00*
Second Turbine-Powered Air Transportation Meeting Proceedings - 1955	3.50	6.00*
7th Anglo-American Aeronautical Conference Proceedings - 1959	20.00	25.00*
5th International Aeronautical Conference Proceedings - 1955	15.00	20.00*
2nd International Aeronautical Conference Proceedings - 1949	5.00	5.00*
National Naval Aviation Meeting Proceedings - 1957 (124 pp.)	3.00	5.00*
Index to Books on Selected Technical Subjects in the IAS Library (up to 1950), unbound	2.00	2.00*

* Add $1.00 for orders outside the U.S.A.

These may be obtained by writing to: **Special Publications Dept., IAS, 2 E. 64th St., N.Y. 21, N.Y.**

occurs in a less efficient manner in this range of fatigue stress than it does in normal static stressing.

On the other hand, in the F range, conditions are significantly different. The deformation is primarily due to fine slip and involves little or no hardening. Failure of the material appears to be due to a gradual deterioration of structure which manifests itself as the "persistent slip bands," and the fissures that lead to eventual failure seem to start in these regions. This process is presumably the result of the to-and-fro motion of a large number of individual dislocations rather than the avalanche release of dislocations characteristic of the Frank-Read sources that are apparently responsible for coarse slip. Wood calls the failure in this region pure fatigue since it appears to be an important feature of low stress level fatigue and is not a significant aspect of plastic deformation leading to failure in static testing.

Because of the distinctly different modes of deformation, it is not reasonable to expect that a quantitative theory of fatigue may be developed which will be valid in a logical manner in both ranges. If one simple theory appears to do so, it must be considered a coincidence. It may be observed in passing that even if a crack develops in the F range, when it grows, the local stresses in the immediate vicinity will be relatively high because of stress concentration. The result will be that at some stage during the propagation, a crack which started in the F range will behave more as if it were in the H range. Consequently, the region of validity of a quantitative theory of high stress level fatigue may be expected to extend somewhat beyond the strictly H range. It will also be shown that by choosing two of the unknown constants judiciously, the range of practical validity of a theory of fatigue developed for the H range may be extended artificially to the F range also.

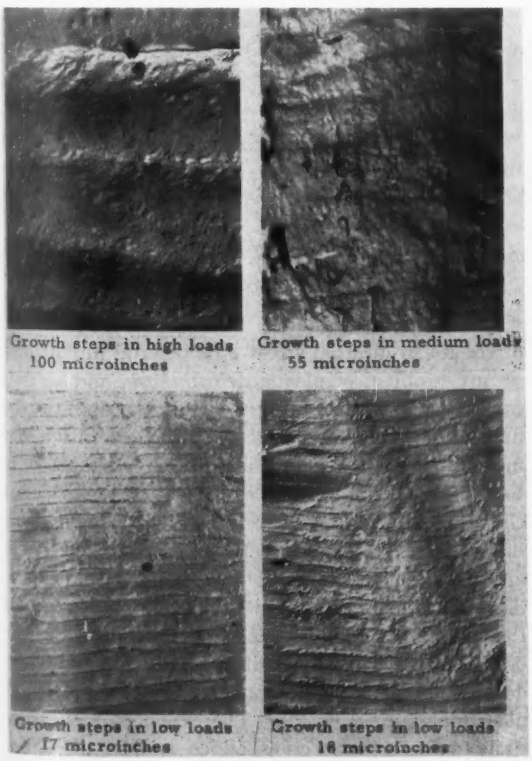

Fig. 4. Electron micrographs of progressive fracture on microscale.

There is evidence to show that crack propagation in fatigue occurs intermittently.[6, 7] Christensen, by focusing attention on the cross sections of broken test specimens in fatigue, was able to show that the rings characteristically observed in fatigue were in fact an aggregate of a large number of finer rings (Figs. 2, 3, and 4). It is suggested that the growth time involved by these rings constitutes a "dormant period" in fatigue. Christensen's pictures show that the dormant period is substantially larger than the active period, and that the incremental increase in length of the crack is much smaller during the former. He finds that, typically, the incremental growth of the crack in the dormant period, which is dependent upon the stress, is of the order of 20 to 100 microns and that corresponding crack growths in the active period are several orders of magnitude larger than these values. The number of cycles during which the crack is dormant is typically about 50 to 500 cycles and the active period approximately 1 cycle. It seems that, macroscopically smooth as the crack growth may appear to be, it is in fact growing in a stepwise manner (Fig. 2). This observation is of fundamental importance in the theory to be presented here.

The discussion that follows is restricted to fatigue failure of materials in the H range. Since plastic deformation in this region proceeds primarily through coarse slip which occurs because of activation of the Frank-Read sources, any characteristic stresses associated with these sources may be expected to play a prominent role in the theory. In view of certain assumptions made, the theory as developed is not expected to be valid below 50 cycles on the high stress range and, strictly speaking, beyond about 5 million cycles on the low stress side. Since the range is sufficiently large, it is hoped that the theory will be of some use in explaining the various aspects of fatigue in a systematic manner from a unified viewpoint.

Basic Assumptions

The material is considered to be a polycrystalline aggregate susceptible to strain hardening with a known statistical distribution of grain size. The mean grain size is L_m and the distribution is assumed to be log-normal in accordance with Beck's observations reported by Lunchick.[8] While there may be a number of cracks generated by the fatigue stresses, it is assumed that the final failure is due

to the growth of a "dominant crack." In accordance with some of the existing findings, this dominant crack in the H range is assumed to grow intermittently and consists of active and dormant periods. The theory concerns itself with developing quantitative expressions for the growth of this dominant crack in terms of the applied stress, the stress range, and the number of cycles of the applied stress. As a corollary, this will result in most of the other quantitative expressions that we desire in order to understand the various aspects of fatigue.

While these assumptions are based substantially on physical observations, we shall make additional assumptions based on broad and plausible conjectures. It is assumed that the dormant period in the crack growth is associated with the strain hardening of a plastic region or enclave that is presumed to be formed ahead of the crack. Completion of the hardening of the enclave is assumed to be followed by a rapid growth of the crack through an incremental length represented approximately by the width of the hardened enclave. It has been found that the hardening process in reversed stressing is less efficient than that occurring during static stressing.[4] In static stressing the process of strain hardening is accomplished by producing an intersecting network of dislocations whose stability is assured by the applied stress. Under repeated loading in fatigue when the stress is reversed, presumably some of the dislocations generated during the increasing part of the stress cycle go back to their sources and get absorbed. In the subsequent cycle, more are generated, and from them additional ones are prevented from going back to their sources. This marginal increase in the number of dislocations that interact and become fixed is apparently a decreasing function of the number of cycles. When the hardening is completed, a stable, intersecting array of dislocations is set up in the sense that their stability is not dependent upon the applied stress. It is postulated that this motion of the dislocations leads to interactions, presumably leading to submicroscopic cracks.[3] It is therefore suggested that growth of the dominant crack at the end of the hardening stage is accomplished through the process of these submicroscopic cracks joining together with the dominant crack to extend the crack through the region of the hardened enclave. This may be termed "advanced submicroscopic crack initiation ahead of the dominant crack in fatigue." It appears, therefore, that inefficient as it may be in the rate of hardening, large amplitude stress reversals play a fundamental part in the fatigue mechanism. Since the number of submicroscopic cracks produced seems to be dependent upon the extent and number of dislocation interactions and since this in turn is dependent upon the stress range, range of stress appears to be an essential parameter in fatigue. These conclusions are in a sense an extension of Wood's hypothesis of fatigue in the H range. This conjectured type of crack growth in fatigue has in fact recently been observed.[9]

It has already been stated that since the Frank-Read sources appear to play a prominent part in deformation in the H range, any characteristic stresses associated with them may be important in the theory. Operation of a Frank-Read source causes a pile-up of dislocations in a slip plane,[5] and such a pile-up has been shown to result in large tensile stresses.[10] It has also been shown that when the number of dislocations in the pile-up is of the order of 1,000, the coalescence of the leading-edge dislocations may take place leading to an incipient crack. This suggestion was made originally by Zener.[11] It can be shown that the number of dislocations in a pile-up is given approximately by the relation[5]

$$\eta \approx [2L_m(\tau_o - \tau_i)]/\mu b \qquad (1)$$

where η is number of dislocations in a pile-up, L_m is grain size, τ_o is resolved shear stress[5] in slip plane in direction of slip, τ_i is a mean internal stress[5] that opposes motion of dislocations, μ is shear modulus, and b is a characteristic lattice spacing called Burger's vector.[5]

The tensile stress σ_M produced at the leading-edge dislocation of the pile-up (Fig. 1) may be shown to be of the order

$$\sigma_m \approx K_1 \frac{L_m (\tau_o - \tau_i)^2}{b \quad \mu} \qquad (2)$$

where K_1 is a constant. The classical theoretical strength[12] of a material is of the order $E/2\pi$ where E is Young's modulus. Assuming that σ_o and σ_i are the tensile stresses for which τ_o and τ_i are the appropriate shear stresses, we may nondimensionally express the tensile stress σ_M as

$$\sigma_m \approx K_2 \frac{L_m (\sigma_o - \sigma_i)^2}{b \quad E^2} \qquad (3)$$

with K_2 again a constant. It appears that the value of the mean internal stress σ_i is of vital importance in any problem of plastic deformation, and so it is in fatigue. If the fatigue failure is due to the nucleation of cracks produced by the generation and motion of dislocations, since these respond only to the stress difference $(\sigma_o - \sigma_i)$, we assert that the applied stress by itself is of no importance, but it is the difference between the applied stress and the mean internal stress that is important. Also, since it is conceived that the propagation of the dominant crack is due to the joining together of the cracks generated within the enclave and the dominant crack, the response is to $(\sigma_o - \sigma_i)^2$ and not simply to $(\sigma_o - \sigma_i)$. The exponent 2 is essentially a factor that gives added weight to higher stresses. It is therefore proposed that the right-

hand side of Eq. (3) must also find a place in a quantitative theory of fatigue.

In order to derive an expression for the rate of crack propagation, we need two important relations. One is an estimate of the width of the plastic enclave which gives the incremental crack growth, and the other is an expression for the rate of hardening of the enclave. These will enable us to determine the rate of crack propagation. If, in addition, we have an estimate of the initial crack length and a relation for the limiting crack length when the catastrophic failure of the specimen occurs, we are in a position to define the fatigue failure expression completely. The estimate of initial length of the crack and its limiting length are provided by the Griffith theory of cracks. Specifically, we shall assume that unless the crack length is at least equal to the equivalent Griffith crack length for failure at ultimate tensile strength, it will not propagate. This would in essence mean that the dominant crack will be that which would have caused failure in a simple tension test. This assumption is untenable in low stress level fatigue. We shall also assume that the limiting length of the crack is also governed by the Griffith theory. Thus, if the tensile stress amplitude in fatigue is σ_o, we write for failure

$$l_{cr}/l_o = \sigma_{ult}^2/\sigma_o^2 \tag{4}$$

where l_{cr} is critical length of fatigue crack for stress σ_o, and l_o is critical Griffith crack length for failure at ultimate tensile strength σ_{ult}. This equation is an alternate statement of the Griffith expression[12]

$$\sigma_o = K_3\sqrt{ES/l_{cr}} \tag{5}$$

where K_3 is a constant and S is the equivalent surface energy.[13] Regarding rate of strain hardening, in the absence of more pertinent information we shall assume that the hardening obeys a rate process and that it can conveniently be measured by collapse of the hysteresis loop of the material in the enclave. This assumption is not inviolate and can be substituted by a more accurate, experimentally observed expression.

Quantitative Development of the Theory

With these assumptions, we are now in a position to formulate the theory quantitatively. In a recent paper on analysis of stress distribution in the vicinity of a crack based upon some calculations of Eaton and Stimpson,[14] Williams[15] estimates the extent of plastic enclave produced ahead of the crack in a material that has a well-defined limiting octahedral stress, the assumption being that as soon as the stress exceeds this value, the distribution changes from elastic to plastic. The expression that he obtains for the area of the plastic enclave is of the form

$$A = K_\sigma(2l^2/81)(\sigma_\infty/\tau_{oct})^4 \tag{6}$$

where A is area of plastic enclave, l is crack length, σ_∞ is applied stress far away from crack, τ_{oct} is limiting octahedral stress, and K_σ is an appropriate plane stress constant. While shape of the enclave is a function of applied stress,[14] it is a satisfactory approximation for the present purpose to assume that the width of the enclave W_p is equal to $(A)^{1/2}$. Hence, for a crack in a sheet specimen, we write

$$W_p \approx \sqrt{(K_\sigma/2)}l(\sigma_\infty/\sigma_t)^2 \tag{7}$$

where σ_t is appropriate tensile stress which produces limiting octahedral stress τ_{oct}. For three-dimensional specimens a similar relation may be expected to hold good except that the constant of multiplication will be different.

The disadvantage of Eq. (7) is that it does not take into account the strain hardening characteristics of the material. Since the stress dependence in Eqs. (7) and (3) is the same and since Eq. (3) describes a realistic state of affairs in a material capable of strain hardening, it is proposed that the width of the plastic enclave for materials susceptible to strain hardening be written intuitively in the form

$$\left.\begin{aligned} W_p &= C_p l \frac{L_m}{b}\left(\frac{\sigma_o - \sigma_i}{E}\right)^2 && \sigma_o \geq \sigma_i \\ &= 0 && \sigma_o \leq \sigma_i \end{aligned}\right\} \tag{8}$$

where C_p is now a constant to be determined experimentally at this stage of development of theory. This intuitive generalization is a fundamental assumption of the theory. If the test specimen is notched with a theoretical stress concentration factor K_T, it will be necessary to modify Eq. (8) so that σ_o will represent actual macroscopic stress in the vicinity of the notch. In such a case, we shall use the results of Hardrath and Ohman[16] to write σ_o as

$$\sigma_o = \sigma_\infty\left\{1 + (K_T - 1)\frac{E_S}{E_\infty}\right\} \tag{9}$$

where E_S is secant modulus of stress-strain curve at stress σ_o, E_∞ is ordinary Young's modulus, K_T is theoretical stress concentration factor, and σ_∞ is stress far away from the notch.

When we proceed to introduce the range factor $[(\sigma_o - \sigma_o')/\sigma_i]^2$ into the expression for the width of the plastic enclave, we can identify enclave width with the incremental crack length Δl. We may therefore write

$$\Delta l \approx C_p l \frac{L_m}{b}\left(\frac{\sigma_o - \sigma_i}{E}\right)^2\left(\frac{\sigma_o - \sigma_o'}{\sigma_i}\right)^2 \tag{10}$$

The exponent two and the nondimensional form of the range factor are introduced intuitively and justified by test results. When the crack extends through this incremental length, the new incremental length when the crack propagates again will be given by

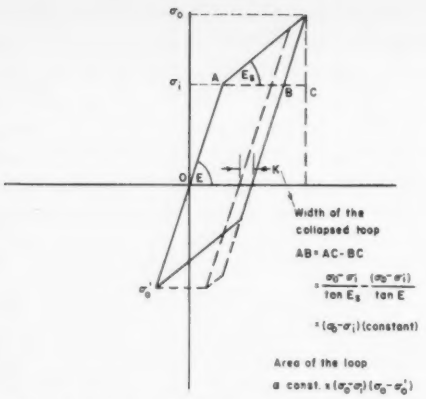

Fig. 5. Schematic representation of collapse of hysteresis loop during strain hardening of plastic enclave ahead of the crack.

$$\Delta l_1 \approx C_p(l + \Delta l)\frac{L_m}{b}\left(\frac{\sigma_o - \sigma_i}{E}\right)^2\left(\frac{\sigma_o - \sigma_o'}{\sigma_i}\right)^2 \quad (11)$$

The significance of this expression is clear. It states that at this stage, while we do not know when the crack suddenly becomes active, we do know the approximate distance through which it moves when it becomes active.

Before we can derive the rate of crack propagation, we need a relation for the rate of hardening of the plastic enclave, for unless the enclave hardens, we cannot (strictly speaking) identify it with the incremental crack length. At the present stage of development of the dislocation theory, it is extremely difficult to determine this from purely theoretical considerations. Therefore, as indicated previously, we shall assume that a rate process law governs the hardening. We shall take the rate of decrease of the area of the hysteresis loop—that is, its collapse—as a measure of this hardening. It may be noted that there will always be a residual hysteresis loop, for—no matter how small—there will always be some free dislocations that will execute a to-and-fro motion and thus dissipate energy, apart from other dissipating mechanisms such as grain boundary relaxation, stress induced ordering, etc. We therefore invoke a relation of the type

$$\log_e (W/W_N) = K_4 \Delta N_1 \quad (12)$$

where ΔN_1 is number of cycles it takes for collapse of a loop of area W to one of area W_N (Fig. 5). It is evident that

$$\Delta N_1 = C_2 \log_e \frac{(\sigma_o - \sigma_o')(\sigma_o - \sigma_i)}{K(\sigma_o - \sigma_o')} \quad (13)$$

where K_4, C_2, and K are constants. K, width of the collapsed loop, is dependent upon the final dislocation structure in the hardened enclave. If ΔN_1 is number of cycles for hardening of the enclave or what amounts to the same, the dormant period, and ΔN_2 is number of cycles for the active period, we have

$$\Delta N_1 \gg \Delta N_2 \quad (14)$$

In fact, Christensen finds that they are of the order 250 to 1. Therefore, the total number of cycles to failure N may be written to a good approximation

$$N = n_D \Delta N_1 \quad (15)$$

where n_D is number of dormant periods (Fig. 6). Incremental propagation rate $\Delta l/\Delta N$ ($\Delta N = \Delta N_1 + \Delta N_2$) may therefore be approximated to $\Delta l/\Delta N_1$. Rate of crack propagation may therefore be written from Eqs. (10) and (13) as

$$\frac{dl}{dN} \approx \frac{\Delta l}{\Delta N_1} = C_1 l \frac{L_m}{b} \frac{\left(\frac{\sigma_o - \sigma_i}{E}\right)^2\left(\frac{\sigma_o - \sigma_o'}{\sigma_i}\right)^2}{\log_e\left(\frac{\sigma_o - \sigma_i}{K}\right)} \quad (16)$$

where C_1 is again a constant. The dependence of rate of crack propagation on crack length is too well known for any additional comment. Liu,[17] Frost and Dugdale,[18,19] and several others have observed this relationship and have given theoretical interpretation of the result. The main difference between Eq. (16) and its counterparts suggested by others is the proposed additional dependence on grain size, stress and its range, and stress σ_i. Integrating Eq. (16), we obtain

$$\log_e \frac{l}{l_o} = C_1 \frac{L_m}{b} \frac{\left(\frac{\sigma_o - \sigma_i}{E}\right)^2\left(\frac{\sigma_o - \sigma_o'}{\sigma_i}\right)^2}{\log_e\left(\frac{\sigma_o - \sigma_i}{K}\right)} (N - N_o) \quad (17)$$

where l_o is crack length appropriate for N_o. We shall interpret, as mentioned already, that l_o is the equivalent Griffith crack length for failure at the ultimate static tensile strength. Therefore, $N_o = 1/4$ and, as a matter of convenience, we shall neglect it compared to the large number of cycles to fatigue failure. An important consequence of this as-

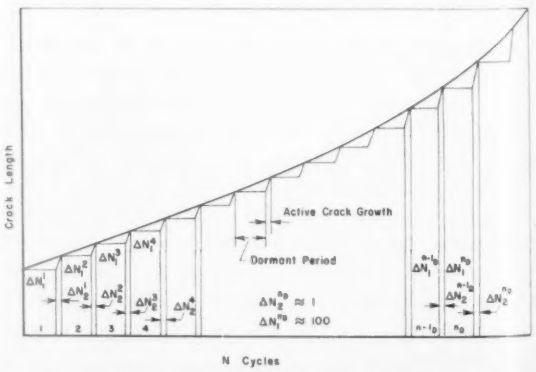

Fig. 6. Schematic representation of crack propagation in high stress level fatigue.

sumption regarding l_o is that, until the crack generated by fatigue is at least equal to l_o, no significant general damage has occurred in the material. The macroscopic residual static strength will then be governed by the pre-existing Griffith cracks or the cracks generated during determination of the tensile strength, rather than by the fatigue cracks. It is entirely possible that the number of cycles it takes for the fatigue cracks to grow to the equivalent Griffith crack length can be substantially large in the low stress level fatigue (F range). Hence, it is here that we explicitly invoke the concept of high stress level fatigue. In the low stress level fatigue, this approximation is not justified since the "crack initiation stage" may be expected to be relatively large compared to the total cycles to failure. Therefore, we have to take into account N_o and introduce a more appropriate value of l_o. Otherwise the expression would predict cycles to failure that are less than what the tests would indicate. Since the grain size is not frequently measured, we may introduce a new constant

$$C = C_1 L_m / b \tag{18}$$

and write

$$\log_e \frac{l}{l_o} = C \frac{\left(\frac{\sigma_o - \sigma_i}{E}\right)^2 \left(\frac{\sigma_o - \sigma_o'}{\sigma_i}\right)^2}{\log_e \left(\frac{\sigma_o - \sigma_i}{K}\right)} N \tag{19}$$

Eq. (17) or (19) may be considered the fundamental equation of this theory of fatigue. In view of Eq. (4), it is a simple matter to determine the cycles to catastrophic failure. The condition clearly is

$$\log_e \frac{l}{l_o} = \log_e \left(\frac{\sigma_{ult}}{\sigma_o}\right)^2 = C \frac{\left(\frac{\sigma_o - \sigma_i}{E}\right)^2 \left(\frac{\sigma_o - \sigma_o'}{\sigma_i}\right)^2}{\log_e \left(\frac{\sigma_o - \sigma_i}{K}\right)} \times N_F \tag{20}$$

so that

$$N_f = \frac{2}{C} \frac{\log_e \frac{\sigma_{ult}}{\sigma_o} \log_e \left(\frac{\sigma_o - \sigma_i}{K}\right)}{\left(\frac{\sigma_o - \sigma_i}{E}\right)^2 \left(\frac{\sigma_o - \sigma_o'}{\sigma_i}\right)^2} \tag{21}$$

where N_f is number of cycles to failure at stress level σ_o and its appropriate range.

Comments Regarding the Value of σ_i

Before determining the constants C and K and examining the explanation of the several observed features of fatigue, some comments are in order regarding σ_i. In the dislocation theory of metals, σ_i is assumed to be the stress that must be overcome before dislocations can move. This stress is supposed to arise from various sources, such as the existing network of dislocations, solute atoms, etc. For certain aspects of the dislocation theory, the additional assumption is made that the material may be looked upon as consisting of potential hills and valleys[5] and that the maximum slope on all these hills is the same and has the value σ_i. The dislocations with their associated stress fields may then be looked upon as climbing up and down these potential hills and valleys. When external stresses are applied, they drive the dislocations up and down these potential hills and valleys. Since the material does not exhibit plastic deformation until the dislocations move and since the external stress has to exceed σ_i before dislocations can move, it is natural to interpret σ_i as the proportional limit of the material. But in fatigue this interpretation causes difficulty for two reasons. First, determination of the proportional limit for a material is an elusive thing, and its value depends upon the accuracy and technique of measurement. Second, it is well known that if a test specimen is subjected to a fatigue stress amplitude somewhat less than the proportional limit commonly measured in engineering practice, the specimen is liable to fatigue failure. We may therefore return to Bairstow's original hypothesis[20] and assume that the real or natural elastic limit of a material is the same as the endurance limit exhibited by the material under completely reversed fatigue stressing. With this interpretation of the σ_i, the contradiction of having fatigue failures at stresses below the normal proportional limits is removed. This interpretation has the natural advantage that variations of the endurance limit under different conditions, such as understressing and overstressing, can be discussed in terms of the variation of the internal stresses due to changes in dislocation structure. A simple example of this is the effect of cold working. It is fairly easy to show that the effect of cold work is to produce an increase in the dislocation density resulting in an increase in the value of σ_i. The result of this on Eq. (21) will be to increase the value of N as compared to that of an annealed material for the same applied stress conditions.

The constants C and K have to be determined from test results at this stage of the theory's development. Thus, given the test specimens of any material, we perform fatigue tests on a statistical basis choosing stress levels that extend all the way from ultimate tensile strength down to endurance limit. Taking two points in the intermediate range of stress, we can determine the constants C and K. By a judicious choice of the points, the region of validity of this equation may be extended well beyond the H range. This artificial extension of the range may well destroy the physical significance of the constants C and K in the sense that, instead of K implying strain hardening, it may imply strain

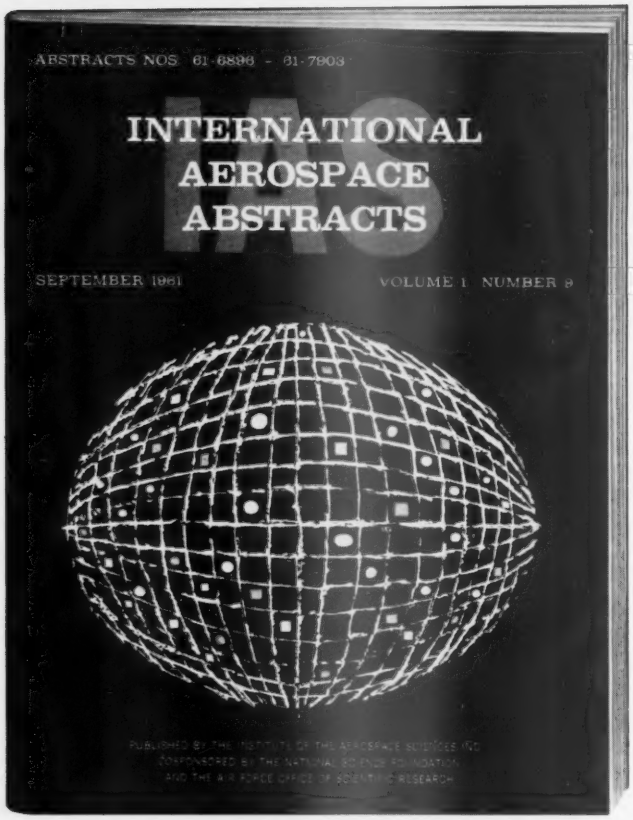

Are you <u>really</u> keeping abreast of aerospace developments?

Today's aerospace technology moves *fast*. Every forward-looking engineer and scientist *must* know the results of all aerospace research related to his own work *wherever accomplished*.

INTERNATIONAL AEROSPACE ABSTRACTS is ideally suited to help you with this task—made enormous by an avalanche of publications.

INTERNATIONAL AEROSPACE ABSTRACTS saves you time. Each monthly issue gives you about a thousand abstracts of the latest reports, articles, meeting papers, and books—selected because they *are* important to aerospace technology. You can immediately put your finger on the work being done in your field. COVERAGE IS WORLD-WIDE.

INTERNATIONAL AEROSPACE ABSTRACTS is cosponsored by the National Science Foundation and the Air Force Office of Scientific Research. For detailed information on this indispensable R & D tool, write to the address below.

Enter Your Subscription Now!

INTERNATIONAL AEROSPACE ABSTRACTS
2 East 64th Street, New York 21, N. Y.

Please enter ____ subscription(s) for the year 1962 at the following rates:

- ☐ Individual IAS Member Rate – $20/yr
- ☐ Corporate IAS Member Rate – $40/yr
- ☐ Nonmember Rate – $60/yr
  - ☐ Payment is enclosed.
  - ☐ Please send bill.

Name_____ Title_____

Company_____

Address_____

City_____ Zone____ State_____

INSTITUTE OF THE AEROSPACE SCIENCES, INC.

softening. But the indications are that the practical utility of the expressions is not destroyed by such a process.

Test results of Illg[21] for 2024-T3 have been used to determine the constants C and K in Eq. (21). The chosen test points are indicated by the big squares in Fig. 7 with the computed curve superposed on the test points. The same constants are used to compute the curves of Eq. (19), the results of which are presented in Fig. 8. In a sense, the curves of Fig. 8 may be considered the fundamental curves of the proposed theory of fatigue since from them stems the discussion of almost all other aspects of fatigue.

At this stage it is desirable to sum up briefly what we have done so far. Fatigue failure of a specimen is attributed to the growth of a dominant crack. This growth is assumed to occur in jerks and is affected by the hardening characteristics of the material and the range of applied stress. On this basis, an expression for the growth of the dominant crack as a function of the number of cycles was derived. Failure is assumed to occur when the growing crack just becomes critical for catastrophic failure at the applied stress. This condition determines the number of cycles to failure. The fundamental equations of the theory, Eqs. (19) and (21), contain essentially four constants of which two are the ultimate tensile strength and the endurance limit. The other two are the constants C and K which have to be determined from statistically reliable fatigue tests. It will be found that, if the statistical mean test points chosen to determine the constants are spaced suitably, the region of practical validity of the equation is extended well beyond the H range.

Dependence of Fatigue on Different Variables

Shape of Fatigue Curve

The expression for the shape of the fatigue curve is given by Eq. (21), and Fig. 7 shows a typical result where the test points for determining the constants have been obtained from Illg.[21] While the theoretical curve appears to fit the test results

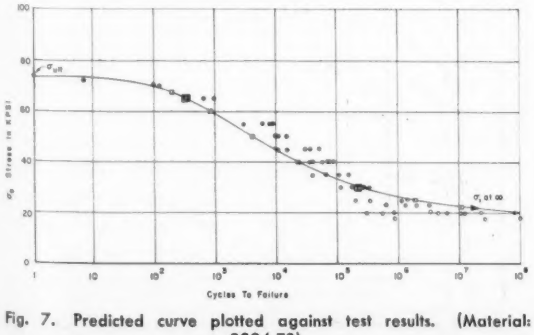

Fig. 7. Predicted curve plotted against test results. (Material: 2024-T3)

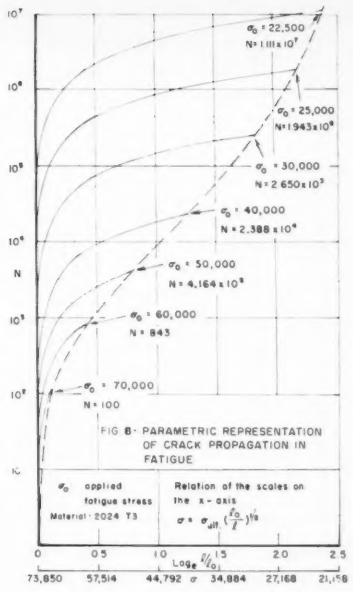

Fig. 8.

in a satisfactory manner, in the high stress level range the predictions will be somewhat spurious. The actual slope of the crack propagation curve dl/dN has been approximated to dl/dN_1 by virtue of the physically justifiable assumption $\Delta N_2 \ll \Delta N_1$. But, in fact, as we approach closer and closer to the σ_{ult}, ΔN_1 will become smaller and smaller and comparable in magnitude to ΔN_2. Hence, this assumption will no longer be justified, and the consequence will be that a higher propagation rate will have been assumed with the result that the predicted life to failure may be less than what may be expected. For this reason the upper limit of stress validity of the theory has been restricted arbitrarily to about 50 cycles. Therefore, the predicted results in this region must be used with some caution. The low stress side of the curve and the artificial extension of the region of practical validity have already been discussed.

Existence or Nonexistence of Endurance Limit

This property is closely related in principle to the value of the mean internal stress σ_i. There are two alternate possibilities for the existence of a well-defined endurance limit. Since it is generally accepted that the fatigue process generates its own cracks, a well-defined endurance limit would imply either that the cracks' formation is prevented or that, if they form, their propagation is inhibited. Since formation of the cracks is due to dislocation movements and interactions, a natural way of obtaining a well-defined endurance limit is to prevent the motion of dislocations. This requires the pinning of existing dislocations to prevent them from moving and also the pinning of any new dislocations generated in isolated places as the result of local stress concentrations. This anchoring can

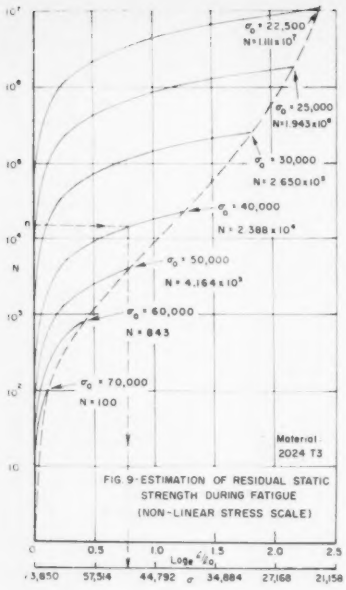

Fig. 9.

be effected fairly easily in interstitial solid solutions (mild steel, for example) through the formation of Cottrell atmospheres,[22] and, consequently, one should expect a well-defined endurance limit in such materials. This fact is well known. It also follows that, since the formation of these atmospheres is a diffusion controlled process and hence time dependent, the endurance limit of such materials should be frequency dependent. It also follows that, if the interstitial solute atoms of such materials are removed by a suitable treatment, the endurance limit must disappear. This is a known fact.[23] The second alternative—preventing propagation of existing cracks—is somewhat more difficult. One possibility for this is an indefinite capacity for plastic deformation—that is, an ideally plastic material. The enclave in such a material will not strain harden, and hence the crack cannot propagate. This alternative appears to be one of theoretical interest only. What this amounts to is that, apart from interstitial solid solutions, one may not in principle expect a well-defined endurance limit. An approximate endurance limit may be defined on the basis of nonfailure at a large number of cycles, say of the order of 500 million.

Residual Static Strength

The determination of the residual static strength after an arbitrary amount of fatigue is straightforward when the curves of Fig. 8 are computed. It is clear from Eq. (4) that the scale of crack length can be converted to a corresponding scale of the critical Griffith stress. Thus, we may convert the scale of log l/l_o to that of the residual static strength by the relation

$$\sigma_{rs} = \sigma_{ult}(l_o/l)^{1/2} \tag{22}$$

where σ_{rs} is residual static stress at which specimen would fail. Residual static strength in pounds will be given by

$$P_{rs} = \sigma_{rs} A_C \tag{23}$$

where A_C is area of cross section of test specimen. Graphical construction for the residual static strength appropriate for σ vs. N curve of Fig. 7 is indicated in Fig. 9. When size of the crack is significant compared to initial area of cross section of the test specimen, a correction factor will be necessary in these expressions. Analytical representation for the residual static strength after application of n cycles of stress at stress level σ_o and range $(\sigma_o - \sigma_o')$ is given by

$$\sigma_{rs} = \sigma_{ult}\left(\frac{l_o}{l}\right)^{1/2} = \sigma_{ult}\exp^{-1/2} \times \left[C\frac{\left(\frac{\sigma_o - \sigma_i}{E}\right)^2\left(\frac{\sigma_o - \sigma_o'}{\sigma_i}\right)^2}{\log_e\left(\frac{\sigma_o - \sigma_i}{K}\right)}\left(n - \frac{1}{4}\right)\right] \tag{24}$$

A parametric representation of Eq. (24) for different values of σ_o is given in Fig. 10. Some inherent limitations of this method of representation of the residual static strength are pointed out in the original report[24] on which this paper is based. The number 1/4 is reintroduced here in order to satisfy the condition that when $\sigma_o = \sigma_{ult}$ and $n = 1/4$, $\sigma_{rs} = \sigma_{ult}$.

Effect of Frequency

The effect of frequency is a straightforward consequence of the theory and has already been treated elsewhere.[25] It is not yet possible to treat it in a quantitative manner, but qualitatively it

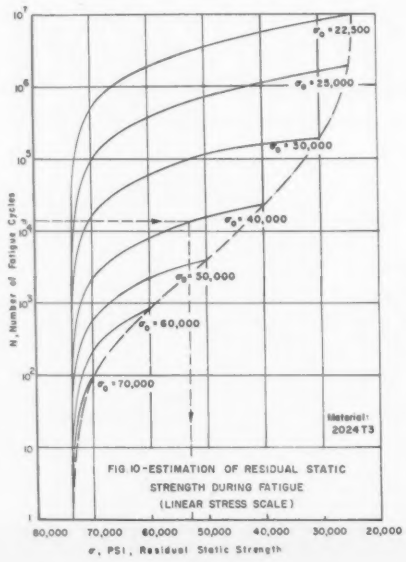

Fig. 10.

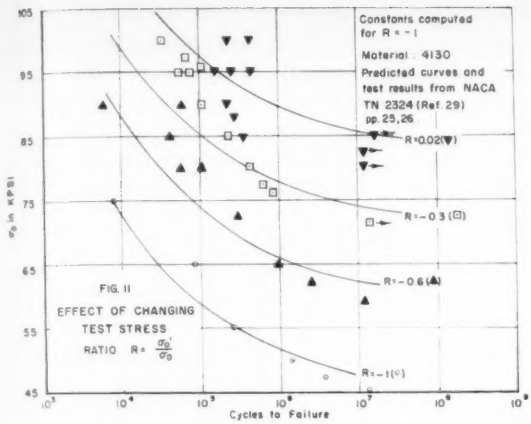

Fig. 11.

can be looked upon as due to the possibility of thermal activation of some partially activated Frank-Read sources in the enclave. Briefly, the principle of approach may be outlined as follows. The stress concentration at the leading-edge dislocation of a pile-up of dislocations is dependent upon the number of dislocations piled up in the slip band. When the external stress σ_o is applied, of the Frank-Read sources with a spectral distribution of lengths $n(l_s)dl_s$, those with lengths defined by the condition

$$l_s \geqslant \mu b/(\sigma_o - \sigma_i) \qquad (25)$$

where l_s is source length, become immediately activated. Sources with lengths smaller than this value are only partially activated in the sense that they assume shapes less than the critical semicircular shape.[5] Under suitable thermal fluctuations, these partially activated sources can become momentarily active, send out an additional dislocation loop into the slip band, and hence cause more local stress concentration. It is presumed that this increase will result in a decrease in fatigue life. The process is similar to the exhaustion theories of creep, and the measured activation energies (34,000 cal/gm mole for aluminum) seem to support a creep-type mechanism since they are of the same order as volume diffusion energies. The frequency effect comes into the picture by virtue of the fact that if the frequency is high, not enough time is available for successful thermal fluctuations, with the result that the number of marginally active sources becomes less and produces fewer sources of stress concentration and presumably, therefore, a higher fatigue life. Some conclusions arrived at on the basis of this approach[25] are briefly summarized:

(1) The effect appears to be marginal. But there are experimental observations which show an increase in life of about 800 percent for high-purity aluminum[26] for a three-decade increase in frequency. This would apparently mean that other, more simply activated mechanisms may also be operative.

(2) The effect is more pronounced at higher stress levels than at lower stress levels—that is, what one may call the endurance limit is not sensibly effected by the frequency. This would imply that the possible frequency dependence of the endurance limit of the interstitial solid solutions (mild steel, etc.) may be insignificant.

(3) Cold worked materials show more pronounced frequency effect than annealed materials.

(4) The effect of frequency for a given temperature is significant only within a certain frequency range. Beyond this range, changes in frequency do not result in significant additional changes in fatigue life.[27]

Effect of Grain Size

This effect appears through variations in L_m. Larger grain size implies larger crack propagation rates, Eq. (16), and hence shorter lives. Coarse grained materials may therefore be expected to have shorter lives. This fact is well known.[28]

Effect of Cold Work

To predict quantitatively the effect of cold work from purely theoretical considerations is somewhat difficult since it is sensitively dependent upon the dislocation structure. Approximate calculations[24] based upon dislocation theory predict more significant effect of cold work than is normally observed. The effect occurs for two possible reasons. One is the increase in the density of dislocations[5] due to the cold work, and this in turn may be shown[5] to increase the mean internal stress σ_i. It is evident that the result of this will be to reduce the net effective stress $(\sigma_o - \sigma_i)$ responsible for fatigue damage, and hence the fatigue life would be higher. The second effect is due to the introduction of compressive stress fields on the surface where cracks generally occur, thus inhibiting their growth.

Effect of Temperature

The dependence on temperature does not appear explicitly in the theory, but it is fairly easy to see how it occurs. In the first place, an increase in temperature means a decrease in the modulus E and hence a higher rate of crack propagation. However, the second and probably more important effect of temperature is in its capacity to reduce the mean internal stress level. The substantially stable array of dislocations that exists at the room temperature will be upset at the elevated temperatures where creep-type mechanisms can operate. Thermally activated dislocation climb[5] and possible mutual annihilation of these activated dislocations can reduce the value of σ_i with the result that the crack propagation rates will again become larger. If the temperatures are higher than the normal recrystallization temperatures of the material, the temperature effect occurs through the grain growth

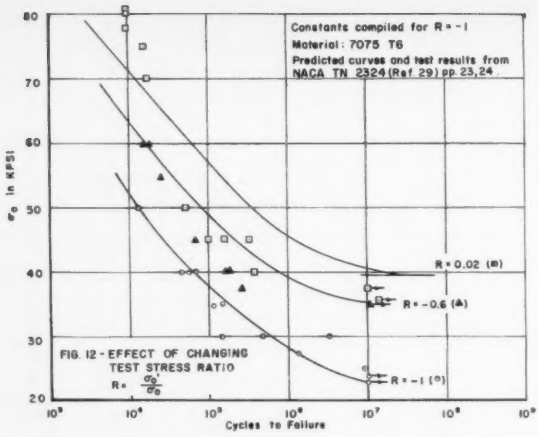
Constants compiled for R = -1
Material: 7075 T6
Predicted curves and test results from
NACA TN 2324 (Ref 29) pp 23,24
R = 0.02 (⊞)
R = -0.6 (Δ)
R = -1 (○)
FIG. 12 - EFFECT OF CHANGING
TEST STRESS RATIO
R = σo'/σo
σo in KPSI
Cycles to Failure

Fig. 12.

during testing leading to larger values of the grain and, hence, again a decrease in the fatigue life. While qualitatively the dependence of fatigue through the variation of E, σ_i, and L_m is fairly easy to understand, we are not yet in a position to take it into account quantitatively in a satisfactory manner, since the dislocation theories pertaining to these aspects are not too well developed.

Effect of Changing Test Stress Ratio

The effect of changing the test ratio may be investigated in a straightforward manner. Introducing the test stress ratio $R = \sigma_o'/\sigma_o$, we can rewrite the expression for cycles to failure in the alternate form

$$N = \frac{2}{C} \frac{\log_e (\sigma_{ult}/\sigma_o) \log_e [(\sigma_o - \sigma_{i_R})/K]}{\left[\frac{\sigma_o(\sigma_o - \sigma_{i_R})}{E\sigma_{i_R}}\right]^2 (1 - R)^2} \quad (26)$$

where σ_{i_R} is "endurance limit" appropriate for given test stress ratio. Thus, for example, when $R = -1$, the minimum stress is in compression and is exactly equal in magnitude to the maximum tensile stress. Test ratio $R = 1$ implies no fatigue stress. If the form of the equation has general validity, it should be possible to compute the constants C and K for one value of R (say, $R = -1$), and the same constants must be valid for different values of R for the same material, provided appropriate values of the endurance limit corresponding to the different test stress ratios are used. No exhaustive or statistically reliable test results are available to explore this idea thoroughly, but Grover *et al.*[29] present test results in which the range was varied from $R = -1$ to $R = +0.80$. Figs. 11 and 12 show the comparison between the theory and their test results which may be considered fair. More exhaustive tests are necessary to confirm these different aspects.

Cumulative Damage

The generally observed results of cumulative damage are among perhaps the most direct consequences of the theory. The Miner[30] theory of cumulative damage suggests that, when different stress levels are applied for a different number of cycles, total life to failure is governed by the condition that

$$\sum_{q=1}^{q} \frac{n_q}{N_q} = 1 \quad (27)$$

where n_q is number of cycles applied at stress level σ_q, and N_q is total number of cycles to failure at this constant stress level. It has been evident from the beginning that this theory is inadequate in the sense that the experimentally observed sum is rarely equal to 1 as the theory predicts. Furthermore, it is well known that if two stress levels σ_1 and $\sigma_2 (\sigma_1 < \sigma_2)$ are used in a two-step cumulative damage test, the sum of the partial life fractions is very much dependent upon the order in which the stresses are applied. If the low stress is applied first, the sum is generally found to be less than one, and if the high stress is applied first, the sum is found to be greater than one. This sensitivity to the order of stressing is not explainable on the basis of Miner's theory. More recently, several theories of an essentially empirical nature have been proposed in order to explain this phenomenon. Among them are those of Freudenthal and Heller,[31] Corten and Dolan,[32] Liu and Corten,[33] and Newmark.[34] These theories suggest, in general, that the damage is not simply proportional to n_q/N_q but to some power of this fraction. All these theories have been able to explain some of the different aspects of cumulative damage with varying degrees of success.

It appears, however, that a cumulative principle sensitive to the order of stressing is a natural consequence of the present theory. The theoretical model has in it the natural means of extension of the theory to program-type loading, random loading, and—as a formal extension—the theory of acoustic fatigue. In view of the importance of the cumulative damage aspects of fatigue to the aircraft industry, the theory will be developed here in some detail.

Two-Step Cumulative Damage

Consider the application of two stresses σ_1 and σ_2 with the corresponding stress ranges $(\sigma_1 - \sigma_1')$ and $(\sigma_2 - \sigma_2')$. Assume $\sigma_1 < \sigma_2$. With this information and the statistically reliable results of a basic curve of stress vs. number of cycles, we can construct curves of Eq. (19) for these two stresses and the appropriate ranges (Fig. 13). Let us now consider the application of n cycles at stress level σ_1 and its appropriate range. As a consequence, the initial crack of length l_0 will grow to

length l_1 as indicated by the vertical line with the open arrow. The crack of the same length can be grown by n_2 cycles at stress level σ_2 and its appropriate range. It is easy to see from Eq. (19) that

$$\frac{\left(\frac{\sigma_1 - \sigma_{1i}}{E}\right)^2\left(\frac{\sigma_1 - \sigma_1'}{\sigma_{1i}}\right)^2}{\log_e\left(\frac{\sigma_1 - \sigma_{1i}}{K}\right)} n = \log_e \frac{l_1}{l_0} = \frac{\left(\frac{\sigma_2 - \sigma_{2i}}{E}\right)^2\left(\frac{\sigma_2 - \sigma_2'}{\sigma_{2i}}\right)^2}{\log_e\left(\frac{\sigma_2 - \sigma_{2i}}{K}\right)} n_2 \quad (28)$$

where the notations σ_{1i} and σ_{2i} indicate that when $|\sigma_1| \neq |-\sigma_1'|$ and $|\sigma_2| \neq |-\sigma_2'|$, then $\sigma_{1i} \neq \sigma_{2i}$ —that is, if there exists a mean stress, the endurance limit is not necessarily the same, as indicated in the discussion of the effect of test stress ratio. We may, therefore, write

$$n_2 = n\left(\frac{\sigma_1 - \sigma_{1i}}{\sigma_2 - \sigma_{2i}}\right)^2\left(\frac{\sigma_1 - \sigma_1'}{\sigma_2 - \sigma_2'}\right)^2\left(\frac{\sigma_{2i}}{\sigma_{1i}}\right)^2 \times \left[\log_e\left(\frac{\sigma_2 - \sigma_{2i}}{K}\right)\right] \Big/ \left[\log_e\left(\frac{\sigma_1 - \sigma_{1i}}{K}\right)\right] \quad (29)$$

Insofar as the test specimen is concerned, it is of little consequence how the damage is caused. An irreversible damage exists in the specimen, and the relationship between the number of cycles of stress at different stress levels and their appropriate ranges for the same amount of damage is given by Eq. (29). In a sense, this is the fundamental equation for the discussion of different aspects of cumulative damage. If now we change over to stress σ_2 and its appropriate range and subject the test specimen to fatigue failure at this stress level, the specimen will fail when the crack reaches the appropriate critical length for failure at this level. The progress of damage therefore follows the line associated with stress σ_2 (indicated by open arrows, Fig. 13) and terminates at point N_2. Therefore, the additional number of cycles to failure sustained by the specimen is $(N_2 - n_2)$, and the total number of cycles to failure is

$$N_{12} = n + (N_2 - n_2) \quad (30)$$

The sum of the familiar damage fractions is given by

$$S_{12} = \frac{n}{N_1} + \frac{N_2 - n_2}{N_2} = \frac{n}{N_1} + 1 - \frac{n_2}{N_2} \quad (31)$$

It may be noted that in the normal practice n/N_1 is plotted against n_2/N_2 of the present notation. In the normal notation this is the same as plotting n_1'/N_1 against $1 - (n_2'/N_2)$ where n_1' and n_2' are the partial lives at the two stress levels. Substituting appropriate values of N_1 and N_2, it may be seen that

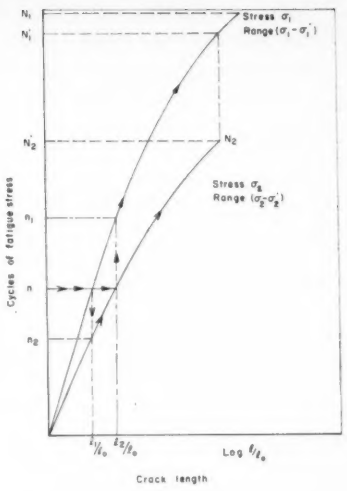

Fig. 13. Schematic representation for discussion of two-step cumulative damage.

$$\frac{n_1'}{N_1} = \frac{n}{N_1} = n\frac{C}{2}\frac{\left(\frac{\sigma_1 - \sigma_{1i}}{E}\right)^2\left(\frac{\sigma_1 - \sigma_1'}{\sigma_{1i}}\right)^2}{\log_e\left(\frac{\sigma_{ult}}{\sigma_1}\right)\log_e\left(\frac{\sigma_1 - \sigma_{1i}}{K}\right)} = \alpha_1 n \quad (32)$$

$$1 - \frac{n_2'}{N_2} = \frac{n_2}{N_2} = n\frac{C}{2} \times \frac{\left(\frac{\sigma_1 - \sigma_{1i}}{E}\right)^2\left(\frac{\sigma_1 - \sigma_1'}{\sigma_{1i}}\right)^2}{\log_e\left(\frac{\sigma_{ult}}{\sigma_2}\right)\log_e\left(\frac{\sigma_1 - \sigma_{1i}}{K}\right)} = \alpha_2 n \quad (33)$$

It is clear from the structure of the two equations that α_1 and α_2 are predetermined constants once the stresses (and their ranges) are given. In similar manner, we can see that if the order of application of stresses is reversed and σ_2 is applied first for n cycles, we obtain

$$N_{21} = n + (N - n_1) \quad (34)$$

where n_1 is equivalent number of cycles to failure at stress level σ_1 to cause the same damage as that due to n cycles at stress level σ_2. The corresponding partial life fractions are

$$\frac{n_2'}{N_2} = \frac{n}{N_2} = n\frac{C}{2}\frac{\left(\frac{\sigma_2 - \sigma_{2i}}{E}\right)^2\left(\frac{\sigma_2 - \sigma_2'}{\sigma_{2i}}\right)^2}{\log_e\left(\frac{\sigma_{ult}}{\sigma_2}\right)\log_e\left(\frac{\sigma_2 - \sigma_{2i}}{K}\right)} = \beta_1 n \quad (35)$$

$$1 - \frac{n_1'}{N_1} = \frac{n_1}{N_1} = n\frac{C}{2} \times \frac{\left(\frac{\sigma_2 - \sigma_{2i}}{E}\right)^2\left(\frac{\sigma_2 - \sigma_2'}{\sigma_{2i}}\right)^2}{\log_e\left(\frac{\sigma_{ult}}{\sigma_1}\right)\log_e\left(\frac{\sigma_2 - \sigma_{2i}}{K}\right)} = \beta_2 n \quad (36)$$

It is immediately seen that the results of this theory are different from those of Miner's theory. In Miner's theory, $\alpha_1 = \beta_1$ and $\alpha_2 = \beta_2$. The sum of the partial life fractions when stress σ_1 is applied first and then σ_2 is $S_{12} = \alpha_1 n + (1 - \alpha_2 n)$. Therefore,

$$S_{12} = 1 - \frac{nC}{2} \frac{\left(\frac{\sigma_1 - \sigma_{1i}}{E}\right)^2 \left(\frac{\sigma_1 - \sigma_1'}{\sigma_{1i}}\right)^2}{\log_e \left(\frac{\sigma_1 - \sigma_{1i}}{K}\right)} \times \left\{ \frac{(\log_e \sigma_2 - \log_e \sigma_1)}{\log_e \left(\frac{\sigma_{ult}}{\sigma_1}\right) \log_e \left(\frac{\sigma_{ult}}{\sigma_2}\right)} \right\} \quad (37)$$

Similarly, $S_{21} = 1 + n(\beta_1 - \beta_2)$. Therefore,

$$S_{21} = 1 + \frac{nC}{2} \frac{\left(\frac{\sigma_2 - \sigma_{2i}}{E}\right)^2 \left(\frac{\sigma_2 - \sigma_2'}{\sigma_{2i}}\right)^2}{\log_e \left(\frac{\sigma_2 - \sigma_{2i}}{K}\right)} \times \left\{ \frac{(\log_e \sigma_2 - \log_e \sigma_1)}{\log_e \left(\frac{\sigma_{ult}}{\sigma_1}\right) \log_e \left(\frac{\sigma_{ult}}{\sigma_2}\right)} \right\} \quad (38)$$

It is easy to see that since $\sigma_1 < \sigma_2$, $S_{12} < 1$ and $S_{21} > 1$, a result that is consistent with the generally observed values. As already mentioned, $\alpha_2 n$ is plotted against $\alpha_1 n$ and $\beta_2 n$ against $\beta_1 n$ to describe cumulative damage. The slopes of the two lines thus obtained are given by

$$\left(\frac{dy}{dx}\right)_{12} = \frac{\alpha_2}{\alpha_1} = \frac{(\log_e \sigma_{ult} - \log_e \sigma_1)}{(\log_e \sigma_{ult} - \log_e \sigma_2)} \quad (39)$$

$$\left(\frac{dy}{dx}\right)_{21} = \frac{\beta_2}{\beta_1} = \frac{(\log_e \sigma_{ult} - \log_e \sigma_2)}{(\log_e \sigma_{ult} - \log_e \sigma_1)} \quad (40)$$

where the notation $(dy/dx)_{12}$ implies the slope of the damage line when stress σ_1 is applied first and then σ_2, and vice versa for $(dy/dx)_{21}$. It is seen from these relations that when the low stress is applied first and then the high stress, the damage line falls above the Miner representation (45° line), and the opposite occurs when the order of application of stress is reversed. We may also note a symmetry relation between the two lines represented by the two Eqs. (39) and (40), by virtue of the fact that

$$(dy/dx)_{12}(dy/dx)_{21} = 1 \quad (41)$$

This symmetry of the damage curves has been observed.[35]

An extremely important aspect of cumulative damage may be pointed out at this stage. Suppose that low stress σ_1 is applied with the expectation that at some stage the stress will be changed to higher stress σ_2 (Fig. 13). When the number of cycles at stress level σ_1 reaches N_1' as indicated in the figure, the length of the crack will have become just critical for stress level σ_2. Therefore, while in single stress fatigue it is meaningful to talk in terms of fatigue cycles beyond N_1', in two-step application it is not meaningful to do so. The value of N_1' is given by the condition

$$\log_e \frac{l}{l_0} = \log_e \left(\frac{\sigma_{ult}}{\sigma_2}\right)^2 = C \frac{\left(\frac{\sigma_1 - \sigma_{1i}}{E}\right)^2 \left(\frac{\sigma_1 - \sigma_1'}{\sigma_{1i}}\right)^2}{\log_e \left(\frac{\sigma_1 - \sigma_{1i}}{K}\right)} N_1' \quad (42)$$

so that

$$N_1' = \frac{2}{C} \frac{\log_e \left(\frac{\sigma_{ult}}{\sigma_2}\right) \log_e \left(\frac{\sigma_1 - \sigma_{1i}}{K}\right)}{\left(\frac{\sigma_1 - \sigma_{1i}}{E}\right)^2 \left(\frac{\sigma_1 - \sigma_1'}{\sigma_{1i}}\right)^2} \quad (43)$$

The maximum value beyond which n has no meaning in two-step cumulative damage is given by the condition

$$n = N_1' \quad (44)$$

Substituting this value, the limiting points of the damage lines in Fig. 14 are found to be

$$\left.\begin{aligned} \alpha_1 n_{max} &= \alpha_1 N_1' = \frac{(\log_e \sigma_{ult} - \log_e \sigma_2)}{(\log_e \sigma_{ult} - \log_e \sigma_1)} &&= X_1 \\ \alpha_2 n_{max} &= \alpha_2 N_1' = 1 &&= Y_1 \\ \beta_1 n_{max} &= 1 \quad = &&= X_2 \\ \beta_2 n_{max} &= \frac{(\log_e \sigma_{ult} - \log_e \sigma_2)}{(\log_e \sigma_{ult} - \log_e \sigma_1)} &&= Y_2 \end{aligned}\right\} \quad (45)$$

It is clear that, given the two stresses σ_1 and σ_2 and the ultimate tensile strength, we can draw the damage lines from the information contained in Eqs. (39), (40), and (45). Thus, for every pair of stresses, we obtain a pair of damage lines. As an example, such a damage line fan is drawn in Fig. 14 for the same numerical data for which curves in Figs. 7 and 8 are appropriate. In the scheme of things presented here, it is not meaningful to join these pairs of lines to the point (1, 1) as is commonly done In fact, it is difficult to see why these curves

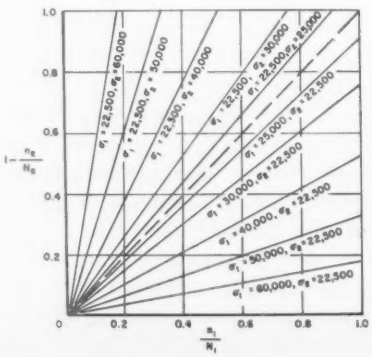

Fig. 14. Cumulative damage curves for different pairs of stresses. (Curves computed for the same specimens as Fig. 7.)

should converge on this point. As an example, test results from Grover *et al.*[29] and the predicted damage lines for a pair of stresses are given in Fig. 15.

Generalization to cumulative damage involving three or more stress levels is straightforward. It is seen that if the stresses are given by σ_1, σ_2, σ_3, ... σ_q; Δn_1, Δn_2, Δn_3, Δn_q are the number of cycles of stress applied at each one of these stress levels, and if σ_r is the last stress to be applied (denoted as a reference stress), we have the number of cycles sustained until failure occurs at the last stress given by

$$\Delta n_r = N_r - \sum_{q=1}^{q} (\Delta n_r)_q \tag{46}$$

where

$$(\Delta n_r)_q = \Delta n_q \left(\frac{\sigma_q - \sigma_{qi}}{\sigma_r - \sigma_{ri}}\right)^2 \left(\frac{\sigma_q - \sigma_q'}{\sigma_r - \sigma_r'}\right)^2 \left(\frac{\sigma_{ri}}{\sigma_{qi}}\right)^2 \times \frac{\log_e\left(\frac{\sigma_r - \sigma_{ri}}{K}\right)}{\log_e\left(\frac{\sigma_q - \sigma_{qi}}{K}\right)} \tag{47}$$

and Δn_r is number of cycles sustained at stress level σ_r applied last after applying Δn_1, Δn_2, Δn_3 ... cycles at stress levels σ_1, σ_2, σ_3, etc., and N_r is cycles to failure at stress level σ_r.

Program-Type Loading

In program-type loading, the common practice is to apply a sequence of cycles of stress at various stress levels and repeat the sequence until failure occurs. The problem then is one of determining the number of times the sequence can be applied before failure occurs.

Let us, for example, assume that stresses σ_1, σ_2, σ_3, ... σ_q are applied for Δn_1, Δn_2, Δn_3, ... Δn_q cycles. Δn_q is arbitrary; the only limitation is that $\Delta n_q < N_q$, where N_q is number of cycles to failure at stress level σ_q. As before, let σ_r be the reference stress. It can be any one of stresses σ_1, σ_2, σ_3, σ_q; the only limitation is that $\sigma_r > \sigma_{ri}$, the endurance limit. During the application of the sequence once, the extent of equivalent life consumed at reference stress σ_r is given by

$$(\Delta n_e)_r = \sum_{q=1}^{q} (\Delta n_r)_q \tag{48}$$

where $(\Delta n_r)_q$ is given by Eq. (47). Failure would then occur when the crack in the specimen reaches a length just critical for the largest stress of the sequence. If σ_L is the largest stress of the sequence, the number of cycles $(N_r)_L$ needed at the reference stress to reach the critical length is given by

$$(N_r)_L = \frac{2}{C} \frac{\log_e \frac{\sigma_{ult}}{\sigma_L} \log_e\left(\frac{\sigma_r - \sigma_{ri}}{K}\right)}{\left(\frac{\sigma_r - \sigma_{ri}}{E}\right)^2 \left(\frac{\sigma_r - \sigma_r'}{\sigma_{ri}}\right)^2} \tag{49}$$

Therefore, the number of times the sequence can be applied before failure occurs is

$$n_S = (N_r)_L / (\Delta n_e)_r \tag{50}$$

It will be noted that $(\Delta n_e)_r$ is essentially the weighted sum of the stress pulses in the sequence. Consequently, the result n_S is sensitive to the number of cycles at each stress level. If the size of the block of the program—that is, $\Delta n_1 + \Delta n_2 + \Delta n_3 \ldots \Delta n_q = \Delta n_{T_F}$—the total number of actual cycles to failure is

$$N_{T_P} = n_S \Delta n_{T_P} \tag{51}$$

For example, let us consider the tests performed by Liu and Corten[36] in which $\sigma_q = -\sigma_q'$, so that $\sigma_{qi} = \sigma_{ri} = \sigma_i$. The program-type loading used by Liu and Corten consists of applying two stress levels in blocks of 10,000 cycles in reversed bending, varying the ratio of cycles corresponding to the two stress levels. Eq. (47) therefore reduces to

$$(\Delta n_r)_q = \Delta n_q \left(\frac{\sigma_q - \sigma_i}{\sigma_r - \sigma_i}\right)^2 \left(\frac{\sigma_q}{\sigma_r}\right)^2 \times \left[\log_e\left(\frac{\sigma_r - \sigma_i}{K}\right)\right] \Big/ \left[\log_e\left(\frac{\sigma_q - \sigma_i}{K}\right)\right] \tag{52}$$

The value obtained for σ_i on a statistical basis was 20,000 psi, and from among the different test levels used by them we shall choose the high stress as 50,000 psi, and the low stress 45,000, 35,000, and 25,000 psi. The percentage of life at high stress was taken as 9.95, 3.97, and 0.95 percent. Let us, for example, consider that $\sigma_1 = 50{,}000$ psi and $\sigma_2 = 45{,}000$ psi, and let us choose σ_1 as the reference stress σ_r. Therefore,

$$\Delta n_{er} = \Delta n_1 + \Delta n_2 \left(\frac{45{,}000\text{–}20{,}000}{50{,}000\text{–}20{,}000}\right)^2 \left(\frac{4.5}{5}\right)^2 \times \frac{\log_e\left(\frac{50{,}000\text{–}20{,}000}{K}\right)}{\log_e\left(\frac{45{,}000\text{–}20{,}000}{K}\right)}$$

$$= \Delta n_1 + \Delta n_2 \times 0.563 \frac{\log_e\left(\frac{3 \times 10^4}{K}\right)}{\log_e\left(\frac{2.5 \times 10^4}{K}\right)}$$

Since the logarithmic terms are so close to each other, considerable simplification results without serious loss of accuracy if we neglect them. Thus,

$$\Delta n_{er} = \Delta n_1 + \Delta n_2 \times 0.563$$

The life to failure at the reference stress level of 50,000 psi on a statistical basis is 18,770 cycles based on 72 tests. Therefore, the number of blocks to failure is

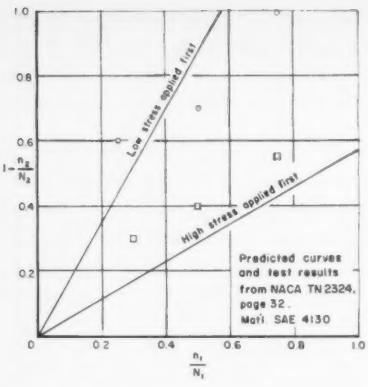

Fig. 15. Response to order of application of stress in cumulative damage.

$$n_S = \frac{18{,}770}{\Delta n_{er}} = \frac{18{,}770}{\Delta n_1 + \Delta n_2 \times 0.563}$$

Since the size of each block is 10,000 cycles, the actual life to failure is

$$10{,}000\, n_S = 10^4 \frac{18{,}770}{\Delta n_1 + \Delta n_2 \times 0.563}$$

In one test $\Delta n_1 = 995$ and $\Delta n_2 = 9{,}005$. Substituting, we obtain the life to failure in this program of loading as

$$N_{T_P} = 10^4 \times \frac{18{,}770}{995 + 9{,}005 \times 0.563} = 30{,}800 \text{ cycles}$$

The actually observed mean statistical life for tests was 30,550 cycles, thereby giving a percentage error of 0.82 percent. Comparing the logarithms of life, the error is approximately 0.1 percent. Some other computed results are presented in Table 1 and Fig. 16. It will be noted, therefore, that where statistically reliable test results are available, comparison between the theory and experiment appears to be good. It is desirable to obtain extensive additional experimental confirmation of this and the other aspects of the present theory of fatigue.

Fatigue Damage in Random Loading

The case of random loading is a simple extension of the preceding equations. We shall assume that a frequency distribution function of Δn_q vs. σ_q is given. The problem then is one of determining the number of cycles to failure for such a loading. The extent of randomness may be one of two types. In one case, while the loading is random, there is regularity in the loading in the sense that after the application of the number of cycles represented by the area under the distribution curve, the load pulses repeat themselves again in a random manner. The second case will be the problem of predicting the probability of failure during the anticipated design life of a specimen. We shall, for example, imagine that the specimen will be subjected to N_T stress pulses in a random manner during its anticipated life, and that the distribution function is known in terms of the maximum, mean, and minimum stresses and the standard deviation. The problem then is one of ascertaining the probability of failure at any stage.

Considering the first case, let us assume, for example, that the stress pulses obey a normal distribution function,

$$\Delta n_q = \frac{1}{\rho_1} \frac{\Delta n_T}{\sqrt{2\pi s}}\, e^{-\frac{1}{2}\left(\frac{\sigma_q - \sigma_m}{s}\right)^2} d\sigma_q \qquad (53)$$

where σ_m is mean stress of the sequence, s is standard deviation, Δn_T is total number of cycles in this random sequential loading, and ρ_1 is a normalization factor introduced by virtue of the fact that the maximum and minimum stresses do not go to infinity. The equivalent number of cycles corresponding to Δn_T at reference σ_r is

$$\Delta n_{er} = \Delta n_T \int_{\sigma_{min} > \sigma_{qi}}^{\sigma_{max}} \frac{1}{\rho_1 \sqrt{2\pi s}} \exp\left\{-\frac{1}{2}\left(\frac{\sigma_q - \sigma_m}{s}\right)^2\right\} \times \left[\frac{\sigma_q - \sigma_{qi}}{\sigma_r - \sigma_{ri}} \frac{\sigma_q - \sigma_q'}{\sigma_r - \sigma_r'} \frac{\sigma_{ri}}{\sigma_{qi}}\right]^2 d\sigma_q \qquad (54)$$

The logarithmic terms are neglected in view of the relatively small change that they cause in the final results and the considerable simplification that results from this approximation. Therefore, the number of blocks of random sequential pulses Δn_T which may be applied before failure occurs is

$$n_{S-1} = (N_r)_L / \Delta n_{er} \qquad (55)$$

where $(N_r)_L$ is given by Eq. (49), with the assumption $\sigma_L = \sigma_{max}$. Because of the randomness of the application of stress pulses, the failure in the n_S block has a probability of failure whose cumulative probability increases from 0 at the beginning of the block to 1 at the number of cycles corresponding to failure at the minimum stress of the block. It must be noted that this probability of failure is quite different from the inherently statistical nature of the fatigue problem and arises by virtue of the randomness of the load application. As before, the actual number of random stress pulses which may be applied before any failure occurs is

$$N_{T_{S-1}} = \Delta n_T \frac{(N_r)_L}{\Delta n_{er}} = \Delta n_T \times n_{S-1} \qquad (56)$$

During application of the next Δn_T cycles, failure would occur as indicated in Eq. (56) and the cumulative probability of failure will apparently be a function of the cumulative distribution function of the applied stress pulses and the instantaneous crack length. This will be discussed in detail elsewhere.

The second problem may be treated as a formal extension of this case. We shall now interpret Δn_T not as the number of pulses applied in a random manner in a block, but as the total number of

cycles N_T that are presumed to be applied during the anticipated design life of the specimen. The minimum number of cycles at which failure may be expected will correspond to the critical crack length for maximum anticipated stress $\sigma_L = \sigma_{max}$. Therefore, the formal number of blocks after which failure may be expected is

$$n_{S,\,min} = (N_r)_L/(N_e)_r \tag{57}$$

where $(N_e)_r$ is given by Eq. (54) with N_T substituted for Δn_T and the appropriate distribution function. The actual number of stress pulses after which failure may be expected is therefore

$$N_a = N_T n_{S,\,min} \tag{58}$$

It is clear that if $n_{S,\,min} < 1$, the failure would occur during the anticipated life of the specimen. Correspondingly, if $n_{S,\,min} > 1$, no failure may be expected. The mean anticipated life, following the same reasoning, is

$$N_{a,\,mean} = N_T \frac{(N_r)_{mean}}{(N_e)_r} \tag{59}$$

where

$$(N_r)_{mean} = \frac{2}{C} \frac{\log_e \left(\frac{\sigma_{ult}}{\sigma_{mean}}\right) \log_e \left(\frac{\sigma_r - \sigma_{ri}}{K}\right)}{\left(\frac{\sigma_r - \sigma_{ri}}{E}\right)^2 \left(\frac{\sigma_r - \sigma_r'}{\sigma_{ri}}\right)^2} \tag{60}$$

The maximum life that may be expected before failure occurs is

$$N_{a,\,max} = N_T\,[(N_r)_{max}/(N_e)_r] \tag{61}$$

where it will be noted that

$$(N_r)_{max} = \frac{2}{C} \frac{\log_e \frac{\sigma_{ult}}{\sigma_{min}} \log_e \frac{\sigma_r - \sigma_{ri}}{K}}{\left(\frac{\sigma_r - \sigma_{ri}}{E}\right)^2 \left(\frac{\sigma_r - \sigma_r'}{\sigma_{ri}}\right)^2} \tag{62}$$

Acoustic Fatigue

Any theory of acoustic fatigue has three essential aspects. The first is an adequate quantitative representation of the acoustic field. The second is the determination of the stress response of a panel to this given acoustic input. The third is the estimation of the time to failure of the panel for the stress response so determined. The emphasis in this section is on the third aspect; it will be treated as a formal extension of the present theory of fatigue. This is possible since it appears that acoustic fatigue is essentially the response of the structure to random excitation.

The stress response of the panel to an acoustic input is given generally in either of the equivalent alternate forms, its power spectrum or an rms stress as a function of the frequency. An additional assumption is frequently made that the amplitude peaks associated with an rms stress peak obey the Rayleigh distribution function given by

$$P = \left(\frac{\sigma_q''}{\bar{\sigma}_q}\right) e^{-1/2\left(\frac{\sigma_q''}{\bar{\sigma}_q}\right)^2} \tag{63}$$

where $\bar{\sigma}_q$ is rms stress peak occurring at frequency ω_q, and P is probability of occurrence of amplitude peak σ_q''. It is apparent that there is an additional complexity in this problem because of the different frequencies at which fatigue stress cycles are simultaneously imposed. Because of this, it will be found necessary to estimate equivalent times for the damage at a reference frequency and stress corresponding to different times for the same damage at the different frequencies and stresses.

Let us consider a frequency ω_q, and let the rms value of the stress at this frequency be $\bar{\sigma}_q$. In unit time, the probable number of stress pulses Δn_q related with each stress amplitude σ_q'' is given by

$$\Delta n_q = \frac{\omega_q}{\rho_2} \frac{\sigma_q''}{\bar{\sigma}_q} \exp\left\{-\frac{1}{2}\left(\frac{\sigma_q''}{\bar{\sigma}_q}\right)^2\right\} d\sigma_q'' \tag{64}$$

where ρ_2 is a normalization constant that takes into account the fact that the maximum and minimum anticipated stresses are finite. There are two additional aspects worth noting in acoustic fatigue. The first is that there is generally a mean stress over which is superposed the vibratory stresses. The second is that the vibrations are taking place over a range of frequencies (Fig. 17), and so pre-

Table 1. Comparison Between Theory and Test Results for Program-Type Loading

High Stress	Low Stress	Percent of Life at High Stress	Predicted Life to Failure	Actual Life to Failure	Percent Variation	Log of Predicted Life	Log of Actual Life	Percent Variation
50,000	45,000	9.95	30,800	30,550	0.82	4.4886	4.4851	0
50,000	45,000	3.97	32,000	33,600	4.72	4.5051	4.5262	0.246
50,000	45,000	0.95	32,600	31,220	4.42	4.4997	4.4945	0
50,000	35,000	9.95	85,100	87,600	2.86	4.9299	4.9424	0.25
50,000	35,000	3.97	118,500	118,100	0.34	5.0737	5.0722	0
50,000	35,000	0.95	143,500	132,500	8.3	5.1568	5.1221	0.68
50,000	25,000	9.95	162,500	163,700	0.75	5.2108	5.214	0
50,000	25,000	3.97	404,000	362,000	11.7	5.6064	5.5583	0.865
50,000	25,000	0.97	1,135,000	1,045,000	8.6	6.0550	6.0191	0.6
				Mean variation	4.7	Mean variation		0.29

Material 7075-T6 aluminum alloy.

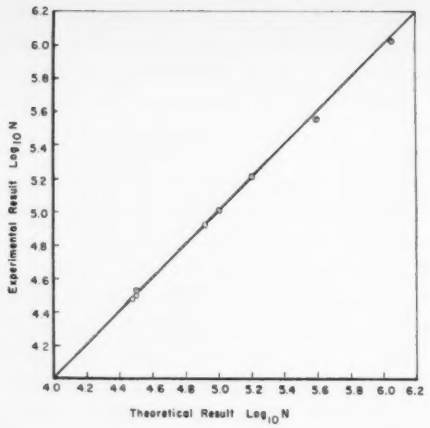

Fig. 16. Comparison between statistical mean values in program-type loading. Test results from NASA D-647.

sumably one has to take into account the effect of frequency on fatigue. It has already been mentioned that in high-purity aluminum one may observe about a decade change in fatigue life for three-decade change in frequency. Apparently, for many alloys, the change is much less. Typically, in the case of acoustic fatigue, the frequency range over which significant rms stress peaks occur is rarely more than one decade. This would probably correspond to a maximum of 200–300 percent change in life, well within the normal scatter band of fatigue. So to obtain a reasonable solution to the problem of acoustic fatigue, the assumption may be made that the effect of frequency as such may be neglected. We can now write the governing equation for acoustic fatigue (neglecting the logarithmic terms)

$$(\Delta n_r)_q = \Delta n_q \left\{ \frac{\sigma_q'' - \sigma_{mqi}}{\sigma_r'' - \sigma_{mri}} \cdot \frac{\sigma_q'' - \sigma_{mq}}{\sigma_r'' - \sigma_{mr}} \cdot \frac{\sigma_{mri}}{\sigma_{mqi}} \right\}^2 \quad (65)$$

where σ_{mqi} is endurance limit at frequency of vibration ω_q corresponding to mean stress σ_{mq}. Eq. (65) is exactly the same as Eq. (47) except that it is rewritten in terms of mean stress instead of stress range. The total equivalent number of cycles per unit time at the reference stress corresponding to stresses $\bar{\sigma}_q$ may therefore be written as

$$\Delta n_{erq} = \int_{\sigma_{mqi}}^{\sigma_L''} \frac{\omega_q}{\rho_2} \cdot \frac{\sigma_q''}{\bar{\sigma}_q} \exp\left\{ -\frac{1}{2}\left(\frac{\sigma_q''}{\bar{\sigma}_q} \right)^2 \right\} \times \left\{ \frac{(\sigma_q'' - \sigma_{mqi})}{(\sigma_r'' - \sigma_{mri})} \cdot \frac{(\sigma_q'' - \sigma_{mq})}{(\sigma_r'' - \sigma_{mr})} \cdot \frac{\sigma_{mri}}{\sigma_{mqi}} \right\}^2 d\sigma_q'' \quad (66)$$

The limit σ_{mqi} is chosen on the basis of the assumption that any stresses below the endurance limit have no effect on the fatigue life. This assumption does not appear to be rigorously true. The stress σ_L'' is an arbitrary upper limit of the Rayleigh distribution function. If the reference frequency is ω_r, the time it takes to impose Δn_{erq} cycles is clearly given by

$$T_{erq} = \Delta n_{erq}/\omega_r \quad (67)$$

It must be noted that there are rms stress amplitude peaks at different frequencies ω_q and these have to be added. The total equivalent time at the reference frequency and the reference stress level is

$$t_{er} = \sum_{q=1}^{q} t_{erq} \quad (68)$$

In order to obtain actual time to failure, we have to divide time to failure t_r at the reference stress level and the reference frequency by t_{er}. Thus, actual time to failure is given by

$$t_A = t_r/t_{er} \quad (69)$$

The time t_r may be seen to be equal to

$$t_r = \frac{(N_r)_L}{\omega_r} = \frac{1}{2c\omega_r} \frac{\log_e \dfrac{\sigma_{ult}}{\sigma_L''} \log_e \left(\dfrac{\sigma_r'' - \sigma_{mri}}{K} \right)}{\left\{ \dfrac{\sigma_r''(\sigma_r'' - \sigma_{mri})}{E\sigma_{mri}} \right\}^2 \left\{ 1 - \dfrac{\sigma_{mr}}{\sigma_r''} \right\}^2} \quad (70)$$

Physically, t_{er} is the sum of the equivalent times at the reference frequency for the damage to which the material is being subjected simultaneously at different frequencies and stress levels in unit standard time. Essentially t_{er} may be looked upon as a coordinate transformation for time. The transformation is from the frequencies ω_q and stress σ_q'' to the reference frequency ω_r and reference stress σ_r''. Eqs. (66–68) may be looked upon as appropriate coordinate transformations.

Simplifying Assumptions and Resulting Equations

Solution to the problem of acoustic fatigue is essentially given by Eq. (69). A comment is in order regarding the choice of the reference frequency and reference stress level. Since the basic stress vs. number of cycles curve of fatigue is to be determined in any case for the panel in order to determine the constants C and K, and since this is most easily done by exciting the panel in its fundamental mode, it simplifies the analysis considerably to choose the frequency of the fundamental mode as the reference frequency. The reference stress may correspondingly be chosen as the largest stress to which the panel may be subjected. The mean stress of vibration which is generally small may be assumed to be approximately the same at the various frequencies. This would also imply the endurance limits to be the same at the different frequencies—that is,

$$\left.\begin{aligned} \sigma_{m1} &= \sigma_{m2} = \sigma_{mr} = \sigma_{mq} = \sigma_m \\ \sigma_{m1i} &= \sigma_{m2i} = \sigma_{mri} = \sigma_{mqi} = \sigma_{mi} \end{aligned}\right\} \quad (71)$$

In addition, it will be noted that t_r is the time to failure at the reference frequency and

the largest stress σ_L'' which may be expected on the test panel. This is a term that can be determined fairly accurately from tests on a statistical basis. In such a case, only the denominator of Eq. (69) needs to be computed. We may therefore write Eqs. (66–69) in the simplified form

$$t_A = t_r/t_{er} = t_r \div \sum_{q=1}^{q} \int_{\sigma_{mi}}^{\sigma_L''} \frac{1}{\rho_2} \left(\frac{\omega_q}{\omega_r}\right) \left(\frac{\sigma_q''}{\bar{\sigma}_q}\right) \exp\left\{-\frac{1}{2}\left(\frac{\sigma_q''}{\bar{\sigma}_q}\right)^2\right\} \times \left\{\frac{\sigma_q'' - \sigma_{mi}}{\sigma_L'' - \sigma_{mi}} \frac{\sigma_q'' - \sigma_{mq}}{\sigma_r'' - \sigma_m}\right\}^2 d\sigma_q'' \quad (72)$$

One implicit assumption made in the formal extension of the present theory of fatigue to the problem of acoustic fatigue must be mentioned. The basic fatigue theory as developed is strictly valid only for high stress levels. In acoustic fatigue, the damage is due more to a large number of cycles of low stress in short time than to a small number of cycles of large stress. Hence, some caution is needed in the extension of the present theory to acoustic fatigue. It will be noted that this item of caution is introduced by using the experimentally determined value of t_r and using the general form of the equations to predict times to failure in acoustic fatigue. Extensive experimental verification is needed to substantiate this approach.

Statistical Aspects

The preceding discussion of the several aspects of fatigue was closely related to the value of σ_i, the internal stress that is presumed to oppose the motion of dislocations. In this theory the value of this internal stress was identified with the endurance limit in fatigue by invoking Bairstow's hypothesis which suggests that the endurance limit of a material is the same as its natural elastic limit. Apart from determining the endurance limit from extensive tests, the determination of the actual value of σ_i is an extremely difficult task at this stage. This is the main disadvantage of the present theory and, in a sense, reflects the bridge between the microscopic and macroscopic approaches.

The difficulty of accurate determination of σ_i brings us directly into the statistical aspects of fatigue, of which there are three items. First, we have assumed that the value σ_i (maximum slope of the potential hills in the material at the level of the lattice structure) is a constant. Actually, it is clear that this is not true. Therefore, in certain regions the plastic enclave will be larger and presumably the deformation more severe than in other regions. In other words, the width of the enclave, and hence the incremental crack length, the rate of strain hardening, and the rate of crack propagation are indeed statistical variables and not the

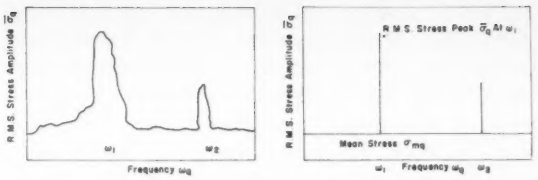

Fig. 17a (*left*). Schematic representation of typical rms stress response in acoustic fatigue. Fig. 17b (*right*). Idealized stress response curve used in discussion of acoustic fatigue.

nonstatistical quantities we have assumed in developing the theory.

The second aspect is concerned with grain size. While in the beginning we assumed that the grain size had a statistical distribution with a mean size L_m and a logarithmic normal distribution, nowhere did we take this specific property into account, although it is not difficult to do so in principle. If grain size distribution is $n(L)dL$, then one can define a mean rate of crack propagation

$$\frac{dl_m}{dN} = \int C_1 \frac{L}{b}\, n(L)\, \frac{\left(\frac{\sigma_o - \sigma_i}{E}\right)^2 \left(\frac{\sigma_o - \sigma_o'}{\sigma_i}\right)^2}{\log_e \frac{\sigma_o - \sigma_i}{K}}\, dL \quad (73)$$

and use this value instead of Eq. (16) in subsequent developments of the theory. In principle, we should do the same thing with σ_i also. But at the present stage of the dislocation theory, we know nothing about its distribution, with the result that there will always be an element of statistical uncertainty in the fatigue results. This will, in principle, be reflected in the theory by a spread of the value σ_i. This necessarily implies that the familiarly defined endurance limit for metals is also a statistical quantity, a fact that has already been shown experimentally by Epremian and Mehl.[37]

The third aspect is concerned with the cracks themselves. The analysis presented here concerned itself with the progress of the "dominant crack" only, and presumably the propagation of this crack proceeds from the opening up of other smaller cracks in its path. In reality, one should expect the possibility of having more than one major crack. In sheet metal structures, this may not be so serious as in other types of three-dimensional structure where it may play a prominent role.

These three aspects therefore seem to indicate that for a considerable time to come, the problem of fatigue will remain essentially statistical in nature. One has to take recourse to extensive tests to obtain statistically reliable data. It appears that the main contribution of the theory is that, when such statistically reliable test data concerning the basic stress vs. number of cycles curve in fatigue are given, most of the other aspects of fatigue may be predicted in a systematic manner without any arbitrary assumptions other than those made or

implied in development of the basic theory. The systematic approach in this method has become possible by virtue of the equivalence relations obtained for determining the number of cycles of stress at any arbitrary reference stress level and range to cause the same damage as the number of cycles of stress at any stress and its appropriate range (and, in acoustic fatigue, its appropriate frequency). This relationship—or, what amounts to the same, the coordinate transformations from the σ_q, $(\sigma_q - \sigma_q')$, Δn_q plane to σ_r, $(\sigma_r - \sigma_r')$, $(\Delta n_r)_q$ plane—are provided by Eq. (47). This equation enables one to treat the problem of fatigue for any arbitrary intermixing of stresses, stress ranges (and, by implication, temperatures and frequencies) as if the whole damage is occurring at one stress amplitude, temperature, and frequency, and discuss the problem at the reference state—i.e., the reference coordinate system.

It was mentioned earlier that any theory is only as good as the assumptions implied in its development. It is therefore highly desirable to call attention to the limitations implied by the assumptions in the present theory. The first is the fact that strain softening, which appears to be an important aspect of fatigue under certain conditions, is not physically taken into account and, hence, cannot be explained by this theory. The second is that there is some evidence to indicate that, if a stress lower than the endurance limit is included in a program, it appears to make some difference in the test results. This would certainly mean that the form of Eq. (17) must respond in some manner to this effect. Presumably, it may be explained on the basis that the value of σ_i changes in some manner in such a test, but there is as yet no way of taking it into account. The third is that there is also some evidence to indicate that the order of application of the loads in program-type loading alters the fatigue life in a more significant manner than the present theory would indicate. The reported test results do not appear to be statistically reliable, and this aspect must be investigated further.

The analysis of cumulative damage in random loading presented here is a first-order approximation only. More detailed investigations are under way at the present. A formal quantitative theory of temperature and frequency which appears to explain many of the known aspects is substantially completed.

Conclusions

An analytical theory of fatigue for high stress levels has been formulated based on a fairly simple model derived from a synthesis of the macroscopic elastoplastic fracture theory and concepts derived from the dislocation theory of metals. The theory (1) predicts the shape of the stress vs. number of cycles curve in fatigue; (2) after determining two of the unknown constants from test results, makes quantitative predictions regarding the residual static strength, changes resulting from change of test stress ratio (and mean stress), cumulative damage due either to multiple step or to random loading; and (3) as a formal extension, gives a quantitative theory of acoustic fatigue. Once the constants have been determined, the theory asserts that no additional assumptions of a fundamental nature are necessary to predict or explain the sensitivity of cumulative damage to the order of stressing and the stress magnitude. The basic statistical nature of the fatigue problem has been attributed to two material variables of which one is grain size and the other, probably more important, a mean internal stress denoted as σ_i which is essentially a stress that opposes the motion of dislocations. This stress, characterized at present by its mean value, depends on the prior stress history and is expected to vary throughout the material with its variation in terms of mean value and its distribution not known. It is suggested that, because of this, the fatigue problem will remain statistical in nature. In the present theory this stress σ_i has been identified with the endurance limit under completely reversed loading. Confirmation of the theory through tests performed by different people has been satisfactory, though considerably more experimental verification is needed. When statistically reliable basic test data are available, quantitative predictions from the theory for program-type loading have been found to be excellent, the average error of prediction being about 5 percent, a value well within the requirements of most designers and engineers. The general form of the equations of this theory of fatigue is such that the treatment of the various aspects of the fatigue problem from a unified viewpoint appears to be feasible.

References

[a] Valluri, S. R., *Comments on Certain Investigations Relative to High Stress-Low Cycle Fatigue*, GALCIT SM 60-21, C.I.T., Dec. 1960, Rev. Jan. 1961.

[b] Valluri, S. R., *A Unified Engineering Theory of High Stress Level Fatigue*, GALCIT SM 61-1, C.I.T., Jan. 1961.

[c] Valluri, S. R., *A Theory of Cumulative Damage in Fatigue*, GALCIT SM 61-2, C.I.T., Jan. 1961.

[d] Valluri, S. R., *Theory of Acoustic Fatigue*, GALCIT SM 61-3, C.I.T., April 1961.

[1] Thompson, N., *Experiments Relating to the Origin of Fatigue Cracks*, in "Fatigue in Aircraft Structures," A. M. Freudenthal (Ed.), Academic Press, 1956.

[2] Forsyth, P. J. E.. *The Fatigue of Aluminum*, in "Fatigue in Aircraft Structures," A. M. Freudenthal (Ed.), Academic Press, 1956.

[3] Cottrell, A. H., *Theoretical Aspects of Fracture*, in "Conference on Fracture," Technology Press of M.I.T., April 1959.

[4] Wood, W. A., *Some Basic Studies in Fatigue of Metals*, in "Conference on Fracture," Technology Press of M.I.T., April 1959.

[5] Cottrell, A. H., *Dislocations and Plastic Flow in Crystals*, Oxford Univ. Press, 1953.

[6] Christensen, R. H., *Fatigue Crack Growth in Metals*,

Douglas Aircraft Co., Engineering Paper No. 985, April 1960.

[7] Lipsitt, H. A., Forbes, F. W., and Baird, R. B., *Crack Propagation in Cold Rolled Aluminum Sheet*, Proc. ASTM, 1959.

[8] Lunchick, M. E., *A Theory of Fatigue Based on a Statistical Distribution of Grain Size*, Univ. of Illinois, ONR Contract N6-ori-71, T.O. IV, July 1952.

[9] Girard, Francois, *Etude Microscopic de la Fissuration Par Fatigue a Haute Frequence*, ONERA France, presented at 2nd International Congress, ICAS, Zurich, Sept. 1960. (Accompanying film shows instances supporting hypothesis of crack propagation due to joining of submicroscopic cracks ahead of propagating crack.)

[10] Koehler, J. S., *The Production of Large Tensile Stresses by Dislocations*, Physical Review, Series 85, 1952.

[11] Zener, C. L., *The Micromechanism of Fracture*, in "Fracturing of Metals," F. Jonassen, W. P. Roop, and R. T. Bayless (Ed.), ASM Symposium, 1952.

[12] Petch, N. J., *The Fracture of Metals*, in "Progress in Metal Physics," Vol. 5, B.Chalmers and R. King (Eds.), Interscience, 1959.

[13] Orowan, E., *Fundamentals of Brittle Behavior in Metals*, in "Fatigue and Fracture of Metals," W. M. Murray (Ed.), Technology Press of M.I.T., 1952.

[14] Eaton, D., and Stimpson, L. D., *The Extent of Elasto-Plastic Yielding at the Crack Point of an Externally Notched Plane Stress Tensile Specimen*, GALCIT SM 60-10, C.I.T., June 1960, Rev., Jan. 1961.

[15] Williams, M. L., *A Review of Recent Research at "GALCIT" Concerning Fracture Initiation*, ARDC, ARL TR-1, Jan. 1961.

[16] Hardrath, H. F., and Ohman, L., *A Study of Elastic and Plastic Stress Concentration Factors Due to Notches and Fillets in a Flat Plate*, NACA TR 1117, 1953.

[17] Liu, H. W., *Crack Propagation in Thin Metal Sheet under Repeated Loading*, Univ. of Illinois, T & AM Report No. 155, Dec. 1959.

[18] Frost, N. E., and Dugdale, D. S., *The Propagation of Fatigue Cracks in Sheet Specimens*, J. Mech. & Physics of Solids, Vol. 6, 1958.

[19] Frost, N. E., and Dugdale, D. S., *Fatigue Tests of Notched Mild Steel Plates with Measurements of Fatigue Cracks*, J. Mech. & Physics of Solids, Vol. 5, 1957.

[20] Bairstow, L., *The Elastic Limits of Iron and Steel under Cyclic Variations of Stress*, Phil. Trans., Royal Society, Vol. 210A, 1911.

[21] Illg, W., *Fatigue Tests on Notched and Unnotched Sheet Specimens of 2024-T3 and 7075-T6 Aluminum Alloys and of SAE 4130 Steel with Special Consideration of the Life Range from 2 to 10,000 Cycles*, NACA TN 3866, Dec. 1956.

[22] Rassweiler, G. M., and Grube, W. L., *Internal Stresses and Fatigue in Metals*, p. 207, 415, Elsevier, 1959.

[23] Lipsitt, H. A., and Wang, D. Y., *The Effect of Interstitial Solute Atoms on the Fatigue Limit Behavior of Titanium*, ARL, Wright-Patterson AFB, May 1960 (also presented at AIME Meeting, Feb. 1960).

[24] Valluri, S. R., *A Unified Engineering Theory of High Stress Level Fatigue*, GALCIT SM 61-1, C.I.T., Jan. 1961.

[25] Valluri, S. R., *A Dislocation Theory Viewpoint of the Effect of Frequency, Temperature and Grain Size on the Fatigue of Metals*, C.I.T., submitted to NASA for publication, Aug. 1959.

[26] Valluri, S. R., *An Experimental Investigation of the Effect of Frequency and Temperature on the Fatigue of High Purity Aluminum*, C.I.T., submitted to NASA for publication, May 1960.

[27] Valluri, S. R., *Effect of Frequency and Temperature on Fatigue of Metals*, NACA TN 3972, Feb. 1957.

[28] Daniels, N. H. G., and Dorn, J. E., *The Effect of Temperature, Frequency and Grain Size on the Fatigue Properties of Pure Aluminum*, WADC TR 54-104, Oct. 1954.

[29] Grover, H. J., Bishop, S. M., and Jackson, L. R., *Fatigue Strength of Aircraft Materials*, NACA TN 2324, March 1951.

[30] Miner, M. A., *Cumulative Damage in Fatigue*, J. Appl. Mech., Vol. 12, No. 3, pp. A-159–164, Sept. 1945.

[31] Freudenthal, A. M., and Heller, R. A., *Accumulation of Fatigue Damage*, in "Fatigue in Aircraft Structures," A. M. Freudenthal (ed.), Academic Press, 1956.

[32] Corten, H. T., and Dolan, T. J., *Cumulative Damage in Fatigue*, International Conf. on Fatigue of Metals, New York, Sept. 1956.

[33] Liu, H. W., and Corten, H. T., *Fatigue Damage During Complex Stress Histories*, NASA TN D-256, Nov. 1959.

[34] Newmark, N. M., *A Review of Cumulative Damage in Fatigue*, in "Fatigue and Fracture of Metals," W. M. Murray (Ed.), Technology Press of M.I.T., 1952.

[35] Douglas Aircraft Co., *Investigation of Thermal Effects on Structural Fatigue*, WADD TR 60-410, Pt. I, Aug. 1960.

[36] Liu, H. W., and Corten, H. T., *Fatigue Damage under Varying Stress Amplitudes*, NASA TN D-647, Nov. 1960.

[37] Epremian, E., and Mehl, R. T., *Investigations of Statistical Nature of Fatigue Properties*, NACA TN 2719, June 1952.

✦ ✦ ✦

AN AUTHORIZED BINDING FOR

Aerospace Engineering

Arrangements have been made by the Institute of the Aerospace Sciences for members and subscribers to have their magazines bound carefully and economically. Simply write for details to:
Publishers' Authorized Bindery Service Ltd., 430 West Erie St., Chicago 10, Ill.

✦ ✦ ✦

Thus the force output required of the operator is seen to be a complex function of a number of quantities, including several variables.

Up to this point we have made no assumptions concerning the primacy of one or another perceptual input, so that the results are perfectly general. If we now assume that the variable ψ is the pilot's primary visual cue in steering and F his primary output, then the function F/ψ represents a simple linear approximation to his transfer function. From Eq. (13), we obtain

$$F/\psi = (1/k)(W/v)[(v - \dot{D})/D] \qquad (14)$$

This statement represents the assumption that the perceptual variable x (lateral distance from centerline) does not play an important part in the steering task. It does not, however, tell us anything about the variable D other than that it must be taken into account by the operator.

Some observations on steering behavior are in order at this point. Most drivers are probably aware of the fact that they tend to look farther ahead at high speeds than at low speeds. This is a logical outgrowth of the fact that, given a particular control task, a human operator is characterized by a more or less constant response time so that his anticipation requirements dictate that he "look ahead" at least a distance equal to response time divided by speed (this is then the distance traveled during the interval of one response time). It may be possible to quantify the relationship experimentally by means of precise eye movement studies to determine fixation point as a function of vehicle speed.

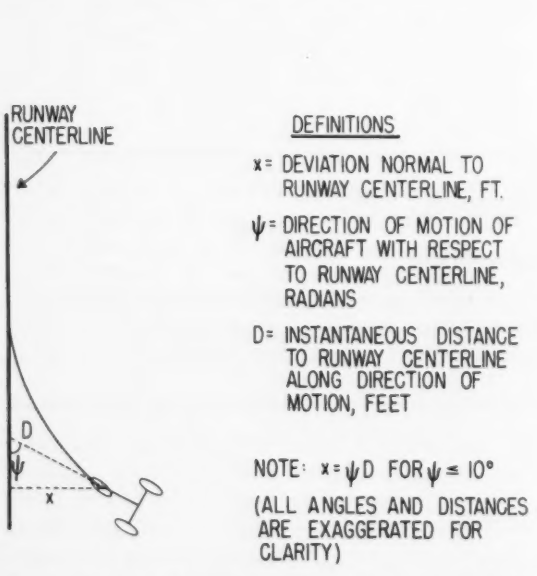
RUNWAY CENTERLINE
DEFINITIONS
x = DEVIATION NORMAL TO RUNWAY CENTERLINE, FT.
ψ = DIRECTION OF MOTION OF AIRCRAFT WITH RESPECT TO RUNWAY CENTERLINE, RADIANS
D = INSTANTANEOUS DISTANCE TO RUNWAY CENTERLINE ALONG DIRECTION OF MOTION, FEET
NOTE: x = ψD FOR ψ ≤ 10°
(ALL ANGLES AND DISTANCES ARE EXAGGERATED FOR CLARITY)
D
ψ
x

Fig. 2. Geometry of visual perception problem associated with steering an aircraft.

In line with these observations and in the absence of definitive data, then, let us make two further extremely important assumptions: (1) that the pilot looks a "distance ahead," d, which is directly proportional to speed—viz., $d = \tau v$, where τ is his response time in seconds; and (2) that he continually attempts to maintain the condition $D = d$ by adjusting ψ via the medium of the nose-wheel control. The latter assumption can best be illustrated by assuming that the pilot extends an imaginary line of length $d = \tau v$ ahead of the aircraft and pointed in the direction of motion, and attempts to keep the far end of this imaginary line exactly on the centerline of the runway by his steering behavior. We may then introduce the resulting relationship representing these two assumptions:

$$D = \tau v \qquad (15)$$

Now $\dot{D} = 0$ since in the present analysis v is also a constant (from a previous assumption). With these relationships in mind we can rewrite Eq. (14) as follows:

$$F/\psi = W/kD = W/\tau kv \qquad (16)$$

[The significance of Eq. (16) will be discussed later.]

Next, let us suppose that x—i.e., lateral deviation from centerline—is the pilot's primary visual input instead of ψ. From Eq. (16) we see that

$$F = (\psi/k)(W/D) \qquad (17)$$

But $\psi = x/D$, from Eq. (7). Substituting this in Eq. (17) we obtain

$$F = (x/k)(W/D^2) \qquad (18)$$

As in Eq. (15), we assume again that $D = \tau v$. Substituting this in Eq. (18) and solving for F/x, we obtain the desired result:

$$F/x = W/k\tau^2 v^2 \qquad (19)$$

It is instructive to assess the relative meanings of Eqs. (16) and (19) as possible human transfer functions. First, we see that both are dependent only upon the three constants W (wheel base), v (speed), and τ (response time). Second, we can determine whether stable steering system operation is possible in either case by solving both Eqs. (16) and (19) for F, then substituting successively in Eqs. (12) and (6).

From Eq. (16), $F = W\psi/k\tau v$. Substituting this in Eqs. (12) and (6) we obtain $\ddot{x} = v\psi/\tau$. But $\psi = x/D$, from Eq. (7). Therefore,

$$\ddot{x} = vx/\tau D \qquad (20)$$

Again applying the assumption of Eq. (15) and substituting for D in Eq. (20), we obtain

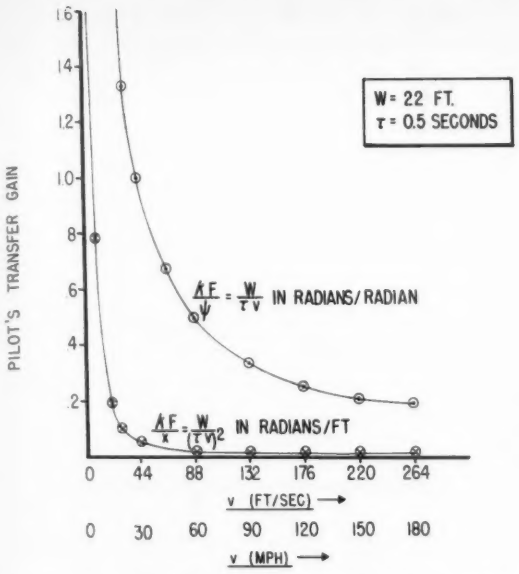

Fig. 3. Human transfer gain required to compensate for different constant vehicle speeds under differing assumptions of perceptual input.

$$\ddot{x} = x/\tau^2 \tag{21}$$

The well-known solution to Eq. (21) is

$$x = x_0 e^{-t/\tau} \tag{22}$$

This means that if the man exhibits the transfer function defined in Eq. (14) and uses ψ as his primary perceptual input, the aircraft will always approach the runway centerline in an exponential manner for any given displacement x_0 (the constant $1/\tau$ represents the decay rate of the resulting exponential).

Now let us look at the second possibility. Eq. (19) represents the case where the man uses x as his primary perceptual input. Substituting Eqs. (19) and (12) in Eq. (6), we obtain directly Eq. (21) again. So it is evident that both methods of perceiving apparently lead to stable operation in the nose-wheel steering task. How then do they differ? To illustrate the difference graphically, both gain functions are plotted in Fig. 3 for $\tau = 0.5$ sec and $W = 22$ ft.

It is clearly evident that the human's transfer gain must vary over a wide range to handle different vehicle speeds—in the one case, his gain must be inversely proportional to *speed*, while in the other case it must be inversely proportional to the *square of speed*. Pilot's transfer gain in either case is seen to be independent of time and/or frequency and may be characterized quite simply as a *velocity-modulated gain*.

It is quite possible that, in general, the operator may include components of both transfer functions. For instance, his output might be characterized as follows:

$$F = c_1 \frac{Wx}{\tau^2 v^2} + c_2 \frac{W\psi}{\tau v} \tag{23}$$

where c_1 and c_2 represent the relative proportions of each function being utilized by the operator at any given time. Indeed, it is possible that these relative proportions may vary with learning, with time, or even with ground speed.

However, it appears more reasonable to assume that, since transfer gain variation with the square of speed is the more difficult task, requiring greatest sensitivity and largest variation, the operator will eventually learn or will prefer to steer the vehicle using only aircraft heading ψ and distance to centerline D. The considerable weight of opinion in favor of this assumption is summarized by Gibson[1] thus: "The behavior involved in steering an automobile, for instance, has usually been misunderstood. It is less a matter of *aligning the car with* the road than it is a matter of *keeping the focus of expansion* in the* direction one must go." (Italics mine.)

That a changing gain as a function of speed is required of the pilot is not a new observation; this requirement has been recognized, at least implicitly, in connection with the steering of all types of ground vehicles (see the previous discussion of "distance ahead"). Nonetheless, the extent of the variation in required gain as indicated in Fig. 3 is rather startling. It derives from the fact that nose-wheel steering effectiveness must be maintained throughout a range of speeds up to that at which the increasing aerodynamic effectiveness of the rudder can provide adequate lateral control of the aircraft. It is likely to be at this speed that nose-wheel lift-off is performed, relieving the pilot or copilot of the extreme nose-wheel steering sensitivity required because of high speed and permitting the lower sensitivity of rudder steering to become effective. In effect, nose-wheel lift-off represents a sudden change in vehicle steering gain of a sort indicated in Fig. 4. This change serves to simplify the pilot's steering task at a crucial point in the ground roll.

In contrast, at the low end of the speed range, very high nose-wheel gain is required for turn-off, taxiing, parking, and initial alignment on runway during start of take-off ground roll.

Taken together, these factors indicate a rather complex steering task. As take-off speeds have increased with the advent of jet aircraft, the inadequacies of linear steering systems with respect to the pilot's steering task have become increasingly

* The *focus of expansion* in the visual field always represents the direction of motion of the observer. In steering on a runway, relative motion of the aircraft with respect to the runway centerline is simply the angle ψ formed by the intersection of the runway centerline with an extended line from the pilot to his *focus of expansion*, as shown in Fig. 2. In the absence of wind, skid, or creep, this line is usually coincident with the centerline of the aircraft as shown in Fig. 1. Nevertheless, the foregoing analysis is perfectly valid in the presence of a crosswind.

serious and, hence, apparent. If, for example, a nose-wheel steering gain is selected for best operation at 60 mph, the gain will be found much too low for low-speed taxiing and parking. In an attempt to overcome this particular difficulty, it has been proposed that a two-valued nonlinear steering gain be incorporated into steering systems as exemplified in Fig. 5. The higher gain would be obtained with the large excursions of the rudder bar normally encountered in taxiing and parking.

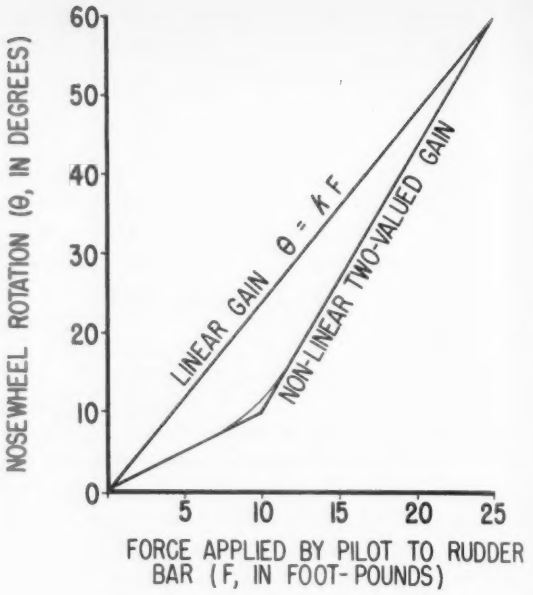

Fig. 5. Steering gains in current use.

Proposed Solution

Of the various solutions proposed, none has gone far enough toward a complete solution valid for all conditions of the ground-roll phase of aircraft operation. It is proposed, then, that such a solution be attempted, based upon known facts and principles of human performance in a servoloop.

It appears desirable from a human factors standpoint for an operator in a servoloop to maintain a high, fixed gain and to act as a simple amplifier. Experimental evidence indicates that such operations will result in least variability and greatest accuracy in performance.[2–5]

Translating this statement into terms of the present problem, it means that a given rudder pedal (or steering wheel) force should always result in the same rate of change of aircraft direction of motion $\dot{\psi}$, regardless of speed [refer back to Eq. (4)]. In order that this may occur, the steering system must be so designed that the nose-wheel angle θ is made directly proportional to the product of applied rudder pedal force F and wheel base W and inversely proportional to ground speed v—viz.,

$$\theta = kF(W/v) \tag{24}$$

where k is the constant of proportionality as in Eq. (12). Eq. (24) specifies the operation of a *velocity-modulated steering system*. To see whether this mechanization has the desired effect, first substitute Eq. (24) in Eq. (11). This results in

$$F = (\psi/k)\ [(v - \dot{D})/D] \tag{25}$$

The contrast between Eq. (25) and Eq. (13) is evident in that the dependency upon wheel base and inverse velocity has been eliminated.

Next substitute Eq. (15) in Eq. (25) to obtain

$$F = (\psi/\tau k)[1 - (\tau\dot{v}/v)] \tag{26}$$

For the assumption of constant speed, Eq. (26) reduces to

$$F = \psi/\tau k \tag{27}$$

This equation says that, with the foregoing mechanization of the steering system, the force output required is simply proportional to the perceived angle ψ regardless of speed.

Since constant speed has been assumed in the development to this point, it is instructive to examine the new requirements which the proposed system of velocity-modulated steering places upon the human operator or pilot under the more usual conditions of *varying* speed. More specifically, the case of particular interest is that of take-off, wherein relatively constant acceleration occurs so that $\dot{v}$ = a constant. For aircraft of interest, this value is of the order of 8.8 ft/sec^2, representing a take-off run of 3,900 ft over 30 sec. The value of τ, or human response time, can be taken as approximately 1/2 sec. Substituting these values in Eq. (26), we obtain

$$F = (\psi/0.5k)[1 - (4.4/v)] \tag{28}$$

The quantity $\tau kF/\psi$ is plotted against $[1 - (4.4/v)]$ in Fig. 6 to indicate the required variation

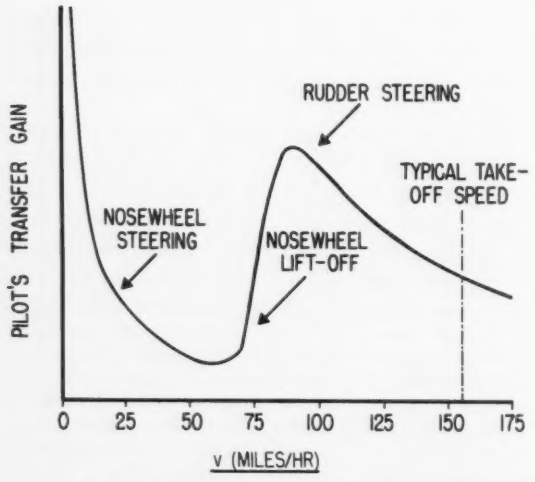

Fig. 4. Variation in required pilot's transfer gain as a function of speed, showing effect of nose-wheel lift-off.

in pilot's gain with constant take-off acceleration using the proposed velocity-modulated steering system On the same graph is plotted the solution for the constant steering gain system. The success of the proposed system in reducing pilot transfer gain variation over a wide range of ground speed is evident. It does not require increasing pilot steering sensitivity with speed as does the normal constant gain system. Over the important speed range of 30–80 mph the pilot gain requirement is essentially constant. Its specific level is fixed by the appropriate selection of k.

The type of mechanization required for such a steering system is indicated schematically in Fig. 7. The portion of the diagram within the dotted lines already exists on most aircraft of interest, the only difference being that a constant voltage is applied across the Request Potentiometer at A″-B″. Introduction of velocity-modulated steering in these aircraft requires only that this applied voltage be made an inverse linear function of ground speed, instead of a constant. The scheme shown in Fig. 7 is only one of a number of possible schemes, the particular choice of which depends upon the type of steering system in an aircraft, the selection of a reliable speed sensor, and the desirability of introducing fail-safe features. References 6 and 7 describe other mechanization techniques which will achieve the same goal after suitable modification. (It is of interest to note that those aircraft presently equipped with anti-skid braking devices have inherent in them a ground-speed sensor.)

Referring back to Fig. 7, it is seen that the steering signal voltage is directly proportional to pilot's

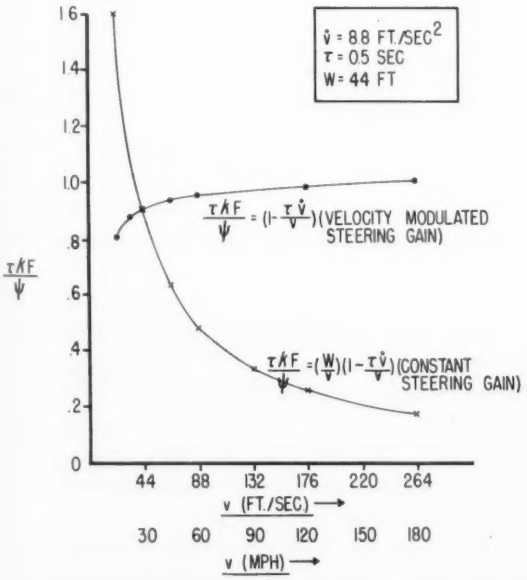

Fig. 6. Comparison of human transfer gain requirements for standard vs. proposed steering systems under conditions of constant longitudinal acceleration.

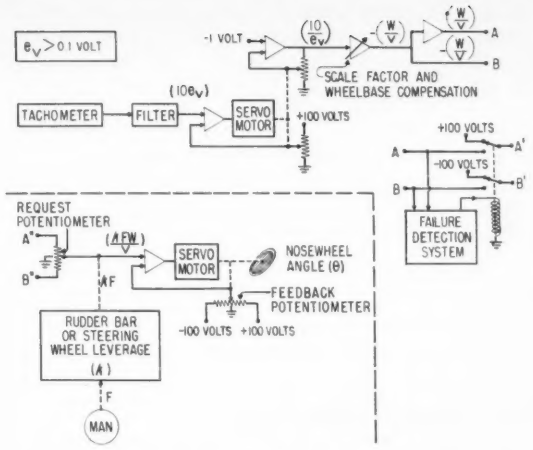

Fig. 7. Schematic diagram of velocity-modulated steering system.

force F (which produces rudder bar or steering wheel deflection), aircraft wheel base W, and a constant of proportionality k; and inversely proportional to speed v; all as required by Eq. (24). Such a scheme would indeed result in high gain at low speeds for turn-off, taxiing and parking, and initial ground roll during take-off, and would result in low gain at high speeds where overcontrol might be critical.

The most attractive result, however, for those aircraft with rudder pedal control of nose-wheel steering is the fact that rudder pedal travel can be large at high speeds, thus permitting full use of the rudder as soon as it becomes aerodynamically effective with no sharp rudder transition.

An additional important advantage is that, through proper choice of the gain constant k, the normal side-load on the aircraft due to nose-wheel steering can be operationally limited to some nominal amount (as required by some current aircraft specifications) while at the same time allowing the pilot to override this limit in certain situations where a ground loop might be the lesser of two evils.

Finally, the proposed velocity-modulated steering system concept retains the safety feature of requiring that the pilot look ahead a distance proportional to speed, without imposing on him the additional burden of varying his steering transfer gain with speed as required by present systems.

References

[1] Gibson, J. J., *The Perception of the Visual World*, Cambridge, Mass., Houghton-Miflin Co., 1950.

[2] Levine, M., *Tracking Performance as a Function of Exponential Delay Between Control and Display*, WADC TR 53-236, Oct. 1953.

[3] Birmingham, H. P., and Taylor, F. V., *A Human Engineering Approach to the Design of Man-Operated Continuous Control Systems*, NRL Report 4333, April 1954.

[4] Chernikoff, R., Bowen, J. H., and Birmingham, H. P., *A Comparison of Zero-Order and Fourth-Order Aided Compensatory Systems as a Function of Course Frequency*, NRL Report 5262, Jan. 1959.

[5] Birmingham, H. P., and Taylor, F. V., *Why Quickening*

Works, Automatic Control, Vol. 8, No. 4, pp. 16–18, 1958.

[6] Helgeson, V. L., *Vehicle Steering System with Lateral Acceleration Computer*, U.S. Patent No. 2,957,535, dated Oct. 25, 1960; U.S. Patent Office, Dept. of Commerce.

[7] Groen, W., *Speed-Responsive Control System for Vehicle Steering Mechanisms*, U.S. Patent No. 2,734,589, dated Feb. 14, 1956; U.S. Patent Office, Dept. of Commerce.

✦ ✦ ✦

Aerospace Technology

(Continued from page 26)

Flight Mechanics Reliability

existent. A much higher level of effort is needed in the collection, correlation, and dissemination of information on components and subsystems. The initiative here can be taken by the Air Force, particularly in improving the organization and unification of the program to place emphasis on all aspects. However, the willing cooperation of the industry is most essential.

The solution of the problem of design of reliable aerospace vehicles demands careful and complete analyses at every level of industry, from the smallest item up to components, subsystems, and systems. After these careful analyses, judgments can be made as to re-examination of the requirement, development of "super" components, redundancy, testing, and inspection rigidity. Fundamentally this job can be done only by industry. The Air Force can exhort, establish requirements and goals, participate in compromises, etc., but it is not close enough, early enough, to the design to be able to do the job. Neither can the job be done well by the specialized reliability groups in industry. These groups have a utility, but the key to the situation is the indoctrination of all levels associated with the design and an almost fanaticism on the part of group leaders to accept nothing less in reliability than what is needed regardless of what it means in discarding old ways of doing things. Only when this indoctrination is accomplished will we be on the way to solution of the problem we face.

References

[1] Durand, T. S., and Johnston D. E., WADD TR 60-330, *A Compilation of Component Field Reliability Data Useful in Systems Preliminary Design*, 1961.

[2] Anderson, R. O., WADC TN 58-346, *Methods of Analyses for Space Vehicle Control System Redundancy*, 1958.

[3] Jex, H. R., Ashkenas, I. L., and Peters, R. A., WADC TR 59-474, *An Application of Airframe Controller Optimization Techniques to a Supersonic Missile*, 1961.

Relating Industrial Research to Company Goals

including whether emphasis will be placed on basic or applied research; over what time spans are the results of research expected to have an economic impact in the company; and how follow-on development is to be supported. Successful research leads to ideas, and ideas lead to product development. The extent to which the research team participates in the development will determine to a large degree the stability of the research organization. If research scientists are encouraged to continue with development, research will be stopped. On the other hand, if development derives little benefit from the research background, the development project may fail. Policy must be established upon which continuity from research to development is maintained with maximum advantage to company goals.

Under the topic of *facilities*, decisions are needed with regard to questions such as whether emphasis will be given to facilities for research or for development; geographic accessibility of the laboratory from the home company, employees' homes, local universities; who will operate the facilities; and does the long-range financing of the facilities provide for all important needs?

Organization of the research function is important because it determines to a large extent the environment in which scientists and engineers doing research must work.[3] Organization determines not only the immediate working environment but also the extent to which the research director may control facilities operation, support services, procurement, etc. Decisions on these details are required.

Finance involves topics such as time span of research budgets (one year or more); pricing policy of research contracts; circumstances under which the company sets aside the requirement for profits in research contracts; impact of Armed Services procurement regulations on research financing; and accounting practices in determining research costs.

Relating the research mission to company goals requires careful consideration of all details just enumerated. Reconciliation of the issues involved in the company goals with the factors involved in the conduct of research requires top management decisions.[4] Although the problems are complex, skilled managers are solving equally difficult problems in other areas.[5]

To SUMMARIZE—a problem exists in matching research with business. The problem is important and complex, but there is no reason to believe that it cannot be adequately solved. A recognition of

the principal details involved in company goals and research, an appreciation for new management techniques involving complicated details, and a willingness for all—including top management—to participate in the approach to the problem are the essential ingredients in its solution.

References

[1] Brozen, Yale, *Trends in Industrial R/D*, Research & Development, Aug. 1960.

[2] Marcson, Simon, *The Scientist in American Industry*, Industrial Relations Section, Princeton Univ., 1960.

[3] Rodert, Lewis A., *Whither Aerospace Industry Research Management*, Aerospace Engineering, March 1961.

[4] Quinn, James Brian, *Long Range Planning of Industrial Research*, H.B.R., Vol. 39, No. 4, July-Aug. 1961.

[5] Ohlinger, Lee A., *A New Scientific Management Technique for the Air Force*, presented at IAS Summer Meeting, June 1961.

✦ ✦ ✦

Adventures in Engineering

(*Continued from page 27*)

(b) Transistors rejected via temperature cycling tests.

(c) "Gettered" transistors.

Tests results were as follows:

(a) Transistors accepted via temperature cycling tests showed approximately 4 percent temperature-sensitive units.

(b) Transistors rejected via temperature cycling tests showed approximately 80 percent temperature-sensitive units.

(c) "Gettered" transistors did not show temperature sensitivity.

This test answered several questions:

(a) The temperature cycle screening was removing the majority of temperature sensitive transistors and removing all that would cause malfunctions at time of screening.

(b) "Gettered" transistors did not show temperature sensitivity at the time of the test.

It asked at least one more: Would time cause temperature sensitivity degradation of temperature cycle screened transistors?

The test groups were subjected to 96 hours at 100°C (equivalent to one year's storage at 25°C). The temperature plateau test was repeated, the groups were subjected to a second 96-hour period at 100°C, and the temperature plateau test was again performed.

It was found that temperature sensitivity degradation increased in transistors that were temperature cycle accepted. An approximately linear increase in the number of transistors exhibiting temperature sensitivity with time was noted. The severity of sensitivities also increased with time. A definite upward shift was noted in temperature sensitivity point with respect to temperature. "Gettered" transistors showed no evidence of degradation or temperature sensitivity.

A program of remedial action was instituted on the basis of test results. On a short-term basis, a temperature plateau test with plateaus at −35, −25, −15, +5, +15, and +25°C was established to screen existing stocks. Steps were taken to reduce transistor high-temperature experience in storage, manufacturing, and test. Long-term corrective action is a change to transistors of "gettered" construction.

The deficiency noted would not affect equipment operating at average or high ambient conditions except as an undesirable shortening of transistor life. However, this phenomenon should be carefully considered in the design of equipments where low-temperature operation is desired.

✦ ✦ ✦

IAS SCRIP COUPONS

IAS SCRIP COUPONS may now be used as payment for IAS Papers, dues, subscriptions, and all other IAS services. This method will save you from writing checks, sending money orders or cash. Sheets of 5- and 25-cent coupons are available in book form of $5, $10, $25, or any amount desired, from the Special Publications Dept. Scrip may be ordered by foreign and domestic members and nonmembers.

✦ ✦ ✦

A word about our Advertisers

The many companies whose advertising appears in this issue are interested in you and your work. They are anxious to let you know what they are doing to help you solve research and design problems in missile, rocket, air, and spacecraft projects.

AEROSPACE ENGINEERING's advertising pages keep you posted on new and improved materials, components, services, and supplies useful to your professional work.

To request more information on any product or service advertised, may we suggest you write to the *advertiser* directly, at no obligation to you. It would be greatly appreciated if you would mention that you saw the ad in AEROSPACE ENGINEERING.

AEROSPACE ENGINEERING
Established 1934
2 E. 64th St., New York 21, N. Y.

Index to Advertisers

AiResearch Mfg. Divs., The Garrett Corp. 8
J. Walter Thompson Co.

American Bosch Arma Corp., Arma Div. 1
Doyle, Kitchen & McCormick, Inc.

American Machine & Foundry Co., Government Products Group 31
Cunningham & Walsh, Inc.

The Boeing Co., Wichita Div. 45
Jones & Hanger, Inc.

Cambridge University Press 59
English & Co.

Components Div., International Telephone & Telegraph Corp. 35
Gaynor & Ducas, Inc.

Douglas Aircraft Co., Inc. ..... inside front cover
J. Walter Thompson Co.

Eastman Kodak Co. 29
The Rumrill Co., Inc.

Electronic Associates, Inc. 37
Gaynor & Ducas, Inc.

The Garrett Corp., AiResearch Mfg. Divs. 8
J. Walter Thompson Co.

Government Products Group, American Machine & Foundry Co. 31
Cunningham & Walsh, Inc.

Howell Instruments, Inc. 33
The Kotula Co., Inc.

International Telephone & Telegraph Corp., Components Div. 35
Gaynor & Ducas, Inc.

Lincoln Laboratory, Massachusetts Institute of Technology 39
Randolph Associates

Lockheed-Georgia Co., A Div. of Lockheed Aircraft Corp. ..... inside back cover
Donahue & Coe, Inc.

Lockheed Missiles & Space Co., A Div. of Lockheed Aircraft Corp. 6, 7
Hal Stebbins, Inc.

Los Angeles Div. of North American Aviation, Inc. 41
Batten, Barton, Durstine & Osborn, Inc.

Massachusetts Institute of Technology, Lincoln Laboratory 39
Randolph Associates

McDonnell Aircraft Corp. ..... outside back cover
John Patrick Starrs, Inc.

Northrop Corp. 2
Doyle, Dane, Bernbach, Inc.

Princeton University Press 43
Franklin Spier, Inc.

United Aircraft Corp., Research Laboratories 5
B. E. Burrell & Associates

Vinco Corp. 47
Rolfe C. Spinning, Inc.

Wichita Div., The Boeing Co. 45
Jones & Hanger, Inc.

John Wiley & Sons, Inc. 49
Needham & Grohmann, Inc.

Wyman-Gordon Co. 57
Davis Advertising, Incorporated

AIRCRAFT DESIGN ENGINEERS

Engineering is now underway on the strange looking bird pictured here. We call it the "Hummingbird," and we are developing it for the U. S. Army.

It is to utilize the jet ejector augmentation principle for VTOL aerial vehicles to fly straight up, straight down, hover in mid-air, and convert to conventional forward flying at speeds in excess of 500 miles per hour. Just one example of what is going on here at our Engineering Center where dreams come true. Like to join us?

Openings in the fields of: Aircraft Design Engineering • Engineering Drawings Checking • Aircraft Structures • Flutter and Vibration • Sonic Fatigue • Aircraft Specifications Engineering • Reliability Engineering • Operations Research • Aircraft Research Engineering.

Write to: Hugh L. Gordon, Professional Employment Mgr., Lockheed-Georgia Co., 834 W. Peachtree St., Atlanta 8, Ga. Dept. Z-77

All qualified applicants will receive consideration for employment without regard to race, creed, color or national origin.

THE ENGINEERING CENTER

LOCKHEED-GEORGIA COMPANY

A DIVISION OF LOCKHEED AIRCRAFT CORPORATION

The Making of History was not only His Privilege

... It was His Goal

If you are an advanced degree physicist, scientist or electronic management engineer who seeks to shape air and space vehicles to their unique environmental problems rather than stretch existing designs for marginal success, you are needed at McDonnell.

Write R. F. Kaletta, Professional Placement, McDonnell Aircraft, St. Louis 66, Missouri

AN EQUAL OPPORTUNITY EMPLOYER

All qualified applicants will receive consideration for employment without regard to race, creed, color or national origin.